



universität
wien

DISSERTATION / DOCTORAL THESIS

Titel der Dissertation /Title of the Doctoral Thesis

„Omics-based physiology of marine nematode
ectosymbioses“

verfasst von / submitted by

Gabriela Fabiola Paredes Rojas

angestrebter akademischer Grad / in partial fulfilment of the requirements for the degree of
Doctor of Philosophy (PhD)

Wien, 2021 / Vienna 2021

Studienkennzahl lt. Studienblatt /
degree programme code as it appears on the
student record sheet:

UA 794 685 437

Dissertationsgebiet lt. Studienblatt /
field of study as it appears on the student record sheet:

Biologie

Betreut von / Supervisor:

Assoz. Prof. Dr. Silvia Bulgheresi, Privatdoz.

"The mind adapts and converts to its own purposes the obstacle to our acting. The impediment to action advances action. What stands in the way becomes the way."

Marcus Aurelius

TABLE OF CONTENTS

ABSTRACT.....	3
CHAPTER I.....	6
INTRODUCTION	7
MAJOR GOALS OF THE THESIS	14
OUTLINE OF THE THESIS.....	15
CHAPTER II	17
Anaerobic sulfur oxidation underlies adaptation of a chemosynthetic symbiont to oxic-anoxic interfaces.....	18
CHAPTER III	64
Differential regulation of degradation and immune pathways underlies adaptation of the ectosymbiotic <i>Laxux oneistus</i> to oxic-anoxic interfaces	65
CHAPTER IV.....	126
A Bidimensional Segregation Mode Maintains Symbiont Chromosome Orientation toward Its Host.....	127
FtsZ-mediated fission of a cuboid bacterial symbiont.....	152
CHAPTER V	177
CONCLUSIVE DISCUSSION.....	178
CONCLUSIVE REMARKS.....	192
OUTLOOK	194
REFERENCES	196
APPENDIX.....	214
ZUSAMMENFASSUNG	215
ACKNOWLEDGEMENTS.....	217

ABSTRACT

My thesis explored a fascinating animal-bacterium symbiosis, the one engaging interstitial marine nematodes belonging to the Stilbonematinae. They are unique as every worm species carries on its surface a single phylotype of sulfur-oxidizing Gammaproteobacteria belonging to the genus *Candidatus* Thiosymbion. Despite being globally distributed in shallow-water marine sediments and at abundances so high as to potentially influence sediment geochemical cycles, we still do not know why these organisms associate. Based on seminal ecological studies, it has long been hypothesized that the symbionts associate with the nematodes to exploit their vertical migrations through the redox zone, that is, to alternatively access O₂ in the upper sand layers and sulfide in the deeper ones. However, up until this work, the physiological response of the holobiont to the conditions encountered while migrating through the sand remained unknown. Therefore, in my Ph.D. studies, I analyzed *Laxus oneistus* physiological response to superficial sand- and deep sand-like conditions by applying a broad array of techniques including comparative transcriptomics, lipidomics, proteomics, and metabolomics, qPCR, stable isotope-based techniques, Raman spectroscopy, and *in situ* physico-chemical measurements. Moreover, to link symbiont physiology to its cell biology, I performed ultrastructural studies and applied DNA fluorescence *in situ* hybridization (FISH).

The results collected in the course of my Ph.D. led to four publications which can be conceptually grouped into three parts: 1) symbiont response to oxygen (Paredes et al., 2021); 2) host response to oxygen (Paredes et al., *under review*); 3) symbiont cell biology (Weber, Moessel, Paredes et al., 2019; Weber, Paredes et al., *accepted*). Concerning part (1), we showed that, under anoxia, sulfur oxidation genes were upregulated, and the symbiont appeared to be less stressed and to proliferate more. In the presence of oxygen, instead, genes involved in carbon and nitrogen assimilation were upregulated. Hence, we proposed that animal-mediated access to oxygen, rather than enhancing sulfur oxidation, would promote carbon storage and the synthesis of vitamins and cofactors. Moreover, the symbiont could profit from host-derived organic compounds and lipids. In part (2), we showed that the anoxic host did not enter suspended animation, nor appeared to suppress its metabolism. Instead, it upregulated degradation pathways (e.g., the ubiquitin-proteasome system, autophagy, and apoptosis), as well as genes that may mediate symbiosis establishment (e.g., lectins, mucins). On the other hand, when oxygen was available, it seemed to engage in costly biological processes such as development,

feeding, mating, and locomotion and also upregulated immune pathways and effectors (e.g., fungicides, bactericidal/permeability-increasing proteins). Finally, in part (3) we showed a fixed chromosome configuration in *Candidatus* Thiosymbion and hypothesized that it might facilitate the localization of membrane proteins involved in symbiosis to the worm-bacterium interface. Finally, we characterized the morphology and reproductive mode of the first-ever reported cuboid bacterium.

CHAPTER I

INTRODUCTION

MAJOR GOALS OF THE THESIS

OUTLINE OF THE THESIS

INTRODUCTION

The art of symbiosis

Symbiosis or "*the living together of differently named organisms*", as coined by the German mycologist and botanist Heinrich Anton de Bary (de Bary 1879), describes associations between dissimilar species. Although the term mostly refers to mutually beneficial associations (mutualism) that may increase fitness for all partners (Douglas and Smith, 1989; Margulis and Fester, 1991; Smith 1991), symbiosis involves a wide array of interactions (Saffo, 1992, Martin and Schwab, 2013). For example, commensalism (beneficial for one without an effect on the other), and parasitism (beneficial for one at the expense of the other) are also among the most common symbiotic alliances (Goff, 1982; Paracer et al., 2000; McFall-Ngai and Gordon, 2006). Additionally, to describe the evolutionary stability of an association, the concept of symbiosis oftentimes involves the word *intimate*. That is, those organisms that reside within their hosts (endosymbionts) are believed to have a higher degree of intimacy than those living attached to the surface (ectosymbionts) (Smith, 1979; Rosati et al., 2004). This definition, however, might be under dispute, as ectosymbiotic associations have proven to be a result of complex coordination and communication between the participating partners and might even display a high degree of phylogenetic congruency (Goffredi, 2010; Zimmerman et al., 2016).

The perpetuation of the symbiotic associations requires transmission events across cycle stages and/or generations (reviewed in Bright and Bulgheresi, 2010, and Russel, 2019). Indeed, the symbionts adopt two main transmission modes: vertical or horizontal. The first describes the symbiont inheritance from parent to offspring, and a well-known example of this type would be the *Aphid-Buchnera* symbiosis. Here, the genome of the *Buchnera* endosymbiont has undergone a dramatic reduction, a hallmark of strict vertical transmission (Shigenobu et al., 2000). On the other hand, horizontal transmission occurs when the symbiotic partner is acquired (e.g., through coprophagy; reviewed in Salem et al., 2015) or “captured” from the surrounding environment as in the case of the symbionts of the squid *Euprymna scolopes* or of the tubeworm *Riftia pachyptila* (Nyholm and McFall-Ngai, 2004; Nussbaumer et al., 2006).

Nevertheless, regardless of the transmission mode, the symbiotic interplay among organisms of the three domains of life (Eukarya, Bacteria, and Archaea) creates genetic, morphological, behavioral, and physiological innovations (Margulis and Fester, 1991; Douglas, 1994; Ott et al., 2004a, b; Cavanaugh et al., 2006; McFall-Ngai, 2008; Moya et al., 2008; Sudakaran et al., 2017).

Nowadays, there is no doubt that we live in a symbiotic Earth, yet the surge of this field only started a couple of decades ago (McFall-Ngai, 2008). That is because symbioses, especially microbial partnerships, were regarded as a mere curiosity more than the norm in biology (Smith and Douglas, 1987; McFall-Ngai, 2015). Thus, it wasn't until the advent of molecular markers (Woese et al., 1977; 1990), followed by the use of high-throughput technologies (e.g., next-generation sequencing) that also uncultivated organisms (see for example Wilbanks et al., 2014; Ghanbari et al., 2015; Trojan et al., 2016; Zaremba-Niedzwiedzka et al., 2017) including a wealth of symbionts (see for example Shigenobu et al., 2000; Woyke et al., 2006; Newton et al., 2007; Moran et al., 2008; Petersen et al., 2016; Bongrand et al., 2016; Jäckle et al., 2019) could be characterized. Crucially, this led to the realization that i) microorganisms virtually rule the world (Woese et al., 1990; Pace et al., 2012), and that ii) host-microbial symbioses are pervasive and a driving force for the evolutionary success of eukaryotes (Dubilier et al., 2008; Lee et al., 2010; Gilbert et al., 2012; McFall-Ngai et al., 2013; Turney, 2020).

Chemosynthetic symbioses

Chemosynthesis describes the use of chemical energy derived from a variety of inorganic compounds (e.g., hydrogen sulfide, H_2S) to produce organic carbon (Winogradsky, 1887, reviewed in Jannasch et al., 1985). Before the *Alvin* dive, which led to the discovery of deep-sea hydrothermal vents in the Galapagos Rift in 1977 (Lonsdale, 1977; Corliss et al., 1979), it was widely assumed that primary production (i.e. the conversion of an inorganic carbon source into organic carbon) was mainly driven by light through photosynthesis (Tyler et al., 2003; Sogin et al., 2021). Therefore, the unexpected encounter of a teeming ecosystem - far away from solar energy - revealed the importance of chemosynthesis for biomass production and life on Earth (Karl et al., 1980; Jannasch et al., 1985; Van Dover, 2000; Dubilier et al., 2008).

Investigations following the discovery evidenced that these communities are primarily composed of chemosynthetic symbiosis between marine invertebrates (or protists) and chemolithotrophic bacteria, and that beyond doubt, these relationships are ubiquitous in the marine environment (reviewed in Jannasch et al., 1985; Cavanaugh et al., 2006; and Dubilier et al., 2008). Moreover, the participation of at least seven animal phyla combined with numerous bacterial lineages highlights the uncontested success of these associations (Cavanaugh et al., 2006; Dubilier et al., 2008). As the ecosystems they inhabit are primordially oligotrophic, it quickly became apparent that the nutrition of the thriving populations was substantially supported by the chemosynthetic microorganisms (reviewed in Ott et al., 2004a, b; Cavanaugh et al., 2006, Taylor and Glover, 2006; and Dubilier et al., 2008, Petersen and Yuen, 2020). Strikingly, these are capable of making use of an astonishing array of electron donors for energy generation (e.g., hydrogen, carbon monoxide, hydrogen sulfide) (reviewed in Cavanaugh et al., 2006; Dubilier et al., 2008, Petersen and Yuen 2020). Among prominent examples evidencing the symbiont's role in host nutrition are the *Riftia*, *Rimicaris*, and *Zoothamnium* symbioses (Minic et al., 2001; Minic and Herve, 2003; Ponsard et al., 2013; Volland et al., 2018).

Ectosymbiotic nematodes: the Stilbonematinae

My thesis focuses on a fascinating invertebrate-bacterium chemosynthetic symbiosis involving marine nematodes belonging to the Stilbonematinae. They are a subfamily of interstitial free-living marine nematodes (Chromadoria, Desmodoridae, Stilbonematinae), and prominent members of the shallow-water meiofauna (Wieser, 1959; Ott and Novak, 1989; Ott et al., 2004a, b; Tchesunov, 2013; Scharhauser et al., 2020). Stilbonematinae comprise a monophyletic group (Kampfer et al., 1998; Bayer et al., 2009; Zimmerman et al., 2016) of approximately 50 different species grouped in 11 genera, and although some have been found in bathyal ecosystems, the majority are globally occurring in intertidal or shallow subtidal marine sediments (Tchesunov, 2013; Armenteros et al., 2014; Ott et al., 2014a, b; Scharhauser et al., 2020). Synapomorphic characteristics of Stilbonematinae include: (i) the presence of unique epidermal glandular sense organs (GSOs; Nebelsick et al., 1992; Bauer-Nebelsick et al., 1995) that may secrete molecules (C-type lectins) mediating specific symbiont attachment (Nussbaumer et al.,

2004; Bulgheresi et al., 2006, 2011), (ii) a reduced oral cavity, with a muscular-glandular pharynx (Ott et al., 2004b), and crucially (iii) every worm species carries on its cuticle a single phylotype of sulfur-oxidizing Gammaproteobacteria belonging to the genus *Candidatus* Thiosymbion (Polz et al., 1994; Bayer et al., 2009; Bulgheresi et al., 2011; Pende et al., 2014, Weber et al., *accepted*), thereby establishing a one-to-one (binary) ectosymbiosis (reviewed in Ott et al., 2004a, b).

On the surface of the worms, the ectosymbionts are arranged in either monolayer or multilayer coats that cover the totality of the nematodes (only the head and tail remain symbiont-free) (Ott et al., 2004a, b). Additionally, the bacteria display a wide array of morphological plasticity. Namely, they range from rod-shaped, crescent-shaped, filamentous, to cuboid-like bacteria (reviewed in Scharhauser et al., 2020; Weber et al., *accepted*). The stable and long codivergent evolutionary history of Stilbonematinae and their ectosymbionts suggests that the transmission mode of *Ca. Thiosymbion* is predominantly vertical (Zimmerman et al., 2016).

The *Laxus oneistus* ectosymbiosis

During my doctoral studies, I mainly focused on studying the physiology of one Stilbonematinae, the nematode *Laxus oneistus*, and its rod-shaped ectosymbiont *Candidatus* Thiosymbion oneisti. The latter stands perpendicular to the surface of the nematode and only attached with one pole, creating a monolayer that covers the whole worm (except its anterior and posterior extremities) (Polz et al., 1994; Ott et al., 1995; Ott et al., 2004a, b). Notably, *Ca. T. oneisti* was estimated to account for up 12 % of the holobiont volume (Ott et al., 2004 b).

As the genus name Thiosymbion evokes, as previously suggested (Powell et al., 1979; Ott et al., 1982), and as supported by ecological and biochemical studies (Ott and Novak, 1989; Schiemer et al., 1990; Ott et al., 1991; Polz et al., 1992; Hentschel et al., 1999), their phylogenetic placement (Zimmermann et al., 2016) and genetic repertoire (Petersen et al., 2016; Paredes et al., 2021), *Ca. T. oneisti* are chemoautotrophic sulfur-oxidizers (thiotrophic). That is, they possess the genetic capability to harness chemical energy from the oxidation of reduced sulfur compounds (e.g., sulfide, thiosulfate) to drive carbon dioxide (CO₂) fixation (Cavanaugh et al., 2006). Indeed, the autotrophic nature of the symbionts was confirmed by detecting RuBisCO (ribulose 1,5 biphosphate carboxylase/oxygenase) (Polz et al., 1992), a key enzyme

for CO₂ fixation in the Calvin-Benson-Bassham (CBB) cycle, and by showing uptake of ¹⁴C-labeled bicarbonate (Schiemer et al., 1990). In addition, my doctoral work unequivocally confirmed CO₂ fixation by the symbionts, by showing for the first time, sites of symbiont ¹³C-labeled bicarbonate uptake using NanoSIMS visualization (Paredes et al., 2021). In 1999, Hentschel et al. expanded the knowledge of *Ca. T. oneisti* physiology, and showed that it was capable of using nitrate (NO₃⁻) as an alternative electron acceptor to oxygen (O₂) and that nitrate respiration to nitrite (NO₂⁻) was stimulated by sulfide but not as much by thiosulfate. Later on, genomic (Petersen et al., 2016) but also transcriptomic and proteomic data (Paredes et al., 2021) confirmed their ability to perform complete denitrification from nitrate to dinitrogen gas (N₂).

Based on seminal ecological studies, it has long been hypothesized that the symbionts associate with the nematodes to exploit their vertical migrations through the redox zone. That is, to alternatively access O₂ (e⁻ acceptor) in the upper sand layers and sulfide (e⁻ donor) in the deeper ones. In return, the symbionts would protect the host from sulfide poisoning (Ott and Novak, 1989; Ott et al., 1991; Hentschel et al., 1999).

In these anoxic layers, the symbionts might use NO₃⁻, NO₂⁻, fumarate, thiosulfate, and polysulfide as alternative e⁻ acceptors (Hentschel et al., 1999; Paredes et al., 2021). Nevertheless, up to this thesis, it was unknown how the *Laxus*-Thiosymbion symbiosis was affected by the different conditions encountered while migrating through the redox zone. More generally, omics-based physiological investigations were lacking, despite the availability of stable isotope-based studies (Ott et al., 1991; Conway et al., 1989; Dando et al., 1993; Volland et al., 2018) and of morphological and ultrastructural analyses (Bauer-Nebelsick et al., 1995; Bright and Sörgo, 2003). In Chapters II and III of this thesis, to provide a comprehensive physiological analysis of the Stilbonematinae-Thiosymbion consortium, for a better understanding of its evolution and its functioning, I applied a palette of omics techniques. The latter inspired by the groundbreaking studies performed on other nematode-bacterium (e.g., the *Xenorhabdus*-*Steinernema* symbiosis; Goodrich-Blair, 2007; Murfin et al., 2015) and chemosynthetic symbioses such as those engaging *Olavius algarvensis* (Kleiner et al., 2012; Wippler et al., 2016), and *R. pachyptila* (Childress and Girguis, 2011; Hinzke et al., 2019).

From Symbiont physiology to Symbiont cell biology

Despite the inability to isolate the ectosymbionts into pure cultures, the growth and division modes responsible for their various shapes (e.g., rod, filaments) and for their spatial arrangement on the worm surface (e.g., rods forming monolayers resembling epithelia) have started to be characterized at the molecular level (Bulgheresi, 2016; Pende et al., 2018; Weber et al., 2019; Weber et al., *accepted*). One unconventional reproductive strategy is that of the ectosymbiont of *L. oneistus*, *Ca. T. oneisti*. Instead of lengthening, this symbiont grows in width and undergoes FtsZ-based longitudinal fission, thereby guaranteeing to both its daughter cells, continuous, transgenerational host attachment (Polz et al., 1992; Leisch et al., 2012). This division mode is likely supported by the arrangement of the bacterial actin homolog MreB into a medial ring-like structure, which does not exclude the poles. Crucially, this led to the hypothesis that in animal symbionts MreB is needed for cell growth and division (Pende et al., 2018). Strikingly, *Ca. T. oneisti* cell division is radically different from that of model rods (such as *Escherichia coli*) that are known to grow in length (excluding MreB from the poles) and then undergo transverse binary fission (Bendezú and de Boer, 2008; den Blaauwen, 2013; Rowlett and Margolin, 2015; Kawazura et al., 2017).

How to explain the evolution of these extraordinary cell division modes? In Chapter II, we show that the symbiont might profit from host-derived lipids and organic compounds. In light of this, the longitudinal division would enable both daughter cells to stay attached to the host and profit from the nutrients diffusing from its cuticle. But longitudinal division raises another important issue: how are the symbiont's chromosomes segregated? In bacterial model rods, chromosomes exist in two main configurations termed longitudinal and horizontal (reviewed Wang et al., 2013). Longitudinal refers to the localization of the origin of chromosome replication (*ori*) and the terminus of replication (*ter*) at opposite cell poles. In the transverse configuration, instead, the *ori* and *ter* co-occur at midcell.

In Chapter IV, we show that the longitudinal dividing *Ca. T. oneisti* exhibits a unique DNA-segregation mode. Namely, the sister *ori* segregate bi-dimensionally (i.e. along both the short and the long cell axis), and localize together with the *ter* (at both the beginning and end of the cell cycle), at the center of the cell. As a result, the chromosome orientation toward the host is maintained throughout the generations (Weber et al., 2019). Therefore, Chapter IV

(Weber et al., 2019) addresses for the first time the chromosome configuration of a free-living bacterial symbiont, and we hypothesize that the fixed chromosome orientation might be an adaption to the symbiotic lifestyle.

In addition, Chapter IV describes the host-polarized and FtsZ-mediated division mode of the cube-like *Candidatus Thiosymbion cuboideus* (Weber et al, *accepted*). The latter is the ectosymbiont of the free-living marine nematode *Catanema sp.* (Stilbonematinae) (Scharhau-ser et al., 2020). Crucially, cuboid cell shapes are rare, and within prokaryotes (and up until this thesis; Chapter IV) they had only been described in halophilic Archaea (Walsby, 1980; Oren, 1999).

MAJOR GOALS OF THE THESIS

Chemosynthetic hosts are believed to have adopted several strategies to fulfill one key nutritional requirement of their thiotrophic symbionts: the use of oxygen as their main electron acceptor. In the case of Stilbonematinae, it is hypothesized that vertical migrations across oxidized and reduced sediments would bridge the gap between oxygen and sulfide. This implies that symbioses with Stilbonematinae evolved for thiotrophic bacteria to regularly access oxygen. However, up to my Ph.D. research, the impact of oxygen on chemosynthetic ectosymbioses has not been studied. Therefore, I focused on *Laxus oneistus* which, like other Stilbonematinae, thrives at oxic-anoxic interfaces (Ott and Novak, 1989), and addressed the following questions:

1. What is the global physiological response of the ectosymbiont *Candidatus* Thiosymbion oneisti to oxygen?
2. What is the global physiological response of the nematode host *Laxus oneistus* to oxygen?
3. How does symbiont cell biology, namely its reproduction mode, serve its physiology?

OUTLINE OF THE THESIS

My Ph.D. thesis is a cumulative thesis (Kumulative Dissertation). The structure is written in the following order: an abstract in English, a general introduction (Chapter I), followed by the corresponding individual publications dealing with: symbiont (Chapter II) and nematode host (Chapter III) physiological response to oxygen, symbiont cell biology (Chapter IV), an all-embracing discussion and conclusive remarks (Chapter V), and finalizing with the corresponding cited literature an abstract in German (Zusammenfassung) and acknowledgments.

The experimental part of the study was mainly carried out at the Smithsonian Field Station on Carrie Bow Cay, located on the Belizean Barrier Reef in Central America, and at Ilet à Cochons in Guadeloupe, France. My thesis comprises four original scientific articles (two first-authored, two second-authored). Below are the published and accepted papers and the manuscript under review, with their corresponding chapters:

Chapter II

Paredes, G. F., Viehboeck, T., Lee, R., Palatinszky, M., Mausz, M. A., Reipert, S., Schintlmeister, A., Maier, A., Volland, JM., S., Hirschfeld, C., Wagner, M., Berry, D., Markert, S., Bulgheresi, S., & Koenig, L. (2021). Anaerobic sulfur oxidation underlies adaptation of a chemosynthetic symbiont to oxic-anoxic interfaces. **mSystems**, 6(3), e01186-20. <https://doi.org/10.1128/mSystems.01186-20>

Chapter III

Paredes, G. F., Viehboeck, T., Mausz, M., Saito, Y., Liebeke, M., Markert, S., Koenig L., & Bulgheresi, S. Differential regulation of degradation and immune pathways underlies adaptation of the symbiotic nematode *Laxus oneistus* to oxic-anoxic interfaces. Under review and available online at <https://doi.org/10.1101/2021.11.11.468236>

Chapter IV

Weber, P. M., Moessel, F. *, **Paredes, G. F.** *, Viehboeck, T., Vischer, N. O., & Bulgheresi, S. (2019). A Bidimensional Segregation Mode Maintains Symbiont Chromosome Orientation toward Its Host. **Current Biology**, 29(18), 3018-3028. <https://doi.org/10.1016/j.cub.2019.07.064> *Contributed equally.

Weber, P., **Paredes, G. F.** *, Viehboeck, T. *, Pende, N., Volland, JM., Gros, O., Ott, J., & Bulgheresi, S. Ftsz-Mediated Fission of a Cuboid Bacterial Symbiont. *Contributed equally. *Accepted at iScience*, and available online at: https://papers.ssrn.com/sol3/papers.cfm?abstract_id=3885987

CHAPTER II

Anaerobic Sulfur Oxidation Underlies Adaptation of a Chemosynthetic Symbiont to Oxic-Anoxic Interfaces



Authors Gabriela F. Paredes, Tobias Viehboeck, Raymond Lee, Marton Palatinszky, Michaela A. Mausz, Siegfried Reipert, Arno Schintlmeister, Andreas Maier, Jean-Marie Volland, Claudia Hirschfeld, Michael Wagner, David Berry, Stephanie Markert, Silvia Bulgheresi* and Lena König*

*these authors contributed equally

Published in: mSystems, 2021



Anaerobic Sulfur Oxidation Underlies Adaptation of a Chemosynthetic Symbiont to Oxic-Anoxic Interfaces

Gabriela F. Paredes,^a  Tobias Viehboeck,^{a,b} Raymond Lee,^c Marton Palatinszky,^b Michaela A. Mausz,^d Siegfried Reipert,^e Arno Schintlmeister,^{b,f} Andreas Maier,^g Jean-Marie Volland,^{a,*} Claudia Hirschfeld,^h Michael Wagner,^{b,i} David Berry,^{b,j} Stephanie Markert,^h  Silvia Bulgheresi,^a Lena König^a

^aUniversity of Vienna, Department of Functional and Evolutionary Ecology, Environmental Cell Biology Group, Vienna, Austria

^bUniversity of Vienna, Center for Microbiology and Environmental Systems Science, Division of Microbial Ecology, Vienna, Austria

^cWashington State University, School of Biological Sciences, Pullman, Washington, USA

^dUniversity of Warwick, School of Life Sciences, Coventry, United Kingdom

^eUniversity of Vienna, Core Facility Cell Imaging and Ultrastructure Research, Vienna, Austria

^fUniversity of Vienna, Center for Microbiology and Environmental Systems Science, Large-Instrument Facility for Environmental and Isotope Mass Spectrometry, Vienna, Austria

^gUniversity of Vienna, Faculty of Geosciences, Geography, and Astronomy, Department of Geography and Regional Research, Geoecology, Vienna, Austria

^hUniversity of Greifswald, Institute of Pharmacy, Department of Pharmaceutical Biotechnology, Greifswald, Germany

ⁱAalborg University, Department of Chemistry and Bioscience, Aalborg, Denmark

^jJoint Microbiome Facility of the Medical University of Vienna and the University of Vienna, Vienna, Austria

Silvia Bulgheresi and Lena König contributed equally to this work.

ABSTRACT Chemosynthetic symbioses occur worldwide in marine habitats, but comprehensive physiological studies of chemoautotrophic bacteria thriving on animals are scarce. Stilbonematinae are coated by thiotrophic *Gammaproteobacteria*. As these nematodes migrate through the redox zone, their ectosymbionts experience varying oxygen concentrations. However, nothing is known about how these variations affect their physiology. Here, by applying omics, Raman microspectroscopy, and stable isotope labeling, we investigated the effect of oxygen on “*Candidatus Thiosymbion oneisti*.” Unexpectedly, sulfur oxidation genes were upregulated in anoxic relative to oxic conditions, but carbon fixation genes and incorporation of ¹³C-labeled bicarbonate were not. Instead, several genes involved in carbon fixation were upregulated under oxic conditions, together with genes involved in organic carbon assimilation, polyhydroxyalkanoate (PHA) biosynthesis, nitrogen fixation, and urea utilization. Furthermore, in the presence of oxygen, stress-related genes were upregulated together with vitamin biosynthesis genes likely necessary to withstand oxidative stress, and the symbiont appeared to proliferate less. Based on its physiological response to oxygen, we propose that “*Ca. T. oneisti*” may exploit anaerobic sulfur oxidation coupled to denitrification to proliferate in anoxic sand. However, the ectosymbiont would still profit from the oxygen available in superficial sand, as the energy-efficient aerobic respiration would facilitate carbon and nitrogen assimilation.

IMPORTANCE Chemoautotrophic endosymbionts are famous for exploiting sulfur oxidation to feed marine organisms with fixed carbon. However, the physiology of thiotrophic bacteria thriving on the surface of animals (ectosymbionts) is less understood. One long-standing hypothesis posits that attachment to animals that migrate between reduced and oxic environments would boost sulfur oxidation, as the ectosymbionts would alternatively access sulfide and oxygen, the most favorable electron acceptor. Here, we investigated the effect of oxygen on the physiology of “*Candidatus Thiosymbion oneisti*,” a gammaproteobacterium which lives attached to marine nematodes inhabiting shallow-water sand. Surprisingly, sulfur oxidation genes were upregulated under anoxic relative

Citation Paredes GF, Viehboeck T, Lee R, Palatinszky M, Mausz MA, Reipert S, Schintlmeister A, Maier A, Volland J-M, Hirschfeld C, Wagner M, Berry D, Markert S, Bulgheresi S, König L. 2021. Anaerobic sulfur oxidation underlies adaptation of a chemosynthetic symbiont to oxic-anoxic interfaces. *mSystems* 6:e01186-20. <https://doi.org/10.1128/mSystems.01186-20>.

Editor Seth Bordenstein, Vanderbilt University

Copyright © 2021 Paredes et al. This is an open-access article distributed under the terms of the [Creative Commons Attribution 4.0 International license](https://creativecommons.org/licenses/by/4.0/).

Address correspondence to Silvia Bulgheresi, silvia.bulgheresi@univie.ac.at, or Lena König, lena.koenig@univie.ac.at.

* Present address: Jean-Marie Volland, Joint Genome Institute/Global Viral, San Francisco, California, USA.

Received 10 November 2020

Accepted 20 April 2021

Published 26 May 2021

to oxic conditions. Furthermore, under anoxia, the ectosymbiont appeared to be less stressed and to proliferate more. We propose that animal-mediated access to oxygen, rather than enhancing sulfur oxidation, would facilitate assimilation of carbon and nitrogen by the ectosymbiont.

KEYWORDS *Gammaproteobacteria*, Thiosymbion, anoxia, chemosynthesis, sulfur oxidation, symbiosis, thiotrophic bacteria

At least six animal phyla and numerous lineages of bacterial symbionts belonging to *Alphaproteobacteria*, *Gammaproteobacteria*, and *Campylobacteria* (formerly *Epsilonproteobacteria*) (1) engage in chemosynthetic symbioses, rendering the evolutionary success of these associations incontestable (2, 3). Many of these mutualistic associations rely on sulfur-oxidizing (thiotrophic), chemoautotrophic bacterial symbionts that oxidize reduced sulfur compounds for energy generation in order to fix inorganic carbon (CO₂) for biomass buildup. Particularly in binary symbioses involving thiotrophic endosymbionts, it is generally accepted that the bacterial chemosynthetic metabolism serves to provide organic carbon for feeding the animal host (reviewed in references 2 to 4). In addition, some chemosynthetic symbionts have been found capable of fixing atmospheric nitrogen, albeit symbiont-to-host transfer of fixed nitrogen remains unproven (5, 6). As for the rarer chemosynthetic bacterial-animal associations in which symbionts colonize exterior surfaces (ectosymbioses), fixation of inorganic carbon and transfer of organic carbon to the host have been unequivocally shown only for the microbial community colonizing the gill chamber of the hydrothermal vent shrimp *Rimicaris exoculata* (7).

The majority of thioautotrophic symbioses have been described to rely on reduced sulfur compounds as electron donors and on oxygen as terminal electron acceptor (3, 4). However, given that sulfidic and oxic zones are often spatially separated, also owing to abiotic sulfide oxidation (8, 9), chemosynthetic symbioses (i) are typically found where sulfide and oxygen occur in close proximity (e.g., hydrothermal vents, shallow-water sediments) and/or (ii) exhibit host behavioral, physiological, and anatomical adaptations enabling the symbionts to access both substrates. Among the former adaptations, host-mediated migration across oxygen and sulfide gradients was proposed for shallow-water interstitial invertebrates and *Kentrophoros* ciliates (reviewed in references 2 and 3). The ectosymbionts of Stilbonematinae, a free-living nematode subfamily of the Desmodoridae that inhabit marine sediments (2, 10), have also long been hypothesized to associate with their motile hosts to maximize sulfur oxidation-fueled chemosynthesis, by alternatively accessing oxygen in upper sand layers and sulfide in deeper, anoxic sand. This hypothesis was based upon the distribution pattern of Stilbonematinae in sediment cores together with their migration patterns observed in agar columns (10–12). However, several chemosynthetic symbionts were subsequently shown to use nitrate as an alternative electron acceptor, and nitrate respiration was stimulated by sulfide, suggesting that some may gain energy by respiring nitrate in addition to oxygen (13–17). Furthermore, although physiological studies on chemosynthetic symbioses are available (e.g., references 18 to 21), the impact of oxygen on the symbionts' central metabolism has not been investigated (remarkably, not even in those symbionts that cover their hosts and are, therefore, directly exposed to fluctuating concentrations of oxygen).

Here, to understand how oxygen affects symbiont physiology, we focused on “*Candidatus* Thiosymbion oneisti,” a gammaproteobacterium belonging to the basal family of *Chromatiaceae* (also known as purple sulfur bacteria), which colonizes the surface of the marine nematode *Laxus oneistus* (Stilbonematinae). This group of free-living roundworms represents the only known animals engaging in monospecific ectosymbioses, i.e., a given nematode species is typically ensheathed by a single “*Ca.* Thiosymbion” phylotype, and in the case of “*Ca.* T. oneisti,” the bacteria form a single layer on the cuticle of their host (22–25). Moreover, the rod-shaped representatives of

this bacterial genus, including “*Ca. T. oneisti*,” divide by FtsZ-based longitudinal fission, a unique reproductive strategy which ensures continuous and transgenerational host attachment (26–28).

Like other chemosynthetic symbionts, “*Ca. Thiosymbion*” bacteria have been considered chemoautotrophic sulfur oxidizers based on several lines of evidence: stable carbon isotope ratios of symbiotic nematodes are comparable to those found in other chemosynthetic symbioses (12); the key enzyme for carbon fixation via the Calvin-Benson-Bassham (CBB) cycle (RuBisCO) along with elemental sulfur and enzymes involved in sulfur oxidation have been detected (29–31); reduced sulfur compounds (sulfide, thiosulfate) have been shown to be taken up from the environment by the ectosymbionts, to be used as energy source, and to be responsible for the white appearance of the symbiotic nematodes (11, 15, 31); and the animals often occur in the sulfidic zone of marine shallow-water sands (10). More recently, the phylogenetic placement and genetic repertoire of “*Ca. Thiosymbion*” species have equally been supporting the chemosynthetic nature of the symbiosis (6, 25).

In this study, we incubated nematodes associated with “*Ca. T. oneisti*” under conditions resembling those encountered in their natural environment and subsequently examined the ectosymbiont transcriptional responses via RNA sequencing (RNA-Seq). In combination with complementary methods such as stable isotope labeling, proteomics, Raman microspectroscopy and lipidomics, we show that the ectosymbiont exhibits specific metabolic responses to oxygen. Most strikingly, sulfur oxidation but not carbon fixation was upregulated in anoxia. Such a response in their natural environment would challenge the current opinion that sulfur oxidation requires oxygen and drives carbon fixation in chemosynthetic symbioses. We finally present a metabolic scheme of a thiotrophic ectosymbiont experiencing ever-changing oxygen concentrations, in which anaerobic sulfur oxidation coupled to denitrification may represent the preferred metabolism for growth.

RESULTS

Hypoxic and oxic conditions induce similar expression profiles. To understand how the movement of the animal host across the chemocline affects symbiont physiology, we exposed symbiotic worms to sulfide (thereafter used for $\sum \text{H}_2\text{S}$) and oxygen concentrations resembling the ones encountered by “*Ca. T. oneisti*” in its natural habitat. Previous studies showed that Stilbonematinae live predominantly in highly reduced sediment zones with sulfide concentrations below $50 \mu\text{M}$ or up to $250 \mu\text{M}$ (10). To assess the sulfide concentration preferred by *Laxus oneistus* (i.e., the host of “*Ca. T. oneisti*”) at our collection site (Carrie Bow Cay Marine Field Station, Belize), we determined the nematode abundance relative to the sampling depth and sulfide concentration. We found the nematode abundance to be the highest between 12 and 24 cm below the seabed. Moreover, we found all *L. oneistus* individuals in pore water containing $\leq 25 \mu\text{M}$ sulfide. Only 1.3% of them inhabited nonsulfidic ($0 \mu\text{M}$ sulfide) surface layers (Fig. 1A; see also Table S1 in the supplemental material). Therefore, we chose anoxic seawater supplemented with $\leq 25 \mu\text{M}$ sulfide as the incubation medium (AS condition) most resembling the natural habitat of “*Ca. T. oneisti*.” To assess the effect of oxygen on symbiont physiology, we additionally incubated the nematodes in hypoxic (H; $< 60 \mu\text{M}$ oxygen after 24 h) and oxic (Ox; $> 100 \mu\text{M}$ after 24 h) seawater (Fig. 1B). Nitrate, nitrite, ammonium, and dissolved organic carbon (DOC) could be detected throughout the sediment core including the surface layer (Table S1).

Differential gene expression analysis comparing H and Ox incubations revealed that only 2.9% of all expressed protein-coding genes differed significantly in their expression (Fig. 1C and D). Crucially, this gene set comprised several hypothetical proteins but did not show any significantly enriched metabolic pathways, processes, or protein families (Table S3B and Data Set S1). Because the presence of oxygen, irrespective of its concentration, resulted in a similar gene expression profile, we treated the samples

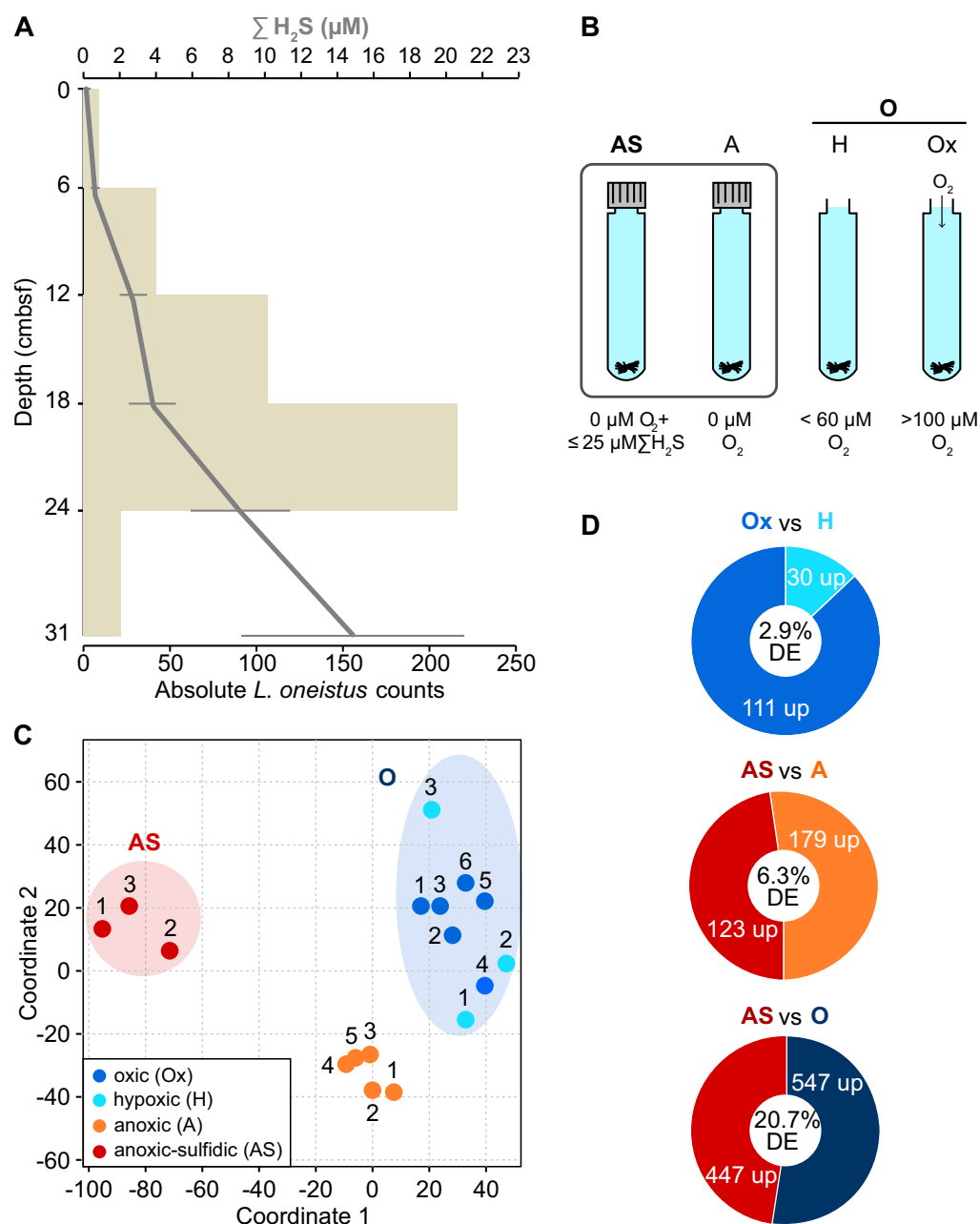


FIG 1 Natural and experimental conditions, transcriptome sample similarity, and differential gene expression. (A) *Laxus oneistus* total counts per 6-cm core subsection from 8 sandbars (horizontal beige bars) and corresponding mean sulfide ($\Sigma \text{H}_2\text{S}$) concentrations (μM , gray line). Error bars represent the standard error of the mean (Table S1). (B) Experimental setup of incubations for RNA-Seq, EA-IRMS, and Raman microspectroscopy. Batches of 50 *L. oneistus* worms were incubated under different oxygen concentrations: AS (0 μM O_2 , $\leq 25 \mu\text{M}$ sodium sulfide added), A (0 μM O_2), H (<60 μM O_2 after 24 h), and Ox (>100 μM O_2 after 24 h). The box around the anoxic incubation vials indicates that these incubations were carried out in a polyethylene isolation chamber. All incubations were performed in 0.2- μm -filtered seawater and in at least biological triplicates (see Table S2). (C) Similarity between transcriptome samples based on Euclidean distances between expression values ($\log_2\text{TPMs}$), visualized by means of multidimensional scaling. Most of the follow-up RNA-Seq analyses were conducted comparing the anoxic-sulfidic conditions (AS, red circle) to all conditions under which oxygen was present (O, blue circle). Samples 1 to 3 were collected in July 2017, whereas samples 4 to 6 were collected in March 2019. (D) Differential gene expression (DE) analysis between H and Ox samples revealed that the number of DE genes was low (2.9% of all expressed genes), and thus, H and Ox samples were treated as biological replicates. Of all expressed genes, 20.7% were differentially expressed between AS and O conditions. Genes were considered differentially expressed if their expression changed 2-fold with a false-discovery rate (FDR) of ≤ 0.05 .

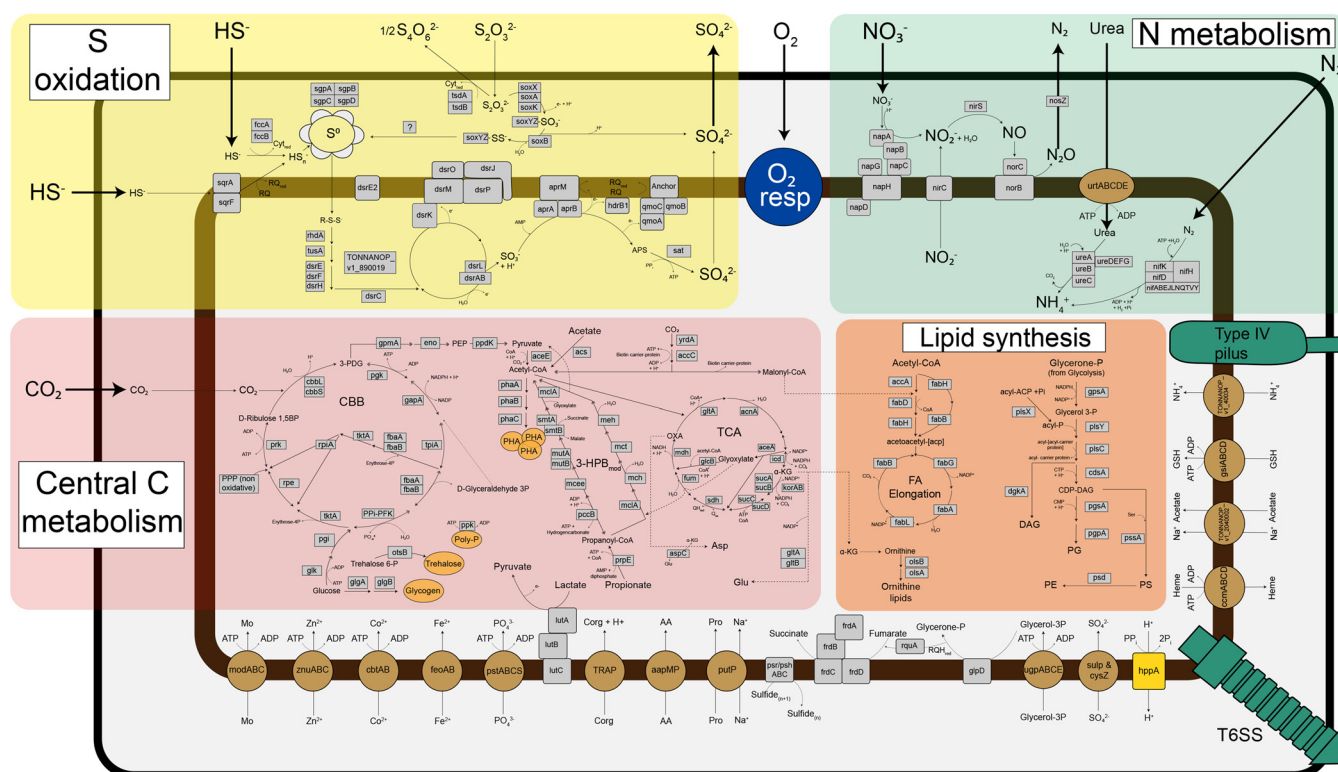


FIG 2 Schematic representation of central metabolic pathways present in the “*Ca. T. oneisti*” genome. All gene names (or locus tags for unidentified gene names) can be found in Data Set S1. The aerobic respiratory chain (O_2 resp, blue) includes NADH dehydrogenase (*nuc* genes, complex I), succinate dehydrogenase (*sdh* genes, complex II), the cytochrome bc_1 complex (*pet* genes, complex III), and an aa_3 -type cytochrome *c* oxidase (*cta* genes, complex IV). The electron transfer reactions in the S oxidation pathways are based on the work of Dahl et al. (32). Electron transfers in the denitrification pathway (N metabolism) are not illustrated but involve complexes I and III and cytochrome *c* (35). Pathways for glycogen, trehalose, and PHA degradation, as well as overall reaction stoichiometry, are not depicted. Organic carbon compounds (Corg) such as acetate, lactate, propionate, and glycerol 3-phosphate (glycerol-3P) could be host derived. Enzymes are shown in gray, transporters are brown, storage compounds are orange, and pilus and secretion system are depicted in green. AA, L-amino acids; Anchor, putative membrane anchor for the Qmo complex (TONNANOP_v1_730022); Asp, aspartate; Biotin carrier-protein, a [biotin carboxyl-carrier-protein dimer]-N6-biotinyl-L-lysine; C, carbon; CBB, Calvin-Benson-Bassham cycle; Co, cobalt; CoA, coenzyme A; DAG, diacylglycerol; FA, fatty acids; Fe, iron; Glu, glutamate; GSH, glutathione; Mo, molybdate; N, nitrogen; OXA, oxaloacetate; PE, phosphatidylethanolamine; PEP, phosphoenolpyruvate; PG, phosphatidylglycerol; PHA, polyhydroxyalkanoate; Poly-P, polyphosphate; PS, phosphatidylserine; Red, reduced; RQ, rhodoquinone; S, sulfur; Ser, serine; TCA, tricarboxylic acid cycle; TONNANOP_v1_890019, Alvin_2107 homolog (32); T6SS, type VI secretion system; Zn, zinc; 3-HPB_{mod}, modified 3-hydroxypropionate cycle according to the work of Kleiner et al. (50); 3-PDG, 3-phospho-D-glycerate; α -KG, 2-oxoglutarate.

derived from H and Ox incubations as biological replicates, and we will hereafter refer to them as the O condition.

Gene expression analysis between the AS and O conditions revealed that 20.7% of all expressed protein-coding genes exhibited significantly different expression (Fig. 1D), as we will present in detail below.

Sulfur oxidation genes are upregulated in anoxia. “*Ca. T. oneisti*” genes encoding a sulfur oxidation pathway similar to that of the related but free-living purple sulfur bacterium *Allochrochromatium vinosum* (Fig. 2) (32) were highly expressed under both AS and O conditions compared with other central metabolic processes, albeit median gene expression was significantly higher under the AS condition (Fig. 3). Consistently, 24 out of the 26 differentially expressed genes involved in sulfur oxidation were upregulated under AS (Fig. 4A). These mostly included genes involved in the cytoplasmic branch of sulfur oxidation, i.e., genes associated with sulfur transfer from sulfur storage globules (*rhd*, *tusA*, *dsrE2*), genes encoding the reverse-acting *dsr* (dissimilatory sulfite reductase) system involved in the oxidation of stored elemental sulfur (S^0) to sulfite, and finally, also the genes required for further oxidation of sulfite to sulfate in the cytoplasm by two sets of adenylylsulfate (APS) reductase (*aprAB*) along with their membrane anchor (*aprM*) and sulfate adenylyltransferase (*sat*) (33, 34). Genes encoding a quinone-interacting membrane-bound oxidoreductase (*qmoABC*) exhibited the same expression pattern. This is noteworthy, as AprM and QmoABC are hypothesized

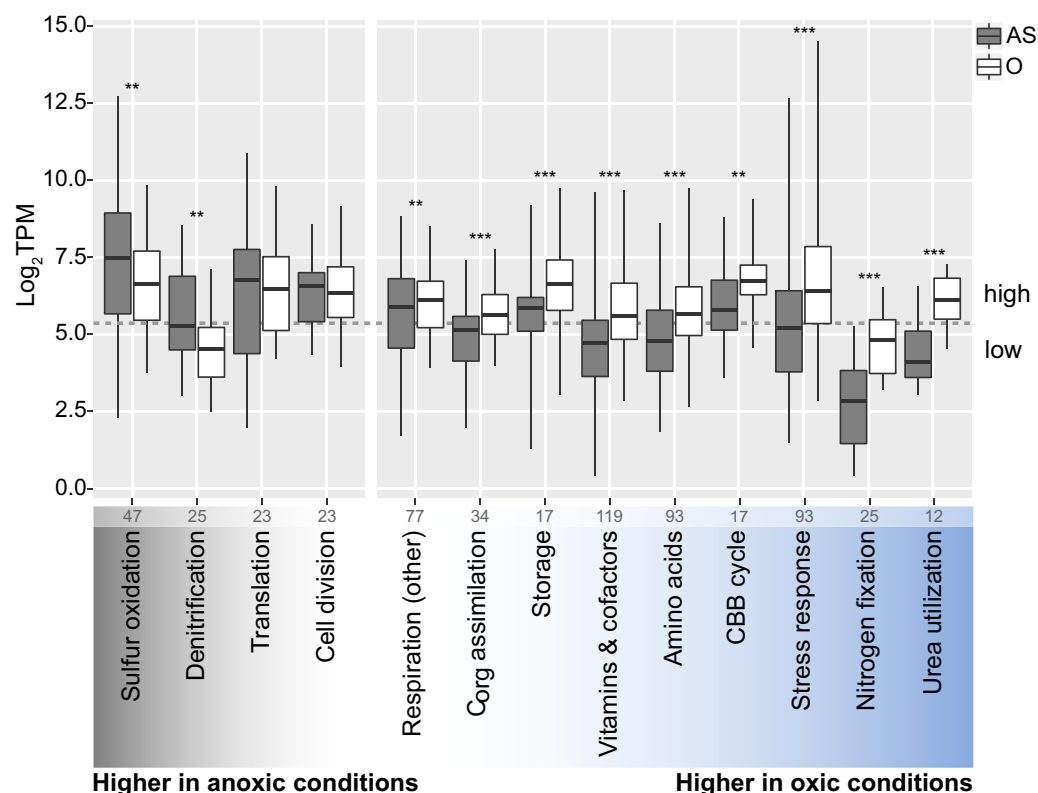


FIG 3 Median gene expression levels of selected “*Ca. T. oneisti*” metabolic processes under anoxic sulfidic (AS) versus oxygenated (O) conditions. All genes involved in a particular process were manually collected, and median expression levels (log₂TPMs, transcripts per kilobase million) per condition and process are shown (horizontal bold lines). Importantly, metabolic processes include both differentially and constitutively expressed genes, and the total number of genes considered is indicated at the bottom of each process. For the specific assignment of genes, see Data Set S1. Note that for the processes designated “Amino acids,” “Storage,” and “Vitamins & cofactors,” only the expression of the biosynthesis genes was considered. Boxes indicate interquartile ranges (25% to 75%); whiskers refer to the minimum and maximum expression values, respectively. The individual processes are ordered according to the difference in median expression between AS and O conditions, i.e., sulfur oxidation (far left) had the largest difference in median expression between the two conditions, with higher median expression under the AS condition, whereas urea utilization (far right) had the largest difference in median expression, with higher median expression under the O condition. Metabolic processes were considered highly expressed when their median expression level was above 5.2 log₂TPM (dashed gray line), which represents the median expression of all expressed protein-coding genes ($n=4,747$) under both conditions. A Wilcoxon signed-rank test was used to test for significantly different median gene expression between conditions (**, $P < 0.01$; ***, $P < 0.001$). CBB cycle, Calvin-Benson-Bassham cycle.

to have an analogous function, and their cooccurrence is rare among sulfur-oxidizing bacteria (33).

Concerning genes involved in the periplasmic branch of sulfur oxidation, such as the two types of sulfide-quinone reductases (*sqrA*, *sqrF*; oxidation of sulfide) and the Sox system (*soxKAXB*, *soxYZ*) and the thiosulfate dehydrogenase (*tsdA*) both involved in the oxidation of thiosulfate, transcript levels were unchanged between the two conditions (Data Set S1). Only the flavoprotein subunit of the periplasmic flavocytochrome *c* sulfide dehydrogenase (*fccB*), as well as a cytochrome *c* family protein (*tsdB*) thought to cooperate with TsdA, was downregulated in the absence of oxygen (Fig. 4A).

To assess whether the upregulation of sulfur oxidation genes under anoxia was due to the absence of oxygen (and not to the presence of supplemented sulfide in the medium), we performed an additional anoxic incubation where sulfide was not provided (A condition). Differential expression analysis between the anoxic conditions with and without sulfide revealed that transcript levels of 6.3% of all expressed protein-coding genes differed significantly between the two anoxic treatments (Fig. 1D). Among them, we found eight genes involved in sulfur oxidation to be upregulated in the presence of sulfide (Data Set S1). Importantly, however, irrespective of sulfide supplementation, most

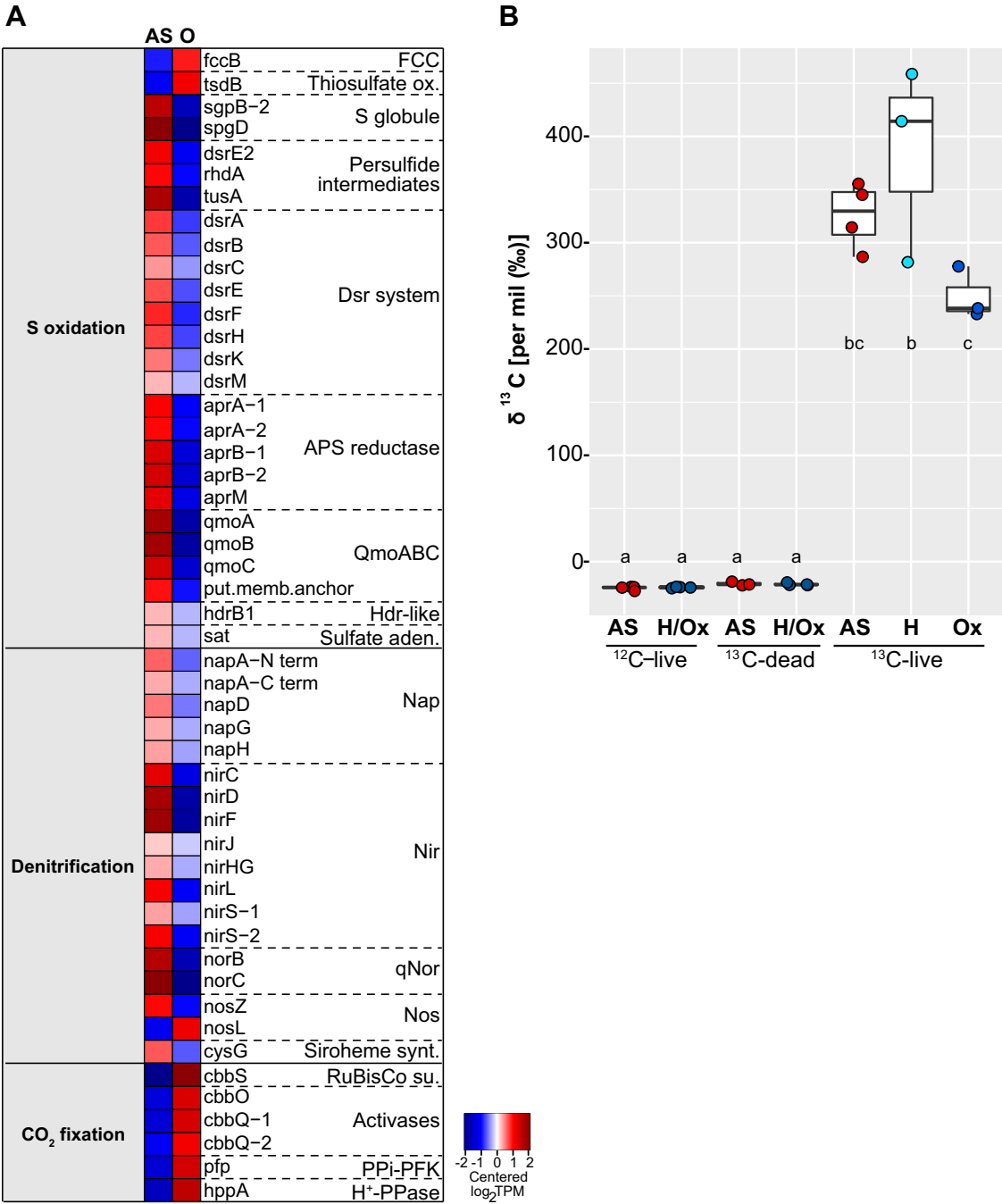


FIG 4 Oxidation of stored sulfur is coupled to denitrification but loosely coupled to CO₂ fixation under anoxic conditions. (A) Heatmap visualizing only differentially expressed genes (2-fold change, FDR ≤ 0.05) involved in sulfur oxidation, denitrification, and CO₂ fixation via the Calvin-Benson-Bassham cycle between the anoxic-sulfidic (AS) and oxygenated (O) conditions after 24 h of incubation. Expression levels are visualized by displaying mean-centered log₂TPMs (transcripts per kilobase million). Upregulation is indicated in red, and downregulation is in blue. Genes are ordered by function in the respective metabolic pathways. FCC, flavocytochrome c; thiosulfate ox., thiosulfate oxidation; S, sulfur; Dsr, dissimilatory sulfite reductase; APS, adenylylsulfate; Qmo, quinone-interacting membrane-bound oxidoreductase; Hdr, heterodisulfide reductase; sat, sulfate adenylyltransferase; Nap, periplasmic nitrate reductase; Nir, cd1 nitrite reductase; qNor, quinol-dependent nitric oxide reductase; Nos, nitrous oxide reductase; Siroheme synt., siroheme biosynthesis (heme d precursor); RuBisCo su., ribulose-1,5-bisphosphate carboxylase/oxygenase small subunit; PPi-PFK, PPi-dependent phosphofructokinase; H⁺-PPase, proton-translocating pyrophosphatase. (B) Relative ¹³C isotope content of symbiotic *L. oneistus* as determined by EA-IRMS after 24-h incubations with ¹³C-labeled bicarbonate under anoxic-sulfidic conditions (AS, red dots), hypoxic condition (H, light blue dots), or oxic conditions (Ox, dark blue dots). Dots refer to the values determined in individual measurements (comprising 50 worms per measurement; for further details, see Table S2). Horizontal lines indicate means; error bars correspond to standard deviations. The categories ¹²C-live and ¹³C-dead refer to the natural isotope abundance control and the dead control, respectively. H/Ox, controls for both hypoxic and oxic conditions. Different lowercase letters indicate significant differences among conditions (one-way ANOVA, Tukey's *post hoc* test, *P* < 0.05).

sulfur oxidation genes were similarly upregulated in the anoxic (AS or A) relative to the O incubation (Fig. S1A, Table S3B, and Data Set S1). In addition, proteome data derived from incubations with and without oxygen, but no added sulfide, showed that one copy of AprA and one of AprM were among the top expressed proteins under anoxia (Data Set S1, column “mean %cOrgNSAF,” and Text S1). Raman microspectroscopy revealed that levels of elemental stored sulfur (S^0) were highest under AS and H conditions and low or below detection limit under Ox conditions and A conditions at the end of the incubations (Fig. S1B and Text S1).

Collectively, sulfur oxidation genes were upregulated under both anoxic conditions (A and AS) irrespective of sulfur storage content and, conversely, were downregulated under hypoxic conditions even though elemental sulfur was detected in most of these symbiont cells.

Upregulation of anaerobic respiratory enzymes under AS conditions. Given that sulfur oxidation was upregulated under AS conditions, we expected this process to be coupled to the reduction of anaerobic electron acceptors, and nitrate respiration has been shown for symbiotic *L. oneistus* (15). Consistently, genes encoding components of the four specific enzyme complexes active in denitrification (*nap*, *nir*, *nor*, *nos*), as well as two subunits of the respiratory chain complex III (*petA* and *petB* of the cytochrome bc_1 complex, which is known for being involved in denitrification and in the aerobic respiratory chain [35]) were upregulated under AS conditions (Fig. 4A, Fig. S1A, and Data Set S1).

Besides nitrate respiration, “*Ca. T. oneisti*” may also utilize polysulfide or thiosulfate as a terminal electron acceptor under AS conditions, since we observed an upregulation of all genes encoding either a respiratory polysulfide reductase or a thiosulfate reductase (*psrA/psrA*, *psrB/psrB*, *prcC/psrC*; dimethyl sulfoxide [DMSO] reductase family, classification based on reference 36). Concerning other anaerobic electron acceptors, the symbiont has the genetic potential to carry out fumarate reduction (*frdABCD* genes; Fig. 2 and Data Set S1), and the fumarate reductase flavoprotein subunit (*frdA*) was indeed upregulated under AS conditions (Data Set S1). We also identified a gene potentially responsible for the biosynthesis of rhodoquinone (*rquA*; Fig. 2 and Data Set S1), which acts as an electron carrier in anaerobic respiration in a few other prokaryotic and eukaryotic organisms (37, 38) and could thus replace the missing menaquinone during anaerobic respiration in “*Ca. T. oneisti*.”

Intriguingly, lipid profiles of the symbiont revealed a change in lipid composition, as well as significantly higher relative abundances of several lysophospholipids under anoxia (Fig. S2A and Text S1), possibly resulting in altered uptake behavior and higher membrane permeability for electron donors and acceptors (39–42). Notably, we also detected lysophosphatidylcholine to be significantly more abundant in anoxia (Fig. S2B). As the symbiont does not possess any known genes for biosynthesis of this lipid, it may be host derived. Incorporation of host lipids into symbiont membranes was indeed reported previously (43, 44).

Furthermore, upregulation of the respiratory enzyme glycerol 3-phosphate (G3P) dehydrogenase gene (*glpD*; Data Set S1), as well as the substrate-binding subunit of a putative G3P transporter gene (*ugpABCD* genes; Data Set S1), suggests that host lipid-derived G3P may serve as carbon and energy source for the symbiont under anoxia.

Taken together, our data indicate that under AS conditions, the ectosymbiont gains energy by coupling sulfur oxidation to the complete reduction of nitrate to dinitrogen gas. Moreover, the symbiont appears to exploit oxygen-depleted environments for energy generation by utilizing G3P as an additional electron donor and nitrate, polysulfide or thiosulfate, and fumarate as electron acceptors.

Upregulation of sulfur oxidation genes is not accompanied by increased expression of carbon fixation genes. Several thioautotrophic symbionts have been shown to use the energy generated by sulfur oxidation for the fixation of inorganic carbon (7, 19, 20, 45–47). Previous studies strongly support that “*Ca. T. oneisti*” is capable of fixing carbon via an energy-efficient Calvin-Benson-Bassham (CBB) cycle (6, 11, 12, 30, 48) (Fig. 2). In this study, bulk isotope ratio mass spectrometry (IRMS) conducted

with symbiotic nematodes confirmed that they incorporate isotopically labeled inorganic carbon, and we detected no significant difference in incorporation between any two incubations in the course of 24 h (Fig. 4B). To localize the sites of carbon incorporation, we subjected symbiotic nematodes incubated with [^{13}C]bicarbonate to nano-scale secondary ion mass spectrometry (NanoSIMS) and detected ^{13}C enrichment predominantly within the ectosymbiont (Fig. S3 and Text S1).

Consistent with the evidence for carbon fixation by the ectosymbiont, all genes related to the CBB cycle were detected, on both the transcriptome and the proteome level, with high transcript levels under both AS and O conditions (Fig. 3 and Data Set S1). However, the upregulation of sulfur oxidation genes observed under AS did not coincide with an upregulation of carbon fixation genes. On the contrary, the median expression level of all CBB cycle genes was significantly higher in the presence of oxygen (Fig. 3). In particular, the transcripts encoding the small subunit of the key autotrophic carbon fixation enzyme ribulose-1,5-bisphosphate carboxylase/oxygenase (RuBisCO) (*cbbS*) together with the transcripts encoding its activases (*cbbQ* and *cbbO*) (49), the PP_i -dependent 6-phosphofructokinase (PP_i -PFK) (50, 51), and the neighboring PP_i -energized proton pump (*hppA*) thought to be involved in energy conservation during autotrophic carbon fixation (50, 51) were upregulated under O conditions (Fig. 4A). The large subunit of the RuBisCO protein (CbbL; type I-A group according to Fig. S4) was among the top expressed proteins irrespective of the presence of oxygen (Data Set S1, column "mean %cOrgNSAF").

In conclusion, (i) upregulation of carbon fixation genes occurred in the presence of oxygen when sulfur oxidation genes were downregulated, while (ii) incorporation of inorganic carbon was detected to a similar extent in the presence and absence of oxygen.

Genes involved in the utilization of organic carbon and polyhydroxyalkanoate (PHA) storage buildup are upregulated in the presence of oxygen. As anticipated, the nematode ectosymbiont may exploit additional reduced compounds besides sulfide for energy generation. Indeed, "*Ca. T. oneisti*" possesses the genomic potential to assimilate glyoxylate, acetate, and propionate via the partial 3-hydroxypropionate cycle (like the closely related *Olavius algarvensis* γ 1-symbiont [50]) and furthermore contains genes for utilizing additional small organic carbon compounds such as G3P, glycolate, ethanol, and lactate (Fig. 2 and Data Set S1). With the exception of G3P utilization genes (see above), the expression of genes involved in the assimilation of organic carbon including their putative transporters was significantly higher under O conditions (Fig. 3). Among the upregulated genes were *lutB* (involved in the oxidation of lactate to pyruvate [52]), propionyl coenzyme A (CoA) synthetase (*prpE*, propionate assimilation [53]), and two components of a TRAP transporter which commonly transports carboxylates (54) (Data Set S1).

These gene expression data imply that the nematode ectosymbiont uses organic carbon compounds in addition to CO_2 under O conditions, thereby increasing the supply of carbon. Consistent with high carbon availability, genes necessary to synthesize storage compounds such as polyhydroxyalkanoates (PHAs), glycogen, and trehalose showed an overall higher median transcript level under O conditions (Fig. 3). In particular, two key genes involved in the biosynthesis of the PHA compound polyhydroxybutyrate (PHB)—acetyl-CoA acetyltransferase (*phaA*) and a class III PHA synthase subunit (*phaC-2*)—were upregulated in the presence of oxygen. Conversely, we observed upregulation of both PHB depolymerases involved in PHB degradation under AS, and Raman microspectroscopy showed that the median PHA content was slightly lower in symbiont cells under AS than under both oxic conditions after the incubation period (Fig. S5).

We propose that in the presence of oxygen, enhanced mixotrophy (i.e., simultaneous assimilation of inorganic and organic carbon) would result in higher carbon availability reflected by PHA storage buildup and facilitating facultative chemolithoautotrophic synthesis of ATP via the aerobic respiratory chain.

Upregulation of nitrogen assimilation in the presence of oxygen. It has been shown that high carbon availability is accompanied by high nitrogen assimilation (55–57). Indeed, despite the sensitivity of nitrogenase toward oxygen (58), its key catalytic MoFe

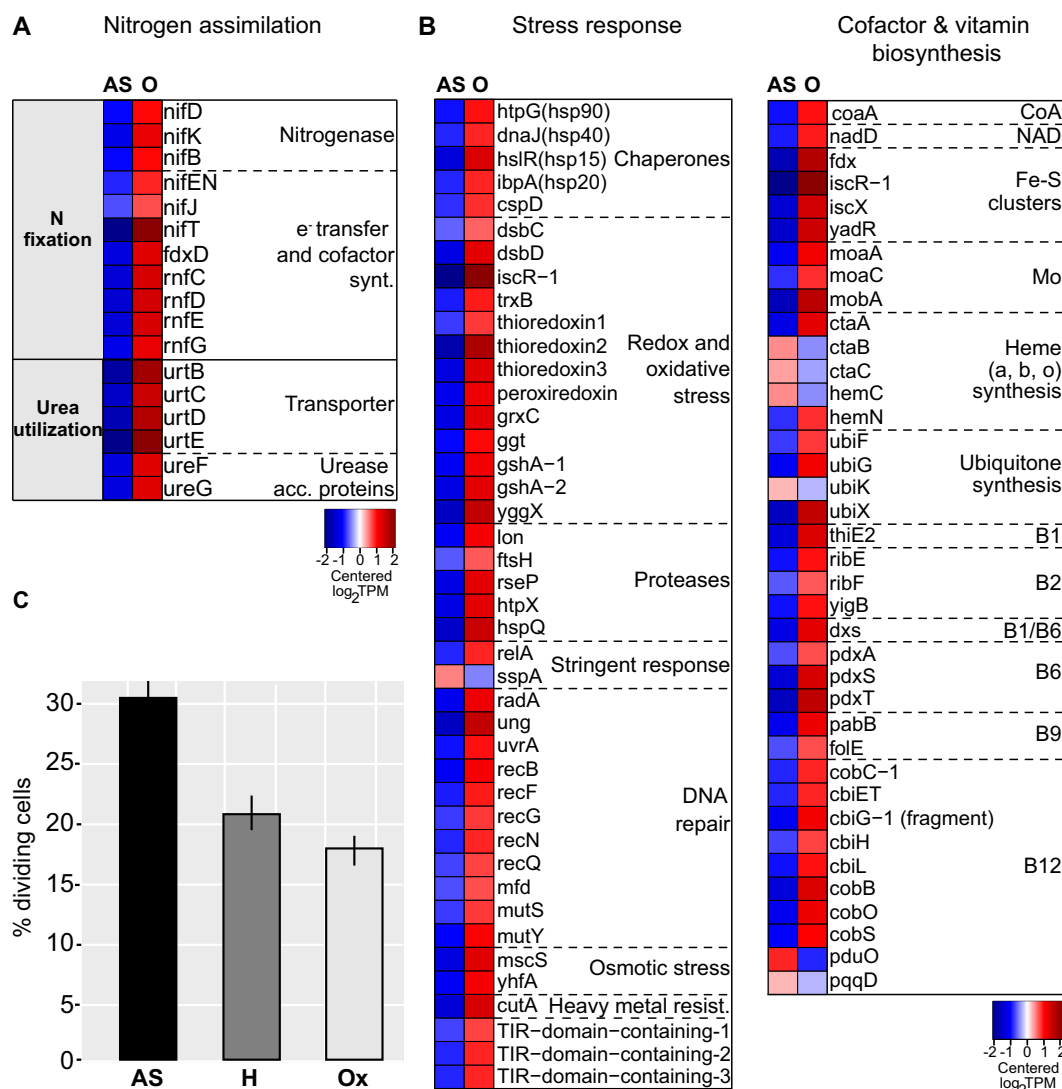


FIG 5 Nitrogen fixation and urea utilization genes as well as stress response and vitamin biosynthesis genes are upregulated, and fewer symbiont cells divide in the presence of oxygen. (A) Heatmap showing transcript levels of differentially expressed genes involved in nitrogen assimilation. Cofactor synt., cofactor biosynthesis; Urease acc. proteins, urease accessory proteins. (B) Heatmaps displaying transcript levels of differentially expressed genes involved in stress response as well as in the biosynthesis of vitamins and cofactors. Heavy metal resist., heavy metal resistance. Both panel A and panel B show genes that were differentially expressed between anoxic sulfidic (AS) and oxygenated (O) conditions after 24 h of incubation (2-fold change, FDR ≤ 0.05). Expression levels are visualized by displaying mean-centered \log_2 TPMs (transcripts per kilobase million). Upregulation is indicated in red, and downregulation is in blue. Genes are ordered by function in the respective metabolic pathways. (C) Bars show the percentage of dividing “*Ca. T. oneisti*” cells upon 24-h incubations under anoxic sulfidic (AS), hypoxic (H), and oxalic (Ox) conditions. A total of 658, 1,009, and 1,923 cells was counted for the AS, H, and Ox condition, respectively. Error bars indicate 95% confidence intervals of the proportions. A chi-square hypothesis test of independence determined that the observed differences between all proportions were highly likely dependent on the incubation condition ($P < 0.00001$).

enzymes (*nifD*, *nifK*) (59) and several other genes involved in nitrogen fixation were drastically upregulated in the presence of oxygen (Fig. 3 and 5A). Moreover, in accordance with a recent study showing the importance of sulfur assimilation for nitrogen fixation (60), genes involved in the assimilation of sulfate, i.e., the sulfate transporters *sulP* and *cysZ*, as well as genes encoding two enzymes responsible for cysteine biosynthesis (*cysM*, *cysE*) were also upregulated in the presence of oxygen (Data Set S1).

Besides nitrogen fixation, genes involved in urea uptake (transporters, *urtCBDE*) and utilization (urease, *ureF* and *ureG*) were also transcribed significantly more highly under O conditions (Fig. 3 and 5A).

In conclusion, genes involved in nitrogen assimilation (from N_2 or urea) were consistently upregulated in the presence of oxygen, when (i) carbon assimilation was likely higher and when (ii) higher demand for nitrogen is expected due to stress-induced synthesis of vitamins (see section below).

Upregulation of biosynthesis of cofactors and vitamins and global stress response in the presence of oxygen. Multiple transcripts and proteins associated with diverse bacterial stress responses were among the most highly expressed in the presence of oxygen (Fig. 3 and Data Set S1). More specifically, heat shock proteins Hsp70 and Hsp90 were highly abundant (Data Set S1, column “mean %cOrgNSAF”), and transcripts of heat shock proteins (Hsp15, Hsp20, Hsp40, and Hsp90) were upregulated (Fig. 5B). Besides chaperones, we also detected upregulation of a transcription factor which induces synthesis of Fe-S clusters under oxidative stress (*iscR*) (61) along with several other genes involved in Fe-S cluster formation (Fig. 5B) (62) and regulators for redox homeostasis, like thioredoxins, glutaredoxins, and peroxiredoxins (63). Furthermore, we observed upregulation of protease genes (*lon*, *ftsH*, *rseP*, *hspX*, *hspQ*) (64–68), genes required for repair of double-strand DNA breaks (such as *radA*, *recB*, *mutSY*, and *mfd*) (69–71), and *relA*, known to initiate the stringent response when cells are starved for amino acids (72) (Fig. 5B). Amino acid starvation could be caused by a high demand for stress-related proteins under O conditions and could also explain the upregulation of amino acid biosynthesis pathways under O conditions (73) (Fig. 3).

SspA, shown to be important for survival under various stress conditions (74–76), was the only stress-related gene upregulated under AS (Fig. 5B).

We hypothesized that the drastic upregulation of stress-related genes observed under O conditions would require an increase in the biosynthesis of vitamins (77–79). Indeed, genes involved in biosynthesis of vitamins such as vitamins B_2 , B_6 , B_9 , and B_{12} were upregulated in the presence of oxygen (Fig. 3 and 5B). Notably, the proposed upregulation of nitrogen fixation and urea utilization (see above section) would support the synthesis of these nitrogen-rich molecules.

The upregulation of stress-related genes under O conditions was accompanied by significantly fewer dividing symbiont cells, i.e., 18.1% and 21.4% (under H and Ox conditions, respectively) versus 30.1% (under AS conditions) (Fig. 5C), and downregulation of both early (*ftsE*, *ftsX*) and late (*damX*, *ftsN*) cell division genes (80) (Fig. 3 and Data Set S1). Oxygen may therefore elicit a stress response that hampers symbiont proliferation.

DISCUSSION

This is the first study reporting on the global transcriptional response to oxygen of a thiotrophic animal ectosymbiont, “*Ca. T. oneisti*.” Here, we detected a strong transcriptional response of “*Ca. T. oneisti*” key metabolic processes to oxygen, as well as shifts in protein abundance and lipid composition. Although ongoing comparative host transcriptomics suggests that also the nematode host responds to oxygen (L. König and G. F. Paredes, unpublished data), and although the host response likely affects that of “*Ca. T. oneisti*,” this study exclusively focused on the effect of oxygen on symbiont physiology.

Experimental design. The concentrations of oxygen and sulfide to which symbiotic nematodes were exposed in our study were chosen based on the distribution of *L. oneistus* and measured sulfide concentrations in their natural environment, that is, shallow-water marine sediment containing up to 25 μ M sulfide (Fig. 1A), with oxidized layers rapidly transitioning to reduced, anoxic sediments (10). Given that in low-sulfide sediments, oxygen and sulfide rarely cooccur (81, 82), nematodes were not supplemented with sulfide when incubated in the presence of oxygen. Moreover, we omitted pre-experimental acclimation to study the symbiont in its close-to-natural state, i.e., replete with intracellular sulfur stores as indicated by the nematode whiteness (15, 31). Indeed, the similar gene expression observed between AS and A, and between H and O, conditions is consistent with the assumption that during the incubations, “*Ca. T. oneisti*” relied on stored sulfur, and its metabolism responded to the presence or absence of oxygen,

irrespective of sulfide supplementation (Fig. 1D and Fig. 4A and see Fig. S1 in the supplemental material).

Although at the beginning of all the incubations “*Ca. T. oneisti*” was likely not depleted of stored sulfur, after 24 h of incubation, the lack of sulfide supplementation resulted in depleted sulfur stores under both the A and Ox conditions. Curiously, sulfur stores were higher following H than following Ox incubations (Fig. S1B). This cannot be explained by transcriptomics, as only a single gene involved in sulfur oxidation (a putative sulfur globule gene, *spgD* [Data Set S1]) was differentially expressed between H and Ox conditions.

Ideally, all the worms should have been subjected to the four different conditions at the same time. Although we did randomly split the worms into replicates, we were able to test a maximum of two conditions (150 nematodes per condition) per day, due to the time needed to manually extract each single nematode from the sand (see Materials and Methods). In spite of this technical limitation, replicates from the same treatment on different dates (e.g., three Ox replicates in July 2017 and three Ox replicates in March 2019) clustered with each other in their gene expression profiles (Fig. 1C).

Another potential source of variability under the conditions experienced by different nematode batches could be the fact that the A and AS conditions were tested in closed vials whereas the H and Ox ones were tested in open vials. Although in this study we measured only oxygen, sulfide, and nitrate, and we cannot, therefore, rule out whether the concentrations of other substrates differed between closed and open vials, the fact that transcriptomes of symbionts incubated in H (on the bench) and Ox (in an aquarium) samples clustered together suggests that differences in unmeasured substrates were negligible (Fig. 1C).

Overall, distinct (treatment-specific) and coherent transcriptional profiles irrespective of sampling date and experimental setup (Fig. 1C) suggest that oxygen is the main factor affecting the symbiont transcriptomes.

Anaerobic sulfur oxidation. Genes involved in sulfur oxidation showed high overall expression compared to other central metabolic processes, indicating that thiotrophy is the predominant energy-generating process for “*Ca. T. oneisti*” under both Ox and anoxic conditions (Fig. 6). Thus, our data strongly support previous observations of Stilbonematinae ectosymbionts performing aerobic and anaerobic sulfur oxidation (11, 15). As the majority of genes involved in denitrification were upregulated under AS conditions (Fig. 4A), nitrate likely serves as terminal electron acceptor for anaerobic sulfur oxidation. Importantly, we detected nitrate in the incubation medium, as well as in all sediment layers (Table S1), at concentrations typical of oligotrophic sediment, in which also the *O. algarvensis* γ -symbiont is predicted to couple sulfur oxidation to denitrification (50).

Sulfur oxidation in chemosynthetic symbioses is commonly described as an aerobic process required for host survival (3). However, many of these symbiotic organisms likely experience periods of oxygen depletion as would be expected from life at the interface of oxidized and reduced marine environments. Together with previous reports demonstrating nitrate reduction (13, 14, 16) and studies showing the genomic potential for using nitrate as terminal electron acceptor (6, 50, 83–85), this study substantiates that nitrate respiration during temporary anoxia could represent an important strategy for energy conservation among thiotrophic symbionts.

While upregulation of sulfur oxidation and denitrification genes in anoxia represents no proof for preferential anaerobic sulfur oxidation, we hypothesize that oxidation of reduced sulfur compounds to sulfate is more pronounced when oxygen is absent. Among the upregulated sulfur oxidation genes, we identified *aprM* and the *qmoABC* complex, both of which are thought to act as electron-accepting units for APS reductase and therefore rarely cooccur in thiotrophic bacteria (33). The presence and expression of the QmoABC complex could provide a substantial energetic advantage to the ectosymbiont by mediating electron bifurcation (33), in which the additional

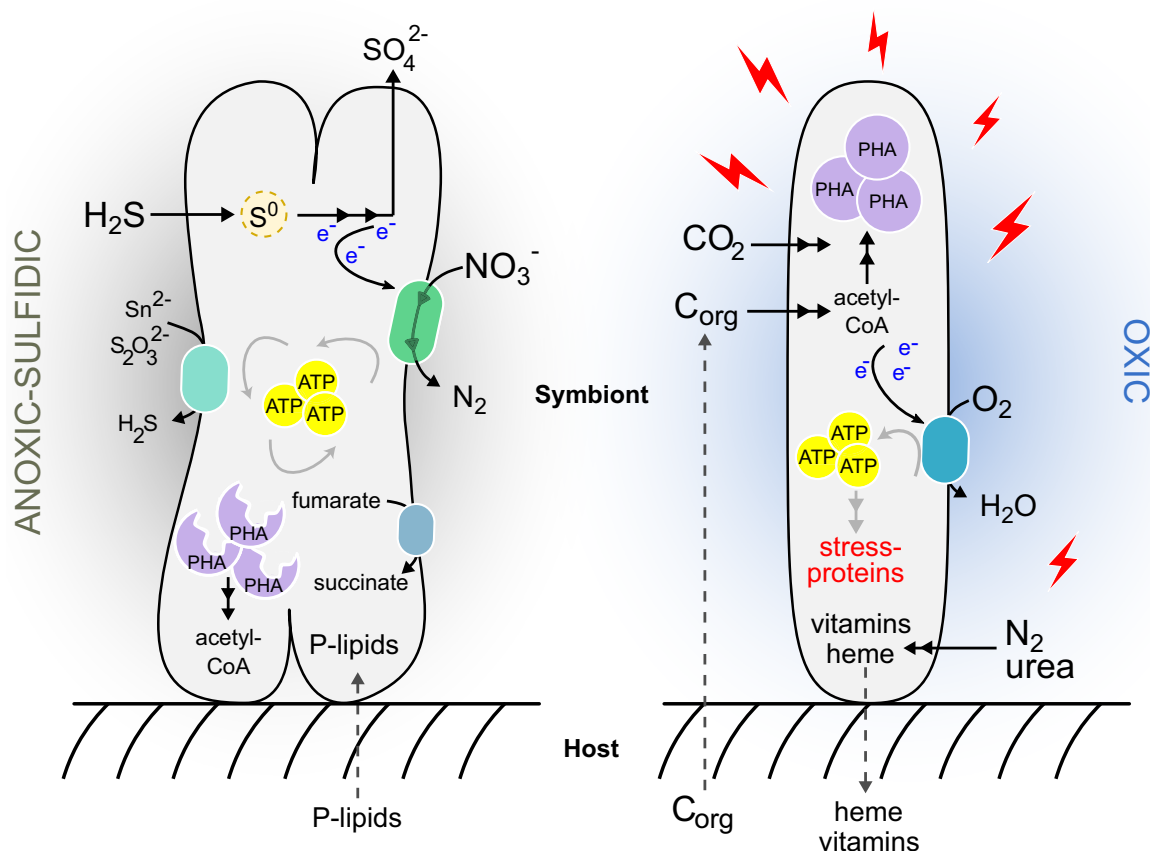


FIG 6 Schematic representation of the metabolism of “*Ca. T. oneisti*” in deep anoxic and upper oxygenated sand. Our study suggests that in anoxic sulfidic sediment zones (left), the ectosymbiont performs enhanced anaerobic sulfur oxidation coupled to nitrate reduction to nitrogen gas (denitrification). Additional electron acceptors such as fumarate, polysulfide (Sn^{2-}), or thiosulfate ($\text{S}_2\text{O}_3^{2-}$) may also be reduced. The storage compound PHA may serve as a carbon source (in addition to CO_2) and an additional electron donor. Host-derived phospholipids (P-lipids) may be incorporated into the ectosymbiont’s membrane to increase permeability. In superficial, oxygenated zones (right), oxygen triggers a global stress response that may not only consume energy and dampen proliferation but may also require vitamin biosynthesis, thereby increasing the demand for nitrogen. Small organic carbon compounds (C_{org}) putatively excreted by the host and incorporated by the ectosymbiont may contribute to energy generation (and carbon) via aerobic respiration, by the conversion of acetyl-CoA via the TCA cycle (not depicted in the figure). Together with autotrophic CO_2 fixation, C_{org} may increase carbon availability, which would enable “*Ca. T. oneisti*” to synthesize PHA. Heme and other essential nutrients may be directly or indirectly transferred to the nematode host. Only processes predicted to dominate under one condition over the other are depicted in this model, although they likely occur under both conditions.

reduction of a low-potential electron acceptor (e.g., ferredoxin, NAD^+) could result in optimized energy conservation under anoxic conditions. The maximization of sulfur oxidation under anoxia might even represent a temporary advantage for the host. Indeed, this would be shielded from sulfide poisoning while crawling in a sediment which is free of predators but rich in decomposed organic matter (detritus) (15, 86–88). Due to the dispensability of oxygen for sulfur oxidation, the ectosymbiont may not need to be shuttled to superficial sand by its nematode hosts to oxidize sulfur. Host migration into upper zones of the sediment may therefore primarily reflect the oxygen dependence of the animal host.

In addition to anaerobic sulfur oxidation, the nematode ectosymbiont’s phylogenetic affiliation with facultative anaerobic, anoxygenic phototrophic sulfur oxidizers such as *Allochromatium vinosum* (6, 32) and the presence and expression of yet other anaerobic respiratory complexes (DMSO reductase family enzyme and fumarate reductase) collectively suggest that “*Ca. T. oneisti*” might be well adapted to anoxic sulfidic sediment zones.

Symbiont proliferation in anoxia. Although a few studies shed light on the molecular cell biology of “*Ca. T. oneisti*” reproduction (26, 28, 89), up to this study, we did

not know how this is influenced by environmental changes. Here, we observed significantly higher numbers of dividing cells under AS conditions (Fig. 5C), and therefore, sulfur oxidation coupled to denitrification might represent the ectosymbiont's preferred strategy to generate energy for growth. We hypothesize that aside from sulfur oxidation, the mobilization of PHA could represent an additional source of ATP (and carbon) supporting symbiont proliferation under AS (Fig. S5 and Fig. 6). Of note, PHA mobilization in anoxia was also shown for *Beggiatoa* spp. (90). On the other hand, several lines of research have shown that stress—experienced by “*Ca. T. oneisti*” in the presence of oxygen (Fig. 5B)—can inhibit bacterial growth (91–97). Importantly, increased proliferation of a thiotroph which uses an anaerobic electron acceptor (such as nitrate) instead of oxygen has not been reported yet (98–101).

Loose coupling of sulfur oxidation and carbon fixation. Reduced sulfur compounds stimulate carbon fixation in thioautotrophic symbionts (7, 11, 19, 20, 45–47, 102, 103). Our bulk isotope ratio mass spectrometry (EA-IRMS) analysis indicates that, even though expression of the sulfur oxidation pathway was stimulated, fixation of [^{13}C]bicarbonate-derived carbon was not the highest under AS conditions (Fig. 3 and 4). Instead, carbon fixation appeared unaffected by oxygen.

Even though, based on EA-IRMS, oxygen did not affect carbon fixation, CBB cycle transcripts in general, and RuBisCO-associated transcripts in particular, were significantly more abundant when oxygen was present (Fig. 3 and 4). Upregulation of these genes could be a mechanism to counteract an increased oxygenase activity of RuBisCO in the presence of oxygen, as competition between its two substrates (CO_2 and O_2) has been reported to constrain the carbon fixation efficiency of the enzyme (104, 105). Phylogenetic analysis of the ectosymbiont RuBisCO large subunit protein (CbbL) placed it within the type I-A group (Fig. S4), whose characterized representatives are adapted to oxic environments (105, 106). The discrepancy between carbon incorporation and transcriptome data could thus reflect a tradeoff between the carboxylase and oxygenase activity of RuBisCO. Of note, fixation of CO_2 by other carboxylating enzymes may not significantly contribute to inorganic carbon incorporation. Indeed, acetyl-CoA carboxylase (*acc* genes) is predicted to act only as a biosynthetic carboxylase, whereas the constitutively expressed propionyl-CoA carboxylase (*pccB*) takes part in the partial 3-hydroxypropionate cycle thought to mainly function in assimilation of organic substrates in some thiotrophic symbionts (48, 50, 107). No other known carboxylases are found in the symbiont genome.

Altogether, both lines of evidence point toward a loose coupling between sulfur oxidation and autotrophic carbon fixation. Notably, sulfide oxidation without matching CO_2 fixation has been described before for the symbiont of *Riftia pachyptila* (108, 109), and an example of extreme decoupling of sulfur oxidation and carbon fixation was recently reported for *Kentrophoros* ectosymbionts. Strikingly, these lack genes for autotrophic carbon fixation altogether and thus represent the first heterotrophic sulfur-oxidizing symbionts (48).

Oxic mixotrophy. Several chemosynthetic symbionts may engage in mixotrophy (6, 20, 50, 51, 110), and also the nematode ectosymbiont possesses genes for transport of small organic carbon compounds, their assimilation, and further metabolism (tricarboxylic acid [TCA] cycle, glyoxylate shunt). Some of the organic carbon compounds represent typical host waste products (acetate, lactate, propionate) and could therefore be host-derived (50).

The expression of genes involved in transport and assimilation pathways was significantly more pronounced under O than under AS conditions (Fig. 3). In addition to assimilating inorganic carbon autotrophically, the ectosymbiont may thus assimilate more organic carbon in the presence of oxygen and, consequently, may experience higher carbon availability (Fig. 6).

While repression of RuBisCO biosynthesis by organic carbon has been demonstrated (111, 112), simultaneous incorporation of organic and inorganic carbon has been described for several facultative autotrophic bacteria (113–119). Concomitant mixotrophy is thought to be an advantage in oligotrophic environments where nutrients are limiting (116, 120), and

CO₂ derived from the breakdown of organic carbon through decarboxylation can subsequently be reutilized via the CBB cycle (117).

The metabolism of these organic carbon compounds ultimately yields acetyl-CoA, which, in turn, can be further oxidized in the TCA cycle and/or utilized for fatty acid and PHA biosynthesis (Fig. 2 and 6). Our transcriptome and Raman microspectroscopy data suggest that “*Ca. T. oneisti*” favors PHA buildup over its degradation under O conditions (Fig. S5). Higher carbon availability in the presence of oxygen resulting in a surplus of acetyl-CoA may cause a nutrient imbalance that could facilitate PHA accumulation as previously shown (121–123). Moreover, it might play a role in resilience against cellular stress, as there is increasing evidence that PHA biosynthesis is enhanced under unfavorable growth conditions such as extreme temperatures, UV radiation, osmotic shock, and oxidative stress (124–132). Similar findings have been obtained for pathogenic (133) and symbiotic (134) bacteria of the genus *Burkholderia*, with the latter study reporting upregulation of stress response genes and PHA biosynthesis in the presence of oxygen. Finally, oxic biosynthesis of PHA might also prevent excessive accumulation and breakdown of sugars by glycolysis and oxidative phosphorylation, which, in turn, would exacerbate oxidative stress (135).

Oxic nitrogen assimilation. Despite the oxygen-sensitive nature of nitrogenase (58), we observed a drastic upregulation of nitrogen fixation genes under O conditions (Fig. 3 and 5A). Besides ammonia production, nitrogen fixation can act as an electron sink under heterotrophic conditions (136, 137). The ectosymbiont may therefore use the nitrogenase to maintain redox balance in the cell when organic carbon is metabolized under oxic conditions.

Urea utilization and uptake genes were also upregulated. Although the nematode host likely lacks the urea biosynthetic pathway (L. König, unpublished data), this compound is one of the most abundant organic nitrogen substrates in marine ecosystems, as well as in animal-inhabited (oxygenated) sand (138, 139). The apparent increase in nitrogen assimilation in the presence of oxygen could thus be a result of an increased demand for nitrogen driven by the biosynthesis of nitrogen-rich compounds such as vitamins and cofactors potentially required to survive oxidative stress (Fig. 3, 5, and 6). Indeed, the upregulation of the urea uptake system and urease accessory proteins, as well as the aforementioned stress-related *relA* gene, has been shown to be a response to nitrogen limitation in other systems (140, 141); nitrogen imbalance may have also induced PHA accumulation under oxic conditions (121–123). The role of vitamins in protecting cells against the deleterious effects of oxygen has been shown for animals (142, 143), and the importance of riboflavin for bacterial survival under oxidative stress has previously been reported (77, 79). Along this line of thought, oxygen-exposed “*Ca. T. oneisti*” upregulated glutathione and thioredoxin, which are known to play a pivotal role in scavenging reactive oxygen species (ROS) (144). Their function directly (or indirectly) requires vitamin B₂, B₆, and B₁₂ as cofactors. More specifically, thioredoxin reductase (*trxB*) requires riboflavin (vitamin B₂) in the form of flavin adenine dinucleotide (FAD) (145); cysteine synthase (*cysM*) and glutamate synthases (two-subunit *gltB/gltD*, one-subunit *gltS*) involved in the biosynthesis of the glutathione precursors L-cysteine and L-glutamate depend on vitamin B₆, FAD, and riboflavin in the form of flavin mononucleotide (FMN) (146, 147). As for cobalamin, it was thought that this vitamin played only an indirect role in oxidative stress resistance (148), by being a precursor of S-adenosylmethionine (SAM), a substrate involved in the synthesis of glutathione via the methionine metabolism (and the transsulfuration pathway), and in preventing the Fenton reaction (149, 150). However, its direct involvement in the protection of chemolithoautotrophic bacteria against oxidative stress has also been illustrated (78).

In summary, in the presence of oxygen, the upregulation of genes involved in biosynthesis of vitamins B₂, B₆, and B₁₂ along with antioxidant systems and their key precursor genes *cysM* and B₁₂-dependent-methionine synthase *metH* suggests that the ectosymbiont requires increased levels of these vitamins to cope with oxidative stress (Fig. 6).

Evolutionary considerations. Anaerobic sulfur oxidation, increased symbiont proliferation, and downregulation of stress-related genes lead us to hypothesize that “*Ca. T. oneisti*”

evolved from a free-living bacterium that mostly, if not exclusively, inhabited anoxic sand zones. In support of this, the closest relatives of the nematode ectosymbionts are free-living sulfur oxidizers thriving under anoxic conditions (i.e., *Allochromatium vinosum*, *Thioflavicoccus mobilis*, and *Marichromatium purpuratum*) (6, 151). Eventually, advantages such as protection from predators or utilization of host waste products (e.g., fermentation products, ammonia) may have been driving forces that led to the “Ca. Thiosymbion”-Stilbonematinae symbioses. As the association became more and more stable, the symbiont optimized (or acquired) mechanisms to resist oxidative stress, as well as metabolic pathways to most efficiently exploit the metabolic potential of oxygenated sand zones (mixotrophy, nitrogen assimilation, and vitamin and cofactor biosynthesis). From the *L. oneistus* nematode perspective, the acquired “symbiotic skin” enabled it to tolerate the otherwise poisonous sulfide and to inhabit sands virtually devoid of predators but rich in decomposed organic matter.

MATERIALS AND METHODS

Sample collection. *Laxus oneistus* individuals were collected on multiple field trips (2017 to 2019) at approximately 1-m depth from a sandbar off the Smithsonian Field Station, Carrie Bow Cay, in Belize (16°48′11.01″N, 88°4′54.42″W). All the nematodes were extracted at the same location by gently stirring the sand and pouring the supernatant seawater through a 212- μ m mesh sieve. The retained meiofauna was collected in a petri dish, and single worms of similar size (10 mm length, representing adult *L. oneistus*) were handpicked by using forceps (Dumont 3; Fine Science Tools, Canada) under a dissecting microscope. *L. oneistus* nematodes were identified based on morphological characteristics (152). Notably, all collected *L. oneistus* nematodes had a white appearance. Upon extraction from the sand, which required approximately 1 h per batch (50 nematodes) and 4 h for the up to 4 batches necessary to test one experimental condition (200 nematodes), the nematodes were subjected to various incubation conditions as described below.

The spatial distribution of *L. oneistus* as well as concentrations of sulfide ($\sum H_2S$, i.e., the sum of H_2S , HS^- , and S^{2-}), dissolved inorganic nitrogen (DIN; nitrate, nitrite, and ammonia), and dissolved organic carbon (DOC) was determined in sediment cores at various depths (Fig. 1A; see also Table S1 and Text S1 in the supplemental material).

Incubations for RNA sequencing (RNA-Seq). Batches of 50 *L. oneistus* individuals were collected and incubated in triplicates or more under different oxygen concentrations during two field trips (Fig. 1B and C). Namely, they were incubated for 24 h in the dark, in either the presence or absence of oxygen, in 13-ml exetainers (Labco, Lampeter, Wales, UK) fully filled with 0.2- μ m filtered seawater collected from seawater overlying the sandbar inhabited by the nematodes. The oxic incubations consisted of two separate experiments of low (hypoxic; three replicates in July 2017) and high (oxic; three replicates in July 2017, three replicates in March 2019) oxygen concentrations. Here, all exetainers were kept open, but only the samples with high oxygen concentrations were submerged in an aquarium constantly bubbled with air (Air Pump Plus; Sera, Heinsberg, Germany). Oxic incubations started with around 195 μ M O_2 and reached an average of 188 μ M after 24 h. Hypoxic incubations started with around 115 μ M O_2 but reached less than 60 μ M O_2 after 24 h. This likely occurred due to nematode oxygen consumption. The anoxic treatments comprised incubations to which either 11 μ M sodium sulfide ($Na_2S \cdot 9H_2O$; Sigma-Aldrich, St. Louis, MO, USA) was added (anoxic-sulfidic; three replicates in July 2017) or no sulfide was supplied (anoxic; three replicates in July 2017, two replicates in March 2019), and $\sum H_2S$ concentrations were checked at the beginning and at the end (24 h) of each incubation by spectrophotometric determination following the protocol of Cline (Text S1). Anoxic incubations were achieved with the aid of a polyethylene glove bag (AtmosBag; Sigma-Aldrich) that was flushed with N_2 gas (Fabrigas, Belize City, Belize), together with incubation media and all vials, for at least 1 h before closing. Dissolved oxygen inside the bag was monitored throughout the 24 h of each incubation using a PreSens Fibox 3 trace fiber-optic oxygen meter and noninvasive trace oxygen sensor spots attached to the exetainers (PSt6 and PSt3; PreSens, Regensburg, Germany). For exact measurements of $\sum H_2S$ and oxygen, see Table S2A. The seawater used for all incubations had an initial concentration of nitrate and nitrite of 4.2 μ M and 0.31 μ M, respectively (Text S1). Temperature and salinity remained constant throughout all incubations, measuring 27 to 28°C and 33 to 34‰, respectively. All worms were moving after the 24-h incubations, indicating that they were alive. Each set of 50 worms was quickly transferred into 2 ml RNA storage solution (13.3 mM EDTA disodium dihydrate [pH 8.0], 16.6 mM sodium citrate dihydrate, 3.5 M ammonium sulfate [pH 5.2]), kept at 4°C overnight, and finally stored in liquid nitrogen until RNA extraction.

RNA extraction, library preparation, and RNA-Seq. RNA from symbiotic *L. oneistus* was extracted using the NucleoSpin RNA XS kit (Macherey-Nagel, Düren, Germany). Briefly, batches of 50 worms in RNA storage solution were thawed and the worms were transferred into 90 μ l lysis buffer RA1 containing Tris (2-carboxyethyl) phosphine (TCEP) according to the manufacturer's instructions. The remaining RNA storage solution was centrifuged to collect any detached bacterial cells (10 min, 4°C, 16,100 $\times g$), and pellets were resuspended in 10 μ l lysis buffer RA1 (plus TCEP) and then added to the worms in lysis buffer. To further disrupt cells, suspensions were vortexed for 2 min followed by three cycles of freeze (−80°C) and thaw (37°C) and homogenization using a pellet pestle (Sigma-Aldrich) for 60 s with a 15-s break after 30 s. Any remaining biological material on the pestle tips was collected by rinsing the tip

with 100 μ l lysis buffer RA1 (plus TCEP). Lysates were applied to NucleoSpin filters, and samples were processed according to the manufacturer's instructions, including an on-filter DNA digest. RNA was eluted in 20 μ l RNase-free water. To remove any residual DNA, a second DNase treatment was performed using the Turbo DNA-free kit (Thermo Fisher Scientific, Waltham, MA, USA), RNA was then dissolved in 17 μ l RNase-free water, and the RNA quality was assessed using a Bioanalyzer (Agilent, Santa Clara, CA, USA). To check whether all DNA was digested, real-time quantitative PCR using the GoTaq qPCR master mix (Promega, Madison, WI, USA) was performed targeting a 158-bp stretch of the *sodB* gene using primers specific for the symbiont (*sodB*-F, GTGAAGGGTAAGGACGGTTC; *sodB*-R, AATCCCAAGTTGACGATCTCC; 10 μ M per primer). Different concentrations of genomic "*Ca. T. oneisti*" DNA were used as positive controls. The program was as follows: 1 \times 95°C for 2 min, 40 \times 95°C for 15 s and 60°C for 1 min, 1 \times 95°C for 15 s, and 55°C to 95°C for 20 min. Next, bacterial and eukaryotic rRNA was removed using the Ribo-Zero Gold rRNA removal kit (Epidemiology) (Illumina, San Diego, CA, USA) following the manufacturer's instructions, but volumes were adjusted for low input RNA (153). In short, 125 μ l magnetic beads solution, 32.5 μ l magnetic bead resuspension solution, 2 μ l Ribo-Zero reaction buffer, and 4 μ l Ribo-Zero removal solution were used per sample. RNA was cleaned up via ethanol precipitation and dissolved in 9 μ l RNase-free water, and rRNA removal was evaluated using the Bioanalyzer RNA Pico kit (Agilent, Santa Clara, CA, USA). Strand-specific, indexed cDNA libraries were prepared using the SMARTer stranded RNA-Seq kit (TaKaRa Bio USA, Mountain View, CA, USA). Library preparation was performed according to the instructions, with 8 μ l of RNA per sample as input, 3-min fragmentation time, two rounds of AMPure XP Beads (Beckman Coulter, Brea, CA, USA) cleanup before amplification, and 18 PCR cycles for library amplification. The quality of the libraries was assessed via the Bioanalyzer DNA high-sensitivity kit (Agilent). Libraries were sequenced on an Illumina HiSeq 2500 instrument (single-read, 100 nucleotides [nt]) at the next-generation sequencing facility of the Vienna BioCenter Core Facilities (VBCF; <https://www.viennabiocenter.org/facilities/>).

Genome sequencing, assembly, and functional annotation. The genome draft of "*Ca. T. oneisti*" was obtained by performing a hybrid assembly using reads from Oxford Nanopore Technologies (ONT) sequencing and Illumina sequencing. To extract DNA for ONT sequencing and dissociate the ectosymbionts from the host, approximately 800 *Laxus oneistus* individuals were incubated three times for 5 min each in TE buffer (10 mM Tris-HCl [pH 8.0], 1 mM disodium EDTA [pH 8.0]). Dissociated symbionts were collected by 10-min centrifugation at 7,000 \times g and subsequent removal of the supernatant. DNA was extracted from this pellet using the blood and tissue kit (Qiagen, Hilden, Germany) according to the manufacturer's instructions. The eluant was further purified using the DNA Clean & Concentrator-5 kit (Zymo Research, Irvine, CA, USA), and the DNA was eluted twice with 10 μ l nuclease-free water.

The library for ONT sequencing was prepared using the ONT rapid sequencing kit (SQK-RAD002) and sequenced on an R9.4 flow cell (FLO-MIN106) on a MinION for 48 h. Basecalling was performed locally with ONT's Metrichor Agent v1.4.2, and resulting fastq files were trimmed using Porechop v0.2.1 (<https://github.com/rwick/Porechop>). Illumina sequencing reads from a previous study (6) were made available by Harald Gruber-Vodicka (MPI Bremen). Raw reads were filtered: adapters were removed and trimmed using BBDuk (BBMap v37.22, <https://sourceforge.net/projects/bbmap/>), with a minimum length of 36 and a minimum Phred score of 2. To keep only reads derived from the symbiont, trimmed reads were mapped onto the available genome draft (NCBI accession FLUZ000000000.1) using BWA-mem v0.7.16a-r1181 (154). Reads that did not map were discarded. The hybrid assembly was performed using SPAdes v3.11 (155) with flags `-careful` and the ONT reads supplied as `-nanopore`. Contigs smaller than 200 bp and a coverage lower than 5 \times were filtered out with a custom Python script. The genome completeness was assessed using CheckM v1.0.18 (156) with the gammaproteobacterial marker gene set using the taxonomy workflow. The genome was estimated to be 96.63% complete and to contain 1.12% contamination and was 4.35 Mb in length on 401 contigs with a GC content of 58.7% and N_{50} value of 27,060 bp.

The genome of "*Ca. T. oneisti*" was annotated using the MicroScope platform (157), which predicted 5,169 protein-coding genes. To expand the functional annotation provided by MicroScope, predicted proteins were assigned to KEGG pathway maps using BlastKOALA and KEGG Mapper-Reconstruct Pathway (158) and gene ontology (GO) terms using Blast2GO v5 (159) and searched for Pfam domains using the hmmscan algorithm of HMMER 3.0 (160, 161). All functional annotations can be found in Data Set S1. Furthermore, all genes, proteins, and pathways mentioned in the paper were manually curated and can be searched by name in Data Set S1.

Gene expression analyses. Based on quality assessment of raw sequencing reads using FastQC v0.11.8 (162) and prinseq-lite v0.20.4 (163), reads were trimmed and filtered using Trimmomatic v0.39 (164) and prinseq-lite as follows: 18 nucleotides were removed from the 5' end (HEADCROP), Illumina adapters were removed (ILLUMINACLIP:TruSeq3-SE.fa:2:30:10), reads were trimmed when the average quality of a five-base sliding window dropped below a Phred score of 20 (SLIDINGWINDOW:5:20), 3' poly(A) tails were trimmed (`-trim_tail_right 1`), and only reads longer than 24 nucleotides were kept (MINLEN:25). Mapping and expression analysis were done as previously described (165). Briefly, reads were mapped to the "*Ca. T. oneisti*" genome draft using BWA-backtrack (154) with default settings, only uniquely mapped reads were kept using SAMtools (166), and the number of strand-specific reads per gene was counted using HTSeq in the union mode of counting overlaps (167). On average, 1.4×10^6 (4.4%) reads uniquely mapped to the "*Ca. T. oneisti*" genome. For detailed read and mapping statistics, see Table S3A.

Gene and differential expression analyses were conducted using the R software environment and the Bioconductor package edgeR v3.28.1 (168–170). Genes were considered expressed if at least two reads in at least two replicates of one of the four conditions could be assigned. Including all four conditions, we found 92.8% of all predicted symbiont protein-encoding genes to be expressed (4,797 genes out of 5,169, Data Set S1). Log₂TPM (transcripts per kilobase million) values were calculated by log-transforming TPMs to which library size-adjusted positive prior counts were added in order to avoid zero TPMs (edgeR function

addPriorCount, prior.count = 4). Log₂TPM values were used to assess sample similarities via multidimensional scaling based on Euclidean distances (R Stats package) (170) (Fig. 1C), and the average of replicate log₂TPM values per expressed gene and condition was used to estimate expression strength. Median gene expression of entire metabolic processes and pathways per condition was determined from average log₂TPMs. A Wilcoxon signed-rank test was applied to test for significantly different median gene expression between metabolic processes and pathways (R Stats package).

For differential expression analysis, raw data were normalized by the trimmed mean of M-values (TMM) normalization method (edgeR function calcNormFactors) (171), and gene-specific biological variation was estimated (edgeR function estimateDisp). Differential expression was determined using the quasiliikelihood F-test (edgeR functions glmQLFit and glmQLFTest) for pairwise comparisons (between all four conditions) and comparing both anoxic conditions individually against the average for both oxic conditions. Expression of genes was considered significantly different if their expression changed 2-fold between two treatments with a false-discovery rate (FDR) of ≤ 0.05 (172). Throughout the paper, all genes meeting these thresholds are either termed differentially expressed or up- or downregulated. However, most follow-up analyses were conducted considering only differentially expressed genes between the anoxic-sulfidic (AS) condition and the two oxygenated conditions combined (O [Results and Fig. 1C]). For the differential expression analyses between all four conditions, see Data Set S1. Heatmaps show mean-centered expression values to highlight gene expression change.

Bulk $\delta^{13}\text{C}$ isotopic analysis by Isoprime isotope ratio mass spectrometry (EA-IRMS). To analyze the assimilation of carbon dioxide (CO_2) by the symbionts in the presence or absence of oxygen, batches of 50 freshly collected, live worms were incubated for 24 h in 150 ml of 0.2- μm -filtered seawater, supplemented with 2 mM (final concentration) either ^{12}C -labeled (natural isotope abundance control) or ^{13}C -labeled sodium bicarbonate (Sigma-Aldrich, St. Louis, MO, USA). In a second control experiment, 50 freshly collected worms were killed by incubating them in a 2% paraformaldehyde/water solution for 12 h prior to 24 h of incubation with ^{13}C -labeled sodium bicarbonate (dead control).

All three incubations were performed in biological triplicates or quadruplets and set up under anoxic-sulfidic and oxic conditions. Like the RNA-Seq experiment, the oxic incubations consisted of two separate experiments of low (hypoxic) and high (oxic) oxygen concentrations. To prevent isotope dilution through exchange with the atmosphere, both the oxic and anoxic incubations remained closed throughout the 24 h. The procedure was as follows: 0.2- μm -filtered anoxic seawater was prepared as described above and was subsequently used for both oxic and anoxic incubations. Then, compressed air (DAN oxygen kit; Divers Alert Network, USA) and 25 μM sodium sulfide ($\text{Na}_2\text{S} \cdot 9\text{H}_2\text{O}$; Sigma-Aldrich, St. Louis, MO, USA) were injected into the oxic and anoxic incubations, respectively, to obtain concentrations resembling the conditions applied in incubations for the RNA-Seq experiment (see Table S2B for details about the number of replicates, incubation conditions, and a compilation of the measurement data).

At the end of each incubation (24 h), the nematodes were weighed (0.3 to 0.7 mg [dry weight]) into tin capsules (Elemental Microanalysis, Devon, United Kingdom) and dried at 70°C for at least 24 h. Samples were analyzed using a Costech (Valencia, CA, USA) elemental analyzer interfaced with a continuous flow Micromass (Manchester, United Kingdom) Isoprime isotope ratio mass spectrometer (EA-IRMS) for determination of $^{13}\text{C}/^{12}\text{C}$ isotope ratios. Measurement values are displayed in δ notation (per mille ‰). A protein hydrolysate, calibrated against NIST reference materials, was used as a standard in sample runs. The achieved precision for $\delta^{13}\text{C}$ was ± 0.2 ‰ (1 standard deviation of 10 replicate measurements on the standard). Statistically significant differences were determined by applying one-way analysis of variance (ANOVA), followed by Tukey's pairwise comparisons.

Assessment of the percentage of dividing cells. Three individual nematodes per EA-IRMS incubation (see Table S2B for O_2 and H_2S measurements at the beginning and at the end of the incubations) were fixed, and ectosymbionts were dissociated from their hosts as described for Raman microspectroscopy (Text S1). A 1.5- μl amount of each bacterial suspension per condition was applied to a 1% agarose-covered slide (173), and cells were imaged using a Nikon Eclipse NI-U microscope equipped with an MFCool camera (Jenoptik). Images were obtained using the ProgRes Capture Pro 2.8.8 software (Jenoptik) and processed with ImageJ (174). Bacterial cells were manually counted (>600 per sample) and grouped into constricted (dividing) and nonconstricted (nondividing) cells based on visual inspection (28). The percentage of dividing cells was calculated by counting the total number of dividing cells and the total amount of cells per condition. The chi-square hypothesis test of independence was applied to test for a significant relationship between percentage of dividing cells and incubation condition.

Data availability. The assembled and annotated genome of “*Ca. T. oneisti*” has been deposited at DDBJ/ENA/GenBank under the accession no. [JAAEFD000000000](https://www.ncbi.nlm.nih.gov/assembly/GCA000000000). RNA-Seq data are available at the Gene Expression Omnibus (GEO) database and are accessible through accession number [GSE146081](https://www.ncbi.nlm.nih.gov/geo/query/acc.cgi?acc=GSE146081).

SUPPLEMENTAL MATERIAL

Supplemental material is available online only.

TEXT S1, DOCX file, 0.1 MB.

FIG S1, PDF file, 0.2 MB.

FIG S2, PDF file, 0.1 MB.

FIG S3, PDF file, 1.3 MB.

FIG S4, PDF file, 0.3 MB.

FIG S5, PDF file, 0.5 MB.

TABLE S1, DOCX file, 0.02 MB.

TABLE S2, DOCX file, 0.02 MB.

TABLE S3, DOCX file, 0.02 MB.

DATA SET S1, XLSX file, 2.1 MB.

ACKNOWLEDGMENTS

This work was supported by the Austrian Science Fund (FWF) grant P28743 (T.V., S.B., and L.K.), FWF grant P28953 (L.K. and G.F.P.), and the FWF DK plus grant W1257: Microbial Nitrogen Cycling (G.F.P.).

We are indebted to Florian Goldenberg, Patrick Hyden, and Thomas Rattei (Division of Computational Systems Biology, University of Vienna) for providing and maintaining the Life Science Compute Cluster (LiSC) and help in preparing the MinION sequencing library for “*Ca. T. oneisti*” at the University of Vienna. Harald Gruber-Vodicka from the MPI Bremen generously provided Illumina raw reads to aid the assemblies of ectosymbiont genomes. We are very grateful to Wiebke Mohr, Nikolaus Leisch, and Nicole Dubilier from the MPI for Marine Microbiology (Bremen) for continuous technical support with the stable isotope-based techniques. We appreciate Tjorven Hinzke’s advice on metaproteome statistics and Carolina Reyes for her input on the nitrogen metabolism. We thank Yin Chen for providing the facilities for lipidomic analysis and Eleonora Silvano for assistance with lipid extractions, and Jana Matulla’s and Sebastian Grund’s excellent technical work during protein sample preparation and MS analysis, respectively. Also, our sincere gratitude to the Carrie Bow Cay Marine Field Station, Caribbean Coral Reef Ecosystem Program, and Station Manager Zach Foltz for his continuous help during field work. Finally, we were very much helped and inspired by insightful discussions with Monika Bright, Jörg A. Ott, Christa Schleper, Simon K.-M. R. Rittmann, Filipa Sousa, and Jillian Petersen.

This work is contribution 1054 from the Carrie Bow Cay Laboratory, Caribbean Coral Reef Ecosystem Programme, the National Museum of Natural History, Washington, DC.

We declare no competing financial interest.

REFERENCES

1. Parks DH, Chuvochina M, Waite DW, Rinke C, Skarshewski A, Chaumeil PA, Hugenholtz P. 2018. A standardized bacterial taxonomy based on genome phylogeny substantially revises the tree of life. *Nat Biotechnol* 36:996–1004. <https://doi.org/10.1038/nbt.4229>.
2. Ott J, Bright M, Bulgheresi S. 2004. Marine microbial thiotrophic ectosymbioses, p 95–118. In Gibson RN, Atkinson RJA, Gordon JDM (ed), *Oceanography and marine biology: an annual review*, 42nd ed. CRC Press, Boca Raton, FL.
3. Dubilier N, Bergin C, Lott C. 2008. Symbiotic diversity in marine animals: the art of harnessing chemosynthesis. *Nat Rev Microbiol* 6:725–740. <https://doi.org/10.1038/nrmicro1992>.
4. Stewart FJ, Newton ILG, Cavanaugh CM. 2005. Chemosynthetic endosymbioses: adaptations to oxic–anoxic interfaces. *Trends Microbiol* 13:439–448. <https://doi.org/10.1016/j.tim.2005.07.007>.
5. König S, Gros O, Heiden SE, Hinzke T, Thürmer A, Poehlein A, Meyer S, Vatin M, Mbéguié-A-Mbéguié D, Toczny J, Ponnudurai R, Daniel R, Becher D, Schweder T, Markert S. 2016. Nitrogen fixation in a chemoautotrophic lucinid symbiosis. *Nat Microbiol* 2:16193. <https://doi.org/10.1038/nmicrobiol.2016.193>.
6. Petersen JM, Kemper A, Gruber-Vodicka H, Cardini U, van der Geest M, Kleiner M, Bulgheresi S, Mußmann M, Herbold C, Seah BKB, Antony CP, Liu D, Belitz A, Weber M. 2016. Chemosynthetic symbionts of marine invertebrate animals are capable of nitrogen fixation. *Nat Microbiol* 2:16195. <https://doi.org/10.1038/nmicrobiol.2016.195>.
7. Ponsard J, Cambon-Bonavita M-A, Zbinden M, Lepoint G, Joassin A, Corbari L, Shillito B, Durand L, Cuffe-Gauchard V, Compère P. 2013. Inorganic carbon fixation by chemosynthetic ectosymbionts and nutritional transfers to the hydrothermal vent host-shrimp *Rimicaris exoculata*. *ISME J* 7:96–109. <https://doi.org/10.1038/ismej.2012.87>.
8. Canfield DE, Thamdrup B. 2009. Towards a consistent classification scheme for geochemical environments, or, why we wish the term ‘sub-oxic’ would go away. *Geobiology* 7:385–392. <https://doi.org/10.1111/j.1472-4669.2009.00214.x>.
9. Luther GW, Findlay AJ, MacDonald DJ, Owings SM, Hanson TE, Beinart RA, Girguis PR. 2011. Thermodynamics and kinetics of sulfide oxidation by oxygen: a look at inorganically controlled reactions and biologically mediated processes in the environment. *Front Microbiol* 2:62. <https://doi.org/10.3389/fmicb.2011.00062>.
10. Ott J, Novak R. 1989. Living at an interface: meiofauna at the oxygen/sulfide boundary in marine sediments, p 415–422. In Ryland JS, Tyler PA (ed), *Reproduction, genetics and distributions of marine organisms*. Olsen & Olsen, Fredensborg, Denmark.
11. Schiemer F, Novak R, Ott J. 1990. Metabolic studies on thiotrophic free-living nematodes and their symbiotic microorganisms. *Mar Biol* 106:129–137. <https://doi.org/10.1007/BF02114683>.
12. Ott JA, Novak R, Schiemer F, Hentschel U, Nebelsick M, Polz M. 1991. Tackling the sulfide gradient: a novel strategy involving marine nematodes and chemoautotrophic ectosymbionts. *Mar Ecol* 12:261–279. <https://doi.org/10.1111/j.1439-0485.1991.tb00258.x>.
13. Wilmet DB, Vetter RD. 1992. Oxygen- and nitrogen-dependent sulfur metabolism in the thiotrophic clam *Solemya reidi*. *Biol Bull* 182:444–453. <https://doi.org/10.2307/1542264>.
14. Hentschel U, Cary SC, Felbeck H. 1993. Nitrate respiration in chemoautotrophic symbionts of the bivalve *Lucinoma aequizonata*. *Mar Ecol Prog Ser* 94:35–41. <https://doi.org/10.3354/meps094035>.
15. Hentschel U, Berger E, Bright M, Felbeck H, Ott J. 1999. Metabolism of nitrogen and sulfur in ectosymbiotic bacteria of marine nematodes (Nematoda, Stilbonematinae). *Mar Ecol Prog Ser* 183:149–158. <https://doi.org/10.3354/meps183149>.
16. Hentschel U, Felbeck H. 1993. Nitrate respiration in the hydrothermal vent tubeworm *Riftia pachyptila*. *Nature* 366:338–340. <https://doi.org/10.1038/366338a0>.
17. Petersen JM, Yuen B. 2020. The symbiotic “all-rounders”: partnerships between marine animals and chemosynthetic nitrogen-fixing bacteria.

- Appl Environ Microbiol 87:e02129-20. <https://doi.org/10.1128/AEM.02129-20>.
18. Freytag JK, Girguis PR, Bergquist DC, Andras JP, Childress JJ, Fisher CR. 2001. A paradox resolved: sulfide acquisition by roots of seep tubeworms sustains net chemoautotrophy. *Proc Natl Acad Sci U S A* 98:13408–13413. <https://doi.org/10.1073/pnas.231589498>.
 19. Cavanaugh CM. 1983. Symbiotic chemoautotrophic bacteria in marine invertebrates from sulphide-rich habitats. *Nature* 302:58–61. <https://doi.org/10.1038/302058a0>.
 20. Seston SL, Beinart RA, Sarode N, Shockey AC, Ranjan P, Ganesh S, Girguis PR, Stewart FJ. 2016. Metatranscriptional response of chemoautotrophic *Ifrimeria nautilei* endosymbionts to differing sulfur regimes. *Front Microbiol* 7:1074. <https://doi.org/10.3389/fmicb.2016.01074>.
 21. Breusing C, Mitchell J, Delaney J, Sylva SP, Seewald JS, Girguis PR, Beinart RA. 2020. Physiological dynamics of chemosynthetic symbionts in hydrothermal vent snails. *ISME J* 14:2568–2579. <https://doi.org/10.1038/s41396-020-0707-2>.
 22. Polz MF, Distel DL, Zarda B, Amann R, Felbeck H, Ott JA, Cavanaugh CM. 1994. Phylogenetic analysis of a highly specific association between ectosymbiotic, sulfur-oxidizing bacteria and a marine nematode. *Appl Environ Microbiol* 60:4461–4467. <https://doi.org/10.1128/AEM.60.12.4461-4467.1994>.
 23. Bayer C, Heindl NR, Rinke C, Lückner S, Ott J, Bulgheresi S. 2009. Molecular characterization of the symbionts associated with marine nematodes of the genus *Robbea*. *Environ Microbiol Rep* 1:136–144. <https://doi.org/10.1111/j.1758-2229.2009.00019.x>.
 24. Pende N, Leisch N, Gruber-Vodicka HR, Heindl NR, Ott J, den Blaauwen T, Bulgheresi S. 2014. Size-independent symmetric division in extraordinarily long cells. *Nat Commun* 5:4803. <https://doi.org/10.1038/ncomms5803>.
 25. Zimmermann J, Wentrup C, Sadowski M, Blazejak A, Gruber-Vodicka HR, Kleiner M, Ott JA, Cronholm B, De Wit P, Erséus C, Dubilier N. 2016. Closely coupled evolutionary history of ecto- and endosymbionts from two distantly related animal phyla. *Mol Ecol* 25:3203–3223. <https://doi.org/10.1111/mec.13554>.
 26. Leisch N, Verheul J, Heindl NR, Gruber-Vodicka HR, Pende N, den Blaauwen T, Bulgheresi S. 2012. Growth in width and FtsZ ring longitudinal positioning in a gammaproteobacterial symbiont. *Curr Biol* 22:R831–R832. <https://doi.org/10.1016/j.cub.2012.08.033>.
 27. Leisch N, Pende N, Weber PM, Gruber-Vodicka HR, Verheul J, Vischer NOE, Abby SS, Geier B, Den Blaauwen T, Bulgheresi S. 2016. Asynchronous division by non-ring FtsZ in the gammaproteobacterial symbiont of *Robbea hypermnestra*. *Nat Microbiol* 2:16182. <https://doi.org/10.1038/nmicrobiol.2016.182>.
 28. Pende N, Wang J, Weber PM, Verheul J, Kuru E, Rittmann S-MR, Leisch N, VanNieuwenhze MS, Brun YV, den Blaauwen T, Bulgheresi S. 2018. Host-polarized cell growth in animal symbionts. *Curr Biol* 28:1039–1051.e5. <https://doi.org/10.1016/j.cub.2018.02.028>.
 29. Powell EN, Crenshaw MA, Rieger RM. 1979. Adaptations to sulfide in the meiofauna of the sulfide system. I. 35S-sulfide accumulation and the presence of a sulfide detoxification system. *J Exp Mar Biol Ecol* 37:57–76. [https://doi.org/10.1016/0022-0981\(79\)90026-1](https://doi.org/10.1016/0022-0981(79)90026-1).
 30. Polz MF, Felbeck H, Novak R, Nebelsick M, Ott JA. 1992. Chemoautotrophic, sulfur-oxidizing symbiotic bacteria on marine nematodes: morphological and biochemical characterization. *Microb Ecol* 24:313–329. <https://doi.org/10.1007/BF00167789>.
 31. Himmel D, Maurin LC, Gros O, Mansot J-L. 2009. Raman microspectrometry sulfur detection and characterization in the marine ectosymbiotic nematode *Eubostrichus diana* (Desmodoridae, Stilbonematidae). *Biol Cell* 101:43–54. <https://doi.org/10.1042/BC20080051>.
 32. Dahl C, Friedrich C, Kletzin A. 2008. Sulfur oxidation in prokaryotes. In *Encyclopedia of life sciences*. John Wiley & Sons, Ltd, Chichester, United Kingdom.
 33. Dahl C. 2017. Sulfur metabolism in phototrophic bacteria, p 27–66. In *Hallenbeck P (ed), Modern topics in the phototrophic prokaryotes*. Springer International Publishing, Cham, Switzerland.
 34. Ghosh W, Dam B. 2009. Biochemistry and molecular biology of lithotrophic sulfur oxidation by taxonomically and ecologically diverse bacteria and archaea. *FEMS Microbiol Rev* 33:999–1043. <https://doi.org/10.1111/j.1574-6976.2009.00187.x>.
 35. Chen J, Strous M. 2013. Denitrification and aerobic respiration, hybrid electron transport chains and co-evolution. *Biochim Biophys Acta* 1827:136–144. <https://doi.org/10.1016/j.bbabi.2012.10.002>.
 36. Wells M, Kanmanij NJ, Al Zadjali AM, Janecka JE, Basu P, Oremland RS, Stolz JF. 2020. Methane, arsenic, selenium and the origins of the DMSO reductase family. *Sci Rep* 10:10946. <https://doi.org/10.1038/s41598-020-67892-9>.
 37. Lonjers ZT, Dickson EL, Chu T-PT, Kreutz JE, Neacsu FA, Anders KR, Shepherd JN. 2012. Identification of a new gene required for the biosynthesis of rhodoquinone in *Rhodospirillum rubrum*. *J Bacteriol* 194:965–971. <https://doi.org/10.1128/JB.06319-11>.
 38. Stairs CW, Erme L, Muñoz-Gómez SA, Cohen A, Delleire G, Shepherd JN, Fawcett JP, Roger AJ. 2018. Microbial eukaryotes have adapted to hypoxia by horizontal acquisitions of a gene involved in rhodoquinone biosynthesis. *Elife* 7:e34292. <https://doi.org/10.7554/eLife.34292>.
 39. Mills JK, Needham D. 2005. Lysolipid incorporation in dipalmitoylphosphatidylcholine bilayer membranes enhances the ion permeability and drug release rates at the membrane phase transition. *Biochim Biophys Acta* 1716:77–96. <https://doi.org/10.1016/j.bbamem.2005.08.007>.
 40. Aroui A, Mouritsen OG. 2013. Membrane-perturbing effect of fatty acids and lysolipids. *Prog Lipid Res* 52:130–140. <https://doi.org/10.1016/j.plipres.2012.09.002>.
 41. Koshy C, Schweikhard ES, Gärtner RM, Perez C, Yildiz Ö, Ziegler C. 2013. Structural evidence for functional lipid interactions in the betaine transporter BetP. *EMBO J* 32:3096–3105. <https://doi.org/10.1038/emboj.2013.226>.
 42. Laganowsky A, Reading E, Allison TM, Ulmschneider MB, Degiacomi MT, Baldwin AJ, Robinson CV. 2014. Membrane proteins bind lipids selectively to modulate their structure and function. *Nature* 510:172–175. <https://doi.org/10.1038/nature13419>.
 43. Wier AM, Nyholm SV, Mandel MJ, Massengo-Tiassé RP, Schaefer AL, Koroleva I, Splinter-Bondurant S, Brown B, Manzella L, Snir E, Almabrazi H, Scheetz TE, Bonaldo MDF, Casavant TL, Soares MB, Cronan JE, Reed JL, Ruby EG, McFall-Ngai MJ. 2010. Transcriptional patterns in both host and bacterium underlie a daily rhythm of anatomical and metabolic change in a beneficial symbiosis. *Proc Natl Acad Sci U S A* 107:2259–2264. <https://doi.org/10.1073/pnas.0909712107>.
 44. Saito HE, Harp JR, Fozo EM. 2014. Incorporation of exogenous fatty acids protects *Enterococcus faecalis* from membrane-damaging agents. *Appl Environ Microbiol* 80:6527–6538. <https://doi.org/10.1128/AEM.02044-14>.
 45. Nelson DC, Hagen KD, Edwards DB. 1995. The gill symbiont of the hydrothermal vent mussel *Bathymodiolus thermophilus* is a psychrophilic, chemoautotrophic, sulfur bacterium. *Mar Biol* 121:487–495. <https://doi.org/10.1007/BF00349457>.
 46. Markert S, Arndt C, Felbeck H, Becher D, Sievert SM, Hügler M, Albrecht D, Robidart J, Bench S, Feldman RA, Hecker M, Schweder T. 2007. Physiological proteomics of the uncultured endosymbiont of *Riftia pachyptila*. *Science* 315:247–250. <https://doi.org/10.1126/science.1132913>.
 47. Volland J-M, Schintlmeister A, Zambalos H, Reipert S, Mozetič P, Espada-Hinojosa S, Turk V, Wagner M, Bright M. 2018. NanoSIMS and tissue autoradiography reveal symbiont carbon fixation and organic carbon transfer to giant ciliate host. *ISME J* 12:714–727. <https://doi.org/10.1038/s41396-018-0069-1>.
 48. Seah BKB, Antony CP, Huettel B, Zarzycki J, Schada von Borzyskowski L, Erb TJ, Kouris A, Kleiner M, Liebecke M, Dubilier N, Gruber-Vodicka HR. 2019. Oxidizing symbionts without canonical genes for autotrophic CO₂ fixation. *mBio* 10:e01112-19. <https://doi.org/10.1128/mBio.01112-19>.
 49. Tsai YCC, Lapina MC, Bhushan S, Mueller-Cajar O. 2015. Identification and characterization of multiple rubisco activases in chemoautotrophic bacteria. *Nat Commun* 6:8883. <https://doi.org/10.1038/ncomms9883>.
 50. Kleiner M, Wentrup C, Lott C, Teeling H, Wetzels S, Young J, Chang Y-J, Shah M, VerBerkmoes NC, Zarzycki J, Fuchs G, Markert S, Hempel K, Voigt B, Becher D, Liebecke M, Lalk M, Albrecht D, Hecker M, Schweder T, Dubilier N. 2012. Metaproteomics of a gutless marine worm and its symbiotic microbial community reveal unusual pathways for carbon and energy use. *Proc Natl Acad Sci U S A* 109:E1173–E1182. <https://doi.org/10.1073/pnas.1121198109>.
 51. Jäckle O, Seah BKB, Tietjen M, Leisch N, Liebecke M, Kleiner M, Berg JS, Gruber-Vodicka HR. 2019. Chemosynthetic symbiont with a drastically reduced genome serves as primary energy storage in the marine flatworm *Paracatenula*. *Proc Natl Acad Sci U S A* 116:8505–8514. <https://doi.org/10.1073/pnas.1818995116>.
 52. Chai Y, Kolter R, Losick R. 2009. A widely conserved gene cluster required for lactate utilization in *Bacillus subtilis* and its involvement in biofilm formation. *J Bacteriol* 191:2423–2430. <https://doi.org/10.1128/JB.01464-08>.
 53. Horswill AR, Escalante-Semerena JC. 1999. The prpE gene of *Salmonella typhimurium* LT2 encodes propionyl-CoA synthetase. *Microbiology* 145:1381–1388. <https://doi.org/10.1099/13500872-145-6-1381>.
 54. Mulligan C, Fischer M, Thomas GH. 2011. Tripartite ATP-independent periplasmic (TRAP) transporters in bacteria and archaea. *FEMS Microbiol Rev* 35:68–86. <https://doi.org/10.1111/j.1574-6976.2010.00236.x>.
 55. Rogers A, Gibon Y, Stitt M, Morgan PB, Bernacchi CJ, Ort DR, Long SP. 2006. Increased C availability at elevated carbon dioxide concentration

- improves N assimilation in a legume. *Plant Cell Environ* 29:1651–1658. <https://doi.org/10.1111/j.1365-3040.2006.01549.x>.
56. Elgharably A, Marschner P. 2011. Microbial activity and biomass and N and P availability in a saline sandy loam amended with inorganic N and lupin residues. *Eur J Soil Biol* 47:310–315. <https://doi.org/10.1016/j.ejsobi.2011.07.005>.
 57. Fellbaum CR, Gachomo EW, Beesetty Y, Choudhari S, Strahan GD, Pfeffer PE, Kiers ET, Bucking H. 2012. Carbon availability triggers fungal nitrogen uptake and transport in arbuscular mycorrhizal symbiosis. *Proc Natl Acad Sci U S A* 109:2666–2671. <https://doi.org/10.1073/pnas.1118650109>.
 58. Hill S. 1988. How is nitrogenase regulated by oxygen? *FEMS Microbiol Rev* 4:111–129. <https://doi.org/10.1111/j.1574-6968.1988.tb02738.x>.
 59. Burgess BK, Lowe DJ. 1996. Mechanism of molybdenum nitrogenase. *Chem Rev* 96:2983–3012. <https://doi.org/10.1021/cr950055x>.
 60. Schneider S, Schintlmeister A, Becana M, Wagner M, Woebken D, Wienkoop S. 2019. Sulfate is transported at significant rates through the symbiosome membrane and is crucial for nitrogenase biosynthesis. *Plant Cell Environ* 42:1180–1189. <https://doi.org/10.1111/pce.13481>.
 61. Yeo W-S, Lee J-H, Lee K-C, Roe J-H. 2006. IscR acts as an activator in response to oxidative stress for the *suf* operon encoding Fe-S assembly proteins. *Mol Microbiol* 61:206–218. <https://doi.org/10.1111/j.1365-2958.2006.05220.x>.
 62. Zeller T, Moskvina OV, Li K, Klug G, Gomelsky M. 2005. Transcriptome and physiological responses to hydrogen peroxide of the facultatively phototrophic bacterium *Rhodobacter sphaeroides*. *J Bacteriol* 187:7232–7242. <https://doi.org/10.1128/JB.187.21.7232-7242.2005>.
 63. Grant CM. 2001. Role of the glutathione/glutaredoxin and thioredoxin systems in yeast growth and response to stress conditions. *Mol Microbiol* 39:533–541. <https://doi.org/10.1046/j.1365-2958.2001.02283.x>.
 64. Alba BM, Leeds JA, Onufryk C, Lu CZ, Gross CA. 2002. DegS and YaeL participate sequentially in the cleavage of RseA to activate the sigma E-dependent extracytoplasmic stress response. *Genes Dev* 16:2156–2168. <https://doi.org/10.1101/gad.1008902>.
 65. Sakoh M, Ito K, Akiyama Y. 2005. Proteolytic activity of HtpX, a membrane-bound and stress-controlled protease from *Escherichia coli*. *J Biol Chem* 280:33305–33310. <https://doi.org/10.1074/jbc.M506180200>.
 66. Puri N, Karzai AW. 2017. HspQ functions as a unique specificity-enhancing factor for the AAA+ Lon protease. *Mol Cell* 66:672–683.e4. <https://doi.org/10.1016/j.molcel.2017.05.016>.
 67. Tomoyasu T, Gamer J, Bukau B, Kanemori M, Mori H, Rutman AJ, Oppenheim AB, Yura T, Yamanaka K, Niki H, Hiraga S, Ogura T. 1995. *Escherichia coli* FtsH is a membrane-bound, ATP-dependent protease which degrades the heat-shock transcription factor σ 32. *EMBO J* 14:2551–2560. <https://doi.org/10.1002/j.1460-2075.1995.tb07253.x>.
 68. Schoemaker JM, Gayda RC, Markovitz A. 1984. Regulation of cell division in *Escherichia coli*: SOS induction and cellular location of the SulA protein, a key to lon-associated filamentation and death. *J Bacteriol* 158:551–561. <https://doi.org/10.1128/JB.158.2.551-561.1984>.
 69. Sargentini NJ, Smith KC. 1986. Quantitation of the involvement of the *recA*, *recB*, *recC*, *recF*, *recN*, *lexA*, *radA*, *radB*, *uvrD*, and *umuC* genes in the repair of X-ray-induced DNA double-strand breaks in *Escherichia coli*. *Radiat Res* 107:58–72. <https://doi.org/10.2307/3576850>.
 70. Au KG, Cabrera M, Miller JH, Modrich P. 1988. *Escherichia coli mutY* gene product is required for specific A-G→C-G mismatch correction. *Proc Natl Acad Sci U S A* 85:9163–9166. <https://doi.org/10.1073/pnas.85.23.9163>.
 71. Deaconescu AM, Darst SA. 2005. Crystallization and preliminary structure determination of *Escherichia coli* Mfd, the transcription-repair coupling factor. *Acta Crystallogr Sect F Struct Biol Cryst Commun* 61:1062–1064. <https://doi.org/10.1107/S1744309105035876>.
 72. Traxler MF, Summers SM, Nguyen H-T, Zacharia VM, Hightower GA, Smith JT, Conway T. 2008. The global, ppGpp-mediated stringent response to amino acid starvation in *Escherichia coli*. *Mol Microbiol* 68:1128–1148. <https://doi.org/10.1111/j.1365-2958.2008.06229.x>.
 73. Magnusson LU, Farewell A, Nyström T. 2005. ppGpp: a global regulator in *Escherichia coli*. *Trends Microbiol* 13:236–242. <https://doi.org/10.1016/j.tim.2005.03.008>.
 74. Rao SG, Ponnalagu D, Sukur S, Singh H, Sanghvi S, Mei Y, Jin DJ, Singh H. 2017. Identification and characterization of a bacterial homolog of chloride intracellular channel (CLIC) protein. *Sci Rep* 7:8500. <https://doi.org/10.1038/s41598-017-08742-z>.
 75. Williams MD, Ouyang TX, Flickinger MC. 1994. Starvation-induced expression of SspA and SspB: the effects of a null mutation in *sspA* on *Escherichia coli* protein synthesis and survival during growth and prolonged starvation. *Mol Microbiol* 11:1029–1043. <https://doi.org/10.1111/j.1365-2958.1994.tb00381.x>.
 76. Hansen A-M, Lehnerr H, Wang X, Mobley V, Jin DJ. 2003. *Escherichia coli* SspA is a transcription activator for bacteriophage P1 late genes. *Mol Microbiol* 48:1621–1631. <https://doi.org/10.1046/j.1365-2958.2003.03533.x>.
 77. Chen J, Shen J, Solem C, Jensen PR. 2013. Oxidative stress at high temperatures in *Lactococcus lactis* due to an insufficient supply of riboflavin. *Appl Environ Microbiol* 79:6140–6147. <https://doi.org/10.1128/AEM.01953-13>.
 78. Ferrer A, Rivera J, Zapata C, Norambuena J, Sandoval Á, Chávez R, Orellana O, Levicán G. 2016. Cobalamin protection against oxidative stress in the acidophilic iron-oxidizing bacterium *Leptospirillum* group II CF-1. *Front Microbiol* 7:748. <https://doi.org/10.3389/fmicb.2016.00748>.
 79. Showman AC, Aranjuez G, Adams PP, Jewett MW. 2016. Gene bb0318 is critical for the oxidative stress response and infectivity of *Borrelia burgdorferi*. *Infect Immun* 84:3141–3151. <https://doi.org/10.1128/IAI.00430-16>.
 80. Typas A, Banzhaf M, Gross CA, Vollmer W. 2011. From the regulation of peptidoglycan synthesis to bacterial growth and morphology. *Nat Rev Microbiol* 10:123–136. <https://doi.org/10.1038/nrmicro2677>.
 81. Meyers M, Fossing H, Powell E. 1987. Microdistribution of interstitial meiofauna, oxygen and sulfide gradients, and the tubes of macro-infauna. *Mar Ecol Prog Ser* 35:223–241. <https://doi.org/10.3354/meps035223>.
 82. Powell E. 1989. Oxygen, sulfide and diffusion: why thioibiotic meiofauna must be sulfide-insensitive first-order respirers. *J Mar Res* 47:887–932. <https://doi.org/10.1357/002224089785076082>.
 83. Jan C, Petersen JM, Werner J, Teeling H, Huang S, Glöckner FO, Golyshina OV, Dubilier N, Golyshin PN, Jebbar M, Cambon-Bonavita M-A. 2014. The gill chamber epibiosis of deep-sea shrimp *Rimicaris exoculata*: an in-depth metagenomic investigation and discovery of *Zetaproteobacteria*. *Environ Microbiol* 16:2723–2738. <https://doi.org/10.1111/1462-2920.12406>.
 84. Ponnudurai R, Sayavedra L, Kleiner M, Heiden SE, Thürmer A, Felbeck H, Schlüter R, Sievert SM, Daniel R, Schweder T, Markert S. 2017. Genome sequence of the sulfur-oxidizing *Bathymodiolus thermophilus* gill endosymbiont. *Stand Genomic Sci* 12:50. <https://doi.org/10.1186/s40793-017-0266-y>.
 85. Ponnudurai R, Kleiner M, Sayavedra L, Petersen JM, Moche M, Otto A, Becher D, Takeuchi T, Satoh N, Dubilier N, Schweder T, Markert S. 2017. Metabolic and physiological interdependencies in the *Bathymodiolus azoricus* symbiosis. *ISME J* 11:463–477. <https://doi.org/10.1038/ismej.2016.124>.
 86. Fenchel T. 1970. Studies on the decomposition of organic detritus derived from the turtle grass *Thalassia testudinum*. *Limnol Oceanogr* 15:14–20. <https://doi.org/10.4319/lo.1970.15.1.0014>.
 87. Fenchel TM, Riedl RJ. 1970. The sulfide system: a new biotic community underneath the oxidized layer of marine sand bottoms. *Mar Biol* 7:255–268. <https://doi.org/10.1007/BF00367496>.
 88. Reise K, Ax P. 1979. A meiofaunal “thiobios” limited to the anaerobic sulfide system of marine sand does not exist. *Mar Biol* 54:225–237. <https://doi.org/10.1007/BF00395785>.
 89. Weber PM, Moessel F, Paredes GF, Viehboeck T, Vischer NOE, Bulgheresi S. 2019. A bidimensional segregation mode maintains symbiont chromosome orientation toward its host. *Curr Biol* 29:3018–3028.e4. <https://doi.org/10.1016/j.cub.2019.07.064>.
 90. Schwedt A, Kreutzmann AC, Polerecky L, Schulz-Vogt HN. 2012. Sulfur respiration in a marine chemolithoautotrophic *Beggiatoa* strain. *Front Microbiol* 2:276. <https://doi.org/10.3389/fmicb.2011.00276>.
 91. Nyström T, Neidhardt FC. 1992. Cloning, mapping and nucleotide sequencing of a gene encoding a universal stress protein in *Escherichia coli*. *Mol Microbiol* 6:3187–3198. <https://doi.org/10.1111/j.1365-2958.1992.tb01774.x>.
 92. Aldsworth TG, Sharman RL, Dodd CER. 1999. Bacterial suicide through stress. *Cell Mol Life Sci* 56:378–383. <https://doi.org/10.1007/s000180050439>.
 93. Nyström T. 2001. Not quite dead enough: on bacterial life, culturability, senescence, and death. *Arch Microbiol* 176:159–164. <https://doi.org/10.1007/s002030100314>.
 94. Nyström T. 2002. Translational fidelity, protein oxidation, and senescence: lessons from bacteria. *Ageing Res Rev* 1:693–703. [https://doi.org/10.1016/s1568-1637\(02\)00028-4](https://doi.org/10.1016/s1568-1637(02)00028-4).
 95. Sat B, Reches M, Engelberg-Kulka H. 2003. The *Escherichia coli mazEF* suicide module mediates thymineless death. *J Bacteriol* 185:1803–1807. <https://doi.org/10.1128/JB.185.6.1803-1807.2003>.
 96. Weber H, Engelmann S, Becher D, Hecker M. 2004. Oxidative stress triggers thiol oxidation in the glyceraldehyde-3-phosphate dehydrogenase of *Staphylococcus aureus*. *Mol Microbiol* 52:133–140. <https://doi.org/10.1111/j.1365-2958.2004.03971.x>.
 97. Page R, Peti W. 2016. Toxin-antitoxin systems in bacterial growth arrest and persistence. *Nat Chem Biol* 12:208–214. <https://doi.org/10.1038/nchembio.2044>.

98. ten Hoor AT. 1981. Cell yield and bioenergetics of *Thiomicrospira denitrificans* compared with *Thiobacillus denitrificans*. Antonie Van Leeuwenhoek 47:231–243. <https://doi.org/10.1007/BF00403394>.
99. Sorokin DY, Tourova TP, Antipov AN, Muyzer G, Kuenen JG. 2004. Anaerobic growth of the haloalkaliphilic denitrifying sulfur-oxidizing bacterium *Thiokallivibrio thiocyanodenitrificans* sp. nov. with thiocyanate. Microbiology (Reading) 150:2435–2442. <https://doi.org/10.1099/mic.0.27015-0>.
100. Nunoura T, Takaki Y, Kazama H, Kakuta J, Shimamura S, Makita H, Hirai M, Miyazaki M, Takai K. 2014. Physiological and genomic features of a novel sulfur-oxidizing gammaproteobacterium belonging to a previously uncultivated symbiotic lineage isolated from a hydrothermal vent. PLoS One 9:e104959. <https://doi.org/10.1371/journal.pone.0104959>.
101. Justin P, Kelly DP. 1978. Growth kinetics of *Thiobacillus denitrificans* in anaerobic and aerobic chemostat culture. J Gen Microbiol 107:123–130. <https://doi.org/10.1099/00221287-107-1-123>.
102. Childress JJ, Fisher CR, Favuzzi JA, Sanders NK. 1991. Sulfide and carbon dioxide uptake by the hydrothermal vent clam, *Calypotegna magnifica*, and its chemoautotrophic symbionts. Physiol Zool 64:1444–1470. <https://doi.org/10.1086/physzool.64.6.30158224>.
103. Scott KM, Cavanaugh CM. 2007. CO₂ uptake and fixation by endosymbiotic chemoautotrophs from the bivalve *Solemya velum*. Appl Environ Microbiol 73:1174–1179. <https://doi.org/10.1128/AEM.01817-06>.
104. Jordan DB, Ogren WL. 1981. Species variation in the specificity of ribulose biphosphate carboxylase/oxygenase. Nature 291:513–515. <https://doi.org/10.1038/291513a0>.
105. Badger MR, Bek EJ. 2008. Multiple Rubisco forms in proteobacteria: their functional significance in relation to CO₂ acquisition by the CBB cycle. J Exp Bot 59:1525–1541. <https://doi.org/10.1093/jxb/erm297>.
106. Tabita FR, Satagopan S, Hanson TE, Krel NE, Scott SS. 2007. Distinct form I, II, III, and IV Rubisco proteins from the three kingdoms of life provide clues about Rubisco evolution and structure/function relationships. J Exp Bot 59:1515–1524. <https://doi.org/10.1093/jxb/erm361>.
107. Erb TJ. 2011. Carboxylases in natural and synthetic microbial pathways. Appl Environ Microbiol 77:8466–8477. <https://doi.org/10.1128/AEM.05702-11>.
108. Wilmet DB, Vetter RD. 1990. The bacterial symbiont from the hydrothermal vent tubeworm *Riftia pachyptila* is a sulfide specialist. Mar Biol 106:273–283. <https://doi.org/10.1007/BF01314811>.
109. Fisher CR, Childress JJ, Minnich E. 1989. Autotrophic carbon fixation by the chemoautotrophic symbionts of *Riftia pachyptila*. Biol Bull 177:372–385. <https://doi.org/10.2307/1541597>.
110. Woyke T, Teeling H, Ivanova NN, Hüntemann M, Richter M, Gloeckner FO, Boffelli D, Anderson IJ, Barry KW, Shapiro HJ, Szeto E, Kyrpides NC, Musmann M, Amann R, Bergin C, Ruehlmann C, Rubin EM, Dubilier N. 2006. Symbiosis insights through metagenomic analysis of a microbial consortium. Nature 443:950–955. <https://doi.org/10.1038/nature05192>.
111. Hagen KD, Nelson DC. 1996. Organic carbon utilization by obligately and facultatively autotrophic *Beggiatoa* strains in homogeneous and gradient cultures. Appl Environ Microbiol 62:947–953. <https://doi.org/10.1128/AEM.62.3.947-953.1996>.
112. Kurian D, Janssen T, Mäenpää P. 2006. Proteomic analysis of heterotrophy in *Synechocystis* sp. PCC 6803. Proteomics 6:1483–1494. <https://doi.org/10.1002/pmic.200500413>.
113. Norris PR, Clark DA, Owen JP, Waterhouse S. 1996. Characteristics of *Sulfolobus acidophilus* sp. nov. and other moderately thermophilic mineral-sulphide-oxidizing bacteria. Microbiology 142:775–783. <https://doi.org/10.1099/00221287-142-4-775>.
114. Breznak JA, Blum JS. 1991. Mixotrophy in the termite gut acetogen, *Sporomusa termitida*. Arch Microbiol 156:105–110. <https://doi.org/10.1007/BF00290981>.
115. Wan N, Abernathy M, Tang JKH, Tang YJ, You L. 2015. Cyanobacterial photo-driven mixotrophic metabolism and its advantages for biosynthesis. Front Chem Sci Eng 9:308–316. <https://doi.org/10.1007/s11705-015-1521-7>.
116. Zarzycki J, Fuchs G. 2011. Coassimilation of organic substrates via the autotrophic 3-hydroxypropionate bi-cycle in *Chloroflexus aurantiacus*. Appl Environ Microbiol 77:6181–6188. <https://doi.org/10.1128/AEM.00705-11>.
117. Shimizu R, Dempo Y, Nakayama Y, Nakamura S, Bamba T, Fukusaki E, Fukui T. 2015. New insight into the role of the Calvin cycle: reutilization of CO₂ emitted through sugar degradation. Sci Rep 5:11617–11612. <https://doi.org/10.1038/srep11617>.
118. Shimizu R, Chou K, Orita I, Suzuki Y, Nakamura S, Fukui T. 2013. Detection of phase-dependent transcriptomic changes and Rubisco-mediated CO₂ fixation into poly (3-hydroxybutyrate) under heterotrophic condition in *Ralstonia eutropha* H16 based on RNA-seq and gene deletion analyses. BMC Microbiol 13:169. <https://doi.org/10.1186/1471-2180-13-169>.
119. Makowka A, Nichelmann L, Schulze D, Spengler K, Wittmann C, Forchhammer K, Gutekunst K. 2020. Glycolytic shunts replenish the Calvin–Benson–Bassham cycle as anaplerotic reactions in Cyanobacteria. Mol Plant 13:471–482. <https://doi.org/10.1016/j.molp.2020.02.002>.
120. Unrein F, Gasol JM, Not F, Forn I, Massana R. 2014. Mixotrophic haptophytes are key bacterial grazers in oligotrophic coastal waters. ISME J 8:164–176. <https://doi.org/10.1038/ismej.2013.132>.
121. Anderson AJ, Dawes EA. 1990. Occurrence, metabolism, metabolic role, and industrial uses of bacterial polyhydroxyalkanoates. Microbiol Rev 54:450–472. <https://doi.org/10.1128/MR.54.4.450-472.1990>.
122. Escapa IF, García JL, Bühler B, Blank LM, Prieto MA. 2012. The polyhydroxyalkanoate metabolism controls carbon and energy spillage in *Pseudomonas putida*. Environ Microbiol 14:1049–1063. <https://doi.org/10.1111/j.1462-2920.2011.02684.x>.
123. Verlinden RAJ, Hill DJ, Kenward MA, Williams CD, Radecka I. 2007. Bacterial synthesis of biodegradable polyhydroxyalkanoates. J Appl Microbiol 102:1437–1449. <https://doi.org/10.1111/j.1365-2672.2007.03335.x>.
124. Tal S, Okon Y. 1985. Production of the reserve material poly-β-hydroxybutyrate and its function in *Azospirillum brasilense* Cd. Can J Microbiol 31:608–613. <https://doi.org/10.1139/m85-115>.
125. Natarajan K, Kishore L, Babu CR. 1995. Characteristics of NaCl stress associated proteins of *Rhizobium* under varying cultural conditions. J Basic Microbiol 35:413–420. <https://doi.org/10.1002/jbm.3620350608>.
126. Steinbüchel A, Fuchtenbusch B. 1998. Bacterial and other biological systems for polyester production. Trends Biotechnol 16:419–427. [https://doi.org/10.1016/s0167-7799\(98\)01194-9](https://doi.org/10.1016/s0167-7799(98)01194-9).
127. Kadouri D, Burdman S, Jurkevitch E, Okon Y. 2002. Identification and isolation of genes involved in poly(β-hydroxybutyrate) biosynthesis in *Azospirillum brasilense* and characterization of a *phbC* mutant. Appl Environ Microbiol 68:2943–2949. <https://doi.org/10.1128/aem.68.6.2943-2949.2002>.
128. Ayub ND, Pettinari MJ, Ruiz JA, López NI. 2004. A polyhydroxybutyrate-producing *Pseudomonas* sp. isolated from antarctic environments with high stress resistance. Curr Microbiol 49:170–174. <https://doi.org/10.1007/s00284-004-4254-2>.
129. Kadouri D, Jurkevitch E, Okon Y, Castro-Sowinski S. 2005. Ecological and agricultural significance of bacterial polyhydroxyalkanoates. Crit Rev Microbiol 31:55–67. <https://doi.org/10.1080/10408410509899228>.
130. Obrucsa S, Sedlacek P, Krzyzanek V, Mravec F, Hrubanova K, Samek O, Kucera D, Benesova P, Marova I. 2016. Accumulation of poly(3-hydroxybutyrate) helps bacterial cells to survive freezing. PLoS One 11:e0157778. <https://doi.org/10.1371/journal.pone.0157778>.
131. Obrucsa S, Sedlacek P, Mravec F, Krzyzanek V, Nebesarova J, Samek O, Kucera D, Benesova P, Hrubanova K, Millerova M, Marova I. 2017. The presence of PHB granules in cytoplasm protects non-halophilic bacterial cells against the harmful impact of hypertonic environments. N Biotechnol 39:68–80. <https://doi.org/10.1016/j.nbt.2017.07.008>.
132. Slaninova E, Sedlacek P, Mravec F, Mullerova L, Samek O, Koller M, Heskó O, Kucera D, Marova I, Obrucsa S. 2018. Light scattering on PHA granules protects bacterial cells against the harmful effects of UV radiation. Appl Microbiol Biotechnol 102:1923–1931. <https://doi.org/10.1007/s00253-018-8760-8>.
133. Hamad MA, Austin CR, Stewart AL, Higgins M, Vázquez-Torres A, Voskuil MI. 2011. Adaptation and antibiotic tolerance of anaerobic *Burkholderia pseudomallei*. Antimicrob Agents Chemother 55:3313–3323. <https://doi.org/10.1128/AAC.00953-10>.
134. Kim JK, Won YJ, Nikoh N, Nakayama H, Han SH, Kikuchi Y, Rhee YH, Park HY, Kwon JY, Kurokawa K, Dohmae N, Fukatsu T, Lee BL. 2013. Polyester synthesis genes associated with stress resistance are involved in an insect-bacterium symbiosis. Proc Natl Acad Sci U S A 110:E2381–E2389. <https://doi.org/10.1073/pnas.1303281110>.
135. Claessen D, Errington J. 2019. Cell wall deficiency as a coping strategy for stress. Trends Microbiol 27:1025–1033. <https://doi.org/10.1016/j.tim.2019.07.008>.
136. McKinlay JB, Harwood CS. 2010. Carbon dioxide fixation as a central redox cofactor recycling mechanism in bacteria. Proc Natl Acad Sci U S A 107:11669–11675. <https://doi.org/10.1073/pnas.1006175107>.
137. Bentzon-Tilia M, Severin I, Hansen LH, Riemann L. 2015. Genomics and ecophysiology of heterotrophic nitrogen-fixing bacteria isolated from estuarine surface water. mBio 6:e00929-15. <https://doi.org/10.1128/mBio.00929-15>.
138. Antia NJ, Harrison PJ, Oliveira L. 1991. The role of dissolved organic nitrogen in phytoplankton nutrition, cell biology and ecology. Phycologia 30:1–89. <https://doi.org/10.2216/i0031-8884-30-1-1.1>.

139. Walsh P, Wang Y, Campbell C, Boeck DG, Wood C. 2001. Patterns of nitrogenous waste excretion and gill urea transporter mRNA expression in several species of marine fish. *Mar Biol* 139:839–844. <https://doi.org/10.1007/s002270100639>.
140. Beckers G, Bendt AK, Krämer R, Burkovski A. 2004. Molecular identification of the urea uptake system and transcriptional analysis of urea transporter- and urease-encoding genes in *Corynebacterium glutamicum*. *J Bacteriol* 186:7645–7652. <https://doi.org/10.1128/JB.186.22.7645-7652.2004>.
141. Brown DR, Barton G, Pan Z, Buck M, Wigneshweraraj S. 2014. Nitrogen stress response and stringent response are coupled in *Escherichia coli*. *Nat Commun* 5:4115. <https://doi.org/10.1038/ncomms5115>.
142. Ashoori M, Saedisomeolia A. 2014. Riboflavin (vitamin B2) and oxidative stress: a review. *Br J Nutr* 111:1985–1991. <https://doi.org/10.1017/S0007114514000178>.
143. Gould RL, Pazdro R. 2019. Impact of supplementary amino acids, micronutrients, and overall diet on glutathione homeostasis. *Nutrients* 11:1056. <https://doi.org/10.3390/nu11051056>.
144. Carmel-Harel O, Storz G. 2000. Roles of the glutathione- and thioredoxin-dependent reduction systems in the *Escherichia coli* and *Saccharomyces cerevisiae* responses to oxidative stress. *Annu Rev Microbiol* 54:439–461. <https://doi.org/10.1146/annurev.micro.54.1.439>.
145. Williams CH. 1995. Mechanism and structure of thioredoxin reductase from *Escherichia coli*. *FASEB J* 9:1267–1276. <https://doi.org/10.1096/fasebj.9.13.7557016>.
146. Vanoni MA, Curti B. 1999. Glutamate synthase: a complex iron-sulfur flavoprotein. *Cell Mol Life Sci* 55:617–638. <https://doi.org/10.1007/s000180050319>.
147. Liang J, Han Q, Tan Y, Ding H, Li J. 2019. Current advances on structure-function relationships of pyridoxal 5'-phosphate-dependent enzymes. *Front Mol Biosci* 6:4. <https://doi.org/10.3389/fmolb.2019.00004>.
148. Banerjee R, Ragsdale SW. 2003. The many faces of vitamin B12: catalysis by cobalamin-dependent enzymes. *Annu Rev Biochem* 72:209–247. <https://doi.org/10.1146/annurev.biochem.72.121801.161828>.
149. Fontecave M, Atta M, Mulliez E. 2004. S-adenosylmethionine: nothing goes to waste. *Trends Biochem Sci* 29:243–249. <https://doi.org/10.1016/j.tibs.2004.03.007>.
150. Caro AA, Cederbaum AI. 2004. Antioxidant properties of S-adenosyl-L-methionine in Fe2+-initiated oxidations. *Free Radic Biol Med* 36:1303–1316. <https://doi.org/10.1016/j.freeradbiomed.2004.02.015>.
151. Imhoff JF. 2017. Diversity of anaerobic anoxygenic phototrophic purple bacteria, p 47–85. In Hallebeek P (ed), *Modern topics in the phototrophic prokaryotes*. Springer International Publishing, Cham, Switzerland.
152. Ott JA, Bauer-Nebelsick M, Novotny V. 1995. The genus *Laxus* Cobb, 1894 (Stilbonematinae, Nematoda) - description of two new species with ectosymbiotic chemoautotrophic bacteria. *Proc Biol Soc Washington* 108:508–527.
153. Alberti A, Belser C, Engelen S, Bertrand L, Orvain C, Brinas L, Cruaud C, Giraut L, Da Silva C, Firmo C, Aury J-M, Wincker P, Gilbert J, Field D, Huang Y, Edwards R, Li W, Gilna P, Joint I, Frias-Lopez J, Shi Y, Tyson G, Coleman M, Schuster S, Chisholm S, Delong E, Poretsky R, Hewson I, Sun S, Allen A, Zehr J, Moran M, Hewson I, Poretsky R, Beinart R, White A, Shi T, Bench S, Moisaner P, Pael R, Tripp H, Montoya J, Moran M, Zehr J, Hewson I, Poretsky R, Dyhrman S, Zielinski B, White A, Tripp H, et al. 2014. Comparison of library preparation methods reveals their impact on interpretation of metatranscriptomic data. *BMC Genomics* 15:912. <https://doi.org/10.1186/1471-2164-15-912>.
154. Li H, Durbin R. 2009. Fast and accurate short read alignment with Burrows-Wheeler transform. *Bioinformatics* 25:1754–1760. <https://doi.org/10.1093/bioinformatics/btp324>.
155. Bankevich A, Nurk S, Antipov D, Gurevich AA, Dvorkin M, Kulikov AS, Lesin VM, Nikolenko SI, Pham S, Pribelski AD, Pyshkin AV, Sirotkin AV, Vyahhi N, Tesler G, Alekseyev MA, Pevzner PA. 2012. SPAdes: a new genome assembly algorithm and its applications to single-cell sequencing. *J Comput Biol* 19:455–477. <https://doi.org/10.1089/cmb.2012.0021>.
156. Parks DH, Imelfort M, Skennerton CT, Hugenholtz P, Tyson GW. 2015. CheckM: assessing the quality of microbial genomes recovered from isolates, single cells, and metagenomes. *Genome Res* 25:1043–1055. <https://doi.org/10.1101/gr.186072.114>.
157. Vallenet D, Calteau A, Dubois M, Amours P, Bazin A, Beuvin M, Burlot L, Bussell X, Fouteau S, Gautreau G, Lajus A, Langlois J, Planel R, Roche D, Rollin J, Rouy Z, Sabatet V, Médigue C. 2020. MicroScope: an integrated platform for the annotation and exploration of microbial gene functions through genomic, pangenomic and metabolic comparative analysis. *Nucleic Acids Res* 48:D579–D589. <https://doi.org/10.1093/nar/gkv926>.
158. Kanehisa M, Sato Y, Kawashima M, Furumichi M, Tanabe M. 2016. KEGG as a reference resource for gene and protein annotation. *Nucleic Acids Res* 44:D457–D462. <https://doi.org/10.1093/nar/gkv1070>.
159. Götz S, Garcia-Gomez JM, Terol J, Williams TD, Nagaraj SH, Nueda MJ, Robles M, Talon M, Dopazo J, Conesa A. 2008. High-throughput functional annotation and data mining with the Blast2GO suite. *Nucleic Acids Res* 36:3420–3435. <https://doi.org/10.1093/nar/gkn176>.
160. Bateman A, Birney E, Cerruti L, Durbin R, Ewinger L, Eddy SR, Griffiths-Jones S, Howe KL, Marshall M, Sonnhammer ELL. 2002. The Pfam protein families database. *Nucleic Acids Res* 30:276–280. <https://doi.org/10.1093/nar/30.1.276>.
161. Finn RD, Clements J, Eddy SR. 2011. HMMER web server: interactive sequence similarity searching. *Nucleic Acids Res* 39:W29–W37. <https://doi.org/10.1093/nar/gkr367>.
162. Andrews S. 2010. FastQC: a quality control tool for high throughput sequence data.
163. Schmieder R, Edwards R. 2011. Quality control and preprocessing of metagenomic datasets. *Bioinformatics* 27:863–864. <https://doi.org/10.1093/bioinformatics/btr026>.
164. Bolger AM, Lohse M, Usadel B. 2014. Trimmomatic: a flexible trimmer for Illumina sequence data. *Bioinformatics* 30:2114–2120. <https://doi.org/10.1093/bioinformatics/btu170>.
165. König L, Siegl A, Penz T, Haider S, Wentrup C, Polzin J, Mann E, Schmitz-Esser S, Domman D, Horn M. 2017. Biphasic metabolism and host interaction of a chlamydial symbiont. *mSystems* 2:e00202-16. <https://doi.org/10.1128/mSystems.00202-16>.
166. Li H, Handsaker B, Wysoker A, Fennell T, Ruan J, Homer N, Marth G, Abecasis G, Durbin R, 1000 Genome Project Data Processing Subgroup. 2009. The sequence alignment/map format and SAMtools. *Bioinformatics* 25:2078–2079. <https://doi.org/10.1093/bioinformatics/btp352>.
167. Anders S, Pyl PT, Huber W. 2015. HTSeq - a Python framework to work with high-throughput sequencing data. *Bioinformatics* 31:166–169. <https://doi.org/10.1093/bioinformatics/btu638>.
168. Gentleman RC, Carey VJ, Bates DM, Bolstad B, Dettling M, Dudoit S, Ellis B, Gautier L, Ge Y, Gentry J, Hornik K, Hothorn T, Huber W, Iacus S, Irizarry R, Leisch F, Li C, Maechler M, Rossini AJ, Sawitzki G, Smith C, Smyth G, Tierney L, Yang JYH, Zhang J. 2004. Bioconductor: open software development for computational biology and bioinformatics. *Genome Biol* 5:R80. <https://doi.org/10.1186/gb-2004-5-10-r80>.
169. Robinson MD, McCarthy DJ, Smyth GK. 2010. edgeR: a Bioconductor package for differential expression analysis of digital gene expression data. *Bioinformatics* 26:139–140. <https://doi.org/10.1093/bioinformatics/btp616>.
170. R Core Team. 2017. R: a language and environment for statistical computing. R Foundation for Statistical Computing, Vienna, Austria.
171. Robinson MD, Oshlack A. 2010. A scaling normalization method for differential expression analysis of RNA-seq data. *Genome Biol* 11:R25. <https://doi.org/10.1186/gb-2010-11-3-r25>.
172. Rapaport F, Khanin R, Liang Y, Pirun M, Krek A, Zumbo P, Mason CE, Socci ND, Betel D. 2013. Comprehensive evaluation of differential gene expression analysis methods for RNA-seq data. *Genome Biol* 14:R95. <https://doi.org/10.1186/gb-2013-14-9-r95>.
173. Koppelman C-M, Aarsman MEG, Postmus J, Pas E, Muijsers AO, Scheffers D-J, Nanninga N, Den Blaauwen T. 2004. R174 of *Escherichia coli* FtsZ is involved in membrane interaction and protofilament bundling, and is essential for cell division. *Mol Microbiol* 51:645–657. <https://doi.org/10.1046/j.1365-2958.2003.03876.x>.
174. Schneider CA, Rasband WS, Eliceiri KW. 2012. NIH Image to ImageJ: 25 years of image analysis. *Nat Methods* 9:671–675. <https://doi.org/10.1038/nmeth.2089>.

Anaerobic sulfur oxidation underlies adaptation of a chemosynthetic symbiont to oxic-anoxic interfaces

Supplemental Materials and Methods

Paredes et al.

Sediment cores analysis. To determine the habitat and spatial distribution of *L. oneistus*, we used cores of 60 cm length and 60 mm diameter (UWITEC, Mondsee, Austria) connected to rhizon samplers of a diameter of 2.5 mm and mean pore size of 0.15 μm (Rhizosphere Research Products, Wageningen, Netherlands). This set up allowed the collection of sand and interstitial pore water (the nematode habitat) down to a depth of 30 cm. In total, nine sediment cores were collected in July 2017 at ~1 m depth from a sand bar off Carrie Bow Cay, Belize (16°48'11.01"N, 88°4'54.42"W).

Immediately after collection, the pore-water sulfide content ($\sum\text{H}_2\text{S}$, i.e. the sum of H_2S , HS^- and S^{2-}) was determined by the methylene-blue method [1]. In short, 670 μL of a 2% zinc acetate solution was mixed with 335 μL sample and subsequently 335 μL 0.5% *N,N*-dimethyl-*p*-phenylenediamine and 17 μL of 10% ferrous ammonium sulfate were added and incubated for 30 min in the dark. Surface seawater was used as a blank. Absorbance was measured at 670 nm and concentrations were quantified via calibration (measurement of $\sum\text{H}_2\text{S}$ standard solutions in the concentration range from 0 to 0.5 mM $\sum\text{H}_2\text{S}$). Samples for dissolved inorganic nitrogen (DIN: nitrate, nitrite, and ammonia) and dissolved organic carbon measurements (DOC) were stored and transported deep-frozen, and analyzed at the University of Vienna, Austria. Nitrate (NO_3^-) and nitrite (NO_2^-) concentrations were determined according to the Griess method [2] using VCl_3 [3], whereas the concentration of ammonium (NH_4^+) was measured according to Solórzano [4]. For the quantification of nitrate, nitrite, and ammonia, freshly prepared KNO_3 , NaNO_2 and NH_4Cl solutions ranging from 0 to 100 μM were used to create standard curves, respectively. Artificial seawater served as a blank (prepared according to [5]) and all measurements were performed in technical triplicates. DOC was measured using a Shimadzu TOC-LCPH analyzer equipped with an ASI-L autosampler. After first acidifying the sample (pH 2 to 3) with hydrochloric acid, synthetic air (carbon dioxide free gas) was bubbled for 90 seconds through the sample to eliminate the inorganic carbon component. Next, the remaining total organic carbon was determined. Thereupon, 100 μL sample were injected into the combustion tube, which was filled with an oxidation platinum standard catalyst and heated to 720°C. The resulting combustion products were subsequently dehydrated, cooled and cleaned from chlorine and other halogens. Carbon dioxide was finally detected on a non-dispersive infrared (NDIR) gas analyzer. Each measurement constituted the mean from three 100 μL sample injections.

To determine the abundance of *L. oneistus*, the sand core was subdivided into 6 cm-thick layers and nematode were extracted from each sand layer by stirring the sand in seawater and pouring the supernatant through a 212 μm -mesh sieve. The retained material was transferred into a Petri dish, and single nematodes were handpicked using pipettes under a dissecting microscope. The number of *L. oneistus* nematodes and average $\Sigma\text{H}_2\text{S}$, nitrate and nitrite concentrations are shown in Figure 1A and Table S1. All measurement data are listed in Table S1.

Raman microspectroscopy. Three individual nematodes per EA-IRMS incubation (see Table S2B for O_2 and H_2S measurements at the beginning and at the end of the incubations), and an additional incubation under anoxic conditions without supplemented sulfide (0 μM of O_2 and H_2S at T0 h and T24 h), were fixed and stored in 0.1 M Trump's fixative solution (0.1 M sodium cacodylate buffer, 2.5% GA, 2% PFA, pH 7.2, 1 000 mOsm L^{-1}) [6]), and washed three times for 10 min in 1x PBS (137 mM NaCl, 2.7 mM KCl, 10 mM Na_2HPO_4 , 1.8 mM KH_2PO_4 , pH 7.4) before their ectosymbionts were dissociated by sonication for 40 s in 10 μl 1x PBS. 1 μl of each bacterial suspension was spotted on an aluminum-coated glass slide and measured with a LabRAM HR Evolution Raman microspectroscope (Horiba, Kyoto, Japan). 50 individual single-cell spectra were measured from each sample. All spectra were aligned by the phenylalanine peak, baselined using the Sensitive Nonlinear Iterative Peak (SNIP) algorithm of the R package "Peaks" (<https://www.rdocumentation.org/packages/Peaks/versions/0.2>), and normalized by total spectrum intensity. For calculating the relative sulfur content, the average intensity value for 212-229 wavenumbers (S_8 peak) was divided by the average intensity of the adjacent flat region of 231-248 wavenumbers. For calculating the relative polyhydroxyalkanoate (PHA) content, the average intensity value for 1 723-1 758 wavenumbers (PHA peak) was divided by the average intensity of the adjacent flat region of 1 759-1 793 wavenumbers [7]. Median relative sulfur and PHA content (shown as relative Raman intensities) were calculated treating all individual symbiont cells per condition as replicates (Figure S1B). Statistically significant differences were determined by applying the non-parametric Kruskal-Wallis test, followed by Dunn post-hoc test for multiple pairwise comparisons.

Nanometer scale secondary ion mass spectrometry (NanoSIMS). NanoSIMS analysis was performed to visualize and quantify the distribution and incorporation of the ^{13}C label into ectosymbiont and host biomass incubated in anoxic conditions without supplemented sulfide. The experimental set up of the incubations was identical with the incubations for EA-IRMS bulk analysis (see main Material and Methods), with the difference that here, we utilized batches of 30 worms in duplicates, and one replicate of 50 worms per incubation was used for EA-IRMS to verify the incorporation of the ^{13}C isotope prior to TEM/NanoSIMS sample preparation. EA-IRMS measurement values ($\delta^{13}\text{C}$) for the ^{13}C -live, ^{13}C -dead and ^{12}C -live incubations were 403.9, -3.71,

and -15.2 %, respectively. At the end of each incubation (24 h), the symbiotic nematodes were fixed and stored in 0.1 M Trump's fixative solution [6], at 4°C until further processing.

To obtain simultaneous information on the isotopic distribution and the site of incorporation, consecutive resin sections for TEM/NanoSIMS analysis were prepared as follows: the fixed samples were washed three times with sodium cacodylate buffer (0.1 M, pH 7.2, 1 000 mOsm L⁻¹), each for 10 min at room temperature (RT). Subsequently, the washing buffer was removed, and the samples were incubated in a solution of 1% osmium tetroxide for 1.5 h at RT in a shaker of low speed. Afterwards, the samples were rinsed two times with milli-Q water, each for 10 min at RT, and dehydrated stepwise by application of a concentration series of ethanol. The series consisted of 10 min incubations in 30%, 50%, 70% and 90% ethanol completed by three times 5 min incubations in 100% ethanol. Subsequently, ethanol was substituted by acetone via three times 10 min incubations in 100% acetone. Simultaneously, a fresh mixture of low viscosity resin was prepared (for 100 ml: 48 g LV resin, 8 g VH1 hardener, 44 g VH2 hardener, 2.5 g accelerator; Electron Microscopy Science). The dehydrated samples were then infiltrated stepwise by application of a resin/acetone concentration series: (i) 1:2 resin:acetone mixture for 15 min, (ii) 1:1 resin:acetone mixture for 30 min, (iii) 2:1 resin:acetone mixture for 2 h 30 min, and (iv) 100% resin for 1 h. The final step was conducted inside a vacuum desiccator. Samples were then polymerized in a laboratory oven at 60°C for 48 h. From the obtained resin blocks, thick sections (1-2 µm) were cut by a Leica Ultracut UCT microtome to assess the quality of the embedded samples and to identify appropriate regions for TEM/NanoSIMS analysis. Subsequently, consecutive sections of 70 nm (ultra-thin) and 120 nm (semi-thin) thickness were prepared using a Leica Ultracut UCT microtome and equipped with a diamond knife (Diatome, Bern, Switzerland). The ultra-thin sections (for TEM) were deposited onto previously coated (0.5% formvar solution) slot grids, and stained with 2.5% gadolinium acetate for 25 min, followed by staining with 3% lead citrate for 8 min. After each staining step, the samples were cleaned by gently dipping into milli-Q water for ten times. TEM imaging was conducted on a Zeiss Libra 120 transmission electron microscope (Carl Zeiss AG, Oberkochen, Germany). The semi-thin sections (for NanoSIMS) were deposited onto antimony-doped silicon wafer platelets (7.1 x 7.1 x 0.7 mm; Active Business Company, Brunnthal, Germany) and analyzed on a NS 50L instrument (Cameca, Gennevilliers, France).

NanoSIMS data were recorded as multilayer image stacks by sequential scanning of a finely focused Cs⁺ primary ion beam (approx. 80 nm probe size at 2 pA beam current) and simultaneous detection of negative secondary ions and secondary electrons. Recorded images had a 512 × 512 pixel resolution and a field-of-view ranging from 30 × 30 to 60 × 60 µm². The mass spectrometer was tuned for achieving a mass resolving power of > 10 000 at mass 26 to separate ¹²C¹⁴N⁻ secondary ions from the isobaric species ¹³C₂⁻. Prior to data acquisition, analysis areas were pre-conditioned *in situ* by rastering of a high intensity, defocused Cs⁺ ion beam in the following

sequence of high and extreme low ion impact energies (HE / 16 keV and EXLIE / 50 eV, respectively): HE at 100 pA beam current to a fluence of 5.0E14 ions/cm²; EXLIE at 400 pA beam current to a fluence of 5.0E16 ions/cm²; HE at 100 pA to a fluence of 2.5E14 ions/cm². All images were recorded at a dwell time of 7.5 – 15 ms/pixel/cycle. Secondary ion signal intensities were corrected for detector dead time and quasi-simultaneous arrival (QSA) of secondary ions, using QSA sensitivity factors (“beta” values) of 1.10 for C⁻ and 1.05 for CN⁻ ions. Image data were evaluated using the WinImage software package v2.0.8 provided by Cameca. The carbon isotope composition is displayed as ¹³C/(¹²C + ¹³C) isotope fraction, given in at%, calculated from C₂⁻ secondary ion signal intensities via $\frac{^{13}\text{C}}{(^{12}\text{C} + ^{13}\text{C})} = \frac{^{12}\text{C}^{13}\text{C}^-}{(2 \cdot ^{12}\text{C}^{12}\text{C}^- + ^{12}\text{C}^{13}\text{C}^-)}$. Numerical data evaluation was performed on manually defined regions of interest (ROI). Individual ROI values from samples of the ¹³C-live incubations were considered significantly enriched in ¹³C if (i) the ¹³C isotope fraction was above the 95th percent confidence interval of the corresponding ROI values determined on the negative control samples (i.e. ¹²C-live and ¹³C-dead: natural isotope abundance control and dead control, respectively) and (ii) the statistical counting error (5σ, Poisson) was smaller than the difference between the considered ROI and the mean value measured on each control.

Preparation of *Ca. T. oneisti* pellets for proteomics. 500 symbiotic *Laxus oneistus* were extracted from the sand as described in the main Materials & Methods, and incubated for 24 h in 13 ml of 0.2 μm filtered seawater in exetainers either in the presence of oxygen (mean concentration of dissolved oxygen at incubation start was 195.9 μM, and 183 μM after 24 h) or in anoxic conditions (O₂ was detected neither at incubation start, nor after 24 h; no sulfide was added). After the incubations, *Ca. T. oneisti* was dissociated from the nematodes by incubating each batch of 500 nematodes in 2 ml ddH₂O for 1 min, then transferring them to 2 ml 0.2 μM-filtered seawater for 5 min. This osmotic shock causes *Ca. T. oneisti* to detach from the nematodes and move into the seawater, which was collected with a pipette under the dissecting microscope to exclude involuntary aspiration of nematode tissue (or fragments thereof). The 2 ml nematode-free, ectosymbiont suspension was then centrifuged for 1 min at 14 000 x g to obtain *Ca. T. oneisti* pellets. Ectosymbiont pellets and aposymbiotic nematodes were flash-frozen in liquid nitrogen and stored at -80°C until further processing. Only *Ca. T. oneisti* proteomic data are shown in this study. *L. oneistus* proteomics will be published separately.

Protein extraction and 1D PAGE. *Ca. T. oneisti* proteins were extracted as described previously [8]. Briefly, both samples, i.e. frozen ectosymbiont cell pellets from oxic and anoxic incubations, were resuspended in 1% (w/v) sodium deoxycholate (SDC), 4% (w/v) sodium dodecyl sulfate (SDS) in 50 mM triethylammonium bicarbonate buffer (lysis buffer). After boiling the samples for 5 min under agitation (600 rpm), they were incubated in an ultrasonic bath for 5 min at RT. After removal of cell debris by a 10 min centrifugation at RT (14 000 x g), protein

concentrations in the supernatants were determined using the Pierce BCA (bicinchoninic acid) assay (Thermo Scientific Pierce, Waltham, MA, USA) according to the manufacturer's instructions in a Tecan microtiter plate reader. For gel-based proteomic analysis (as previously described by [9]), 25 µg of protein per sample were mixed with loading buffer (2 % (w/v) SDS, 10 % glycerol, 12.5 mM dithiothreitol, 0.001 % (w/v) bromophenol blue in 0.06 M Tris-HCl) and separated in precast 4 – 20 % SDS mini gels (BioRad TGX). Per sample, three replicates (3 x 25 µg protein) were separated (giving a total of 6 samples). After staining with Coomassie Brilliant Blue, protein-containing gel lanes were excised and subdivided into 10 equal-sized pieces each, which were destained at 37 °C in 200 mM NH₄HCO₃ 30 % acetonitrile under agitation at 600 rpm and digested overnight at 37 °C with trypsin (sequencing grade; Promega, Madison, WI, USA). Finally, peptides were eluted in an ultrasonic bath and subjected to LC-MS/MS analysis.

LC-MS/MS analysis. Peptides were analyzed by reversed phase liquid chromatography (LC) electrospray ionization (ESI) MS/MS using an LTQ Orbitrap Velos (Thermo Fisher Scientific, Waltham, MA, USA) according to [10]. Briefly, in-house self-packed nano-LC columns (100 µm x 20 cm) containing reverse-phase C18 material (3 µm, ReproSil-Pur 120-AQ; Dr. Maisch GmbH, Ammerbuch-Entringen, Germany) were used to perform LC with an Easy-nLC1000 system (Thermo Fisher Scientific). The peptides were loaded with solvent A (0.1% acetic acid (v/v)). Subsequently, the peptides were eluted by a non-linear binary gradient of 80 minutes from 5% to 99% solvent B (0.1% acetic acid (v/v), 99.9% acetonitrile (v/v)) in solvent A at a constant flow rate of 300 nl/min. MS data were acquired in data-dependent MS/MS mode for the 20 most abundant precursor ions. After a full scan in the Orbitrap (m/z 300 – 1 700) with a resolution of 30 000 at m/z 400, ions were fragmented via collision-induced dissociation (CID) and recorded in the linear trap quadrupole LTQ analyzer.

Protein identification and quantification. For protein identification, a database was constructed, containing 18 364 *Laxus oneistus* host protein sequences (derived from a *de novo* assembled transcriptome; will be published separately), 5 169 *Ca. T. oneisti* protein sequences (JAAEFD000000000, see main Materials and Methods) and a set of 42 common laboratory contaminants. All sequences were reversed and appended to the database as decoys to allow for false-discovery rate (FDR) assessment. Mass spectra were searched against this target-decoy database using the Sorcerer SEQUEST algorithm (Sage-N Research) and filtered using Scaffold (version 4.8.4, <http://www.proteomesoftware.com>) applying the following thresholds: i) protein FDR and peptide FDR were set to 1% and ii) at least two unique peptides were required for a protein or protein group to be identified. Proteins were expressed if they were detected in at least two out of the three replicates in at least one condition. This way, 1 137 ectosymbiont proteins (22.0% of all predicted proteins in the database) were identified in total. [Data S1](#) indicates all detected proteins in the column “Proteome detection” (Column AB). Relative abundance of

identified proteins was calculated from total spectrum counts as normalized spectral abundance factor (%NSAF) values – giving the percentage of each protein relative to all proteins in the respective sample [11], and as %OrgNSAF, giving a protein's percentage relative to all ectosymbiont proteins in the respective sample [12]. As ectosymbiont protein identification rates varied substantially between oxic and anoxic samples, which may negatively affect comparability of relative abundances between samples, we included only such proteins in the final quantitation, which were detected under both conditions (824 proteins). This additional normalization step provided corrected %OrgNSAF values (%cOrgNSAF), which give a protein's percentage relative to all symbiont proteins that were expressed under both conditions. %cOrgNSAF values are listed in [Data S1](#) (columns AC and AD), and values are highlighted in yellow when the respective proteins were among the top 30 most abundant proteins.

Intact polar lipid extraction and analysis. Five batches of 100 freshly collected *Laxus oneistus* were incubated for 24 h in oxic or anoxic (no sulfide added) conditions as described in the main Materials and Methods (RNA-Seq incubations). At the beginning of the incubations, mean concentrations of dissolved oxygen in the 0.2 µm filtered seawater were 180.9 µM (oxic) and 0.47 µM (anoxic). After 24 h, we measured on average 86 µM (oxic) and 0 µM (anoxic) oxygen, respectively. Sulfide ($\Sigma\text{H}_2\text{S}$) could not be detected in any of the incubations. At the end of the incubations, *Ca. T. oneisti* (from either the oxic or anoxic conditions) were dissociated from 500 nematodes, as described above (Proteomics). Symbiont pellets were flash-frozen in liquid nitrogen and stored at -80°C until further processing.

Lipids of the ectosymbionts were extracted using a modified Folch extraction [13] previously applied for lipid extraction from bacteria [14]. Briefly, pelleted bacteria were taken up in 1.6 ml 0.2 µm filtered seawater and 0.5 ml were transferred to 2 ml glass vials obtaining three analytical replicates. Bacteria were then pelleted by centrifugation, resuspended in 0.5 ml methanol and extracted using chloroform-methanol (all solvents LC-MS grade, Sigma-Aldrich, St. Louis, MS, USA). Extracted lipids were dried under nitrogen gas on a Techne Sample Concentrator and re-suspended in 1 ml of acetonitrile: 10 mM ammonium acetate at a 95:5 (v:v) ratio. Samples were analyzed by liquid chromatography mass spectrometry (LC-MS) as follows: lipids were separated on a Dionex UltiMate 3000RS UHPLC (Thermo Fisher Scientific) equipped with a XBridge BEH amide XP column (Waters, Milford, MA, USA) and coupled to an amaZon SL quadrupole ion trap MS (Bruker, Billerica, MA, USA) for detection. The column was maintained at 30°C with a flow rate of 150 µl min⁻¹. Samples were separated by a 15 min gradient from 95% (v:v) acetonitrile (Solvent A) to 30% (w:v) 10 mM ammonium acetate (pH 9.2, Solvent B) with 10 min equilibration between samples. Sample analysis was carried out in both positive and negative ion mode and fragmentation performed by the autoMSⁿ function in Compass HyStar (Bruker, Bremen, Germany). We used the Bruker Compass software package for lipid data

analysis: DataAnalysis for peak detection and lipid identification, and QuantAnalysis for quantification of the relative abundances of lipids. Peak integration was manually corrected where necessary. Consecutively, for data normalization the peak area of each lipid was divided by the sum of the peak areas of all detected lipids in each sample. Statistical analysis of significant differences in ectosymbiont lipids between the anoxic and oxic condition was carried out using a Student's t-test.

RuBisCO phylogenetic tree. Amino acid sequences of the RuBisCO forms I-IV were obtained from GenBank and SwissProt databases, and aligned using mafft v7.397 [15]. Please note that the accession numbers are provided next to the names of the organisms (Figure S4). Misaligned sequences were manually inspected. Gaps in more than 70% of the sequences were removed using TrimAl 1.4.rev15 [16]. The maximum-likelihood tree with SH-aLRT support values (10 000 replicates) was inferred using IQ-TREE v1.6.2 with automatic model selection [17, 18].

Data availability. The proteomics raw data and the combined *L. oneistus* host and ectosymbiont database used for proteomic analyses have been deposited to the ProteomeXchange Consortium via the PRIDE [19] partner repository with the data set identifier PXD017709.

Data Set S1 is available online <https://doi.org/10.1128/mSystems.01186-20>

Supplemental References

1. Cline JD. Spectrophotometric determination of hydrogen sulfide in natural waters. *Limnol Oceanogr* 1969; **14**: 454–458.
2. Green LC, Wagner DA, Glogowski J, Skipper PL, Wishnok JS, Tannenbaum SR. Analysis of nitrate, nitrite, and [15N]nitrate in biological fluids. *Anal Biochem* 1982; **126**: 131–138.
3. Schnetger B, Lehnert C. Determination of nitrate plus nitrite in small volume marine water samples using vanadium(III)chloride as a reduction agent. *Mar Chem* 2014; **160**: 91–98.
4. Solórzano L. Determination of ammonia in natural waters by the phenylhypochlorite method. *Limnol Oceanogr* 1969; **14**: 799–801.
5. Kester DR, Duedall IW, Connors DN, Pytkowicz RM. Preparation of artificial seawater. *Limnol Oceanogr* 1967; **12**: 176–179.
6. Trump BF, Ericsson JL. The effect of the fixative solution on the ultrastructure of cells and tissues. A comparative analysis with particular attention to the proximal convoluted tubule of the rat kidney. *Lab Invest* 1965; **14**: 1245–1323.
7. Samek O, Obruča S, Šiler M, Sedláček P, Benešová P, Kučera D, et al. Quantitative Raman spectroscopy analysis of polyhydroxyalkanoates produced by *Cupriavidus necator* H16. *Sensors* 2016; **16**:1808.
8. Hinzke T, Markert S. Efficient protein extraction for proteomics and metaproteomics (also suitable

251 for low biomass samples). *Protocols.io*. 2017; **10**, kg6ctze.

252 9. Ponnudurai R, Kleiner M, Sayavedra L, Petersen JM, Moche M, Otto A, et al. Metabolic and
 253 physiological interdependencies in the *Bathymodiolus azoricus* symbiosis. *ISME J* 2017; **11**: 463–
 254 477.

255 10. Chambers MC, MacLean B, Burke R, Amodei D, Ruderman DL, Neumann S, et al. A cross-
 256 platform toolkit for mass spectrometry and proteomics. *Nat Biotechnol* 2012; **30**: 918–920.

257 11. Florens L, Carozza MJ, Swanson SK, Fournier M, Coleman MK, Workman JL, et al. Analyzing
 258 chromatin remodeling complexes using shotgun proteomics and normalized spectral abundance
 259 factors. *Methods* 2006; **40**: 303–311.

260 12. Mueller RS, Denev VJ, Kalnejais LH, Suttle KB, Thomas BC, Wilmes P, et al. Ecological
 261 distribution and population physiology defined by proteomics in a natural microbial community.
 262 *Mol Syst Biol* 2010; **6**.

263 13. Folch J, Lees M, Sloane Stanley GH. A simple method for the isolation and purification of total
 264 lipides from animal tissues. *J Biol Chem* 1957; **226**: 497–509.

265 14. Smith AF, Rihtman B, Stirrup R, Silvano E, Mausz MA, Scanlan DJ, et al. Elucidation of
 266 glutamine lipid biosynthesis in marine bacteria reveals its importance under phosphorus deplete
 267 growth in Rhodobacteraceae. *ISME J* 2019; **13**: 39–49.

268 15. Katoh K, Standley DM. MAFFT Multiple Sequence Alignment Software Version 7:
 269 Improvements in Performance and Usability. *Mol Biol Evol* 2013; **30**: 772–780.

270 16. Capella-Gutiérrez S, Silla-Martínez JM, Gabaldón T. trimAl: a tool for automated alignment
 271 trimming in large-scale phylogenetic analyses. *Bioinformatics* 2009; **25**: 1972–3.

272 17. Nguyen L-T, Schmidt HA, von Haeseler A, Minh BQ. IQ-TREE: A Fast and Effective Stochastic
 273 Algorithm for Estimating Maximum-Likelihood Phylogenies. *Mol Biol Evol* 2015; **32**: 268–274.

274 18. Kalyaanamoorthy S, Minh BQ, Wong TKF, Von Haeseler A, Jermini LS. ModelFinder: Fast
 275 model selection for accurate phylogenetic estimates. *Nat Methods* 2017; **14**: 587–589.

276 19. Vizcaino JA, Côté RG, Csordas A, Dienes JA, Fabregat A, Foster JM, et al. The Proteomics
 277 Identifications (PRIDE) database and associated tools: Status in 2013. *Nucleic Acids Res* 2013;
 278 **41**.

Anaerobic sulfur oxidation underlies adaptation of a chemosynthetic symbiont to oxic-anoxic interfaces

Supplemental Legends

Paredes et al.

FIG S1

Gene expression heatmaps for sulfur oxidation and denitrification including the anoxic condition without sulfide. (A) Centered expression values ($\log_2\text{TPM}$) of all genes that were differentially expressed between at least two conditions are shown, with genes that were differentially expressed between the AS and O conditions, as well as the A and O conditions, in bold (twofold change, $\text{FDR} \leq 0.05$). Genes are ordered by function in the respective metabolic pathways. Note that the expression of many of the genes follows a clear pattern depending on whether oxygen is present or not. (B) Relative elemental sulfur (S_0) content in ectosymbionts as determined by Raman microspectroscopy after 24-h incubations under anoxic-sulfidic (AS, red dots), hypoxic (H, light blue dots), oxic (Ox, dark blue dots), and anoxic without added sulfide (A, orange dots) conditions. Each dot refers to the value obtained from measuring an individual ectosymbiont cell. Fifty cells were measured per condition. Horizontal lines display medians, boxes show the interquartile ranges (25 to 75%), whiskers indicate minimum and maximum values, and different lowercase letters indicate significant differences among conditions (Kruskal-Wallis test and Dunn *post hoc* test for multiple pairwise comparisons; P [AS versus A] = $3.5\text{E}-17$, P [AS versus hypoxic] = 0.011, P [AS versus oxic] = $7.4\text{E}-13$, P [A versus hypoxic] = $3.2\text{E}-09$, P [A versus oxic] = 0.188, P [hypoxic versus oxic] = $3.6\text{E}-06$). Relative intensities below 1 (gray dashed line) indicate that elemental sulfur could not be detected. Percentage of cells with sulfur detected: 92% (AS), 16% (A), 76% (hypoxic), and 28% (oxic). For details on methodology, see Text S1.

FIG S2

lipid composition of ectosymbionts after incubation of symbiotic nematodes under anoxic and oxic conditions. (A) Major lipid classes and their abundance relative to all lipids detected. (B) Relative abundance of significantly changed glycerophospholipids. Lipid class, fatty acid chain length, and saturation are depicted on the x axis. Note that PG is composed of two fatty acids, while lysophospholipids (LPG, LPE, and LPC) contain only one fatty acid. Bars show mean abundances relative to total lipids (%) and their standard deviations derived from three analytical replicates. The number of asterisks refers to the

significance level (Student's *t* test; *, $P < 0.05$; **, $P < 0.01$; ***, $P < 0.001$). Note that “*Ca. T. oneisti*” does not encode any known phosphatidylcholine biosynthesis genes. PG, phosphatidylglycerol; LPG, lysophosphatidylglycerol; LPE, lysophosphatidylethanolamine; LPC, lysophosphatidylcholine. For details on methodology see Text S1.

FIG S3

anoSIMS analysis of ^{13}C isotope incorporation in *L. oneistus* and its ectosymbiont after incubation in ^{13}C -labeled bicarbonate for 24 h under anoxic conditions without sulfide. The ^{13}C content is displayed as $^{13}\text{C}/(^{12}\text{C} + ^{13}\text{C})$ isotope fraction, given in atom%. (A) NanoSIMS images showing cellular ultrastructure, as displayed by the $^{12}\text{C}^{14}\text{N}$ - secondary ion signal intensity (left) and isotope label distribution (right) in cross sections of *L. oneistus* after incubation of living worms in isotopically labeled (^{13}C -live, top row) and unlabeled (^{12}C -live, bottom row) bicarbonate. Incubation of 2% PFA-fixed worms under identical conditions in isotopically labeled bicarbonate (^{13}C -dead, central row) served as a control for exclusion of unspecific (nonmetabolic) label uptake. Bars, 5 μm . (B) Region of interest (ROI)-specific evaluation of the isotopic label content, revealing significant ^{13}C enrichment both in the ectosymbiont cells and, within particular regions, also in the host tissue. For details on methodology, see Text S1.

FIG S4

hylogenetic tree of the large subunit protein of the ribulose-1,5-bisphosphate carboxylase/oxygenase (RuBisCO). Unrooted phylogenetic tree illustrating the four forms of RuBisCO from diverse organisms, such as plants and free-living and symbiotic bacteria. The CbbL protein of “*Ca. T. oneisti*” is highlighted in red. Type I (IA, IB, IC, ID), CbbL; type II, CbbM, type III; type IV, RuBisCO-like. The analysis is based on a MAFFT alignment of full-length amino acid sequences (accession numbers are provided next to the names of the organisms) and was estimated under the LG+I+G4 model using maximum likelihood phylogeny (IQ-TREE) with node support calculated by SH-aLRT. The scale bar represents 0.5% estimated sequence divergence. SH-aLRT values at the nodes are based on 10,000 replicates. For details on methodology, see Text S1.

FIG S5

Differentially expressed genes involved in biosynthesis and utilization of storage compounds and detection of PHA via Raman spectroscopy. (A) Only differentially expressed genes involved in PHA and trehalose metabolism are shown (2-fold change, $\text{FDR} \leq 0.05$). (B) Relative PHA content measurement of 50 ectosymbiont cells per condition after 24 h of incubation analyzed by Raman spectroscopy. Horizontal lines indicate medians, boxes show interquartile ranges (25 to 75%), and whiskers denote minimum and

maximum measurements. Each dot represents a single ectosymbiont cell. PHA was detected in all cells and conditions, although more PHA was detected in cells incubated in hypoxic incubations ($P < 0.05$; Kruskal Wallis test, followed by Dunn's multiple-pairwise-comparison test; P [AS versus hypoxic] = 0.022, P [AS versus oxic] = 0.057, P [hypoxic versus oxic] = 0.054). Different lowercase letters indicate significant differences among conditions. For details on methodology, see Text S1. AS, anoxic-sulfidic incubation; H, hypoxic incubation; Ox, oxic incubation.

TABLE S1

Sediment core nematode counts and chemical measurements.

TABLE S2

(A) RNA-Seq and (B) EA-IRMS incubation measurements. Replicates in bold were specifically used for Raman microspectroscopy (for further details, see Text S1) and for the assessment of the percentage of dividing cells, and thus, they were not used for EA-IRMS analysis. Each replicate consisted of a 50-worm batch. Note that RNA-Seq and EA-IRMS incubations were performed separately. Samples 1 to 3 were collected in July 2017, whereas samples 4 to 6 were collected in March 2019. T0, start of the incubation; T24, after 24 h of incubation; $\delta^{13}\text{C}$, per mille (‰)

TABLE S3

A) RNA sequencing and mapping statistics. Sequencing reads were mapped to the symbiont genome assembly consisting of 401 contigs and 5,169 protein-coding genes. The total number of reads refers to the number of reads after quality filtering and trimming, and the number of reads mapped to the genome (i.e., genes, intergenic regions, and antisense regions) includes only uniquely mapped reads. (B) Functional enrichments of selected gene sets. Statistical enrichment of functional categories was tested for GO terms (GO), Pfam domains (PF), KEGG metabolic maps (map), COG category (COG), and COG general category (uppercase letter) using the Bioconductor software package Goseq (M. D. Young, M. J. Wakefield, G. K. Smyth, and A. Oshlack, *Genome Biol* 11(2):R14, 2010, <https://doi.org/10.1186/gb-2010-11-2-r14>). Functional categories among sets of protein-coding genes were significantly enriched if the adjusted P value (false-discovery rate [FDR]) was ≤ 0.1 . Only FDR values below that threshold are shown; nonsignificant FDR values are indicated (NS). AS, anoxic-sulfidic; O, hypoxic + oxic.

Figure S1

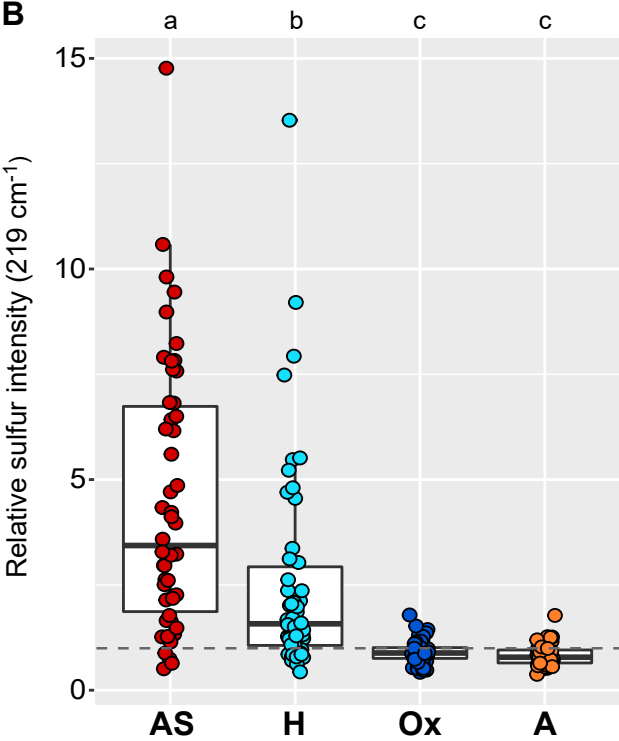
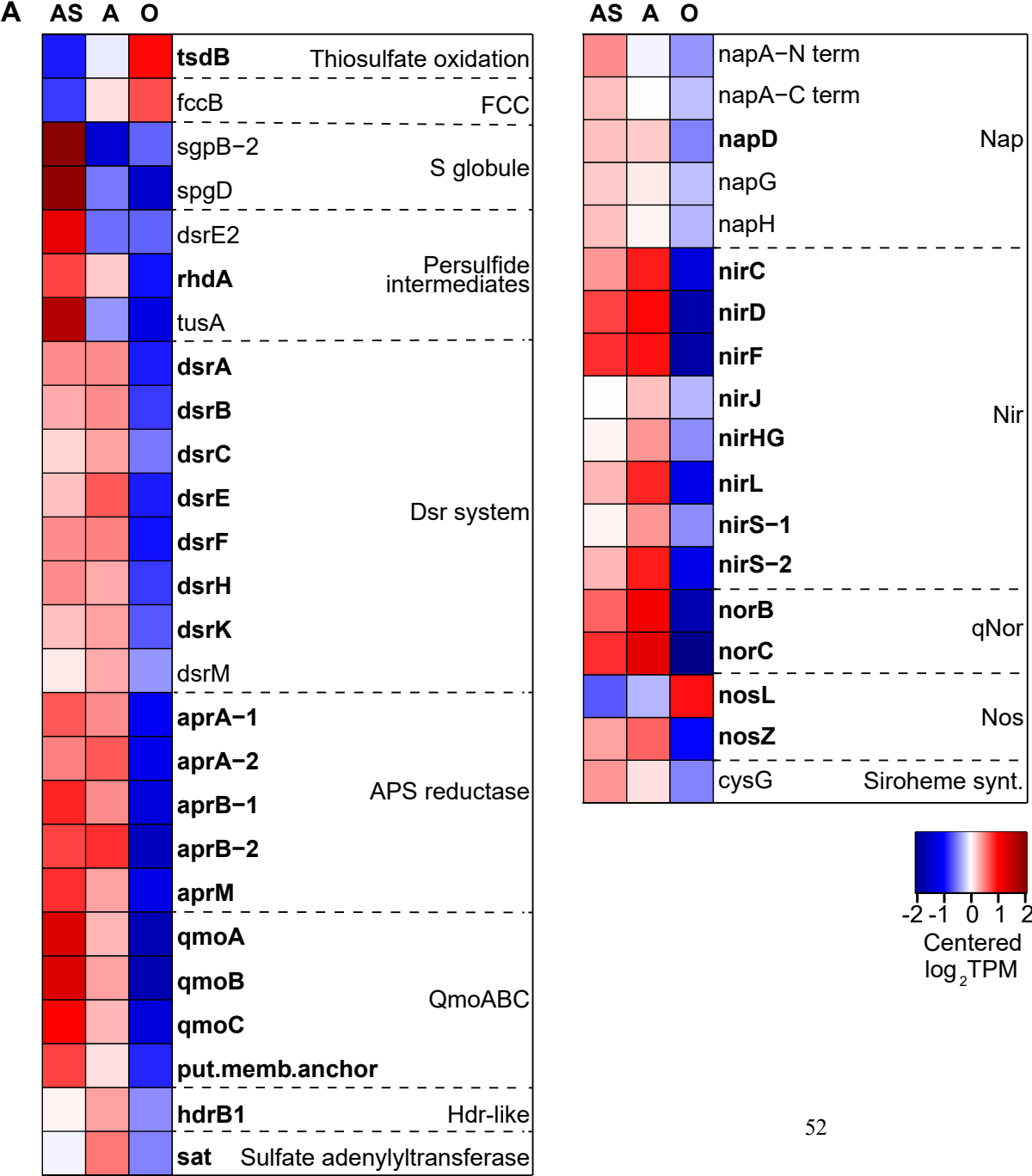
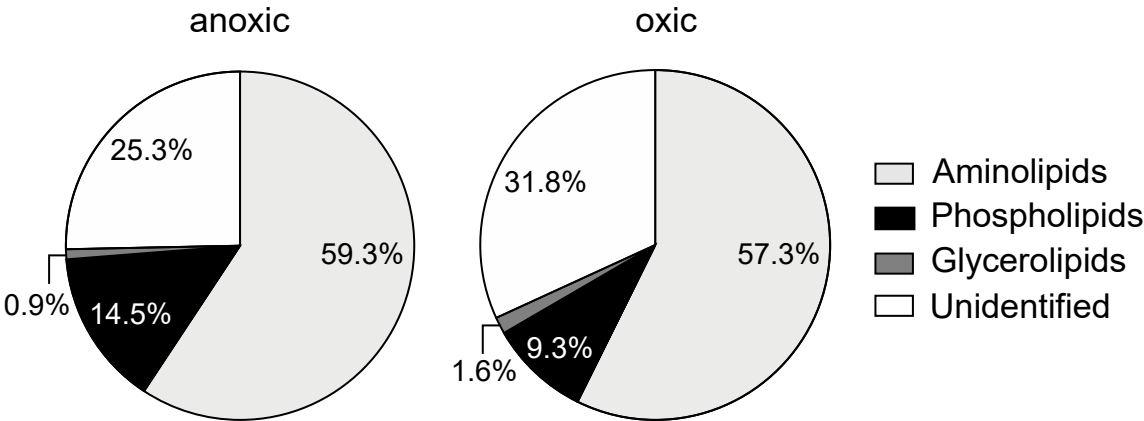


Figure S2

A



B

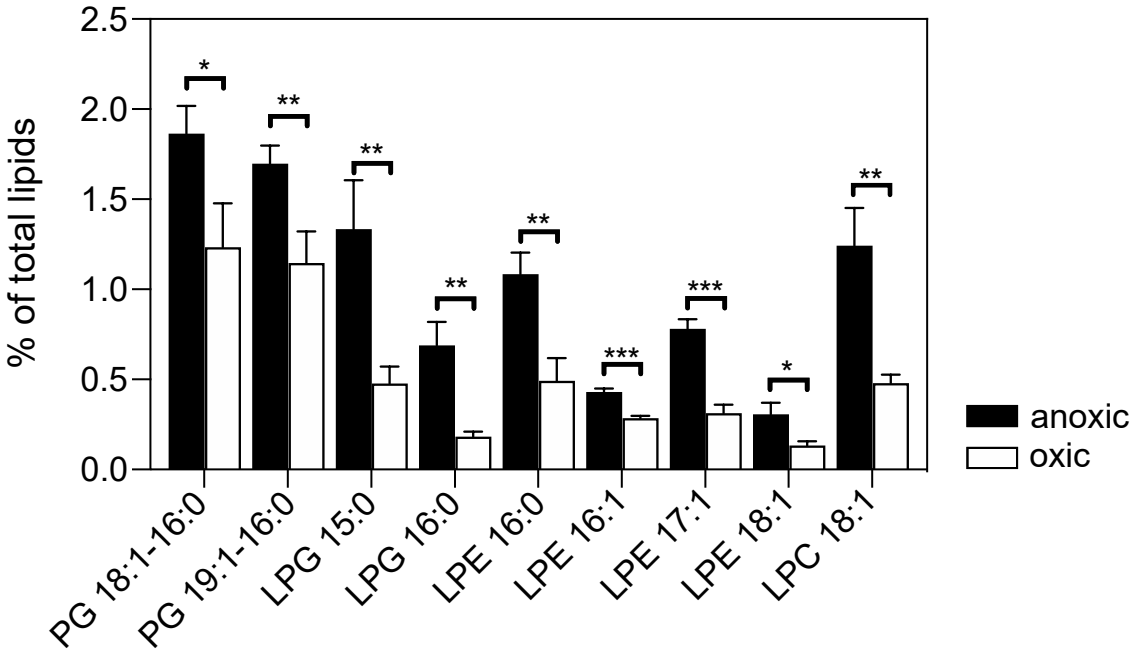
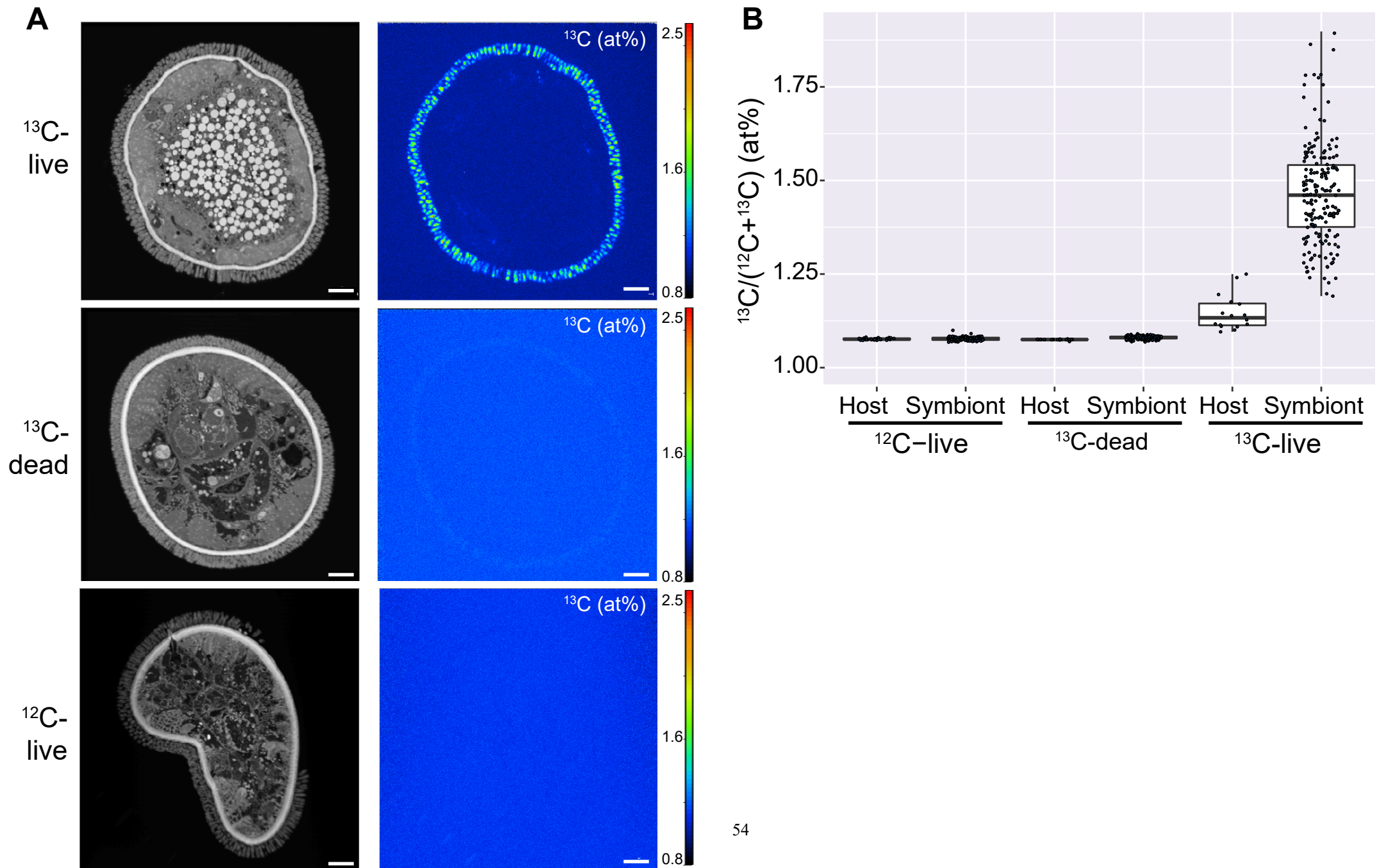


Figure S3



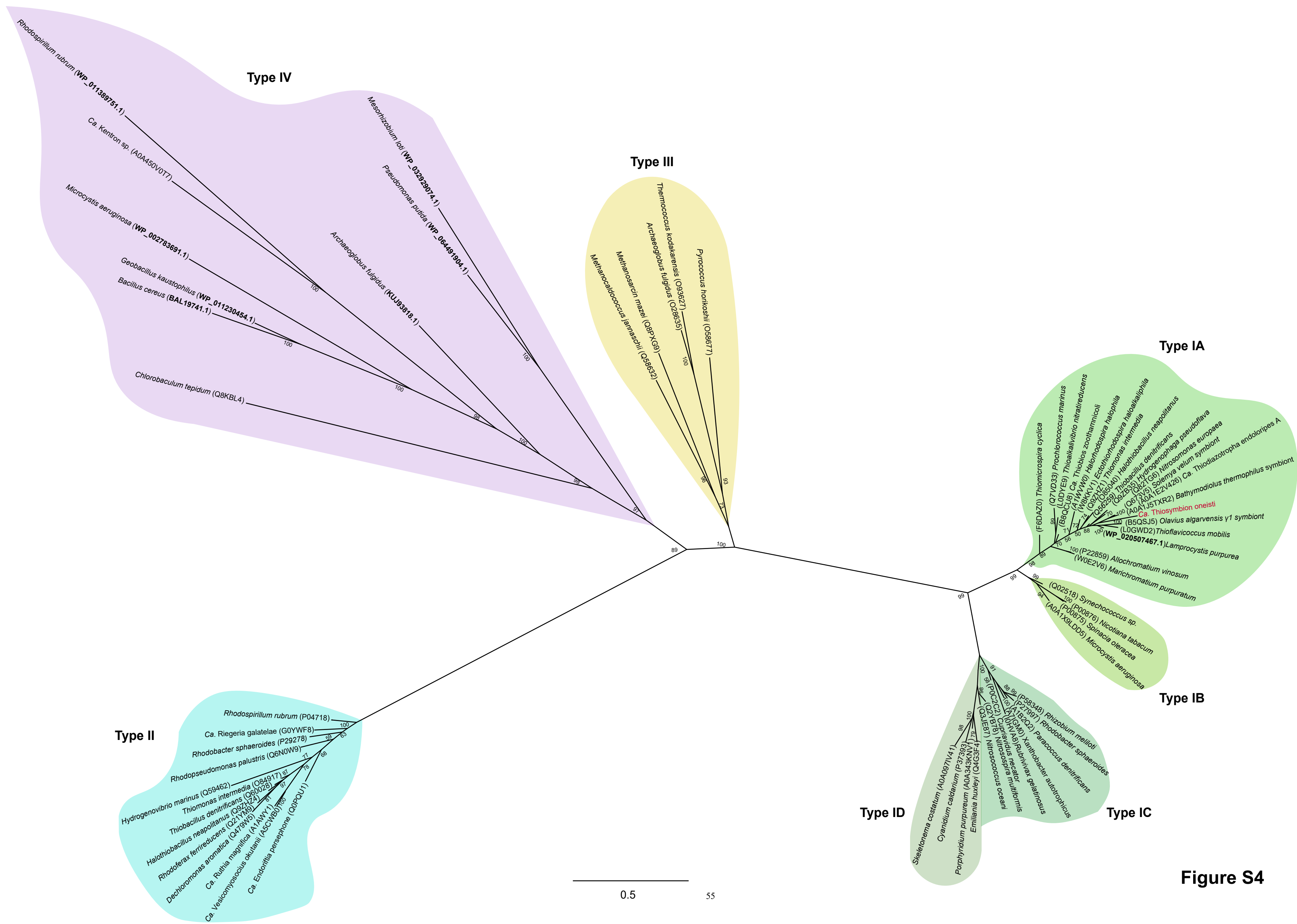


Figure S5

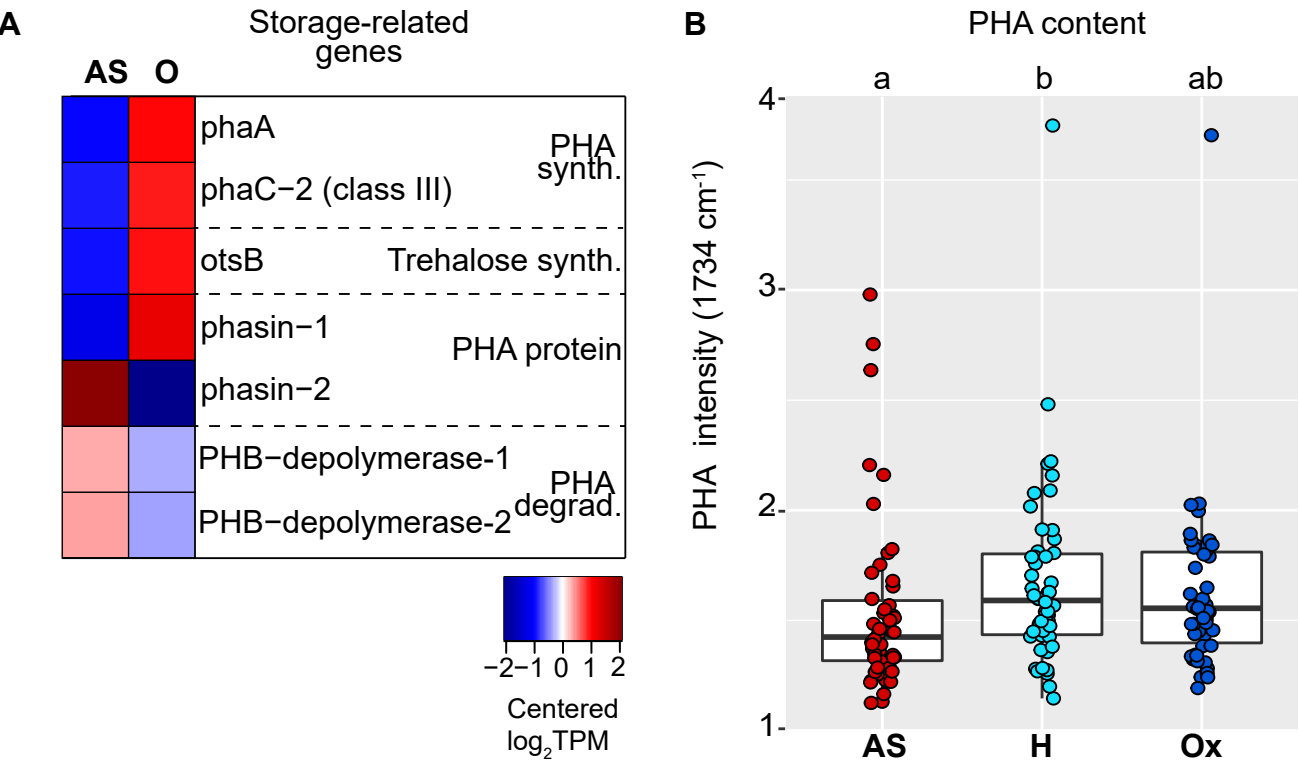


Table S1

Sediment core											
<i>L. oneistus</i> counts											
Depth (cmbsf)	A	B	C	D	E	F	G	H	I	Total	
0 to 6	0	3	1	4	1	0	1	0	0	10	
6 to 12	0	4	2	22	9	1	1	3	0	42	
12 to 18	15	8	6	13	31	6	3	20	5	107	
18 to 24	27	26	2	10	9	21	4	67	50	216	
24 to 31	ND	ND	12	ND	10	0	ND	ND	ND	22	
Relative <i>L. oneistus</i> abundance (%)											
Depth (cmbsf)	A	B	C	D	E	F	G	H	I	Mean	SE
0 to 6	0.00	7.32	4.35	8.16	1.67	0.00	11.11	0.00	0.00	3.62	1.35
6 to 12	0.00	9.76	8.70	44.90	15.00	3.57	11.11	3.33	0.00	10.71	4.34
12 to 18	35.71	19.51	26.09	26.53	51.67	21.43	33.33	22.22	9.09	27.29	3.78
18 to 24	64.29	63.41	8.70	20.41	15.00	75.00	44.44	74.44	90.91	50.73	9.37
24 to 31	ND	ND	52.17	ND	16.67	0.00	ND	ND	ND	22.95	12.56
$\Sigma\text{H}_2\text{S}$ (μM)											
Depth (cmbsf)	A	B	C	D	E	F	G	H	I	Mean	SE
0	0.63	0.00	0.00	0.85	0.00	0.00	ND	ND	ND	0.25	0.14
6	0.84	0.42	0.63	1.48	1.90	0.00	0.00	0.11	0.95	0.70	0.21
12	1.69	0.63	2.95	1.48	6.55	3.70	6.34	0.32	1.58	2.80	0.73
18	2.11	1.90	2.11	1.69	13.10	0.95	6.34	2.22	4.33	3.86	1.20
24	5.30	1.90	ND	1.90	22.82	1.80	14.58	15.11	6.23	8.70	2.60
31	ND	ND	4.75	ND	16.90	6.44	31.38	ND	ND	14.87	5.30
Ammonium (μM)											
Depth (cmbsf)	A	B	C	D	E	F	G	H	I	Mean	SE
0	ND	7.75	ND	ND	2.7	18.74	ND	ND	ND	9.73	3.87
6	ND	5.47	ND	ND	12.84	3.64	ND	ND	ND	7.32	2.30
12	ND	11.56	ND	ND	22.54	8.69	ND	ND	ND	14.26	3.45
18	ND	10.56	ND	ND	21.31	5.69	23.45	ND	ND	15.25	4.26
24	ND	29.73	ND	ND	20.44	13.95	20.28	ND	ND	21.11	2.81
31	ND	ND	ND	ND	5.33	11.7	37.34	ND	ND	18.12	7.99

Nitrate (μM)											
Depth (cmbsf)	A	B	C	D	E	F	G	H	I	Mean	SE
0	ND	ND	ND	ND	1.41	1.13	0.79	ND	ND	1.11	0.25
6	ND	0.00	ND	ND	0.29	ND	1.08	ND	ND	0.46	0.46
12	ND	ND	ND	ND	0.15	ND	0.33	ND	ND	0.24*	0.06*
18	ND	ND	ND	ND	0.00	ND	0.42	ND	ND	0.21*	0.14*
24	ND	ND	ND	ND	0.38	0.48	0.34	ND	ND	0.38	0.48
31	ND	ND	ND	ND	ND	ND	0.47	ND	ND	0.47*	NA
Nitrite (μM)											
Depth (cmbsf)	A	B	C	D	E	F	G	H	I	Mean	SE
0	ND	ND	ND	ND	0.08	0.09	0.07	ND	ND	0.08	0.01
6	ND	0.14	ND	ND	0.07	ND	0.07	ND	ND	0.09	0.02
12	ND	ND	ND	ND	0.03	ND	0.03	ND	ND	0.03*	0.0*
18	ND	ND	ND	ND	0.01	ND	0.02	ND	ND	0.015*	0.004*
24	ND	ND	ND	ND	0.04	0.18	0.00	ND	ND	0.07	0.05
31	ND	ND	ND	ND	ND	ND	0.07	ND	ND	0.07*	NA
DOC (mg/L)											
Depth (cmbsf)	A	B	C	D	E	F	G	H	I	Mean	SE
0	ND	ND	2.77	2.86	4.29	1.24	ND	6.52	2.38	3.34	0.75
6	ND	1.4	5.34	1.91	11.15	2.50	ND	ND	1.70	4.00	1.54
12	ND	ND	1.39	4.41	2.10	6.10	ND	1.99	16.44	5.41	2.32
18	ND	3.10	3.48	3.28	4.14	ND	ND	4.63	2.60	3.54	0.30
24	ND	5.56	4.75	4.53	1.42	9.51	ND	22.66	9.08	8.22	2.63
31	ND	ND	3.47	ND	1.78	20.40	ND	ND	ND	8.55	5.95

*: Measurements that were taken in fewer than 3 sediment cores due to technical problems and thus, means and SE were formed only to visualize the profile trends. Abbreviations: cmbsf, centimeter below seafloor; ND: not determined due to technical difficulties, SE: standard error of the mean, NA: not applicable due to just a single measurement.

Table S2**(A) RNA-Seq incubations**

Sample	O ₂ (μM)		H ₂ S (μM)	
	T0 h	T24 h	T0 h	T24 h
anoxic-sulfidic-1	0.0	0.0	11.0	7.0
anoxic-sulfidic-2	0.0	0.0	11.0	7.0
anoxic-sulfidic-3	0.0	0.0	11.0	7.0
anoxic-1	0.0	0.0	0.0	0.0
anoxic-2	0.0	0.0	0.0	0.0
anoxic-3	0.0	0.0	0.0	0.0
anoxic-4	0.0	0.0	0.0	0.0
anoxic-5	0.0	0.0	0.0	0.0
hypoxic-1	111.6	31.4	0.0	0.0
hypoxic-2	118.9	0.2	0.0	0.0
hypoxic-3	114.8	17.4	0.0	0.0
oxic-1	192.0	184.8	0.0	0.0
oxic-2	196.0	185.0	0.0	0.0
oxic-3	195.0	188.3	0.0	0.0
oxic-4	198.3	192.4	0.0	0.0
oxic-5	196.7	190.5	0.0	0.0
oxic-6	196.9	189.7	0.0	0.0

(B) EA-IRMS incubations

Sample	EA-IRMS Incubation	Replicates	Weight (mg)	$\delta^{13}\text{C}$	O_2 (μM)		H_2S (μM)	
					T0 h	T24 h	T0 h	T24 h
anoxic-sulfidic	^{13}C live nematodes	1	1.4	314.4	0	0	25	1.5
		2	1.1	345	0	0	25	0.8
		3	0.9	355.4	0	0	25	1.5
		4	1.2	286.7	0	0	25	1.2
		5	n.a.	n.a.	0	0	25	1.3
	^{13}C dead nematodes	1	1.1	-18.8	0	0	25	0.7
		2	0.8	-22.3	0	0	25	0.5
		3	0.9	-21.5	0	0	25	1.5
	^{12}C live nematodes	1	1.1	-23.8	0	0	25	1.3
		2	1.2	-24	0	0	25	1
		3	1.2	-24.5	0	0	25	0.7
		4	1	-25.8	0	0	25	0.9
hypoxic	^{13}C live nematodes	1	1.3	281.7	60	45	0	0
		2	1.2	414.2	60	45	0	0
		3	1	458.7	59	45	0	0
		4	n.a.	n.a.	60	45	0	0
	^{13}C dead nematodes	1	1.2	-22.2	59	42	0	0
		2	0.3	-21.9	54	45	0	0
		3	1.8	-21.5	61	44	0	0
	^{12}C live nematodes	1	1	-25	57	50	0	0
		2	1.7	-24.1	55	49	0	0
		3	1.4	-24.4	59	52	0	0
		4	1.4	-24.4	59	52	0	0
oxic	^{13}C live nematodes	1	1	232.9	197	119	0	0
		2	1.1	277.7	196	109	0	0
		3	1.4	238.3	196	111	0	0
		4	n.a.	n.a.	197	113	0	0

n.a.: not applicable

Table S3

(A) RNA sequencing and mapping statistics						
Samples	Total number of reads	Number of reads mapped to symbiont genome	Number of reads mapped to symbiont genes	% reads mapped to symbiont genome	% reads mapped to symbiont genes	% mapped to rRNA genes
oxic-1	39,788,652	935,582	571770	1.4	61.1	2.1
oxic-2	35,270,773	1,308,826	795913	2.3	60.8	1.6
oxic-3	40,645,573	1,140,752	680586	1.7	59.7	1.5
oxic-4	25,823,639	1,422,342	786363	3.0	55.3	1.9
oxic-5	36,002,778	1,401,873	757557	2.1	54.0	1.9
oxic-6	61,503,518	2,065,340	1178912	1.9	57.1	2.5
hypoxic-1	37,528,019	2,064,723	1328297	3.5	64.3	1.8
hypoxic-2	36,704,147	2,246,543	1430114	3.9	63.7	0.5
hypoxic-3	39,087,262	868,032	555176	1.4	64.0	1.0
anoxic-1	36,848,477	1,755,816	1180245	3.2	67.2	0.7
anoxic-2	36,720,206	1,767,472	1219640	3.3	69.0	0.8
anoxic-3	37,438,972	1,757,143	1153214	3.1	65.6	1.2
anoxic-4	57,013,563	1,816,539	971290	1.7	53.5	2.8
anoxic-5	41,002,474	1,738,244	1133192	2.8	65.2	2.7
anoxic-sulfidic-1	55,241,503	508,069	341801	0.6	67.3	2.8
anoxic-sulfidic-2	36,482,028	418,210	281620	0.8	67.3	2.1
anoxic-sulfidic-3	39,792,029	349,853	234535	0.6	67.0	2.5

(B) Functional enrichments of selected gene sets

		FDR (threshold 0.1)										
Category ID	Description	anoxic vs AS ¹		hypoxic vs oxic ¹		anoxic vs O ¹		AS vs O ¹		unchanged over 4 conditions ²		
		AS up n = 124	anoxic up n = 179	oxic up n = 111	hypoxic up n = 30	O up n = 433	anoxic up n = 366	O up n = 548	AS up n = 448	high n = 163	low n = 2184	medium n = 1128
C	Energy production and conversion	NS	NS	NS	NS	NS	2.9E-05	NS	2.4E-04	NS	NS	NS
O	Post-translational modification, protein turnover, and chaperones	NS	NS	NS	NS	0.009	NS	0.022	NS	0.085	NS	NS
J	Translation, ribosomal structure and biogenesis	NS	NS	NS	NS	NS	NS	NS	NS	0.018	NS	3.4E-05
P	Inorganic ion transport and metabolism	NS	NS	NS	NS	NS	0.015	NS	NS	NS	NS	NS
K	Transcription	NS	NS	NS	NS	NS	0.044	NS	NS	NS	NS	NS
M	Cell wall/membrane/envelope biogenesis	NS	NS	NS	NS	NS	NS	NS	NS	NS	NS	0.001
T	Signal transduction mechanisms	NS	NS	NS	NS	NS	NS	NS	NS	0.078	NS	NS
E	Amino acid transport and metabolism	NS	NS	NS	NS	NS	NS	0.087	NS	NS	NS	NS
H	Coenzyme transport and metabolism	NS	NS	NS	NS	NS	NS	0.087	NS	NS	NS	NS
map03010	Ribosome	NS	NS	NS	NS	NS	NS	NS	NS	0.019	NS	1.3E-05
map00710	Carbon fixation in photosynthetic organisms	NS	NS	NS	NS	NS	NS	NS	NS	NS	NS	0.021
map00920	Sulfur metabolism	NS	NS	NS	NS	NS	0.017	NS	0.066	NS	NS	NS
map00550	Peptidoglycan biosynthesis	NS	NS	NS	NS	NS	NS	NS	NS	NS	NS	0.044
map01230	Biosynthesis of amino acids	NS	NS	NS	NS	NS	NS	NS	NS	NS	NS	0.096
COG1053	Succinate dehydrogenase/fumarate reductase, flavoprotein subunit	NS	NS	NS	NS	NS	0.023	NS	0.051	NS	NS	NS

COG2010	Cytochrome C, mono- and diheme variants	NS	NS	NS	NS	NS	0.017	NS	0.046	NS	NS	NS
COG1708	Predicted nucleotidyltransferase	NS	NS	NS	NS	NS	0.045	NS	NS	NS	NS	NS
GO:0051912	CoB—CoM heterodisulfide reductase activity	0.041	NS	NS	NS	NS	0.021	NS	0.046	NS	NS	NS
GO:0020037	Heme binding	NS	NS	NS	NS	NS	0.001	NS	0.046	NS	NS	NS
GO:0015934	Large ribosomal subunit	NS	NS	NS	NS	NS	NS	NS	NS	NS	NS	0.007
GO:0005840	Ribosome	NS	NS	NS	NS	NS	NS	NS	NS	0.053	NS	0.047
GO:0019843	rRNA binding	NS	NS	NS	NS	NS	NS	NS	NS	NS	NS	9.0E-05
GO:0003735	Structural constituent of ribosome	NS	NS	NS	NS	NS	NS	NS	NS	0.018	NS	9.0E-05
GO:0006412	Translation	NS	NS	NS	NS	NS	NS	NS	NS	0.030	NS	9.0E-05
GO:0006508	Proteolysis	NS	NS	NS	NS	NS	NS	NS	NS	NS	NS	0.015
GO:0009055	Electron transfer activity	NS	NS	NS	NS	NS	0.081	NS	NS	NS	NS	NS
PF13442	Cytochrome C oxidase, cbb3-type, subunit III	NS	NS	NS	NS	NS	0.024	NS	0.087	NS	NS	NS
PF05168	HEPN domain	NS	NS	NS	NS	NS	0.023	NS	0.073	NS	NS	NS
PF13609	Gram-negative porin	NS	0.100	NS	NS	NS	NS	NS	NS	NS	NS	NS

¹ These gene sets only comprise genes that were differentially expressed between indicated conditions (FDR \leq 0.05, fold-change of 2).

² These gene sets comprise genes that were not significantly different between any of the four conditions (oxic, hypoxic, anoxic, and anoxic-sulfidic), and were furthermore, classified based on expression level (low, medium, high) over all four conditions based on hierarchical clustering with Euclidean distances.

CHAPTER III

Differential regulation of degradation and immune pathways underlies adaptation of the ectosymbiotic nematode *Laxus oneistus* to oxic-anoxic interfaces

Authors Gabriela F. Paredes, Tobias Viehboeck, Stephanie Markert, Michaela A. Mausz, Yui Sato, Manuel Liebeke, Lena König* and Silvia Bulgheresi*

*these authors contributed equally

Under *review* and available online at <https://doi.org/10.1101/2021.11.11.468236>

1 **Differential regulation of degradation and immune pathways underlies adaptation**
2 **of the ectosymbiotic nematode *Laxus oneistus* to oxic-anoxic interfaces**

3

4 Running title: Transcriptomics and proteomics of an ectosymbiotic marine nematode

5

6 Gabriela F. Paredes¹, Tobias Viehboeck^{1,5}, Stephanie Markert², Michaela A. Mausz³, Yui Sato⁴,
7 Manuel Liebeke⁴, Lena König^{1,#} and Silvia Bulgheresi^{1,#}

8

9 ¹ University of Vienna, Department of Functional and Evolutionary Ecology, Environmental Cell
10 Biology Group, Vienna, Austria

11 ² University of Greifswald, Institute of Pharmacy, Department of Pharmaceutical Biotechnology,
12 Greifswald, Germany

13 ³ University of Warwick, School of Life Sciences, Coventry, United Kingdom

14 ⁴ Max Planck Institute for Marine Microbiology, Bremen, Germany

15 ⁵ Division of Microbial Ecology, Center for Microbiology and Environmental Systems Science
16 University of Vienna, A-1090 Vienna, Austria

17

18 Address correspondence to Silvia Bulgheresi, silvia.bulgheresi@univie.ac.at.

19 # Contributed equally to this work.

20

ABSTRACT

Eukaryotes may experience oxygen deprivation under both physiological and pathological conditions. Because oxygen shortage leads to a reduction in cellular energy production, all eukaryotes studied so far conserve energy by suppressing their metabolism. However, the molecular physiology of animals that naturally and repeatedly experience anoxia is underexplored. One such animal is the marine nematode *Laxus oneistus*. It thrives, invariably coated by its sulfur-oxidizing symbiont *Candidatus Thiosymbion oneisti*, in anoxic sulfidic or hypoxic sand. Here, transcriptomics and proteomics showed that, whether in anoxia or not, *L. oneistus* mostly expressed genes involved in ubiquitination, energy generation, oxidative stress response, immune response, development, and translation. Importantly, ubiquitination genes were also upregulated when the nematode was subjected to anoxic sulfidic conditions, together with genes involved in autophagy, detoxification and ribosome biogenesis. We hypothesize that these degradation pathways were induced to recycle damaged cellular components (mitochondria) and misfolded proteins into nutrients. Remarkably, when *L. oneistus* was subjected to anoxic sulfidic conditions, lectin and mucin genes were also upregulated, potentially to promote the attachment of its thiotrophic symbiont. Furthermore, the nematode appeared to survive oxygen deprivation by using an alternative electron carrier (rhodoquinone) and acceptor (fumarate), to rewire the electron transfer chain. On the other hand, under hypoxia, genes involved in costly processes (e.g., amino acid biosynthesis, development, feeding, mating) were upregulated, together with the worm's Toll-like innate immunity pathway and several immune effectors (e.g., Bacterial Permeability Increasing proteins, fungicides).

In conclusion, we hypothesize that, in anoxic sulfidic sand, *L. oneistus* upregulates degradation processes, rewires oxidative phosphorylation and by reinforces its coat of bacterial sulfur-oxidizers. In upper sand layers, instead, it appears to produce broad-range antimicrobials and to exploit oxygen for biosynthesis and development.

INTRODUCTION

Fluctuations that lead to a decrease in oxygen availability are common in nature (Hermes-Lima and Zenteno-Savin, 2002). The physiological and behavioral response to oxygen deprivation has been studied in animals that naturally experience oxygen deprivation, such as frogs, goldfish, and turtles (Hochachka et al., 1996; 1997, 2001; Hermes-Lima and Zenteno-Savin, 2002), as well as in invertebrate genetic models (Clegg 1997; Nystul et al., 2003; Teodoro and O'Farrell, 2003; Haddad 2006). When oxygen deprived, these organisms must face the challenge of a drastic drop in ATP (the energy-storing metabolite adenosine triphosphate) production, which leads to the failure of energy-demanding processes that are crucial for maintaining cellular homeostasis. Anoxia-tolerant organisms, however, are capable to save

energy by stopping energy-costly cellular functions (e.g., protein synthesis, ion pumping, cell cycle progression), maintain stable and low permeability of membranes, and produce ATP by anaerobic glycolysis (Hochachka et al., 1996; Teodoro and O'Farrell, 2003; Liu & Simon, 2004; Liu et al., 2006; Galli et al., 2014).

When parasitic and free-living nematodes, including the model organism *Caenorhabditis elegans*, are experimentally exposed to anoxia (<0.001 kPa O_2), the intracellular ATP/ADP ratio drops dramatically and, within 10 h, they enter a state of reversible metabolic arrest called *suspended animation*. Namely, they stop to eat, move, develop or lay eggs, implying that oxygen deprivation affects their growth and behavior (Van Voorhies et al., 2000; Padilla et al., 2002; Nystul and Roth, 2004; Powell-Coffmann 2010; Fawcett et al., 2015; Kitazume et al., 2018). If these effects can be reversed upon oxygen reestablishment, the latter can also provoke a massive and sudden production of reactive oxygen species (ROS) that may overwhelm the organism's antioxidant defense, and cause its death (reviewed in Hermes-Lima and Zenteno-Savin, 2002). Of note, an increase of mitochondrial ROS production was also observed in worms under hypoxia, because of the inefficient transfer of electrons to molecular oxygen (Nystul and Roth, 2004; Kim and Jin, 2015).

Because oxygen diffuses slowly through aqueous solutions, sharp concentration gradients of this electron acceptor may occur in marine environments and wet soil (Denny et al., 1993; Fawcett et al., 2015). It is at oxic-anoxic interfaces of marine sands that free-living nematodes coated with sulfur-oxidizing Gammaproteobacteria (Stilbonematinae) abound (Ott et al., 1989, 1991; Schiemer et al., 1990; Paredes et al., 2021). However, up to this study, the molecular mechanisms allowing symbiotic nematodes to withstand anoxia, and the inherent stress it is known to inflict upon metazoans, were unknown. Here, we incubated *Laxus oneistus* (Ott et al., 1995) in conditions resembling those it encounters in its natural environment (i.e. anoxic sulfidic or hypoxic), and applied comparative transcriptomics, proteomics and lipidomics, to understand how it copes with oxygen deprivation. Contrarily to our expectations, in anoxic sulfidic water *Laxus oneistus* did not appear to enter suspended animation. However, it upregulated genes required for ribosome biogenesis and energy generation, and for degradation pathways (e.g., ubiquitination-proteasome systems, autophagy) likely involved in recycling damaged cellular components and misfolded proteins into nutrients. Notably, under anoxic sulfidic conditions, it also upregulated putative symbiont-binding molecules such as lectins. In the presence of oxygen, on the other hand, the worm appeared to overexpress genes involved in energy-demanding processes (e.g., amino acid synthesis, development, feeding, and mating) and upregulated the synthesis of broad-range antimicrobials, likely via triggering the Toll/NF- κ B pathway.

RESULTS AND DISCUSSION

The nematode *Laxus oneistus* did not enter suspended animation upon 24 h anoxia

To survive anoxia, nematodes enter suspended animation to suppress metabolism and conserve energy. The most notorious sign of suspended animation is the arrest of motility (Nystul et al., 2003; Chan et al., 2010; Kitazume et al., 2018).

Surprisingly, although the whole population of four tested nematode species, including *C. elegans*, was reported to be in suspended animation upon 10 h in anoxia (Kitazume et al., 2018), *L. oneistus* kept moving not only after 24-h-long incubations, but also upon 6-day-long incubations in anoxic seawater (three batches of 50 worms were incubated under each condition). Additionally, the symbiotic nematodes appeared morphologically normal ([Supplemental movies 1-4](#)).

The fact that we could not observe suspended animation, led us to hypothesize that *L. oneistus* evolved different strategies to survive oxygen deprivation.

Stable transcriptional profile under hypoxic or anoxic sulfidic conditions

To understand the molecular mechanisms underlying *L. oneistus* response to oxygen, we subjected it to various oxygen concentrations. Namely, nematode batches were incubated under either normoxic (100% air saturation; O), hypoxic (30% air saturation; H) or anoxic (0% air saturation; A) conditions for 24 h. Additionally, given that *L. oneistus* thrives in reduced sand containing up to 25 μ M sulfide (Ott and Novak., 1989; Paredes et al., 2021), we also incubated it in anoxic seawater supplemented with < 25 μ M sulfide (anoxic sulfidic condition; AS).

While transcriptional differences of its symbiont (*Candidatus Thiosymbion oneisti*), incubated under normoxic (O) and hypoxic (H) conditions were negligible (Paredes et al., 2021), the expression profiles of nematode batches incubated under O conditions varied so much that they did not cluster ([Figure S1](#)). Consequently, there was no detectable differential expression between the transcriptomes of O nematodes and any of the other transcriptomes (H, A or AS; [Figure S1B, C](#)). We attribute the erratic transcriptional response of *L. oneistus* to normoxia to the fact that this concentration is not typically experienced by *L. oneistus* (Ott et al., 1989; Paredes et al., 2021).

As for the expression profiles of nematodes subjected to the H, A or AS conditions, replicates of each condition behaved more congruently ([Figure S1B](#)). While we did not find any significant difference between the A and AS nematodes, only 0.05% of the genes (8 genes; [Data S1](#)) were differentially expressed between the H and A nematodes and there was no significant difference between the H and A proteomes (t-test, FDR, Benjamini-Hochberg correction, $p < 0.05$; [Figure S2A, Data S1](#)). However, 4.8% of the expressed genes (787 out of 16,526) were differentially expressed between H and AS nematodes, with 434 upregulated under AS and 353 genes upregulated under H conditions ([Figure S1C, Data S1](#)).

Collectively, our data suggests that *L. oneistus* may be ill-equipped to handle normoxic sediment, but it maintains a largely stable physiological profile under both hypoxic and anoxic sulfidic conditions. Before discussing the subset of biological processes differentially upregulated in AS versus H nematodes and vice versa, we will present the physiological processes the worm appears to mostly engage with, irrespectively of the environmental conditions we experimentally subjected it to.

Top-expressed transcripts under all tested conditions

To gain insights on *L. oneistus* basal physiology, we treated all the 16 transcriptomes as biological replicates (i.e., O, H, A and AS transcriptomes were pooled) and identified the 100 most abundant transcripts out of 16,526 based on functional categories extracted from the UniProt database (2021) and comprehensive literature search (Figure 1, Data S2). Our manual classification was supported by automatic eggNOG classification (Data S2). Similarly, the H and A proteomes were pooled, and the 100 most abundant proteins out of 2,626 were detected (Figure S2).

Based on median gene expression values of the top 100 expressed genes, we found that some of the processes *L. oneistus* mostly engages with were ubiquitination (*ubq-1*, Stringham et al., 1992), energy generation (globin *glb-1*-like (Geuens et al., 2010), cytochrome c oxidase I subunit *ctc-1* (UniProtKB P24893), *nduo-4*-like (UniProtKB P24892), stress response and detoxification (e.g., *hsp-1*, *hsp-90*, *hsp12.2*, and catalases *ctl-1* and *ctl-2*; Birnby et al., 2000; Chávez et al., 2007), and immune defense (lysozyme-like proteins and *lec-3*) (Figure 1, Data S2).

Lastly, 48 out of the top 100 most expressed genes, were also detected among the top 100 proteins (Figure 1, Figure S2, and Data S2, Supplemental material). Despite the modest correlation between transcript and protein expression levels ($r = 0.4$) (Figure S3), there was an overlap in the detected biological processes (e.g., energy generation, stress response or detoxification categories, carbohydrate metabolism, cytoskeleton, locomotion, nervous system) (Figure S2).

All in all, except for those encoding for immune effectors, top-transcribed *L. oneistus* genes could not be ascribed to its symbiotic lifestyle. This differs to what observed for other chemosynthetic hosts, such as giant tubeworms and clams. Indeed, it is perhaps because these animals acquire their symbionts horizontally and feed on them as they are housed in their cells (and not on their surface) that they were found to abundantly express genes involved in symbiont acquisition, proliferation control and digestion (Sun et al., 2017, Hinzke et al., 2019; Yuen et al., 2019). Notably, we did observe a partial overlap of the most expressed gene categories (e.g., oxidative stress, energy generation, immune response), when *L. oneistus* was compared to the marine gutless annelid *Olavius algarvensis*. We ascribe the overlap to the fact that, albeit

endosymbiotic, *O. algarvensis* also inhabits shallow water sand (Figure S4, Supplemental material) and, as hypothesized for *L. oneistus*, it may also acquire its symbionts vertically (Woyke et al., 2006; Dubilier et al., 2008; Wippler et al., 2016; Zimmermann et al., 2016).

To conclude, although both symbiont- (Paredes et al., 2021) and host-transcriptomics do not suggest a high degree of inter-partner metabolic dependence in the *L. oneistus* ectosymbiosis, the nematode seems well-adapted to both anoxic sulfidic (AS) and hypoxic (H) sand (Figure 2, Data S1). The transcriptional response of the worm to these two conditions is, however, significant (Figure 2, Data S1), and it will be reported next.

Genes upregulated in anoxic sulfidic (AS) nematodes

Chaperones and detoxification. The expression of chaperone-encoding (e.g., *hsp12.2*, *grpE*, *dnaJ/dnj-2*, *pfd-1*, *pfd-6*; Naylor et al., 1996; Lundin et al., 2008; Bar-Lavan et al., 2016), and ROS-detoxifying-related genes (e.g., superoxide dismutase *sod-2* and a putative glutathione peroxidase, involved in the detoxification of superoxide dismutase and hydrogen peroxide, respectively; Suzuki et al., 1996; Margis et al., 2008) were higher in AS nematodes (Figures 2 and 3). Notably, transcripts encoding for the heme-binding cytochrome P450 *cyp-13B1* were also more abundant in AS (Figure 3), perhaps to increase the worm's capacity to cope with putative ROS formation (Oliveira et al., 2009). Indeed, as cells start being oxygen-depleted, mitochondrial ROS accumulate because of the inefficient transfer of electrons to molecular oxygen (Semenza, 1999; Nystul and Roth, 2004; Selivanov et al., 2009; Kim and Jin, 2015). Alternatively, the upregulation of antioxidant-related genes in AS worms could represent an anticipation response to an imminent reoxygenation. In animals alternating between anoxic and oxygenated habitats, the re-exposure to oxygen can be very dangerous, as it creates a sudden ROS overproduction that may overwhelm the organism's oxidative defense mechanisms (Hermes-Lima and Zenteno-Savin, 2002; Hashimoto et al., 2004). Although it has not been reported for nematodes, overexpression of ROS-counteracting genes is consistent with what has been reported for vertebrates and marine gastropods which, just like *L. oneistus*, alternate between oxygen-depletion and reoxygenation (Hermes-Lima and Zenteno-Savin, 2002).

Mitochondrial and cytoplasmic ribosome biogenesis. In the cellular stress imposed by oxygen deprivation, mitochondria are central to both death and survival (Borutaite et al., 1995; Brookes et al., 2004; Brenner et al., 2012; Hawrysh et al., 2013; Galli et al., 2014). In this scenario, calcium regulation, the scavenging of ROS or the suppression of their production, and/or inhibition of the mitochondrial permeability transition pore (MPTP) opening, might help to preserve mitochondrial function and integrity (Horwitz et al., 1994; Murphy et al., 2008; Galli et al., 2014; Fanter et al., 2020). In addition, removal of specific mitochondrial components (mitochondrial-associated protein degradation, MAD), might also arise to maintain the overall mitochondrial homeostasis (Chatenay-Lapointe and Shadel, 2010; Heo et al., 2010). Perhaps

as a response to anoxia-induced stress (reviewed in Galli et al., 2014), a gene involved in MAD (*vms-1*) (Chatenay-Lapointe and Shadel, 2010; Heo et al., 2010), was upregulated in AS worms (Figure 4). More abundant in this condition were also transcripts encoding for mitochondrial transmembrane transporters *tin-44*, *slc-25A26* and *C16C10.1* (UniProtKB O02161, Q18934, Q09461), putatively transporting, peptide-containing proteins from the inner membrane into the mitochondrial matrix, such as S-Adenosyl Methionine (Figure 6). Surprisingly, although the translation elongation factor *eef-1A.2* (Tullet, 2015) was downregulated in AS worms, not only various mitochondrial ribosome structural components (28S: *mrps*, 39S: *mrpl*; Kaushal et al., 2014), and mitochondrial translation-related genes (e.g., *C24D10.6* and *W03F8.3*; Sharika et al., 2018) were upregulated in AS nematodes, but also several cytoplasmic ribosome biogenesis (40S: *rps*, 60S: *rpl*; Melnikov et al., 2012) and subunit assembly genes (e.g., RRP7A-like, You et al., 2015) (Figure 4).

Taken together, the maintenance of mitochondrial homeostasis, an anticipatory response to a potential upcoming ROS insult (see Chaperones and detoxification section) and/or their involvement in extra-ribosomal functions (Chen et al., 2010; Savada et al., 2014; Xu et al., 2016) might explain the upregulation of ribosomal biogenesis-related genes in AS nematodes. Although upregulation of ribosomal proteins has also been observed in anoxic gastropods (Larade et al., 2001), increased ribosomal biogenesis (which oftentimes directly correlates with an increase of protein synthesis) is not expected in animals that must repress their metabolism to cope with oxygen deprivation (Thomas et al., 2000; Hochachka and Lutz 2001; Shukla et al., 2012).

Energy generation. Equally surprising was the upregulation of all differentially expressed genes related to energy generation in AS nematodes (Figure 4). Namely, besides putative oxygen-binding globulin-like genes (e.g., *glb-1*, *glb-14*, Geuens et al., 2010), the following were upregulated in AS nematodes: key structural genes (e.g., *atp-3*, *atp-5*, Xu et al., 2018), assembly-related genes (H⁺-transport ATP synthase, Maglioni et al., 2016) of the mitochondrial ATP synthase (complex V), genes related to complex I (*lpd-5*, *nuo-2*, McKay et al., 2003; Rea et al., 2007), a subunit of the succinate dehydrogenase involved in complex II (*mev-1*, Hartman et al., 2001), a mitochondrial cytochrome C oxidase subunit II assembly gene related to complex IV (*sco-1*, Williams et al., 2005), and a mitochondrial gene (*coq-5*), involved in the synthesis of either ubiquinone (Q, aerobic) or rholoquinone (RQ, anaerobic) electron carriers (Buceta et al., 2019) (Figure 4). This suggests that, under anoxia, the electron transfer chain (ETC) is rewired in such way that electrons still enter the ETC at complex I, but instead of reaching complex III and IV they are transferred to RQ. This, in turn, shuttles the electrons to succinate dehydrogenase. The latter enzyme uses fumarate as an alternative electron acceptor, reducing it to succinate. This mechanism would maintain the flow of electrons through the ETC,

and, it would prevent mitochondrial ATP generation (complex V) from shutting down (Buceta et al., 2019; Del Borrello et al., 2019).

In short, under AS, similarly to what has been observed in other free-living and parasitic nematodes, complex I appears to be the sole proton pump in this truncated form of ETC (Buceta et al., 2019; Del Borrello et al., 2019). In accordance with this hypothesis, tryptophan (Trp) degradation-related genes (*acsd-1*, *acsd-2*) and the Trp RNA ligase (*wars-1*; Tsai et al., 2017) that might be required to synthesize RQ (Buceta et al., 2019; Del Borrello et al., 2017; Tan et al., 2020) were upregulated under AS. Intriguingly, upregulated was also an isocitrate dehydrogenase gene (*idh-1*). This produces reducing equivalent (NADPH) carrying electrons that may fuel complex I (Smolková et al., 2012; Martínez-Reyes et al., 2020), but it might also add to the stimulation of the antioxidant capacity or to the maintenance of redox homeostasis by regenerating reduced glutathione (Hermes-Lima and Zenteno-Savin, 2002; Penkov et al., 2015; Yang et al., 2019).

If glycolysis is a key process for ATP generation in anoxia (Lutz et al., 1997; Semenza et al., 2001; Hochachka et al., 2001; Huang et al., 2008; Larade et al., 2009) and if, consistently, *hvk-2* was upregulated under this condition (Figure 6), based on the expression levels of transcripts encoding for alpha-amylases (see Carbohydrate metabolism in Figure 6), starch and/or glycogen (Jackson and McLaughlin, 2009) may be the prominent carbon sources under anoxic sulfidic conditions.

Ubiquitin-proteasome system and proteases. Proteolysis supplies amino acids or polypeptides to the cells, while impeding the accumulation of damaged or misfolded proteins. The two main mechanisms of cellular proteolysis are the lysosome-mediated intracellular protein degradation (autophagy) and the proteasome-mediated protein degradation (ubiquitin-proteasome system, UPS). In the latter, ubiquitin-protein ligases covalently attach ubiquitin to proteins, allowing their recognition and further degradation by the proteasome (Lodish et al., 2008; Papaevgeniou and Chondrogianni, 2014).

As shown in Figure 1, transcripts encoding for polyubiquitin (*ubq-1*), had the highest median gene expression across all transcriptomes. However, all ubiquitination-related genes detected in the differential gene expression analysis between the AS and H conditions, were upregulated in AS worms (Figure 2 and 3, Data S1). For example, *aos-1*, encoding for a subunit of the ubiquitin-activating enzyme (E1) (Jones et al., 2001), two ubiquitin-protein ligases (E3s without detected cullin domains; Papaevgeniou and Chondrogianni, 2014), and kelch-like genes (e.g., *kel-8*-like and *kel-20*). The former are BTB-domain containing proteins known to interact with E3 enzymes, with *kel-8* being involved in the degradation of glutamate neuroreceptors (Schaefer and Rongo 2006; Stogios et al., 2005; Kim et al., 2018). Additional ubiquitination-related genes upregulated in AS were *csn-2*, encoding for a component of the COP9

signalosome complex (Pintard et al., 2003; Brockway et al., 2014), and proteasome genes (*pas-2* and *pas-3*; Fraser et al., 2000; Blumenthal et al., 2002).

Among the proteases that were upregulated in AS worms, aspartyl proteases have been involved in neurodegeneration (Syntichaki et al., 2002), whereas plasminogen and the zinc matrix metalloproteinase ZMP-2 were both reported to mediate degradation of extracellular matrix (ECM) (Vassalli et al., 1991; Altincicek et al., 2010; Fischer, et al., 2014) (Figure 3). *C. elegans* ZMP-2 was also shown to prevent the accumulation of oxidized lipoproteins (Fischer et al., 2014), and, therefore it may contribute to the enhanced antioxidant response observed in this condition.

Autophagy and amino acid degradation. Besides acting coordinately to withstand stress, autophagy cooperates with apoptotic UPS for the recovery and supply of nutrients when these are scarce (Vabulas et al., 2005; Scott et al., 2004; Huber and Teis, 2016; reviewed in Wang RC et al., 2010 and Russel et al., 2014). Transcripts of two autophagy-related genes, *bec-1* (Liang et al., 1999) and the Ragulator complex protein LAMTOR4 (C7orf59-like) (Bar-Peled et al., 2012) were more abundant in AS nematodes (Figure 3). While the former positively regulates autophagy (Liang et al., 1999; Meléndez et al., 2003), the latter interacts with the mTOR Complex I (mTORC1), and tethers small GTPases (Rags and Rheb) to the lysosomal surface (Bar-Peled et al., 2012). When amino acid levels are low, mTORC1 is not translocated to the lysosomal surface (Wang et al., 2009; Bar-Peled et al., 2012), thereby favoring catabolic processes such as autophagy (Thompson et al., 2005). We propose that amino acid scarcity might result from the upregulation of genes involved in the degradation of lysin, glycine, tyrosine, cysteine, leucine, isoleucine, valine or tryptophan (Figure 3, Data S1). This would decrease mTORC1 activity and, in turn, stimulates nutrient recycling via autophagy in AS worms.

Conversely, we hypothesize that in H worms, active mTORC1 interacts with the ribosomal protein S6 kinase (S6K), encoded by the *rsks-1* gene which is also up in H worms (Ladevaia et al., 2014) (Figure 3). This direct interaction, upon a cascade of phosphorylation events, would stimulate translation, and ultimately cell growth and proliferation (Ma et al., 2009, Howell et al., 2011, and Ladevaia et al., 2014).

All in all, although it is currently unclear whether increased autophagy is beneficial or detrimental, under AS conditions, the upregulation of genes involved in self-digestion might play a protective role and foster recovery from starvation (Thompson et al., 2005), pathogens (Huber and Teis, 2016) or from neuronal and muscular degeneration induced by oxygen deprivation (Murphy and Steenbergen 2008).

Lectins and mucins. Given that symbiont attachment may be mediated by Ca²⁺-dependent lectins (Nussbaumer et al. 2004, Bulgheresi et al., 2006, 2011) and given that, under anoxia, the symbiont appeared to proliferate more (Paredes et al., 2021), we expected nematode lectins to be upregulated under this condition. Indeed, nine C-type lectin domain (CTLD)-

containing proteins were upregulated in AS *L. oneistus* adults and only two (*cllec-78* and *cllec-78-like-2*) were upregulated in the presence of oxygen (Figure 4). In addition to CTLD-containing proteins, mucins, a class of glycoproteins with more than 50% of its mass attributable to O-glycans, were also upregulated in AS nematodes. Considering that mucin glycans are used by vertebrate gut commensals for attachment, as well as a source of nutrients (Koropatkin et al., 2012), it is conceivable that their upregulation in anoxia (Figure 4), together with that of CTLD-containing proteins, would foster symbiont attachment.

We hypothesize that overexpression of two classes of putative symbiont-binding molecules, lectins and mucins, under conditions favoring symbiont proliferation (i.e., AS condition, Paredes et al., 2021) may mediate bacterial coat reinforcement.

Apoptosis. Mitochondria play an important role in apoptosis induction (Simon et al., 2000; Martínez-Reyes et al., 2020). Indeed, MPTP opening due to ROS (or the severe ATP decline imposed by the absence of oxygen) may cause cytochrome C release from mitochondria and this, in turn, triggers caspase activation (Martinou et al., 2000; Simon et al., 2000; Gogvadze et al., 2006; Galli et al., 2014). We observed that transcripts encoding for *sco-1*, a gene needed for the synthesis and assembly of mitochondrial cytochrome C (Williams et al., 2005) were more abundant in AS worms (Figure 4). Further, we observed upregulation of Caspase-3 (*ced-3*) which belongs to a family of cysteine proteases involved in apoptosis (Mangahas et al., 2005; Kaufmann et al., 2008) and which is activated upon mitochondrial cytochrome C release into the cytosol (Liu et al., 1996; Tafani et al., 2000; Kaufmann et al., 2008; Martínez-Reyes et al., 2020). Additional apoptosis-related genes that appeared to be upregulated in AS worms were: *bec-1* (Figure 3), a gene that promotes autophagy and fine-tunes the Ced-3-mediated apoptosis (Liang et al., 1999; Takacs-Vellai et al., 2005); *ttr-52*, which mediates apoptotic cell recognition prior to engulfment (Wang, X. et al., 2010; Chen et al., 2013); a BAG family molecular chaperone regulator 1 (BAG1-regulator); a cell-death-related nuclease *crn-2* (Parrish et al., 2003; Samejima et al., 2005) and phagolysosome forming *arl-8* (Sasaki et al., 2013), and a tyrosine kinase Abl-1, (*abl-1*) that modulates apoptotic engulfment pathways (Hurwitz et al., 2009).

Lipid catabolism. Genes involved in lipid metabolism were similarly expressed between the AS and H conditions (Figure 2, Data S1). In accordance, lipidomes of nematodes incubated in the presence or absence of oxygen were not significantly different (Figure S5, Supplemental material). However, in line with the overall upregulation of degradation pathways, we observed upregulation of genes involved in FA beta-oxidation (*kat-1*; Berdichevsky et al., 2010), in lipid digestion (the lipase *lipf-6*; UniProtKB E2S7J2), and lipid degradation (a peripilin-2-like protein; Chughtai et al., 2015). Moreover, a gene that might be involved in oxidative-stress tolerance (a stearic acid desaturase *fat-7* regulating the first step of the fatty acid desaturation pathway (Horikawa et al., 2009) was also upregulated in AS worms. Lipid degradation under anoxia might be a strategy to overcome starvation (Krivoruchko and Storey, 2015).

Notably, we also observed an upregulation of two genes involved in phosphatidylcholine (PC) synthesis (*pmt-1*, *pmt-2*, Brendza et al., 2007) (Figure 5). Intriguingly, PC was more abundant in the anoxic symbiont (Paredes et al., 2021), although the latter cannot synthesize it. Thus, their upregulation in AS worms suggests worm-symbiont lipid transfer.

GABA- and glutamate-mediated neurotransmission. Upregulated genes related to GABA synthesis were, *unc-25*, *unc-104* and *pdxk-1* (pyridoxal phosphate hexokinase) (Thomas et al., 1990; McIntire et al., 1993; Jin et al., 1999; Gally et al., 2003; Nordquist et al., 2018; Risley et al., 2016) (Figure 5, Data S1). Consistent with an expected increase in glutamate requirement as a direct GABA precursor (Martin et al., 1993), we observed downregulation of two glutamine synthetases and a delta-1-pyrroline-5-carboxylate synthase (*gln-3* and *alh-13* respectively; van der Vos et al., 2012; Yen et al., 2021; Figure 6), known to convert glutamate to glutamine or to proline, respectively. Furthermore, an *mgl-2* like gene encoding for a glutamate receptor, which is activated in the presence of glutamate (Tharmalingam et al., 2012), was up in AS worms. Note that, when oxygen is limited, glutamate may act as a neurotoxic amino acid (Baker et al., 1991; Lutz et al., 2003a). Therefore, increased GABA biosynthesis might, beneficially, prevent its accumulation (Milton et al., 2002; Mathews et al., 2003).

GABA-mediated neurotransmission has been documented for facultative anaerobic animals thriving in anoxic conditions (Lutz et al., 1997; Milton et al., 1998; Lutz et al., 2003a, b). Due to its inhibitory nature, it contributes to avoid membrane depolymerization (Nilsson et al., 1990; Milton et al., 1998). Moreover, given that it relaxes muscles, the increment of GABA may impact the movement of the animal (McIntire et al., 1993; Schuske et al., 2004). Therefore, upregulation of GABA-mediated neuronal activity might explain why anoxic *L. oneistus* did not form tight worm clusters after 24h (Supplemental movie 3).

Dopamine-mediated neurotransmission. A gene encoding for the tyrosine hydroxylase Cat-2 (*cat-2*), which is needed for dopamine biosynthesis (Sawin et al., 2000) and two putative dopamine receptors (*protein-D2-like* and a G_PROTEIN_RECEP_F1_2 domain-containing protein (*dop-5*); Sanyal et al., 2004) were upregulated in AS worms. Moreover, a *dat-1*-like gene mediating dopamine reuptake into the presynaptic terminals was downregulated (Gainetdinov et al., 2002; McDonald et al., 2006) in AS worms (Figure 5).

Calcium-binding and -sensing proteins. Finally, in AS worms several calcium-binding or -sensing proteins (e.g., *ncs-2*, *cex-2*, and a calbindin-like (CALB1 homologue); Soontornniyomkij et al., 2012; Hobert et al., 2018; Figure 5), as well as calcium transporters (*cca-1*, Steger et al., 2005; Transport category, Figure 6) were upregulated. On the one hand, we hypothesize their involvement in the inhibitory neural signaling described above (for example, Ncs-2 mediates the cholinergic and GABAergic expression of *C. elegans* (Zhou et al., 2017). On the other, they may protect cells against the stress inflicted by anoxia, which involves calcium

overload and consequent cellular acidification (Bickler et al., 1992; Dell'Anna et al., 1996; Galli et al., 2014).

Genes upregulated in hypoxic (H) nematodes

Innate immune pathways and effectors. Animals recognize and respond to microbes by means of immunoreceptors including Toll-like receptors, conserved from sponges to humans (Akira et al., 2006). We identified almost all genes belonging to this pathway, including the one encoding for the NF- κ B transcription factor. This came as a surprise given that, up to now, the has not been identified in any other nematode NF- κ B (Pujol and Ewbank, submitted). As surprising, was the fact that not only two Toll-like receptors (*tol-1* and *tol-1-like*), but also genes encoding for antimicrobial proteins such as a peroxisome assembly factor involved in defense against Gram- (*prx-11-like*, Wang, D. (2019), a putatively antifungal endochitinase (Dravid et al., 2015) and Bactericidal Permeability Increasing proteins (BPIs) were also more abundant in H worms. BPIs may bind LPS and perforate Gram- membranes and have shown to play a symbiostatic role in other invertebrates (Bruno et al., 2019; Krasity et al., 2015; Chen et al., 2017). However, it is unclear whether activation of the *L. oneistus* Toll pathway leads to the nuclear NF- κ B switching on the expression of antimicrobial genes or whether, as shown in *C. elegans*, the Toll pathway mediates behavioral avoidance of pathogens (Pradel et al., 2007; Brandt et al., 2015).

Overall, the apparent oxygen stimulation of a central innate immunity pathway and, directly or indirectly, of broad range anti-defense mechanisms could be adaptations to the fact that in oxygenated environments (when crawling in superficial sand layers), *L. oneistus* is exposed to predation from bigger animals, but also to pathogenic members of the bacterioplankton. Overexpression of broad-range antimicrobials in response to oxygen might therefore help *L. oneistus* to avoid colonization by potentially deleterious, fouling bacteria (e.g., *Vibrios*, *Roseobacters* and *Pseudoaltermonas/Alteromonadales*) when crawling close to the water column (Dang and Lovell, 2016; M. Mussmann, personal communication).

Development. Although development-related genes were some of the most expressed under all conditions (Figure 1), many were upregulated in H nematodes (Figure 2 and 5). Among the development-related genes upregulated in H nematodes were those related to molting (e.g., *nas-36*, *nas-38*, *chs-2*, *ptr-5*, *ptr-18*, *apl-1*, *myrf-1*; Suzuki et al., 2004; Zhang et al., 2005; Zugasti et al., 2005; Hornsten et al., 2007; Russel et al., 2011), germ line establishment (e.g., *ccm-3*, *rsks-1*; Pan et al., 2007; Pal et al., 2017), oogenesis/spermatogenesis (*crt-1*, Park et al., 2001), embryonic development and yolk production (*smp-1*, *cpna-1*, *plt-1*, *vit-6*, *crt-1*, *arrd-17*, *mhc-5*; Clark et al., 1997; Goedert et al., 1996; Gatewood et al., 1997; Fuji et al., 2002; Gally et al., 2009; Zahreddine et al., 2010; Jee et al., 2012; Warner et al., 2013; Fisher et al., 2014; Perez and Lehner, 2019), and/or larval development (*nmy-1*, *ifb-1*; Ding et al., 2004; Osório et al.,

2019), as well as male tip (*Cdt1*, *plx-1*, *ver-3*; Nelson et al., 2011; Dalpé et al., 2004; Dalpe et al., 2013), vulva morphogenesis (*hda-1*, *unc-62*), and a hermaphrodite-related gene (*hda-1*; Dufourcq et al., 2002; Choy et al., 2007) (Figure 5). Moreover, transcripts encoding for a number of proteases shown to be involved in *C. elegans* molting (e.g., *nas-38*, *nas-6*-like; Park et al., 2010), development (e.g., teneurin-a-like; Topf and Drabikowski, 2019), neuronal regrowth or locomotion (*tep-1*; Kim et al., 2018) and pharyngeal pumping (e.g., neprilysin *nep-1*; Spanier et al., 2005) were also more abundant in H worms. Remarkably, *vav-1*, which, besides being involved in male tip and vulva morphogenesis (Nelson et al., 2011), may also regulate the concentration of intracellular calcium (Norman et al., 2005), was one of the few development-related genes to be downregulated in H nematodes (see previous section on Ca-binding proteins).

To sum up, and as expected, the host appears to exploit oxygen availability to undertake energetically costly processes, such as development and molting (De Cuyper and Vanfleteren 1982; Uppaluri and Brangwynne 2015).

Carbohydrate metabolism. If in AS nematodes, glycogen or starch appeared prominent carbon sources, H worms seemed to exploit trehalose and cellulose instead. Indeed, genes that degrade trehalose (*tre-1*, Pellerone et al., 2003) and cellulose (*Ppa-cel-2*, Schuster et al., 2012) were upregulated in H worms, as well as a putative ADP-dependent glucokinase (C50D2.7) involved in glycolysis (Yuan et al., 2012). The use of this pathway was supported by the overexpression of four genes encoding for sugar transporters (*Slc2-A1*, *C35A11*, *K08F9.1*, *F53H8.3*; Kitaoka et al., 2013; Bertoli et al., 2015), perhaps switched on by active mTOR (see above) (Figure 6) (Howell et al., 2011).

Additionally, *L. oneistus* appeared to exploit oxygen to synthesize complex polysaccharides, such as heparan sulfate (*hst-1*-like; Miyagawa et al. 1988; Bhattacharya et al., 2009) and glycan (*Gcnt3*-like) (Figure 6), as an ortholog of the N-deacetylase/N-sulfotransferase *hst-1*, related to heparin biosynthesis was also upregulated (Bhattacharya et al., 2009).

Although glycolysis seems to generate ATP in both AS and H worms, it is not clear why the latter would prefer to respire cellulose or trehalose instead of starch. Given its role as a membrane stabilizer, we speculate that AS worms might prioritize the storage of trehalose over its degradation to preserve membrane integrity (Figure 6) (Crowe et al 1987; Carpenter et al., 1988; Clegg et al., 1997; Chen et al., 2002; Haddad 2006). Of note, based on its genome draft, the symbiont may synthesize and transport trehalose, but it may not use it (Paredes et al., 2021). Therefore, we hypothesize symbiont-to-host transfer of trehalose under hypoxia. Consistently, the symbiont's trehalose synthesis-related gene (*otsB*; Paredes et al., 2021), and the host trehalase (*tre-1*; Figure 6) were both upregulated under hypoxia and metabolomics could detect trehalose in both partners (Table S1). Metabolomics also detected sucrose in both the holobiont

and the symbiont fraction (Table S1). Given that, based on transcriptomics and proteomics, the nematode can utilize sucrose but cannot synthesize it (Data S1), whereas the symbiont can (Paredes et al., 2021), as in the case for trehalose, we hypothesize symbiont-to-host sucrose transfer.

Acetylcholine-mediated neurotransmission. Instead of upregulating genes involved in inhibitory (GABA and dopamine-mediated) neurotransmission, hypoxic worms appeared to use excitatory acetylcholine-mediated neurotransmission as indicated by the upregulation of *molo-1*, *acr-20*, *cup-4*, *lev-9*, and sphingosine kinase *sphk-1* that promotes its release (Mongan et al., 2002; Patton et al., 2005; Gendrel et al., 2009; Boulin et al., 2012; Chan et al., 2012) (Figure 5). On the one hand, acetylcholine-mediated neurotransmission might promote ROS detoxification in H worms (Sun et al., 2014). On the other hand, its downregulation in AS worms may beneficially decrease calcium influx (Hochachka and Lutz, 2001).

Feeding, mating, mechanosensory behavior and axon guidance and fasciculation. Transcripts related to the neuronal regulation of energy-demanding activities such as feeding, mating, motion, as well as nervous system development were more abundant in H nematodes (Figure 5, and Data S1). More precisely, upregulated genes were involved in pharyngeal pumping (*nep-1*, *lat-2*; Spanier et al., 2005; Guest et al., 2007), male mating behavior and touch (*pdf-1*, *tbb-4*, *ebax-1*, Hurd et al., 2010; Wang, Z. et al., 2013), axon guidance and fasciculation (*spon-1*, *igcm-1*, *ebax-1*, *tep-1*; Kim et al., 2018; Woo et al., 2008; Schwarz et al., 2009; Wang, Z et al., 2013), mechanosensory behavior (e.g., *mec-12*, *delm-2*; Gu et al., 1996; Han et al., 2013). Additionally, we also observed the upregulation of a gene encoding for a glutamate receptor (*glr-7*) possibly involved in feeding facilitation (Li et al., 2012).

Amino acid biosynthesis. Transcripts of genes involved in the synthesis of glutamine and proline (*gln-3* and *alh-13*, respectively), aspartate (L-asparaginases; Tsuji et al., 1999) and S-adenosyl-L-methionine (SAM) (*sams-4*; Chen et al., 2020) were all upregulated in H worms (Figure 6), as well as one encoding for the ornithine decarboxylase *odc-1* which is involved in biosynthesis of the polyamine putrescine, and is essential for cell proliferation and tissue growth (Russell et al., 1968; Heby, 1981). Moreover, polyamines, with their high charge-to-mass ratio may protect against superoxide radicals, which, as mentioned, harm cell membranes and organelles, oxidize proteins, and damage DNA (Gilad et al., 1991; Longo et al., 1993).

Lipid biosynthesis. Genes upregulated in H worms mediate the biosynthesis of long chain fatty acids (*acs-3*, *acs-14*, *elo-3* but not *acs-5*; Yuan et al., 2012; Ward et al., 2014; Wang et al., 2021), sphingolipids (a sphingosine kinase-1 (*sphk-1*) and *egl-8*, which controls egg laying and pharyngeal pumping in *C. elegans* (Bastiani et al., 2003). Notably, sphingolipids may be anti-apoptotic (Taha et al., 2006) or result in acetylcholine release (Chan et al., 2012).

On the other hand, ceramides, which have antiproliferative properties and who may mediate resistance to severe oxygen deprivation (Deng et al., 2008; Menuz, et al. 2009),

appeared to be mainly synthesized in AS worms, as indicated by the upregulation of genes involved in ceramide biosynthesis (*asm-3*, *ttm-5*; Watts et al., 2017) (Figure 6).

Transport. As anticipated in the introduction, anoxia-tolerant animals switch off ATP-demanding processes such as ion pumping (Lutz et al., 1996; Galli et al., 2014). Indeed, transcripts encoding for proteins involved in cation channel activity (*gtl-2*, voltage gated H channel 1; Teramoto et al., 2010), sodium transport (*delm-2*-like; Han et al., 2013), chloride transport (*anoh-1*, *best-13*, *best-14*; Tsunenari et al., 2013; Wang, Y. et al., 2013; Goh et al., 2018), ABC transport (*wht-2*, *pgp-2*, *slcr-46.3*, *F23F12.3*, *hmit-1.3*; Currie et al., 2007; Schroeder et al., 2007; Kage-Nakadai et al., 2011) and organic transport (*F47E1.2*, *oct-2*; Pao et al., 1998) were all more abundant in H than AS worms (Figure 6).

Sulfur metabolism. The *mpst-7* gene which is involved in organismal response to selenium and it is switched on in hypoxic *C. elegans* (Romanelli-Credrez et al., 2020) was upregulated in H nematodes (Figure 6). Given that the latter is thought to catalyze the conversion of sulfite and glutathione persulfide (GSSH) to thiosulfate and glutathione (GSH) (Filipovic et al., 2018), hypoxia-experiencing *L. oneistus* might express this enzyme to recharge the cells with GSH and hence, help to cope with oxidative stress (Hayes and McLellan, 1999; Mytilineou et al., 2002; Diaz-Vivancos et al., 2015). Also more abundant in H worms were transcripts encoding for the sulfatases 2 (*sul-2*) (Morimoto-Tomita et al., 2002) and a PAPS-producing *pps-1* (3'-phospho-adenosine-5'-phosphosulfate (PAPS) considered the universal sulfur donor; Bhattacharya et al., 2009), as well as for the chaperones *pdi-6* and protein-disulfide-isomerase A5-like which require oxygen to mediate correct disulfide bond formation in protein folding (Teodoro and O'Farrell, 2003; Rose et al., 2017; Livshits et al., 2017) (Figure 6).

Conversely, a putative sulfide-producing enzyme (*mpst-1*) who protects *C. elegans* from mitochondrial damage (Qabazard et al., 2014; Ng et al., 2019; Kimura, 2020) was upregulated in AS nematodes. Notably, under AS, *L. oneistus* might detoxify sulfide by producing glutathione and taurine (Rose et al., 2017), as a persulfide dioxygenase (*ethe-1*) and a cysteine dioxygenase (*cdo-1*) which catalyzes taurine synthesis via cysteine degradation were upregulated. Sulfide detoxification via taurine accumulation is a common strategy in chemosynthetic animals (reviewed in Cavanaugh et al., 2006).

All in all, *L. oneistus* appeared to limit excess accumulation of free sulfide in anoxia and to free sulfate when oxygen was available.

Conclusions

Overall and irrespectively of the conditions it was subjected to, *L. oneistus* mostly expressed genes involved in degradation, energy generation, stress response and immune defense. Astonishingly, *L. oneistus* did not enter suspended animation when subjected to anoxic sulfidic conditions for days. We hypothesize that in the absence of oxygen, ATP production is

supported by trehalose and cellulose catabolism, and by rewiring the ETC in such way as to use rodoquinone (RQ) as electron carrier, and fumarate as electron acceptor. Moreover, the nematode activates several degradation pathways (e.g., ubiquitin-proteasome system (UPS), autophagy, and apoptosis) to gain nutrients from anoxia- or ROS-damaged proteins and mitochondria. Further, AS worms also upregulated genes encoding for ribosomal proteins and putative symbiont-binding proteins (lectins). Finally, as proposed for other anoxic-tolerant animals, the worm seems to upregulate its antioxidant capacity in anticipation of reoxygenation. When in hypoxic conditions (Figure 7, left), instead, we speculate that the worm uses starch for energy generation to engage in costly developmental processes such as molting, feeding, and mating, likely relying on excitatory neurotransmitters (e.g., acetylcholine), and it upregulates the Toll immune pathway and, directly or indirectly, the synthesis of broad range antimicrobials (e.g., fungicides, bactericidal permeability increasing proteins).

When looking at the *Laxus-Thiosymbion* symbiosis in light of what was recently published (Paredes et al., 2021), we could identify two signs of inter-partner metabolic dependence: in anoxia worms might transfer lipids to their symbionts, and in hypoxia the symbionts might transfer trehalose to their hosts.

Furthermore, we may conclude that, wherever in the sand the consortium is, one of the two partners is bound to be stressed: in anoxia, the symbiont appear to proliferate more, while its animal host engages in degradation of damaged proteins and mitochondria and in detoxification. In the presence of oxygen, the situation is inverted: the symbiont seems massively stressed, while the host can afford energy costly biosynthetic processes to develop and reproduce (Figure 7). It is therefore fascinating that, in spite of the dramatically different needs a bacterium and animal must have, the *Laxus-Thiosymbion* symbiosis evolved.

ACKNOWLEDGEMENTS

This work was supported by the Austrian Science Fund (FWF) grant P28743 (T.V., S.B., and L.K.), the FWF DK plus grant W1257: Microbial Nitrogen Cycling (G.F.P., L.K.), the FWF DOC 69 doc.fund (T.V). We thank Yin Chen for providing the facilities for lipidomics analysis, and Marvin Weinhold's, Jana Matulla's and Sebastian Grund's excellent technical work during metabolite analysis, and protein sample preparation and MS analysis, respectively. We are grateful to the Carrie Bow Cay Marine Field Station, Caribbean Coral Reef Ecosystem Program, and Station Manager Zach Foltz and Scott Taylor for their continuous support during field work. We thank Nicole Dubilier for access to data on *Olavius algarvensis*, and Jonathan Ewbank and Marc Musmann for insightful comments on the manuscript. Finally, we were inspired by insightful discussions with Monika Bright and Jörg A. Ott. This is contribution number XXX of the Carrie Bow Cay Marine Field Station, Caribbean Coral Reef Ecosystem Program.

MATERIALS AND METHODS

Sample collection

Laxus oneistus individuals were collected on multiple field trips (2016-2019) at approximately 1 m depth from sand bars off the Smithsonian Field Station, Carrie Bow Cay in Belize (16°48'11.01"N, 88°4'54.42"W). The collection of the nematodes, the incubations set up for RNA sequencing, lipidomics, proteomics and metabolomics, as well as the RNA extraction, and library preparation are described in Paredes et al., 2021. Importantly, the nematodes had a bright white appearance and replicate incubations were started simultaneously. Note that the [Supplemental material](#) describes changes in the lipidomics and proteomics pipelines, as well as the metabolomics, and sequencing data of *Olavius algarvensis*.

Host transcriptome de novo assembly

In preparation for the assembly, reads from each sample were first mapped to the symbiont as described before (Paredes et al., 2021), and remaining rRNA reads from all domains of life were removed from unmapped reads using sortmerna v2.1 in combination with the SSURef_NR99_119_SILVA_14_07_14 and LSURef_119_SILVA_15_07_14 databases. Further, exact duplicate reads were removed using PRINSEQ lite's derep option. Read files free of symbiont reads, rRNA reads and exact duplicates were used as input for transcriptome sub-assemblies via Trinity v2.6.6 with the strand-specific option (--SS_lib_type F) (Grabherr et al., 2011). Two sub-assemblies differing in the number and type of input read files were performed: (1) 9 input read files including biological triplicates from 3 incubation conditions (O, H, A) and (2) 4 input read files including a single replicate from 4 incubation conditions (O, H, A and hyper-O). Hyper-O refers to an incubation in which air was pumped directly into the exetainers for the entire incubation period to supersaturate the seawater (300 %O₂). However, as this incubation condition yielded an incongruous transcriptional response by the symbiont (data not shown), these read data were only used to extend the host transcriptome's coding repertoire. The qualities of both sub-assemblies were assessed as described below.

We then performed an intra-assembly clustering step as described in (Cerveau and Jackson, 2016), during which identical transcripts were removed from the sub-assemblies using CD-HIT-EST (Fu et al., 2012). To further reduce redundant transcripts, only the longest isoform for each 'gene' identified by Trinity was kept using Trinity's get_longest_isoform_seq_per_trinity_gene.pl utility. The remaining transcripts of each sub-assembly were then concatenated to produce a merged transcriptome assembly. The final assembly was created by applying another sequence clustering using CD-HIT-EST to avoid inter-assembly redundancy. Here, the identity parameter of 80% (-c 0.8) combined with a minimal coverage ratio of the shorter sequence of 80% (-aS 0.8) and minimal coverage ratio of the longest sequence of 0.005% (-aL 0.005) yielded the best-performing assembly in terms of number of transcripts (162,455) and contiguity (N50 value of 770) (data not shown).

Assembly completeness was assessed by estimating completeness via BUSCO nematode single-copy orthologs (Simão et al., 2015). Importantly, the merged assembly yielded a higher BUSCO-based completeness compared with the two sub-assemblies; 79.2% of the BUSCO nematode single-copy orthologs were found to be present and complete in the final assembly (636 single-copy/142 duplicated), whereas assembly (1) scored 77.8% (233 single-copy/531 duplicated) and assembly (2) was 76.2% complete (314 single-copy/434 duplicated). Further, assembled transcripts were filtered based on taxonomic classification. Transcripts were matched against the RefSeq protein database using blastx (E value 1E-3), and the output was then used as input for taxonomic assignment via MEGAN v5 (Huson et al., 2007). Only transcripts classified as belonging to 'Eukarya' were kept (MEGAN parameters: Min Score: 50, Max Expected: 1E-2, Top Percent: 2), which reduced the number of putative *L. oneistus* transcripts to 30,562. Assembled transcripts were also functionally annotated using Trinotate (Bryant et al., 2017). Briefly, predicted protein coding regions were extracted using TransDecoder (<https://github.com/TransDecoder>), both transcripts and predicted protein sequences were searched for protein homology via blastx and blastp, respectively, and predicted protein sequences were annotated for protein domains (hmmscan), signal peptides (signalP) and transmembrane domains (THMM). 85,859 transcripts exhibited at least one functional annotation. Finally, only taxonomy-filtered transcripts with at least one functional annotation were kept, thereby further reducing the number of putative host transcripts to 27,984, with 22,072 thereof predicted to contain protein coding regions. BUSCO-based completeness for this filtered host transcriptome assembly was 78.8% (635 single-copy/139 duplicated).

Gene expression analysis

Raw sequencing reads quality assessment and preprocessing of data was followed as described in Paredes et al., 2021. Trimmed reads were mapped to the de novo transcriptome assembly and transcript abundance was estimated using RSEM v1.3.1 (Li and Dewey 2011) in combination with bowtie with default settings except for the application of strandedness (--strandedness forward). Read counts per transcript were used for differential expression analysis, and TPM (transcripts per kilobase million) values were transformed to log₂TPMs as described in Paredes et al. 2021.

Gene and differential expression analyses were conducted using the R software environment and the Bioconductor package edgeR v3.28.1 (Gentleman et al., 2004; Robinson et al., 2010; R core Team, 2013), and as shown in Paredes et al., 2021. Here, we only describe the modifications that were made to the pipeline. Genes were considered expressed if at least ten reads in at least three replicates of one of the four conditions could be assigned. Excluding the replicates of the oxic condition, we found that 74.9% of all predicted nematode protein-encoding genes to be expressed (16,526 genes out of 22,072). Log₂TPM were used to assess sample similarities via multidimensional scaling based on Euclidean distances (R Stats package)

(R core Team, 2013) (Figure S1B), and the average of replicate log₂TPM values per expressed gene and condition was used to estimate expression strength. Median gene expression of entire metabolic processes and pathways per condition was determined from average log₂TPM values.

Expression of genes was considered significantly different if their expression changed 1.5-fold between two treatments with a false-discovery rate (FDR) ≤ 0.05 (Rapaport et al., 2013). Throughout the paper, all genes meeting these thresholds are either termed differentially expressed or up- or downregulated. For the differential expression analyses between the AS, H and A conditions see Data S1. Heatmaps show mean-centered log₂TPM expression values to highlight gene expression change.

All predicted *L. oneistus* proteins were automatically annotated using eggNOG-mapper v2 (Cantalapiedra et al., 2021) against eggNOG 5.0 (Huerta-Cepas et al., 2019) using diamond v2.0.4 (Buchfink et al., 2021). All genes that are shown and involved in a particular process were manually curated by blasting them against both the NCBI BLASTP nr database (Altschul et al., 1990) and the WormBase (Harris et al., 2020; https://wormbase.org/tools/blast_blat).

Data availability. This Transcriptome Shotgun Assembly project has been deposited at DDBJ/EMBL/GenBank under the accession GJNO000000000. The version described in this paper is the first version, GJNO01000000. RNA-Seq data are available at the Gene Expression Omnibus (GEO) database and are accessible through accession number GSE188619.

REFERENCES

1. Hermes-Lima, M., & Zenteno-Savín, T. (2002). Animal response to drastic changes in oxygen availability and physiological oxidative stress. *Comparative Biochemistry and Physiology Part C: Toxicology & Pharmacology*, 133(4), 537-556.
2. Hochachka, P. W., Buck, L. T., Doll, C. J., & Land, S. C. (1996). Unifying theory of hypoxia tolerance: molecular/metabolic defense and rescue mechanisms for surviving oxygen lack. *Proceedings of the National Academy of Sciences*, 93(18), 9493-9498.
3. Hochachka, P. W., Land, S. C., & Buck, L. T. (1997). Oxygen sensing and signal transduction in metabolic defense against hypoxia: lessons from vertebrate facultative anaerobes. *Comparative Biochemistry and Physiology Part A: Physiology*, 118(1), 23-29.
4. Hochachka, P. W., & Lutz, P. L. (2001). Mechanism, origin, and evolution of anoxia tolerance in animals☆. *Comparative Biochemistry and Physiology Part B: Biochemistry and Molecular Biology*, 130(4), 435-459.

5. Clegg, J. (1997). Embryos of *Artemia franciscana* survive four years of continuous anoxia: the case for complete metabolic rate depression. *The Journal of Experimental Biology*, 200(3), 467-475.
6. Nystul, T. G., Goldmark, J. P., Padilla, P. A., & Roth, M. B. (2003). Suspended animation in *C. elegans* requires the spindle checkpoint. *Science*, 302(5647), 1038-1041.
7. Teodoro, R. O., and O'Farrell, P. H. (2003). Nitric oxide-induced suspended animation promotes survival during hypoxia. *The EMBO Journal*, 22(3), 580-587.
8. Haddad, G. G. (2006). Tolerance to low O₂: lessons from invertebrate genetic models. *Experimental physiology*, 91(2), 277-282.
9. Liu, L., & Simon, M. C. (2004). Regulation of transcription and translation by hypoxia. *Cancer biology & therapy*, 3(6), 492-497.
10. Liu, L., Cash, T. P., Jones, R. G., Keith, B., Thompson, C. B., & Simon, M. C. (2006). Hypoxia-induced energy stress regulates mRNA translation and cell growth. *Molecular cell*, 21(4), 521-531.
11. Galli, G. L., & Richards, J. G. (2014). Mitochondria from anoxia-tolerant animals reveal common strategies to survive without oxygen. *Journal of Comparative Physiology B*, 184(3), 285-302.
12. Van Voorhies, W. A., & Ward, S. A. M. U. E. L. (2000). Broad oxygen tolerance in the nematode *Caenorhabditis elegans*. *Journal of Experimental Biology*, 203(16), 2467-2478.
13. Padilla, P. A., Nystul, T. G., Zager, R. A., Johnson, A. C., & Roth, M. B. (2002). Dephosphorylation of cell cycle-regulated proteins correlates with anoxia-induced suspended animation in *Caenorhabditis elegans*. *Molecular biology of the cell*, 13(5), 1473-1483.
14. Nystul, T. G., & Roth, M. B. (2004). Carbon monoxide-induced suspended animation protects against hypoxic damage in *Caenorhabditis elegans*. *Proceedings of the National Academy of Sciences*, 101(24), 9133-9136.
15. Powell-Coffman, J. A. (2010). Hypoxia signaling and resistance in *C. elegans*. *Trends in Endocrinology & Metabolism*, 21(7), 435-440.
16. Fawcett, E. M., Hoyt, J. M., Johnson, J. K., & Miller, D. L. (2015). Hypoxia disrupts proteostasis in *Caenorhabditis elegans*. *Aging Cell*, 14(1), 92-101.
17. Kitazume, H., Dayi, M., Tanaka, R., & Kikuchi, T. (2018). Assessment of the behaviour and survival of nematodes under low oxygen concentrations. *PloS one*, 13(5), e0197122.
18. Kim, K. W., & Jin, Y. (2015). Neuronal responses to stress and injury in *C. elegans*. *FEBS letters*, 589(14), 1644-1652.
19. Denny, M. (1993). *Air and Water: the Biology and Physics of Life's Media*. Princeton, NJ: Princeton University Press. 341pp.

20. Ott, J. A., & Novak, R. (1989). Living at an interface: Meiofauna at the oxygen/sulfide boundary of marine sediments.
21. Ott, J. A., Novak, R., Schiemer, F., . Hentschel, U., Nebelsick, M., & Polz, M. (1991). Tackling the sulfide gradient: a novel strategy involving marine nematodes and chemoautotrophic ectosymbionts. *Marine Ecology*, 12(3), 261-279.
22. Schiemer, F., Novak, R., & Ott, J. (1990). Metabolic studies on thiobiotic free-living nematodes and their symbiotic microorganisms. *Marine Biology*, 106(1), 129-137.
23. Paredes, G. F., Viehboeck, T., Lee, R., Palatinszky, M., Mausz, M. A., Reipert, S., ... & König, L. (2021). Anaerobic sulfur oxidation underlies adaptation of a chemosynthetic symbiont to oxic-anoxic interfaces. *mSystems*, 6(3), e01186-20.
24. Ott, J. A., Bauer-Nebelsick, M., & Novotny, V. (1995). The genus *Laxus* Cobb, 1984 (Stilbonematinae: Nematoda): description of two new species with ectosymbiotic chemoautotrophic bacteria. *Proceedings of the Biological Society of Washington*, 108(3), 508-527.
25. Chan, K., Goldmark, J. P., & Roth, M. B. (2010). Suspended animation extends survival limits of *Caenorhabditis elegans* and *Saccharomyces cerevisiae* at low temperature. *Molecular biology of the cell*, 21(13), 2161-2171.
26. UniProt: the universal protein knowledgebase in 2021. *Nucleic Acids Research*, 2021, 49. Jg., Nr. D1, S. D480-D489.
27. Stringham, E. G., Jones, D., & Candido, E. P. M. (1992). Expression of the polyubiquitin-encoding gene (ubq-1) in transgenic *Caenorhabditis elegans*. *Gene*, 113(2), 165-173.
28. Geuens, E., Hoogewijs, D., Nardini, M., Vinck, E., Pesce, A., Kiger, L., ... & Dewilde, S. (2010). Globin-like proteins in *Caenorhabditis elegans*: in vivo localization, ligand binding and structural properties. *BMC biochemistry*, 11(1), 1-15.
29. Birnby, D. A., Link, E. M., Vowels, J. J., Tian, H., Colacurcio, P. L., & Thomas, J. H. (2000). A transmembrane guanylyl cyclase (DAF-11) and Hsp90 (DAF-21) regulate a common set of chemosensory behaviors in *Caenorhabditis elegans*. *Genetics*, 155(1), 85-104.
30. Chávez, V., Mohri-Shiomi, A., Maadani, A., Vega, L. A., & Garsin, D. A. (2007). Oxidative stress enzymes are required for DAF-16-mediated immunity due to generation of reactive oxygen species by *Caenorhabditis elegans*. *Genetics*, 176(3), 1567-1577.
31. Sun, J., Zhang, Y., Xu, T., Zhang, Y., Mu, H., Zhang, Y., ... & Qian, P. Y. (2017). Adaptation to deep-sea chemosynthetic environments as revealed by mussel genomes. *Nature Ecology & Evolution*, 1(5), 1-7.
32. Hinzke, T., Kleiner, M., Breusing, C., Felbeck, H., Häsler, R., Sievert, S. M., ... & Markert, S. (2019). Host-microbe interactions in the chemosynthetic *Riftia pachyptila* symbiosis. *Mbio*, 10(6), e02243-19.

33. Yuen, B., Polzin, J., & Petersen, J. M. (2019). Organ transcriptomes of the lucinid clam *Loripes orbiculatus* (Poli, 1791) provide insights into their specialized roles in the biology of a chemosymbiotic bivalve. *BMC genomics*, 20(1), 1-14.
34. Woyke, T., Teeling, H., Ivanova, N. N., Huntemann, M., Richter, M., Gloeckner, F. O., ... & Dubilier, N. (2006). Symbiosis insights through metagenomic analysis of a microbial consortium. *Nature*, 443(7114), 950-955.
35. Dubilier, N., Bergin, C., & Lott, C. (2008). Symbiotic diversity in marine animals: the art of harnessing chemosynthesis. *Nature Reviews Microbiology*, 6(10), 725-740.
36. Wippler, J., Kleiner, M., Lott, C., Gruhl, A., Abraham, P. E., Giannone, R. J., ... & Dubilier, N. (2016). Transcriptomic and proteomic insights into innate immunity and adaptations to a symbiotic lifestyle in the gutless marine worm *Olavius algarvensis*. *BMC genomics*, 17(1), 1-19.
37. Zimmermann, J., Wentrup, C., Sadowski, M., Blazejak, A., Gruber-Vodicka, H. R., Kleiner, M., ... & Dubilier, N. (2016). Closely coupled evolutionary history of ecto-and endosymbionts from two distantly related animal phyla. *Molecular ecology*, 25(13), 3203-3223.
38. Naylor, D. J., Hoogenraad, N. J., & Høj, P. B. (1996). Isolation and characterisation of a cDNA encoding rat mitochondrial GrpE, a stress-inducible nucleotide-exchange factor of ubiquitous appearance in mammalian organs. *FEBS letters*, 396(2-3), 181-188.
39. Lundin, V. F., Srayko, M., Hyman, A. A., & Leroux, M. R. (2008). Efficient chaperone-mediated tubulin biogenesis is essential for cell division and cell migration in *C. elegans*. *Developmental biology*, 313(1), 320-334.
40. Bar-Lavan, Y., Shemesh, N., Dror, S., Ofir, R., Yeger-Lotem, E., & Ben-Zvi, A. (2016). A differentiation transcription factor establishes muscle-specific proteostasis in *Caenorhabditis elegans*. *PLoS genetics*, 12(12), e1006531.
41. Suzuki, N., Inokuma, K., Yasuda, K., & Ishii, N. (1996). Cloning, sequencing and mapping of a manganese superoxide dismutase gene of the nematode *Caenorhabditis elegans*. *DNA research*, 3(3), 171-174.
42. Margis, R., Dunand, C., Teixeira, F. K., & Margis-Pinheiro, M. (2008). Glutathione peroxidase family—an evolutionary overview. *The FEBS journal*, 275(15), 3959-3970.
43. Oliveira, R. P., Abate, J. P., Dilks, K., Landis, J., Ashraf, J., Murphy, C. T., & Blackwell, T. K. (2009). Condition-adapted stress and longevity gene regulation by *Caenorhabditis elegans* SKN-1/Nrf. *Aging cell*, 8(5), 524-541.
44. Selivanov, V. A., Votyakova, T. V., Zeak, J. A., Trucco, M., Roca, J., & Cascante, M. (2009). Bistability of mitochondrial respiration underlies paradoxical reactive oxygen species generation induced by anoxia. *PLoS computational biology*, 5(12), e1000619.
45. Semenza, G. L. (1999). Perspectives on oxygen sensing. *Cell*, 98(3), 281-284.

46. Hashimoto, T., Yonetani, M., & Nakamura, H. (2004). Selective brain hypothermia protects against hypoxic-ischemic injury in newborn rats by reducing hydroxyl radical production. *Kobe Journal of Medical Sciences*, 49(3/4), 83-92.
47. Borutaite, V., Mildaziene, V., Brown, G. C., & Brand, M. D. (1995). Control and kinetic analysis of ischemia-damaged heart mitochondria: which parts of the oxidative phosphorylation system are affected by ischemia?. *Biochimica et Biophysica Acta (BBA)-Molecular Basis of Disease*, 1272(3), 154-158.
48. Brookes, P. S., Yoon, Y., Robotham, J. L., Anders, M. W., & Sheu, S. S. (2004). Calcium, ATP, and ROS: a mitochondrial love-hate triangle. *American Journal of Physiology-Cell Physiology*, 287(4), C817-C833.
49. Brenner, C., & Moulin, M. (2012). Physiological roles of the permeability transition pore. *Circulation research*, 111(9), 1237-1247.
50. Hawrysh, P. J., & Buck, L. T. (2013). Anoxia-mediated calcium release through the mitochondrial permeability transition pore silences NMDA receptor currents in turtle neurons. *Journal of Experimental Biology*, 216(23), 4375-4387.
51. Horwitz, L. D., Fennessey, P. V., Shikes, R. H., & Kong, Y. (1994). Marked reduction in myocardial infarct size due to prolonged infusion of an antioxidant during reperfusion. *Circulation*, 89(4), 1792-1801.
52. Murphy, E., & Steenbergen, C. (2008). Mechanisms underlying acute protection from cardiac ischemia-reperfusion injury. *Physiological reviews*, 88(2), 581-609.
53. Fanter, C. E., Lin, Z., Keenan, S. W., Janzen, F. J., Mitchell, T. S., & Warren, D. E. (2020). Development-specific transcriptomic profiling suggests new mechanisms for anoxic survival in the ventricle of overwintering turtles. *Journal of Experimental Biology*, 223(4), jeb213918.
54. Chatenay-Lapointe, M., & Shadel, G. S. (2010). Stressed-out mitochondria get MAD. *Cell metabolism*, 12(6), 559-560.
55. Heo, J. M., Livnat-Levanon, N., Taylor, E. B., Jones, K. T., Dephoure, N., Ring, J., ... & Rutter, J. (2010). A stress-responsive system for mitochondrial protein degradation. *Molecular cell*, 40(3), 465-480.
56. Tullet, J. M. (2015). DAF-16 target identification in *C. elegans*: past, present and future. *Biogerontology*, 16(2), 221-234.
57. Kaushal, P. S., Sharma, M. R., Booth, T. M., Haque, E. M., Tung, C. S., Sanbonmatsu, K. Y., ... & Agrawal, R. K. (2014). Cryo-EM structure of the small subunit of the mammalian mitochondrial ribosome. *Proceedings of the National Academy of Sciences*, 111(20), 7284-7289.
58. Sharika, R., Subbaiah, P., & Balamurugan, K. (2018). Studies on reproductive stress caused by candidate Gram positive and Gram negative bacteria using model organism,

- 828 *Caenorhabditis elegans*. *Gene*, 649, 113-126.
- 829 59. Melnikov S, Ben-Shem A, Garreau de Loubresse N, Jenner L, Yusupova G, Yusupov M.
830 One core, two shells: bacterial and eukaryotic ribosomes. *Nat Struct Mol*
831 *Biol.* 2012;19(6):560–567
- 832 60. You, K. T., Park, J., & Kim, V. N. (2015). Role of the small subunit processome in the
833 maintenance of pluripotent stem cells. *Genes & development*, 29(19), 2004-2009.
- 834 61. Chen, J., & Kastan, M. B. (2010). 5'–3'-UTR interactions regulate p53 mRNA translation
835 and provide a target for modulating p53 induction after DNA damage. *Genes &*
836 *development*, 24(19), 2146-2156.
- 837 62. Savada, R. P., & Bonham-Smith, P. C. (2014). Differential transcript accumulation and
838 subcellular localization of *Arabidopsis* ribosomal proteins. *Plant Science*, 223, 134-145.
- 839 63. Xu, X., Xiong, X., & Sun, Y. (2016). The role of ribosomal proteins in the regulation of cell
840 proliferation, tumorigenesis, and genomic integrity. *Science China Life Sciences*, 59(7),
841 656-672.
- 842 64. Larade, K., Nimigan, A., & Storey, K. B. (2001). Transcription pattern of ribosomal protein
843 L26 during anoxia exposure in *Littorina littorea*. *Journal of Experimental Zoology*, 290(7),
844 759-768.
- 845 65. Thomas, G. (2000). An encore for ribosome biogenesis in the control of cell
846 proliferation. *Nature cell biology*, 2(5), E71-E72.
- 847 66. Shukla, S. K., & Kumar, V. (2012). Hepatitis B virus X protein and c-Myc cooperate in
848 the upregulation of ribosome biogenesis and in cellular transformation. *The FEBS*
849 *journal*, 279(20), 3859-3871.
- 850 67. Xu, C., Hwang, W., Jeong, D. E., Ryu, Y., Ha, C. M., Lee, S. J. V., ... & He, Z. M. (2018).
851 Genetic inhibition of an ATP synthase subunit extends lifespan in *C. elegans*. *Scientific*
852 *reports*, 8(1), 1-14.
- 853 68. Maglioni, S., & Ventura, N. (2016). *C. elegans* as a model organism for human
854 mitochondrial associated disorders. *Mitochondrion*, 30, 117-125.
- 855 69. McKay, R. M., McKay, J. P., Avery, L., & Graff, J. M. (2003). *C. elegans*: a model for
856 exploring the genetics of fat storage. *Developmental cell*, 4(1), 131-142.
- 857 70. Rea, S. L., Ventura, N., & Johnson, T. E. (2007). Relationship between mitochondrial
858 electron transport chain dysfunction, development, and life extension in *Caenorhabditis*
859 *elegans*. *PLoS biology*, 5(10), e259.
- 860 71. Hartman, P. S., Ishii, N., Kayser, E. B., Morgan, P. G., & Sedensky, M. M. (2001).
861 Mitochondrial mutations differentially affect aging, mutability and anesthetic sensitivity in
862 *Caenorhabditis elegans*. *Mechanisms of ageing and development*, 122(11), 1187-1201.
- 863 72. Williams, J. C., Sue, C., Banting, G. S., Yang, H., Glerum, D. M., Hendrickson, W. A., &
864 Schon, E. A. (2005). Crystal structure of human SCO1: implications for redox signaling

by a mitochondrial cytochrome c oxidase “assembly” protein. *Journal of Biological Chemistry*, 280(15), 15202-15211.

73. Buceta, P. M. R., Romanelli-Cedrez, L., Babcock, S. J., Xun, H., VonPaige, M. L., Higley, T. W., ... & Salinas, G. (2019). The kynurenine pathway is essential for rodoquinone biosynthesis in *Caenorhabditis elegans*. *Journal of Biological Chemistry*, 294(28), 11047-11053.

74. Del Borrello, S., Lautens, M., Dolan, K., Tan, J. H., Davie, T., Schertzberg, M. R., ... & Fraser, A. G. (2019). Rodoquinone biosynthesis in *C. elegans* requires precursors generated by the kynurenine pathway. *Elife*, 8, e48165.

75. Tsai, P. C., Soong, B. W., Mademan, I., Huang, Y. H., Liu, C. R., Hsiao, C. T., ... & Lee, Y. C. (2017). A recurrent WARS mutation is a novel cause of autosomal dominant distal hereditary motor neuropathy. *Brain*, 140(5), 1252-1266.

76. Tan, J. H., Lautens, M., Romanelli-Cedrez, L., Wang, J., Schertzberg, M. R., Reinl, S. R., ... & Salinas, G. (2020). Alternative splicing of *coq-2* controls the levels of rodoquinone in animals. *Elife*, 9, e56376.

77. Smolková, K., & Ježek, P. (2012). The role of mitochondrial NADPH-dependent isocitrate dehydrogenase in cancer cells. *International journal of cell biology*, 2012.

78. Martínez-Reyes, I., & Chandel, N. S. (2020). Mitochondrial TCA cycle metabolites control physiology and disease. *Nature communications*, 11(1), 1-11.

79. Penkov, S., Kaptan, D., Erkut, C., Sarov, M., Mende, F., & Kurzchalia, T. V. (2015). Integration of carbohydrate metabolism and redox state controls dauer larva formation in *Caenorhabditis elegans*. *Nature communications*, 6(1), 1-10.

80. Yang, H. C., Yu, H., Liu, Y. C., Chen, T. L., Stern, A., Lo, S. J., & Chiu, D. T. Y. (2019). IDH-1 deficiency induces growth defects and metabolic alterations in GSPD-1-deficient *Caenorhabditis elegans*. *Journal of Molecular Medicine*, 97(3), 385-396.

81. Lutz, P. L., & Nilsson, G. E. (1997). Contrasting strategies for anoxic brain survival--glycolysis up or down. *The Journal of experimental biology*, 200(2), 411-419.

82. Semenza, G. L. (2001). HIF-1, O₂, and the 3 PHDs: how animal cells signal hypoxia to the nucleus. *Cell*, 107(1), 1-3.

83. Huang, S., Colmer, T. D., & Millar, A. H. (2008). Does anoxia tolerance involve altering the energy currency towards PPI?. *Trends in plant science*, 13(5), 221-227.

84. Larade, K., & Storey, K. B. (2009). Living without oxygen: anoxia-responsive gene expression and regulation. *Current Genomics*, 10(2), 76-85.

85. Jackson, A. D., & McLaughlin, J. (2009). Digestion and absorption. *Surgery (oxford)*, 27(6), 231-236.

86. Lodish, H., Berk, A., Kaiser, C. A., Kaiser, C., Krieger, M., Scott, M. P., ... & Matsudaira, P. (2008). *Molecular cell biology*. Macmillan.

87. Papaevgeniou, N., & Chondrogianni, N. (2014). The ubiquitin proteasome system in *Caenorhabditis elegans* and its regulation. *Redox biology*, 2, 333-347.
88. Jones, D., Crowe, E., Stevens, T. A., & Candido, E. P. M. (2001). Functional and phylogenetic analysis of the ubiquitylation system in *Caenorhabditis elegans*: ubiquitin-conjugating enzymes, ubiquitin-activating enzymes, and ubiquitin-like proteins. *Genome biology*, 3(1), 1-15.
89. Schaefer, H., & Rongo, C. (2006). KEL-8 is a substrate receptor for CUL3-dependent ubiquitin ligase that regulates synaptic glutamate receptor turnover. *Molecular biology of the cell*, 17(3), 1250-1260.
90. Stogios, P. J., Downs, G. S., Jauhal, J. J., Nandra, S. K., & Privé, G. G. (2005). Sequence and structural analysis of BTB domain proteins. *Genome biology*, 6(10),
91. Kim, K. W., Tang, N. H., Piggott, C. A., Andrusiak, M. G., Park, S., Zhu, M., ... & Jin, Y. (2018). Expanded genetic screening in *Caenorhabditis elegans* identifies new regulators and an inhibitory role for NAD⁺ in axon regeneration. *Elife*, 7, e39756.
92. Pintard, L., Kurz, T., Glaser, S., Willis, J. H., Peter, M., & Bowerman, B. (2003). Neddylation and deneddylation of CUL-3 is required to target MEI-1/Katanin for degradation at the meiosis-to-mitosis transition in *C. elegans*. *Current Biology*, 13(11), 911-921.
93. Brockway, H., Balukoff, N., Dean, M., Alleva, B., & Smolikove, S. (2014). The CSN/COP9 signalosome regulates synaptonemal complex assembly during meiotic prophase I of *Caenorhabditis elegans*. *PLoS genetics*, 10(11), e1004757.
94. Fraser, A. G., Kamath, R. S., Zipperlen, P., Martinez-Campos, M., Sohrmann, M., & Ahringer, J. (2000). Functional genomic analysis of *C. elegans* chromosome I by systematic RNA interference. *Nature*, 408(6810), 325-330.
95. Blumenthal, T., Evans, D., Link, C. D., Guffanti, A., Lawson, D., Thierry-Mieg, J., ... & Kim, S. K. (2002). A global analysis of *Caenorhabditis elegans* operons. *Nature*, 417(6891), 851-854.
96. Syntichaki, P., Xu, K., Driscoll, M., & Tavernarakis, N. (2002). Specific aspartyl and calpain proteases are required for neurodegeneration in *C. elegans*. *Nature*, 419(6910), 939-944.
97. Vassalli, J. D., Sappino, A. P., & Belin, D. (1991). The plasminogen activator/plasmin system. *The Journal of clinical investigation*, 88(4), 1067-1072.
98. Altincicek, B., Fischer, M., Fischer, M., Lüersen, K., Boll, M., Wenzel, U., & Vilcinskas, A. (2010). Role of matrix metalloproteinase ZMP-2 in pathogen resistance and development in *Caenorhabditis elegans*. *Developmental & Comparative Immunology*, 34(11), 1160-1169.

99. Fischer, M., Fitzenberger, E., Kull, R., Boll, M., & Wenzel, U. (2014). The zinc matrix metalloproteinase ZMP-2 increases survival of *Caenorhabditis elegans* through interference with lipoprotein absorption. *Genes & nutrition*, 9(4), 414.
100. Vabulas, R. M., & Hartl, F. U. (2005). Protein synthesis upon acute nutrient restriction relies on proteasome function. *Science*, 310(5756), 1960-1963.
101. Scott, R. C., Schuldiner, O., & Neufeld, T. P. (2004). Role and regulation of starvation-induced autophagy in the *Drosophila* fat body. *Developmental cell*, 7(2), 167-178.
102. Huber, L. A., & Teis, D. (2016). Lysosomal signaling in control of degradation pathways. *Current opinion in cell biology*, 39, 8-14.
103. Wang, R. C., & Levine, B. (2010). Autophagy in cellular growth control. *FEBS letters*, 584(7), 1417-1426.
104. Russell, R. C., Yuan, H. X., & Guan, K. L. (2014). Autophagy regulation by nutrient signaling. *Cell research*, 24(1), 42-57.
105. Liang, X. H., Jackson, S., Seaman, M., Brown, K., Kempkes, B., Hibshoosh, H., & Levine, B. (1999). Induction of autophagy and inhibition of tumorigenesis by beclin 1. *Nature*, 402(6762), 672-676.
106. Bar-Peled, L., Schweitzer, L. D., Zoncu, R., & Sabatini, D. M. (2012). Ragulator is a GEF for the rag GTPases that signal amino acid levels to mTORC1. *Cell*, 150(6), 1196-1208.
107. Meléndez, A., Tallóczy, Z., Seaman, M., Eskelinen, E. L., Hall, D. H., & Levine, B. (2003). Autophagy genes are essential for dauer development and life-span extension in *C. elegans*. *Science*, 301(5638), 1387-1391.
108. Wang, X., & Proud, C. G. (2009). Nutrient control of TORC1, a cell-cycle regulator. *Trends in cell biology*, 19(6), 260-267.
109. Thompson, A. R., & Vierstra, R. D. (2005). Autophagic recycling: lessons from yeast help define the process in plants. *Current opinion in plant biology*, 8(2), 165-173.
110. Ladevaia, V., Liu, R., & Proud, C. G. (2014, December). mTORC1 signaling controls multiple steps in ribosome biogenesis. In *Seminars in cell & developmental biology* (Vol. 36, pp. 113-120). Academic Press.
111. Ma, X. M., & Blenis, J. (2009). Molecular mechanisms of mTOR-mediated translational control. *Nature reviews Molecular cell biology*, 10(5), 307-318.
112. Howell, J. J., & Manning, B. D. (2011). mTOR couples cellular nutrient sensing to organismal metabolic homeostasis. *Trends in Endocrinology & Metabolism*, 22(3), 94-102.

- 973 113. Nussbaumer, A.D., Bright, M., Baranyi, C., Beisser, C.J., and Ott, J.A. (2004)
974 Attachment mechanism in a highly specific association between ectosymbiotic bacteria
975 and marine nematodes. *Aquat Microb Ecol* 34:239–246
- 976 114. Bulgheresi S, Schabussova I, Chen T, Mullin NP, Maizels RM, Ott JA. A new C-
977 type lectin similar to the human immunoreceptor DC-SIGN mediates symbiont acquisition
978 by a marine nematode. *Appl Environ Microbiol.* 2006;72:2950–2956
- 979 115. Bulgheresi S, Gruber-Vodicka HR, Heindl NR, Dirks U, Kostadinova M,
980 Breiteneder H, Ott JA. Sequence variability of the pattern recognition receptor Mermaid
981 mediates specificity of marine nematode symbioses. *ISME J.* 2011;5:986–998
- 982 116. Koropatkin, N. M., Cameron, E. A., & Martens, E. C. (2012). How glycan
983 metabolism shapes the human gut microbiota. *Nature Reviews Microbiology*, 10(5), 323-
984 335.
- 985 117. Simon, H. U., Haj-Yehia, A., & Levi-Schaffer, F. (2000). Role of reactive oxygen
986 species (ROS) in apoptosis induction. *Apoptosis*, 5(5), 415-418.
- 987 118. Martinou, J. C., Desagher, S., & Antonsson, B. (2000). Cytochrome c release
988 from mitochondria: all or nothing. *Nature cell biology*, 2(3), E41-E43.
- 989 119. Gogvadze, V., Orrenius, S., & Zhivotovsky, B. (2006). Multiple pathways of
990 cytochrome c release from mitochondria in apoptosis. *Biochimica et Biophysica Acta*
991 *(BBA)-Bioenergetics*, 1757(5-6), 639-647.
- 992 120. Mangahas, P. M., & Zhou, Z. (2005, April). Clearance of apoptotic cells in
993 *Caenorhabditis elegans*. In *Seminars in cell & developmental biology* (Vol. 16, No. 2, pp.
994 295-306). Academic Press.
- 995 121. Kaufmann, S. H., Lee, S. H., Meng, X. W., Loegering, D. A., Kottke, T. J.,
996 Henzing, A. J., ... & Earnshaw, W. C. (2008). Apoptosis-associated caspase activation
997 assays. *Methods*, 44(3), 262-272.
- 998 122. Liu, X., Kim, C. N., Yang, J., Jemmerson, R., & Wang, X. (1996). Induction of
999 apoptotic program in cell-free extracts: requirement for dATP and cytochrome
1000 c. *Cell*, 86(1), 147-157.
- 1001 123. Tafani, M., Schneider, T. G., Pastorino, J. G., & Farber, J. L. (2000). Cytochrome
1002 c-dependent activation of caspase-3 by tumor necrosis factor requires induction of the
1003 mitochondrial permeability transition. *The American journal of pathology*, 156(6), 2111-
1004 2121.
- 1005 124. Takacs-Vellai, K., Vellai, T., Puoti, A., Passannante, M., Wicky, C., Streit, A., ...
1006 & Müller, F. (2005). Inactivation of the autophagy gene bec-1 triggers apoptotic cell death
1007 in *C. elegans*. *Current biology*, 15(16), 1513-1517.

125. Wang, X., Li, W., Zhao, D., Liu, B., Shi, Y., Chen, B., ... & Xue, D. (2010). *Caenorhabditis elegans* transthyretin-like protein TTR-52 mediates recognition of apoptotic cells by the CED-1 phagocyte receptor. *Nature cell biology*, 12(7), 655-664.
126. Chen, Y. Z., Mapes, J., Lee, E. S., Skeen-Gaar, R. R., & Xue, D. (2013). Caspase-mediated activation of *Caenorhabditis elegans* CED-8 promotes apoptosis and phosphatidylserine externalization. *Nature communications*, 4(1), 1-9.
127. Parrish, J. Z., & Xue, D. (2003). Functional genomic analysis of apoptotic DNA degradation in *C. elegans*. *Molecular cell*, 11(4), 987-996.
128. Samejima, K., & Earnshaw, W. C. (2005). Trashing the genome: the role of nucleases during apoptosis. *Nature reviews Molecular cell biology*, 6(9), 677-688.
129. Sasaki, A., Nakae, I., Nagasawa, M., Hashimoto, K., Abe, F., Saito, K., ... & Kontani, K. (2013). Arl8/ARL-8 functions in apoptotic cell removal by mediating phagolysosome formation in *Caenorhabditis elegans*. *Molecular biology of the cell*, 24(10), 1584-1592.
130. Hurwitz, M. E., Vanderzalm, P. J., Bloom, L., Goldman, J., Garriga, G., & Horvitz, H. R. (2009). Abl kinase inhibits the engulfment of apoptotic cells in *Caenorhabditis elegans*. *PLoS biology*, 7(4), e1000099.
131. Berdichevsky, A., Nedelcu, S., Boulias, K., Bishop, N. A., Guarente, L., & Horvitz, H. R. (2010). 3-Ketoacyl thiolase delays aging of *Caenorhabditis elegans* and is required for lifespan extension mediated by sir-2.1. *Proceedings of the National Academy of Sciences*, 107(44), 18927-18932.
132. Chughtai, A. A., Kaššák, F., Kostrouchová, M., Novotný, J. P., Krause, M. W., Saudek, V., ... & Kostrouchová, M. (2015). Perilipin-related protein regulates lipid metabolism in *C. elegans*. *PeerJ*, 3, e1213.
133. Horikawa, M., & Sakamoto, K. (2009). Fatty-acid metabolism is involved in stress-resistance mechanisms of *Caenorhabditis elegans*. *Biochemical and biophysical research communications*, 390(4), 1402-1407.
134. Krivoruchko, A., & Storey, K. B. (2015). Turtle anoxia tolerance: biochemistry and gene regulation. *Biochimica et Biophysica Acta (BBA)-General Subjects*, 1850(6), 1188-1196.
135. Brendza, K. M., Haakenson, W., Cahoon, R. E., Hicks, L. M., Palavalli, L. H., Chiapelli, B. J., ... & Jez, J. M. (2007). Phosphoethanolamine N-methyltransferase (PMT-1) catalyses the first reaction of a new pathway for phosphocholine biosynthesis in *Caenorhabditis elegans*. *Biochemical Journal*, 404(3), 439-448.
136. Thomas, J. H. (1990). Genetic analysis of defecation in *Caenorhabditis elegans*. *Genetics*, 124(4), 855-872.

137. McIntire, S. L., Jorgensen, E., Kaplan, J., & Horvitz, H. R. (1993). The GABAergic nervous system of *Caenorhabditis elegans*. *Nature*, 364(6435), 337-341.
138. Jin, Y., Jorgensen, E., Hartwig, E., & Horvitz, H. R. (1999). The *Caenorhabditis elegans* gene *unc-25* encodes glutamic acid decarboxylase and is required for synaptic transmission but not synaptic development. *Journal of Neuroscience*, 19(2), 539-548.
139. Gally, C., & Bessereau, J. L. (2003). GABA is dispensable for the formation of junctional GABA receptor clusters in *Caenorhabditis elegans*. *Journal of Neuroscience*, 23(7), 2591-2599.
140. Nordquist, S. K., Smith, S. R., & Pierce, J. T. (2018). Systematic functional characterization of human 21st chromosome orthologs in *Caenorhabditis elegans*. *G3: Genes, Genomes, Genetics*, 8(3), 967-979.
141. Risley, M. G., Kelly, S. P., Jia, K., Grill, B., & Dawson-Scully, K. (2016). Modulating behavior in *C. elegans* using electroshock and antiepileptic drugs. *PLoS One*, 11(9), e0163786.
142. Martin, D. L., & Rimvall, K. (1993). Regulation of γ -aminobutyric acid synthesis in the brain. *Journal of neurochemistry*, 60(2), 395-407.
143. van der Vos KE, Coffey PJ. Glutamine metabolism links growth factor signaling to the regulation of autophagy. *Autophagy*. 2012;8:1862–1864
144. Yen, C. A., & Curran, S. P. (2021). Incomplete proline catabolism drives premature sperm aging. *Aging cell*, 20(2), e13308.
145. Tharmalingam, S., Burns, A. R., Roy, P. J., & Hampson, D. R. (2012). Orthosteric and allosteric drug binding sites in the *Caenorhabditis elegans mgl-2* metabotropic glutamate receptor. *Neuropharmacology*, 63(4), 667-674.
146. Baker, A. J., Zornow, M. H., Scheller, M. S., Yaksh, T. L., Skilling, S. R., Smullin, D. H., ... & Kuczenski, R. (1991). Changes in extracellular concentrations of glutamate, aspartate, glycine, dopamine, serotonin, and dopamine metabolites after transient global ischemia in the rabbit brain. *Journal of neurochemistry*, 57(4), 1370-1379.
147. Lutz, P. L., Nilsson, G. E., & Prentice, H. M. (2003a). The brain without oxygen: causes of failure-physiological and molecular mechanisms for survival. Springer Science & Business Media.
148. Milton, S. L., Thompson, J. W., & Lutz, P. L. (2002). Mechanisms for maintaining extracellular glutamate levels in the anoxic turtle striatum. *American Journal of Physiology-Regulatory, Integrative and Comparative Physiology*, 282(5), R1317-R1323.
149. Mathews, G. C., & Diamond, J. S. (2003). Neuronal glutamate uptake contributes to GABA synthesis and inhibitory synaptic strength. *Journal of Neuroscience*, 23(6), 2040-2048.

150. Milton, S. L., & Lutz, P. L. (1998). Low extracellular dopamine levels are maintained in the anoxic turtle (*Trachemys scripta*) striatum. *Journal of Cerebral Blood Flow & Metabolism*, 18(7), 803-807.
151. Lutz, P. L., Prentice, H. M., & Milton, S. L. (2003b). Is turtle longevity linked to enhanced mechanisms for surviving brain anoxia and reoxygenation?. *Experimental Gerontology*, 38(7), 797-800.
152. Nilsson, G. E. (1990). Long-term anoxia in crucian carp: changes in the levels of amino acid and monoamine neurotransmitters in the brain, catecholamines in chromaffin tissue, and liver glycogen. *Journal of Experimental Biology*, 150(1), 295-320.
153. Schuske, K., Beg, A. A., & Jorgensen, E. M. (2004). The GABA nervous system in *C. elegans*. *Trends in neurosciences*, 27(7), 407-414.
154. Sawin, E. R., Ranganathan, R., & Horvitz, H. R. (2000). *C. elegans* locomotory rate is modulated by the environment through a dopaminergic pathway and by experience through a serotonergic pathway. *Neuron*, 26(3), 619-631.
155. Sanyal, S., Wintle, R. F., Kindt, K. S., Nuttley, W. M., Arvan, R., Fitzmaurice, P., ... & Van Tol, H. H. (2004). Dopamine modulates the plasticity of mechanosensory responses in *Caenorhabditis elegans*. *The EMBO journal*, 23(2), 473-482.
156. Gainetdinov, R. R., Sotnikova, T. D., & Caron, M. G. (2002). Monoamine transporter pharmacology and mutant mice. *Trends in pharmacological sciences*, 23(8), 367-373.
157. McDonald, P. W., Jessen, T., Field, J. R., & Blakely, R. D. (2006). Dopamine signaling architecture in *Caenorhabditis elegans*. *Cellular and molecular neurobiology*, 26(4), 591-616.
158. Soontornniyomkij, V., Risbrough, V. B., Young, J. W., Soontornniyomkij, B., Jeste, D. V., & Achim, C. L. (2012). Hippocampal calbindin-1 immunoreactivity correlate of recognition memory performance in aged mice. *Neuroscience letters*, 516(1), 161-165.
159. Hobert, O. (2018). The neuronal genome of *Caenorhabditis elegans*. *WormBook: The Online Review of C. elegans Biology*
160. Steger, K. A., Shtonda, B. B., Thacker, C., Snutch, T. P., & Avery, L. (2005). The *C. elegans* T-type calcium channel CCA-1 boosts neuromuscular transmission. *Journal of Experimental Biology*, 208(11), 2191-2203.
161. Zhou, K., Cherra III, S. J., Goncharov, A., & Jin, Y. (2017). Asynchronous cholinergic drive correlates with excitation-inhibition imbalance via a neuronal Ca²⁺ sensor protein. *Cell reports*, 19(6), 1117-1129.
162. Bickler, P. E. (1992). Cerebral anoxia tolerance in turtles: regulation of intracellular calcium and pH. *American Journal of Physiology-Regulatory, Integrative and Comparative Physiology*, 263(6), R1298-R1302.

163. Dell'Anna, E., Geloso, M. C., Magarelli, M., & Molinari, M. (1996). Development of GABA and calcium binding proteins immunoreactivity in the rat hippocampus following neonatal anoxia. *Neuroscience letters*, 211(2), 93-96.
164. Akira, S., Uematsu, S., & Takeuchi, O. (2006). Pathogen recognition and innate immunity. *Cell*, 124(4), 783-801.
165. Wang, D. (2019). Epidermal Barrier for Nematodes Against Toxicity of Environmental Toxicants or Stresses. In *Target Organ Toxicology in Caenorhabditis elegans* (pp. 97-122). Springer, Singapore.
166. Dravid, P., Kaushal, D. C., Saxena, J. K., & Kaushal, N. A. (2015). Isolation and characterization of endochitinase and exochitinase of *Setaria cervi*. *Parasitology international*, 64(6), 579-586.
167. Krasity, B. C., Troll, J. V., Lehnert, E. M., Hackett, K. T., Dillard, J. P., Apicella, M. A., ... & McFall-Ngai, M. J. (2015). Structural and functional features of a developmentally regulated lipopolysaccharide-binding protein. *MBio*, 6(5), e01193-15.
168. Chen, F., Krasity, B. C., Peyer, S. M., Koehler, S., Ruby, E. G., Zhang, X., & McFall-Ngai, M. J. (2017). Bactericidal permeability-increasing proteins shape host-microbe interactions. *MBio*, 8(2), e00040-17.
169. Pradel, E., Zhang, Y., Pujol, N., Matsuyama, T., Bargmann, C. I., & Ewbank, J. J. (2007). Detection and avoidance of a natural product from the pathogenic bacterium *Serratia marcescens* by *Caenorhabditis elegans*. *Proceedings of the National Academy of Sciences*, 104(7), 2295-2300.
170. Brandt, J. P., & Ringstad, N. (2015). Toll-like receptor signaling promotes development and function of sensory neurons required for a *C. elegans* pathogen-avoidance behavior. *Current Biology*, 25(17), 2228-2237.
171. Dang, H., & Lovell, C. R. (2016). Microbial surface colonization and biofilm development in marine environments. *Microbiology and molecular biology reviews*, 80(1), 91-138.
172. Suzuki, M., Sagoh, N., Iwasaki, H., Inoue, H., & Takahashi, K. (2004). Metalloproteases with EGF, CUB, and thrombospondin-1 domains function in molting of *Caenorhabditis elegans*.
173. Zhang, Y., Foster, J. M., Nelson, L. S., Ma, D., & Carlow, C. K. (2005). The chitin synthase genes *chs-1* and *chs-2* are essential for *C. elegans* development and responsible for chitin deposition in the eggshell and pharynx, respectively. *Developmental biology*, 285(2), 330-339.
174. Zugasti, O., Rajan, J., & Kuwabara, P. E. (2005). The function and expansion of the Patched-and Hedgehog-related homologs in *C. elegans*. *Genome research*, 15(10), 1402-1410.

175. Hornsten, A., Lieberthal, J., Fadia, S., Malins, R., Ha, L., Xu, X., ... & Li, C. (2007). APL-1, a *Caenorhabditis elegans* protein related to the human β -amyloid precursor protein, is essential for viability. *Proceedings of the National Academy of Sciences*, 104(6), 1971-1976.
176. Russel, S., Frand, A. R., & Ruvkun, G. (2011). Regulation of the *C. elegans* molt by pqn-47. *Developmental biology*, 360(2), 297-309.
177. Pan, K. Z., Palter, J. E., Rogers, A. N., Olsen, A., Chen, D., Lithgow, G. J., & Kapahi, P. (2007). Inhibition of mRNA translation extends lifespan in *Caenorhabditis elegans*. *Aging cell*, 6(1), 111-119.
178. Pal, S., Lant, B., Yu, B., Tian, R., Tong, J., Krieger, J. R., ... & Derry, W. B. (2017). CCM-3 promotes *C. elegans* germline development by regulating vesicle trafficking cytokinesis and polarity. *Current Biology*, 27(6), 868-876.
179. Park, B. J., Lee, D. G., Yu, J. R., Jung, S. K., Choi, K., Lee, J., ... & Ahnn, J. (2001). Calreticulin, a calcium-binding molecular chaperone, is required for stress response and fertility in *Caenorhabditis elegans*. *Molecular Biology of the Cell*, 12(9), 2835-2845.
180. Clark, S. G., Shurland, D. L., Meyerowitz, E. M., Bargmann, C. I., & Van Der Bliek, A. M. (1997). A dynamin GTPase mutation causes a rapid and reversible temperature-inducible locomotion defect in *C. elegans*. *Proceedings of the National Academy of Sciences*, 94(19), 10438-10443.
181. Goedert, M., Baur, C. P., Ahringer, J., Jakes, R., Hasegawa, M., Spillantini, M. G., ... & Hill, F. (1996). PTL-1, a microtubule-associated protein with tau-like repeats from the nematode *Caenorhabditis elegans*. *Journal of cell science*, 109(11), 2661-2672.
182. Gatewood, B. K., & Bucher, E. A. (1997). The mup-4 locus in *Caenorhabditis elegans* is essential for hypodermal integrity, organismal morphogenesis and embryonic body wall muscle position. *Genetics*, 146(1), 165-183.
183. Fujii, T., Nakao, F., Shibata, Y., Shioi, G., Kodama, E., Fujisawa, H., & Takagi, S. (2002). *Caenorhabditis elegans* PlexinA, PLX-1, interacts with transmembrane semaphorins and regulates epidermal morphogenesis.
184. Gally, C., Wissler, F., Zahreddine, H., Quintin, S., Landmann, F., & Labouesse, M. (2009). Myosin II regulation during *C. elegans* embryonic elongation: LET-502/ROCK, MRCK-1 and PAK-1, three kinases with different roles. *Development*, 136(18), 3109-3119.
185. Zahreddine, H., Zhang, H., Diogon, M., Nagamatsu, Y., & Labouesse, M. (2010). CRT-1/calreticulin and the E3 ligase EEL-1/HUWE1 control hemidesmosome maturation in *C. elegans* development. *Current Biology*, 20(4), 322-327.

186. Jee, C., Choi, T. W., Kalichamy, K., Yee, J. Z., Song, H. O., Ji, Y. J., ... & Lee, S. K. (2012). CNP-1 (ARRD-17), a novel substrate of calcineurin, is critical for modulation of egg-laying and locomotion in response to food and lysine sensation in *Caenorhabditis elegans*. *Journal of molecular biology*, 417(3), 165-178.
187. Warner, A., Xiong, G., Qadota, H., Rogalski, T., Vogl, A. W., Moerman, D. G., & Benian, G. M. (2013). CPNA-1, a copine domain protein, is located at integrin adhesion sites and is required for myofilament stability in *Caenorhabditis elegans*. *Molecular biology of the cell*, 24(5), 601-616.
188. Perez, M. F., & Lehner, B. (2019). Vitellogenins-yolk gene function and regulation in *Caenorhabditis elegans*. *Frontiers in physiology*, 10, 1067.
189. Ding, M., Woo, W. M., & Chisholm, A. D. (2004). The cytoskeleton and epidermal morphogenesis in *C. elegans*. *Experimental cell research*, 301(1), 84-90.
190. Osório, D. S., Chan, F. Y., Saramago, J., Leite, J., Silva, A. M., Sobral, A. F., ... & Carvalho, A. X. (2019). Crosslinking activity of non-muscle myosin II is not sufficient for embryonic cytokinesis in *C. elegans*. *Development*, 146(21), dev179150.
191. Nelson, M. D., Zhou, E., Kiontke, K., Fradin, H., Maldonado, G., Martin, D., ... & Fitch, D. H. (2011). A bow-tie genetic architecture for morphogenesis suggested by a genome-wide RNAi screen in *Caenorhabditis elegans*. *PLoS genetics*, 7(3), e1002010.
192. Dalpé, G., Zhang, L. W., Zheng, H., & Culotti, J. G. (2004). Conversion of cell movement responses to Semaphorin-1 and Plexin-1 from attraction to repulsion by lowered levels of specific RAC GTPases in *C. elegans*.
193. Dalpe, G., Tarsitano, M., Persico, M. G., Zheng, H., & Culotti, J. (2013). *C. elegans* PVF-1 inhibits permissive UNC-40 signalling through CED-10 GTPase to position the male ray 1 sensillum. *Development*, 140(19), 4020-4030.
194. Dufourcq, P., Victor, M., Gay, F., Calvo, D., Hodgkin, J., & Shi, Y. (2002). Functional requirement for histone deacetylase 1 in *Caenorhabditis elegans* gonadogenesis. *Molecular and cellular biology*, 22(9), 3024-3034.
195. Choy, S. W., Wong, Y. M., Ho, S., & Chow, K. L. (2007). *C. elegans* SIN-3 and its associated HDAC corepressor complex act as mediators of male sensory ray development. *Biochemical and biophysical research communications*, 358(3), 802-807.
196. Park, J. O., Pan, J., Möhrlen, F., Schupp, M. O., Johnsen, R., Baillie, D. L., ... & Hutter, H. (2010). Characterization of the astacin family of metalloproteases in *C. elegans*. *BMC developmental biology*, 10(1), 1-13.
197. Topf, U., & Drabikowski, K. (2019). Ancient function of teneurins in tissue organization and neuronal guidance in the nematode *Caenorhabditis elegans*. *Frontiers in neuroscience*, 13, 205.

198. Spanier, B., Stürzenbaum, S. R., Holden-Dye, L. M., & Baumeister, R. (2005). *Caenorhabditis elegans* neprilysin NEP-1: an effector of locomotion and pharyngeal pumping. *Journal of molecular biology*, 352(2), 429-437.
199. Norman, K. R., Fazio, R. T., Mellem, J. E., Espelt, M. V., Strange, K., Beckerle, M. C., & Maricq, A. V. (2005). The Rho/Rac-family guanine nucleotide exchange factor VAV-1 regulates rhythmic behaviors in *C. elegans*. *Cell*, 123(1), 119-132.
200. De Cuyper, C., & Vanfleteren, J. R. (1982). Oxygen consumption during development and aging of the nematode *Caenorhabditis elegans*. *Comparative Biochemistry and Physiology Part A: Physiology*, 73(2), 283-289.
201. Uppaluri, S., & Brangwynne, C. P. (2015). A size threshold governs *Caenorhabditis elegans* developmental progression. *Proceedings of the Royal Society B: Biological Sciences*, 282(1813), 20151283.
202. Pellerone, F. I., Archer, S. K., Behm, C. A., Grant, W. N., Lacey, M. J., & Somerville, A. C. (2003). Trehalose metabolism genes in *Caenorhabditis elegans* and filarial nematodes. *International journal for parasitology*, 33(11), 1195-1206.
203. Schuster, L. N., & Sommer, R. J. (2012). Expressional and functional variation of horizontally acquired cellulases in the nematode *Pristionchus pacificus*. *Gene*, 506(2), 274-282.
204. Yuan, Y., Kadiyala, C. S., Ching, T. T., Hakimi, P., Saha, S., Xu, H., ... & Feng, Z. (2012). Enhanced energy metabolism contributes to the extended life span of calorie-restricted *Caenorhabditis elegans*. *Journal of Biological Chemistry*, 287(37), 31414-31426.
205. Kitaoka, S., Morielli, A. D., & Zhao, F. Q. (2013). FGT-1 is a mammalian GLUT2-like facilitative glucose transporter in *Caenorhabditis elegans* whose malfunction induces fat accumulation in intestinal cells. *PLoS One*, 8(6), e68475.
206. Bertoli, S., Neri, I. G., Trentani, C., Ferraris, C., De Amicis, R., Battezzati, A., ... & Tagliabue, A. (2015). Short-term effects of ketogenic diet on anthropometric parameters, body fat distribution, and inflammatory cytokine production in GLUT1 deficiency syndrome. *Nutrition*, 31(7-8), 981-987.
207. Miyagawa, K., Sakamoto, H., Yoshida, T., Yamashita, Y., Mitsui, Y., Furusawa, M.... & Terada, M. (1988). hst-1 transforming protein: expression in silkworm cells and characterization as a novel heparin-binding growth factor. *Oncogene*, 3(4), 383-389.
208. Bhattacharya, R., Townley, R. A., Berry, K. L., & Bülow, H. E. (2009). The PAPS transporter PST-1 is required for heparan sulfation and is essential for viability and neural development in *C. elegans*. *Journal of cell science*, 122(24), 4492-4504.
209. Crowe, J. H., Crowe, L. M., Carpenter, J. F., & Wistrom, C. A. (1987). Stabilization of dry phospholipid bilayers and proteins by sugars. *Biochemical Journal*, 242(1), 1.

- 1263 210. Carpenter, J. F., & Crowe, J. H. (1988). Modes of stabilization of a protein by
1264 organic solutes during desiccation. *Cryobiology*, 25(5), 459-470.
- 1265 211. Chen, Q., Ma, E., Behar, K. L., Xu, T., & Haddad, G. G. (2002). Role of trehalose
1266 phosphate synthase in anoxia tolerance and development in *Drosophila*
1267 *melanogaster*. *Journal of Biological Chemistry*, 277(5), 3274-3279.
- 1268 212. Mongan, N. P., Jones, A. K., Smith, G. R., Sansom, M. S., & Sattelle, D. B. (2002).
1269 Novel $\alpha 7$ -like nicotinic acetylcholine receptor subunits in the nematode *Caenorhabditis*
1270 *elegans*. *Protein Science*, 11(5), 1162-1171.
- 1271 213. Patton, A., Knuth, S., Schaheen, B., Dang, H., Greenwald, I., & Fares, H. (2005).
1272 Endocytosis function of a ligand-gated ion channel homolog in *Caenorhabditis elegans*.
1273 *Current biology*, 15(11), 1045-1050.
- 1274 214. Gendrel, M., Rapti, G., Richmond, J. E., & Bessereau, J. L. (2009). A secreted
1275 complement-control-related protein ensures acetylcholine receptor clustering. *Nature*,
1276 461(7266), 992-996.
- 1277 215. Boulin, T., Rapti, G., Briseño-Roa, L., Stigloher, C., Richmond, J. E., Paoletti, P.,
1278 & Bessereau, J. L. (2012). Positive modulation of a Cys-loop acetylcholine receptor by
1279 an auxiliary transmembrane subunit. *Nature neuroscience*, 15(10), 1374-1381.
- 1280 216. Chan, J. P., Hu, Z., & Sieburth, D. (2012). Recruitment of sphingosine kinase to
1281 presynaptic terminals by a conserved muscarinic signaling pathway promotes
1282 neurotransmitter release. *Genes & development*, 26(10), 1070-1085.
- 1283 217. Sun, L., Zang, W. J., Wang, H., Zhao, M., Yu, X. J., He, X., ... & Zhou, J. (2014).
1284 Acetylcholine promotes ROS detoxification against hypoxia/reoxygenation-induced
1285 oxidative stress through FoxO3a/PGC-1 α dependent superoxide dismutase. *Cellular*
1286 *Physiology and Biochemistry*, 34(5), 1614-1625.
- 1287 218. Guest, M., Bull, K., Walker, R. J., Amliwala, K., O'Connor, V., Harder, A., ... &
1288 Hopper, N. A. (2007). The calcium-activated potassium channel, SLO-1, is required for
1289 the action of the novel cyclo-octadepsipeptide anthelmintic, emodepside, in
1290 *Caenorhabditis elegans*. *International journal for parasitology*, 37(14), 1577-1588.
- 1291 219. Hurd, D. D., Miller, R. M., Núñez, L., & Portman, D. S. (2010). Specific α -and β -
1292 tubulin isotypes optimize the functions of sensory cilia in *Caenorhabditis elegans*.
1293 *Genetics*, 185(3), 883-896.
- 1294 220. Wang, Z., Hou, Y., Guo, X., van der Voet, M., Boxem, M., Dixon, J. E., ... & Jin,
1295 Y. (2013). The EBAX-type Cullin-RING E3 ligase and Hsp90 guard the protein quality of
1296 the SAX-3/Robo receptor in developing neurons. *Neuron*, 79(5), 903-916.
- 1297 221. Woo, W. M., Berry, E. C., Hudson, M. L., Swale, R. E., Goncharov, A., &
1298 Chisholm, A. D. (2008). The *C. elegans* F-spondin family protein SPON-1 maintains cell
1299 adhesion in neural and non-neural tissues.

222. Schwarz, V., Pan, J., Voltmer-Irsch, S., & Hutter, H. (2009). IgCAMs redundantly control axon navigation in *Caenorhabditis elegans*. *Neural development*, 4(1), 1-15.
223. Gu, G. U. O. Q. I. A. N. G., Caldwell, G. A., & Chalfie, M. (1996). Genetic interactions affecting touch sensitivity in *Caenorhabditis elegans*. *Proceedings of the National Academy of Sciences*, 93(13), 6577-6582.
224. Han, L., Wang, Y., Sangaletti, R., D'Urso, G., Lu, Y., Shaham, S., & Bianchi, L. (2013). Two novel DEG/ENaC channel subunits expressed in glia are needed for nose-touch sensitivity in *Caenorhabditis elegans*. *Journal of Neuroscience*, 33(3), 936-949.
225. Li, Z., Li, Y., Yi, Y., Huang, W., Yang, S., Niu, W., ... & Xu, T. (2012). Dissecting a central flip-flop circuit that integrates contradictory sensory cues in *C. elegans* feeding regulation. *Nature communications*, 3(1), 1-8.
226. Tsuji, N., Morales, T. H., Ozols, V. V., Carmody, A. B., & Chandrashekar, R. (1999). Identification of an asparagine amidohydrolase from the filarial parasite *Dirofilaria immitis*. *International journal for parasitology*, 29(9), 1451-1455.
227. Chen, C. C., Lim, C. Y., Lee, P. J., Hsu, A. L., & Ching, T. T. (2020). S-adenosyl methionine synthetase SAMS-5 mediates dietary restriction-induced longevity in *Caenorhabditis elegans*. *PloS one*, 15(11), e0241455.
228. Russell, D., & Snyder, S. H. (1968). Amine synthesis in rapidly growing tissues: ornithine decarboxylase activity in regenerating rat liver, chick embryo, and various tumors. *Proceedings of the National Academy of Sciences of the United States of America*, 60(4), 1420.
229. Heby, O. (1981). Role of polyamines in the control of cell proliferation and differentiation. *Differentiation*, 19(1-3), 1-20.
230. Gilad, G. M., & Gilad, V. H. (1991). Polyamines can protect against ischemia-induced nerve cell death in gerbil forebrain. *Experimental neurology*, 111(3), 349-355.
231. Longo, L. D., Packianathan, S., McQueary, J. A., Stagg, R. B., Byus, C. V., & Cain, C. D. (1993). Acute hypoxia increases ornithine decarboxylase activity and polyamine concentrations in fetal rat brain. *Proceedings of the National Academy of Sciences*, 90(2), 692-696.
232. Ward, J. D., Mullaney, B., Schiller, B. J., He, L. D., Petnic, S. E., Couillault, C., ... & Yamamoto, K. R. (2014). Defects in the *C. elegans* acyl-CoA synthase, *acs-3*, and nuclear hormone receptor, *nhr-25*, cause sensitivity to distinct, but overlapping stresses. *PloS one*, 9(3), e92552.
233. Wang, F., Dai, Y., Zhu, X., Chen, Q., Zhu, H., Zhou, B., ... & Pang, S. (2021). Saturated very long chain fatty acid configures glycosphingolipid for lysosome homeostasis in long-lived *C. elegans*. *Nature Communications*, 12(1), 1-14.

234. Bastiani, C. A., Gharib, S., Simon, M. I., & Sternberg, P. W. (2003). *Caenorhabditis elegans* Gαq regulates egg-laying behavior via a PLCβ-independent and serotonin-dependent signaling pathway and likely functions both in the nervous system and in muscle. *Genetics*, 165(4), 1805-1822.
235. Taha, T. A., Kitatani, K., El-Alwani, M., Bielawski, J., Hannun, Y. A., & Obeid, L. M. (2006). Loss of sphingosine kinase-1 activates the intrinsic pathway of programmed cell death: modulation of sphingolipid levels and the induction of apoptosis. *The FASEB journal*, 20(3), 482-484.
236. Deng, X., Yin, X., Allan, R., Lu, D. D., Maurer, C. W., Haimovitz-Friedman, A., ... & Kolesnick, R. (2008). Ceramide biogenesis is required for radiation-induced apoptosis in the germ line of *C. elegans*. *Science*, 322(5898), 110-115.
237. Menuz, V., Howell, K. S., Gentina, S., Epstein, S., Riezman, I., Fornallaz-Mulhauser, M., ... & Martinou, J. C. (2009). Protection of *C. elegans* from anoxia by HYL-2 ceramide synthase. *Science*, 324(5925), 381-384.
238. Watts, J. L., & Ristow, M. (2017). Lipid and carbohydrate metabolism in *Caenorhabditis elegans*. *Genetics*, 207(2), 413-446.
239. Lutz, P. L., Nilsson, G. E., & Pérez-Pinzón, M. A. (1996). Anoxia tolerant animals from a neurobiological perspective. *Comparative Biochemistry and Physiology Part B: Biochemistry and Molecular Biology*, 113(1), 3-13.
240. Teramoto, T., Sternick, L. A., Kage-Nakadai, E., Sajjadi, S., Siembida, J., Mitani, S., ... & Lambie, E. J. (2010). Magnesium excretion in *C. elegans* requires the activity of the GTL-2 TRPM channel. *PloS one*, 5(3), e9589.
241. Tsunenari, T., Sun, H., Williams, J., Cahill, H., Smallwood, P., Yau, K. W., & Nathans, J. (2003). Structure-function analysis of the bestrophin family of anion channels. *Journal of Biological Chemistry*, 278(42), 41114-41125.
242. Wang, Y., Alam, T., Hill-Harfe, K., Lopez, A. J., Leung, C. K., Iribarne, D., ... & Choe, K. P. (2013). Phylogenetic, expression, and functional analyses of anoctamin homologs in *Caenorhabditis elegans*. *American Journal of Physiology-Regulatory, Integrative and Comparative Physiology*, 305(11), R1376-R1389.
243. Goh, K. Y., & Inoue, T. (2018). A large transcribed enhancer region regulates *C. elegans* bed-3 and the development of egg laying muscles. *Biochimica et Biophysica Acta (BBA)-Gene Regulatory Mechanisms*, 1861(5), 519-533.
244. Currie, E., King, B., Lawrenson, A. L., Schroeder, L. K., Kershner, A. M., & Hermann, G. J. (2007). Role of the *Caenorhabditis elegans* multidrug resistance gene, mrp-4, in gut granule differentiation. *Genetics*, 177(3), 1569-1582.
245. Schroeder, L. K., Kremer, S., Kramer, M. J., Currie, E., Kwan, E., Watts, J. L., ... & Hermann, G. J. (2007). Function of the *Caenorhabditis elegans* ABC transporter PGP-

- 1373 2 in the biogenesis of a lysosome-related fat storage organelle. *Molecular biology of the*
1374 *cell*, 18(3), 995-1008.
- 1375 246. Kage-Nakadai, E., Uehara, T., & Mitani, S. (2011). H⁺/myo-inositol transporter
1376 genes, hmit-1.1 and hmit-1.2, have roles in the osmoprotective response in
1377 *Caenorhabditis elegans*. *Biochemical and biophysical research communications*, 410(3),
1378 471-477.
- 1379 247. Pao, S. S., Paulsen, I. T., & Saier Jr, M. H. (1998). Major facilitator superfamily.
1380 *Microbiology and molecular biology reviews*, 62(1), 1-34.
- 1381 248. Romanelli-Credrez, L., Doitsidou, M., Alkema, M. J., & Salinas, G. (2020). HIF-1
1382 Has a Central Role in *Caenorhabditis elegans* Organismal Response to
1383 Selenium. *Frontiers in genetics*, 11, 63.
- 1384 249. Filipovic, M. R., Zivanovic, J., Alvarez, B., & Banerjee, R. (2018). Chemical
1385 biology of H₂S signaling through persulfidation. *Chemical reviews*, 118(3), 1253-1337.
- 1386 250. Hayes, J. D., & McLellan, L. I. (1999). Glutathione and glutathione-dependent
1387 enzymes represent a coordinately regulated defense against oxidative stress. *Free*
1388 *radical research*, 31(4), 273-300.
- 1389 251. Mytilineou, C., Kramer, B. C., & Yabut, J. A. (2002). Glutathione depletion and
1390 oxidative stress. *Parkinsonism & related disorders*, 8(6), 385-387.
- 1391 252. Diaz-Vivancos, P., de Simone, A., Kiddle, G., & Foyer, C. H. (2015). Glutathione–
1392 linking cell proliferation to oxidative stress. *Free Radical Biology and Medicine*, 89, 1154-
1393 1164.
- 1394 253. Morimoto-Tomita, M., Uchimura, K., Werb, Z., Hemmerich, S., & Rosen, S. D.
1395 (2002). Cloning and characterization of two extracellular heparin-degrading
1396 endosulfatases in mice and humans. *Journal of Biological Chemistry*, 277(51), 49175-
1397 49185.
- 1398 254. Rose, P., Moore, P. K., & Zhu, Y. Z. (2017). H₂S biosynthesis and catabolism:
1399 new insights from molecular studies. *Cellular and Molecular Life Sciences*, 74(8), 1391-
1400 1412.
- 1401 255. Livshits, L., Chatterjee, A. K., Karbian, N., Abergel, R., Abergel, Z., & Gross, E.
1402 (2017). Mechanisms of defense against products of cysteine catabolism in the nematode
1403 *Caenorhabditis elegans*. *Free Radical Biology and Medicine*, 104, 346-359.
- 1404 256. Qabazard, B., Li, L., Gruber, J., Peh, M. T., Ng, L. F., Kumar, S. D., ... & Moore,
1405 P. K. (2014). Hydrogen sulfide is an endogenous regulator of aging in *Caenorhabditis*
1406 *elegans*. *Antioxidants & redox signaling*, 20(16), 2621-2630.
- 1407 257. Ng, L. F., Ng, L. T., van Breugel, M., Halliwell, B., & Gruber, J. (2019).
1408 Mitochondrial DNA damage does not determine *C. elegans* lifespan. *Frontiers in*
1409 *genetics*, 10, 311.

1410 258. Kimura, H. (2020). Hydrogen sulfide signaling in the central nervous system-
1411 Comparison with nitric oxide. Authorea Preprints.

1412 259. Cavanaugh, C. M., McKiness, Z. P., Newton, I. L., & Stewart, F. J. (2006). Marine
1413 chemosynthetic symbioses. *The prokaryotes*, 1, 475-507.

1414 260. Grabherr, M.G., Haas, B.J., Yassour, M., Levin, J.Z., Thompson, D.A., Amit, I., et
1415 al. (2011) Full-length transcriptome assembly from RNA-Seq data without a reference
1416 genome. *Nat Biotechnol* 29: 644–52

1417 261. Cerveau, N., and Jackson, D.J. (2016) Combining independent de novo
1418 assemblies optimizes the coding transcriptome for nonconventional model eukaryotic
1419 organisms. *BMC Bioinformatics* 17: 525

1420 262. Fu, L., Niu, B., Zhu, Z., Wu, S., and Li, W. (2012) CD-HIT: Accelerated for
1421 clustering the next-generation sequencing data. *Bioinformatics* 28: 3150–3152

1422 263. Simão, F.A., Waterhouse, R.M., Ioannidis, P., Kriventseva, E. V., and Zdobnov,
1423 E.M. (2015) BUSCO: assessing genome assembly and annotation completeness with
1424 single-copy orthologs. *Bioinformatics* 31: 3210–3212

1425 264. Huson, D.H., Auch, A.F., Qi, J., and Schuster, S.C. (2007) MEGAN analysis of
1426 metagenomic data. *Genome Res* 17: 377–386.

1427 265. Bryant, D.M., Johnson, K., DiTommaso, T., Tickle, T., Couger, M.B., Payzin-
1428 Dogru, D., et al. (2017) A Tissue-Mapped Axolotl De Novo Transcriptome Enables
1429 Identification of Limb Regeneration Factors. *Cell Rep* 18: 762–776

1430 266. Li, B., & Dewey, C. N. (2011). RSEM: accurate transcript quantification from
1431 RNA-Seq data with or without a reference genome. *BMC bioinformatics*, 12(1), 1-16.

1432 267. Gentleman, R. C., Carey, V. J., Bates, D. M., Bolstad, B., Dettling, M., Dudoit, S.,
1433 ... & Zhang, J. (2004). Bioconductor: open software development for computational
1434 biology and bioinformatics. *Genome biology*, 5(10), 1-16.

1435 268. Robinson, M. D., McCarthy, D. J., & Smyth, G. K. (2010). edgeR: a Bioconductor
1436 package for differential expression analysis of digital gene expression data.
1437 *Bioinformatics*, 26(1), 139-140.

1438 269. Team, R. C. (2013). R: a language and environment for statistical computing. R
1439 Foundation for Statistical Computing, Vienna, Austria.

1440 270. Rapaport, F., Khanin, R., Liang, Y., Pirun, M., Krek, A., Zumbo, P., ... & Betel, D.
1441 (2013). Comprehensive evaluation of differential gene expression analysis methods for
1442 RNA-seq data. *Genome biology*, 14(9), 1-13.

1443 271. Cantalapiedra, C. P., Hernández-Plaza, A., Letunic, I., Bork, P., & Huerta-Cepas,
1444 J. (2021). eggNOG-mapper v2: Functional Annotation, Orthology Assignments, and
1445 Domain Prediction at the Metagenomic Scale. *Molecular Biology and Evolution*.
1446 msab293.

1447 272. Huerta-Cepas, J., Szklarczyk, D., Heller, D., Hernández-Plaza, A., Forslund, S.
1448 K., Cook, H., ... & Bork, P. (2019). eggNOG 5.0: a hierarchical, functionally and
1449 phylogenetically annotated orthology resource based on 5090 organisms and 2502
1450 viruses. *Nucleic acids research*, 47(D1), D309-D314.

1451 273. Buchfink, B., Reuter, K., & Drost, H. G. (2021). Sensitive protein alignments at
1452 tree-of-life scale using DIAMOND. *Nature methods*, 18(4), 366-368.

1453 274. Altschul, S. F., Gish, W., Miller, W., Myers, E. W., & Lipman, D. J. (1990). Basic
1454 local alignment search tool. *Journal of molecular biology*, 215(3), 403-410.

1455 275. Harris, T. W., Arnaboldi, V., Cain, S., Chan, J., Chen, W. J., Cho, J., ... &
1456 Sternberg, P. W. (2020). WormBase: a modern model organism information resource.
1457 *Nucleic Acids Research*, 48(D1), D762-D767.

Figure legends

Figure 1. Relative transcript abundance and expression levels of the top 100 expressed genes of *L. oneistus* across all conditions. (A) Relative transcript abundance (%) of the top 100 expressed genes with a manually curated functional category. The top 100 expressed genes were collected by averaging the expression values ($\log_2\text{TPM}$) across all replicates of all incubations (Figure S1A, Data S1, and S2). Functional classifications were extracted from the curated database UniProt and from comprehensive literature search focused mainly on *C. elegans*, and confirmed with the automatic annotated eggNOG classification (Data S1). (B) Median gene expression levels of selected *L. oneistus* manually annotated functional categories of the top 100 expressed genes. Metabolic processes include both differentially and constitutively expressed genes. Each dot represents the average $\log_2\text{TPM}$ value per gene across all replicates of all incubations. All gene names (or locus tags for unidentified gene names) are listed in Data S2.

Figure 2. Median gene expression levels of selected *L. oneistus* metabolic processes among the differentially expressed genes between the hypoxic (H) and anoxic sulfidic (AS) conditions after 24 h. Individual processes among the differentially expressed genes are ordered according to their difference in median expression between the AS and H incubations. Namely, detoxification (far left) had the largest difference in median expression in the AS condition, whereas immune response (far right) had the largest median expression difference in the H condition. The absolute number of genes are indicated at the top of each process. Metabolic processes were manually assigned and confirmed with the automatic annotated eggNOG classification. For specific gene assignments see Data S1. Some genes are present in more than one functional category and processes comprising only one gene are not displayed in the figure but listed in Data S1.

Figure 3. Genes involved in detoxification, ubiquitin-proteasome, autophagy, apoptosis, and amino acids degradation were predominantly expressed in AS worms. Heatmap displaying genes upregulated in AS (anoxic sulfidic) relative to H (hypoxic) worms after 24 h-long incubations under one of the two conditions (1.5-fold change, $\text{FDR} \leq 0.05$). Expression levels are displayed as mean-centered $\log_2\text{TPM}$ value (transcripts per kilobase million). Genes are ordered by function in their respective metabolic pathways. For each process, the minority of genes that were upregulated in H worms is shown in Data S1. Red denotes upregulation, and blue downregulation. Prot. protein, COP9: Constitutive photomorphogenesis 9. Dcp: domain-containing proteins. Put. glut. peroxid.: putative glutamate peroxidase. Put. sarc. oxid.: putative sarcosine oxidase.

Figure 4. Genes involved in translation and energy generation and genes encoding for C-type lectins and mucins were predominantly expressed in AS worms. Heatmap displaying

genes upregulated in AS (anoxic sulfidic) relative to H (hypoxic) worms, upon 24 h-long incubations under one of the two conditions (1.5-fold change, $FDR \leq 0.05$). Expression levels are displayed as mean-centered \log_2 TPM values (transcripts per kilobase million). Genes are ordered by function in their respective metabolic pathways. For each process, the minority of genes that were upregulated in H worms is shown in [Data S1](#). Red denotes upregulation, and blue downregulation. Fp: family-containing protein. Cytoch. C ox. su. II.: cytochrome c oxidase subunit II. Ubiqu./rhodoq biosynth.: Ubiquinone or rhodoquinone biosynthesis.

Figure 5. Genes involved in immune response, development and nervous system were predominantly expressed in hypoxic (H) worms. Heatmap displaying genes upregulated in H relative to AS worms, upon 24 h-long incubations under one of the two conditions (1.5-fold change, $FDR \leq 0.05$). Expression levels are displayed as mean-centered \log_2 TPM value (transcripts per kilobase million). Genes are ordered by function in their respective metabolic pathways. For each process, the minority of genes that were upregulated in AS worms is shown in [Data S1](#). Red denotes upregulation and blue downregulation. MN: mechanosensory neurons. Embr. body wall muscle posit.: Embryonic body wall muscle positioning. Put.: putative.

Figure 6. Genes involved in carbohydrate, lipid- and sulfur-metabolism, amino acids biosynthesis, and transport were predominant expressed in hypoxic (H) worms. Heatmap displaying genes upregulated in H relative to AS worms, upon 24 h-long incubations under one of the two conditions (1.5-fold change, $FDR \leq 0.05$). Expression levels are displayed as mean-centered \log_2 TPM values (transcripts per kilobase million). Genes are ordered by function in their respective metabolic pathways. For each process, the minority of genes that were upregulated in AS worms is shown in [Data S1](#). Red denotes upregulation, and blue downregulation. FA: fatty acids. PC: phosphatidylcholine. PL: phospholipids. Metab: metabolism. Synth: synthesis. Assim: assimilation. Oxid: oxidation. Transp: transporters.

Figure 7. Schematic representation of *Laxus oneistus* physiology in anoxic and hypoxic sand. In anoxic sulfidic sand (left) *L. oneistus* does not enter suspended animation. Instead, it upregulates the expression of genes mediating inhibitory neurotransmission, involved in symbiosis establishment (e.g., lectins, mucins) and in ribosome biogenesis. Metabolism may be supported by the degradation of starch and by rewiring the electron transfer chain: rhodoquinone (RQ) is used as electron carrier and fumarate as electron acceptor. Moreover, the worm activates degradation pathways (e.g., ubiquitin-proteasome system (UPS), autophagy, and apoptosis) and may anticipate reoxygenation by upregulating superoxide dismutase (SOD) and glutathione peroxidase (GP).

In hypoxic sand (right), instead, *L. oneistus* appears to use trehalose and cellulose for energy generation, while engaging in costly processes such as development, molting, feeding, and mating. Genes involved in excitatory neurotransmission are also upregulated, together with

Toll receptors and immune effectors (e.g., fungicides, bactericidal permeability increasing proteins).

SUPPLEMENTAL MATERIAL LEGENDS

Figure S1. Experimental conditions, sample similarity and differential expression. (A) Experimental setup was previously described (Paredes et al. 2021). Briefly, nematodes were subjected to different oxygen concentrations for 24 h: anoxic with sulfide (AS: 0mM O₂, 25mM sodium sulfide added), anoxic without sulfide (A, 0mM O₂), hypoxic (H, 60mM O₂ after 24 h), and oxic (O, 100mM O₂ after 24 h). The box around the anoxic incubation vials illustrates that these incubations were carried out in a polyethylene glove bag. (B) Similarity between transcriptome samples based on Euclidean distances between expression values (log₂TPM), and visualized by means of multidimensional scaling (C) Differential gene expression (DE) analysis between incubations showed that the number of DE genes was low (maximum value was 4.8% of all expressed genes for the H vs AS conditions). Genes were considered differentially expressed if their expression changed 1.5-fold with a false-discovery rate (FDR) of ≤ 0.05 .

Figure S2. Statistical analysis, relative transcript abundance and expression levels of the top 100 detected proteins of *L. oneistus* across all conditions. (A) Relative protein abundance (%) of the top 100 detected proteins present in a particular manually curated functional category. The top 100 proteins were collected by averaging the expression values across all replicates of all incubations (Figure S1A, Data S2). Functional classifications were extracted from the curated database UniProt and from comprehensive literature search focused mainly on *C. elegans*, and confirmed with the automatic annotated eggNOG classification (Data S1). (B) Median gene expression levels of selected *L. oneistus* manually annotated functional categories of the top 100 expressed proteins. Each dot represents the average %cOrgNSAF per protein across all replicates of all incubations. Notice that some categories were created with genes of overlapping functions (e.g., cytoskeleton/locomotion/nervous system). All protein names (or locus tags for unidentified protein names) are listed in Data S2.

Figure S3. Transcriptomics vs proteomics comparison. Pearson correlation between all transcripts and proteins (Data S1) automatically classified based on their functional category. The Pearson correlation between all expressed transcripts and all detected proteins ($r = 0.4$) was found to be low (Figure S3).

Figure S4. Relative transcript abundance and expression levels of the top 100 expressed genes of *O. algarvensis* across all conditions. (A) Relative transcript abundance (%) of the top 100 expressed genes with a manually curated functional category. The top 100 expressed genes were collected by averaging the expression values (log₂TPM) across all replicates of all

incubations (see [Supplemental material](#)). Functional classifications were extracted from the curated database UniProt and from comprehensive literature search focused mainly on *C. elegans*). (B) Median gene expression levels of selected *O. algarvensis* manually annotated functional categories of the top 100 expressed genes. Metabolic processes include both differentially and constitutively expressed genes. Each dot represents the average log2TPM value per gene across all replicates of all incubations.

Figure S5. *L. oneistus* lipid composition in anoxic and oxic conditions after 24 h. Major lipid classes and their abundance relative to all lipids detected showed no statistical difference between both conditions. For details on methodology see [Supplemental material](#).

Table S1. Metabolites detected in at least two biological replicates of either the holobiont fraction (*Laxus oneistus* and its ectosymbiont) or in the symbiont fraction (see [Supplemental material](#)). RT: retention time. Area: area of a peak from a specific compound detected in the GC-MS chromatograms. Grey boxes: no metabolites detected. Blank boxes: Unknown metabolites that are either below the detected threshold (< 700) or might be products of derivatization reagents. Note that cholestane and ribitol were used as internal standards.

Data S1. *Ca. T. oneisti* genes, functional annotations, transcript and protein expression.

Data S2. Top 100 expressed genes (RNA-Seq) and detected proteins (proteomics data).

Supplemental video 1. A batch of 50 *Laxus oneistus* after 6 days in anoxic seawater.

Supplemental video 2. A batch of 50 *Laxus oneistus* at the beginning (T0) of the incubations.

Supplemental video 3. A batch of 50 *Laxus oneistus* after 1 day (T24 h) in anoxic sulfidic seawater (0 % air saturation, 25 μ M H₂S).

Supplemental video 4. A batch of 50 *Laxus oneistus* after 1 day (T24 h) in oxic seawater (87 % air saturation, 0 μ M H₂S).

Differential regulation of degradation and immune pathways underlie adaptation of an ectosymbiotic nematode to oxic-anoxic interfaces

Supplemental Materials and Methods

Paredes et al.

***Olavius algarvensis* transcriptome analysis.** For transcriptomic analyses of *O. algarvensis*, RNA sequences were obtained from 12 individuals collected from Sant' Andrea bay off the island of Elba (42°48'31"N / 10°08'33"E). Six animals were incubated in anoxic artificial seawater in gas-tight serum bottles for 24 hours before fixed in RNAlater (anoxic treatment). Separate six animals were incubated first in anoxic artificial seawater for 24 hours and subsequently incubated in oxygenated artificial seawater for 12 hours before fixation (oxic treatment). RNA was separately extracted from the 12 individuals with the AllPrep DNA/RNA kit (Qiagen), following the default protocol with a 3 min bead-beating step at 20 Hz. Their cDNA was synthesized with the Ovation RNA-Seq System (NuGEN Technologies Inc., Redwood City, CA) and sheared with the Covaris ultrasonicator (Covaris, Woburn, MA). Sequencing libraries were prepared with the NEBNext Ultra DNA Library Prep Kit for Illumina (New England Biolabs, Ipswich, MA), targeting the insert size of 250 bp. Paired-end metatranscriptomic reads of approximately 6 giga bases (100 bases x 2; 30 million read pairs) per sample were generated, using the HiSeq2500 System (Illumina) at the Max-Planck-Genome-Centre Cologne.

A transcriptomic reference of *O. algarvensis* was generated by *de novo* co-assembly of the metatranscriptomes from the 12 individuals. Raw sequences were first de-contaminated from residual Illumina adapters and PhiX sequences and quality-filtered, using bbduk (BBTools; <https://jgi.doe.gov/data-and-tools/bbtools/>). Sequencing errors were corrected using SEECER (Le et al. 2013). Sequences of *O. algarvensis* mitochondrial genome (mtDNA) and symbiotic bacteria, any ribosomal RNA (rRNA) and DNA contaminants (e.g., *Drosophila* sp.) were removed using bmap (BBTools). Mapping references were mtDNA and symbiont genomes in *O. algarvensis* (Woyke et al. 2006, Sato et al. 2020), rRNA sequences from sortMeRNA database (Kopylova et al. 2012), and the *Drosophila melanogaster* genome (GenBank assembly accession: GCA_000001215.4). Reads were assembled using Trinity v2.4.0 (Grabherr et al. 2011). Contigs shorter than 600 bases and with less than 4× coverage were removed to minimize the assembly artifact. Contigs without open reading frames (ORFs) were further removed using TransDecoder v3.0.1 (Haas et al. 2013). To remove contaminating viral, bacterial, archaeal and contaminating eukaryotic (e.g. Cnidaria, Viridiplantae)

36 sequences, taxonomic affiliations of contigs were identified using DIAMOND blastx
37 search v0.8.36.98 (Buchfink et al. 2015) against the NCBI-nr protein database
38 (<https://www.ncbi.nlm.nih.gov/>; accessed 2018 February), and contigs assigned to
39 Bilateria were exported using MEGAN v6.19.6 (Huson et al. 2007). Redundant contigs
40 due to isoforms and allelic variations were removed with Corset v1.06 (Davidson and
41 Oshlack 2014), with the anoxic vs. oxic treatments used as a grouping factor to
42 differentiate paralogs. Only the longest contigs per gene were kept based on Trinity
43 isoform tags. Completeness of the final transcriptomic assembly was scored at 73.9%
44 with BUSCO v2.01 (Simão et al. 2015) using the metazoan single copy orthologous gene
45 database (odb9). Functional annotation was performed with Blast2GO using OmicsBox
46 v1.4.12 (BioBam Bioinformatics, Valencia) with NCBI-blast against the nr_v5 database
47 and InterPro scan against GO mapping v2019.06.

48 For gene expression analyses of the 12 *O. algarvensis* individuals treated with the
49 anoxic and oxic treatments above (n = 6 each), the quality controlled sequences were
50 mapped against the transcriptomic reference using RSEM v1.3.1 (Li and Dewey 2011).
51 The TPM values were analyzed as described in the main document. As gene expression
52 profiles were not clustered based on the treatment (data not shown), the log₂TPM values
53 were averaged across all the individuals, and the top 100 expressed gene categories
54 were identified.

55 **Proteomics on *L. oneistus*.** Sample collection and preparation of *L. oneistus* pellets
56 for proteomics, as well as the proteins extraction procedure followed by LC-MS/MS
57 analysis were described previously (Paredes et al., 2021)

58 **Protein identification and quantification.** The database for protein identification
59 was constructed as described previously (Paredes et al., 2021), but with optimized host
60 sequences derived from host transcriptome *de novo* assembly (see main text), and
61 contained 21,721 *Laxus oneistus* host proteins, 5,145 *Ca. T. oneisti* proteins
62 (JAAEFD000000000), and a set of 42 common laboratory contaminants. In this way,
63 2,626 host proteins and 1,348 symbiont proteins were identified in total. [Data S1](#) indicates
64 all identified host proteins in the column “Proteome detection” (Column AB). Relative
65 abundance of identified proteins was calculated from total spectrum counts as normalized
66 spectral abundance factor (%NSAF) values – giving the percentage of each protein
67 relative to all proteins in the respective sample (Florens et al., 2006), and as %OrgNSAF,
68 giving a protein’s percentage relative to all host proteins in the respective sample (Mueller
69 et al., 2010). %OrgNSAF values are listed in [Data S1](#) (columns AI and AJ).

70 **Intact polar lipid extraction and analysis.** Sample collection and preparation of *L.*
71 *oneistus* pellets for lipidomics, as well as lipid extraction from the nematodes were

described previously (Paredes et al., 2021). Modifications on the latter are described next.

Briefly, pelleted nematodes were taken up in 1.5 ml 0.2 µm filtered seawater and 0.5 ml were transferred to 2 ml glass vials obtaining three analytical replicates. Nematodes were then pelleted by centrifugation and d17:1/12:0 sphingosylphosphoethanolamine (SPE; Sigma-Aldrich, 50 nM final concentration) added as internal standard. Lipids were extracted using LC-MS grade methanol, HPLC-grade chloroform (both Sigma-Aldrich) and Milli-Q water. After phase separation the lipid-containing chloroform phase was dried under nitrogen gas on a Techne Sample Concentrator. Lipids were re-suspended in 1 ml of acetonitrile: 10 mM ammonium acetate (pH 9.2) at a 95:5 (v:v) ratio. Samples were analyzed by liquid chromatography mass spectrometry (LC-MS) as follows: Five µl lipid extract were injected onto a Dionex UltiMate 3000RS UHPLC (Thermo Fisher Scientific) and separated on a hydrophilic interaction column (XBridge BEH amide XP column, Waters) according to their polar headgroup. The column was maintained at 30°C with a flow rate of 150 µl min⁻¹. Samples were separated by a 15 min gradient from 95% (v:v) acetonitrile (Solvent A) to 30% (w:v) 10 mM ammonium acetate (pH 9.2, Solvent B) with 10 min equilibration between samples. Sample detection was carried out on an amaZon SL quadrupole ion trap MS (Bruker) in both positive and negative ion mode and fragmentation performed by the autoMSⁿ function in Compass HyStar (Bruker). We used the Bruker Compass software package for lipid data analysis: DataAnalysis for peak detection and lipid identification, and QuantAnalysis for quantification against the internal standard SPE. Peak integration was manually corrected where necessary. The abundance of each lipid was normalized against the internal standard SPE and expressed as relative abundance.

Sample preparation and analysis for metabolomics. Batches of 25 *Laxus oneistus* were extracted from the sand as described in Paredes et al., 2021. Sample collection to create triplicates lasted around 2 h, whereby the samples were always exposed to atmospheric oxygen. We aimed at comparing the metabolites present in the holobiont (*L. oneistus* and its ectosymbiont) and in the symbiont fraction (the dissociated bacteria). For the latter *Ca. T. oneisti* was dissociated from the nematodes by subjecting them to sonication for 1 min in 2 ml of seawater. The 2 ml nematode-free, ectosymbiont suspension was then centrifuged for 1 min at 14 000 x g to obtain *Ca. T. oneisti* pellets. Ectosymbiont and holobiont pellets were fixed in 500 µL of methanol and flash-frozen in liquid nitrogen and transported and stored at -80°C until further processing. Note that one biological replicate of the holobiont fraction was lost during transportation ([Table S1](#)).

For metabolite detection and quantification a gas-chromatography- mass spectrometry method was used. Nematode tissue or symbiont cells were separately

extracted with an acetonitrile: methanol: water mixture as described previously (Liebeke and Bundy, 2012) including a mechanical disruption of cells with ceramic beads in a bead beater (2x 30 sec, 4 m*s, Precellys, Bertin Instruments). The extracts were dried and later derivatized for GC-MS analysis (Liebeke and Puskás, 2019). The GC-MS analysis and metabolite identification was performed as described in Koch et al 2020). An in-house metabolite database of pure chemical standards was used for the identification and qualification of selected compounds.

Data availability. The mass spectrometry proteomics data have been deposited to the ProteomeXchange Consortium via the PRIDE (Perez-Riverol et al., 2019) partner repository (<https://www.ebi.ac.uk/pride/>) with the data set identifier PXD017709.

Supplemental Tables, movies, datasets and Figure S4 are available online <https://doi.org/10.1101/2021.11.11.468236>

Supplemental References

1. Le, H. S., Schulz, M. H., McCauley, B. M., Hinman, V. F., & Bar-Joseph, Z. (2013). Probabilistic error correction for RNA sequencing. *Nucleic acids research*, 41(10), e109-e109.
2. Woyke, T., Teeling, H., Ivanova, N. N., Huntemann, M., Richter, M., Gloeckner, F. O., ... & Dubilier, N. (2006). Symbiosis insights through metagenomic analysis of a microbial consortium. *Nature*, 443(7114), 950-955.
3. Sato, Y., Wippler, J., Wentrup, C., Ansorge, R., Sadowski, M., Gruber-Vodicka, H., ... & Kleiner, M. (2021). Fidelity varies in the symbiosis between a gutless marine worm and its microbial consortium. *bioRxiv*.
4. Kopylova, E., Noé, L., & Touzet, H. (2012). SortMeRNA: fast and accurate filtering of ribosomal RNAs in metatranscriptomic data. *Bioinformatics*, 28(24), 3211-3217.
5. Grabherr, M. G., Haas, B. J., Yassour, M., Levin, J. Z., Thompson, D. A., Amit, I., ... & Regev, A. (2011). Trinity: reconstructing a full-length transcriptome without a genome from RNA-Seq data. *Nature biotechnology*, 29(7), 644.
6. Haas, B. J., Papanicolaou, A., Yassour, M., Grabherr, M., Blood, P. D., Bowden, J., ... & Regev, A. (2013). De novo transcript sequence reconstruction from RNA-seq using the Trinity platform for reference generation and analysis. *Nature protocols*, 8(8), 1494-1512.
7. Buchfink, B., Xie, C., & Huson, D. H. (2015). Fast and sensitive protein alignment using DIAMOND. *Nature methods*, 12(1), 59-60.
8. Huson, D. H., Auch, A. F., Qi, J., & Schuster, S. C. (2007). MEGAN analysis of metagenomic data. *Genome research*, 17(3), 377-386.

145 9. Davidson, N. M., & Oshlack, A. (2014). Corset: enabling differential gene expression
146 analysis for de novo assembled transcriptomes. *Genome biology*, 15(7), 1-14.

147 10. Simão, F. A., Waterhouse, R. M., Ioannidis, P., Kriventseva, E. V., & Zdobnov, E. M.
148 (2015). BUSCO: assessing genome assembly and annotation completeness with single-
149 copy orthologs. *Bioinformatics*, 31(19), 3210-3212.

150 11. Li, B., & Dewey, C. N. (2011). RSEM: accurate transcript quantification from RNA-Seq
151 data with or without a reference genome. *BMC bioinformatics*, 12(1), 1-16.

152 12. Florens, L., Carozza, M. J., Swanson, S. K., Fournier, M., Coleman, M. K., Workman, J.
153 L., & Washburn, M. P. (2006). Analyzing chromatin remodeling complexes using shotgun
154 proteomics and normalized spectral abundance factors. *Methods*, 40(4), 303-311

155 13. Mueller, R. S., Denef, V. J., Kalnejais, L. H., Suttle, K. B., Thomas, B. C., Wilmes, P., ...
156 & Banfield, J. F. (2010). Ecological distribution and population physiology defined by
157 proteomics in a natural microbial community. *Molecular systems biology*, 6(1), 374.

158 14. Paredes, G. F., Viehboeck, T., Lee, R., Palatinszky, M., Mausz, M. A., Reipert, S., ... &
159 König, L. (2021). Anaerobic sulfur oxidation underlies adaptation of a chemosynthetic
160 symbiont to oxic-anoxic interfaces. *mSystems*, 6(3), e01186-20.

161 15. Liebeke, M., & Bundy, J. G. (2012). Tissue disruption and extraction methods for
162 metabolic profiling of an invertebrate sentinel species. *Metabolomics*, 8(5), 819-830.

163 16. Liebeke, M., & Puskás, E. (2019). Drying enhances signal intensities for global GC-MS
164 metabolomics. *Metabolites*, 9(4), 68.

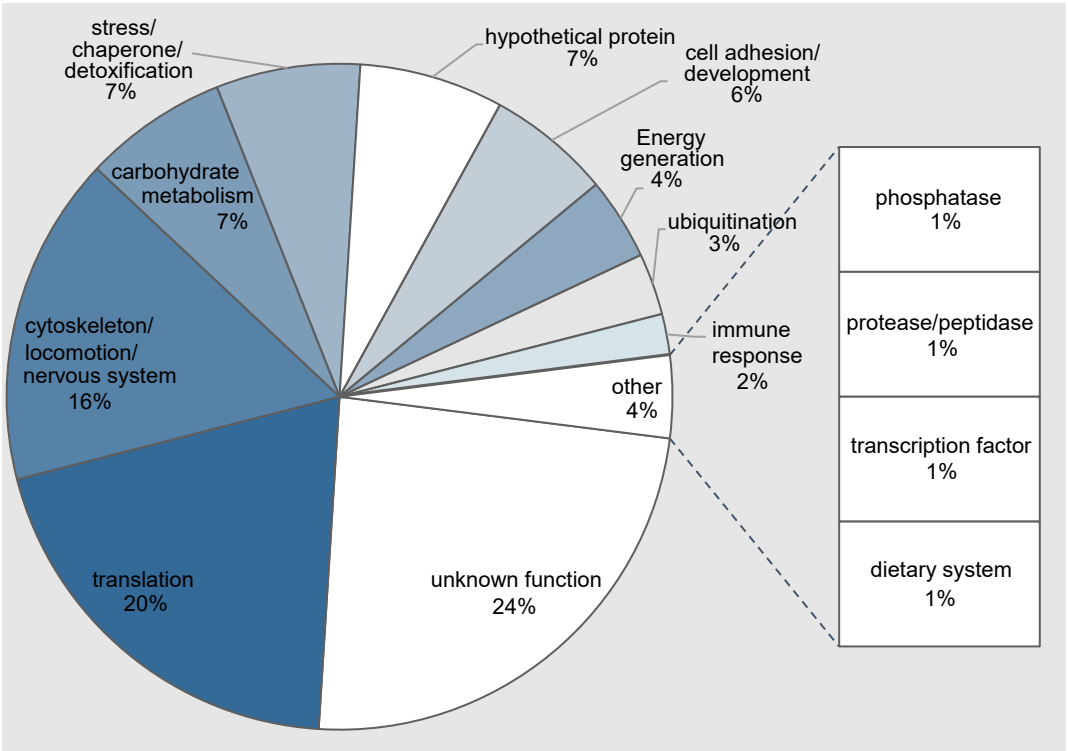
165 17. Koch, E. J., Moriano-Gutierrez, S., Ruby, E. G., McFall-Ngai, M., & Liebeke, M. (2020).
166 The impact of persistent colonization by *Vibrio fischeri* on the metabolome of the host
167 squid *Euprymna scolopes*. *Journal of Experimental Biology*, 223(16), jeb212860.

168 18. Vizcaíno, J. A., Côté, R. G., Csordas, A., Dienes, J. A., Fabregat, A., Foster, J. M., ... &
169 Hermjakob, H. (2012). The PRoteomics IDentifications (PRIDE) database and
170 associated tools: status in 2013. *Nucleic acids research*, 41(D1), D1063-D1069.

171 19. Perez-Riverol, Y., Csordas, A., Bai, J., Bernal-Llinares, M., Hewapathirana, S., Kundu,
172 D. J., ... & Vizcaíno, J. A. (2019). The PRIDE database and related tools and resources
173 in 2019: improving support for quantification data. *Nucleic acids research*, 47(D1), D442-
174 D450.

Figure 1

A



B

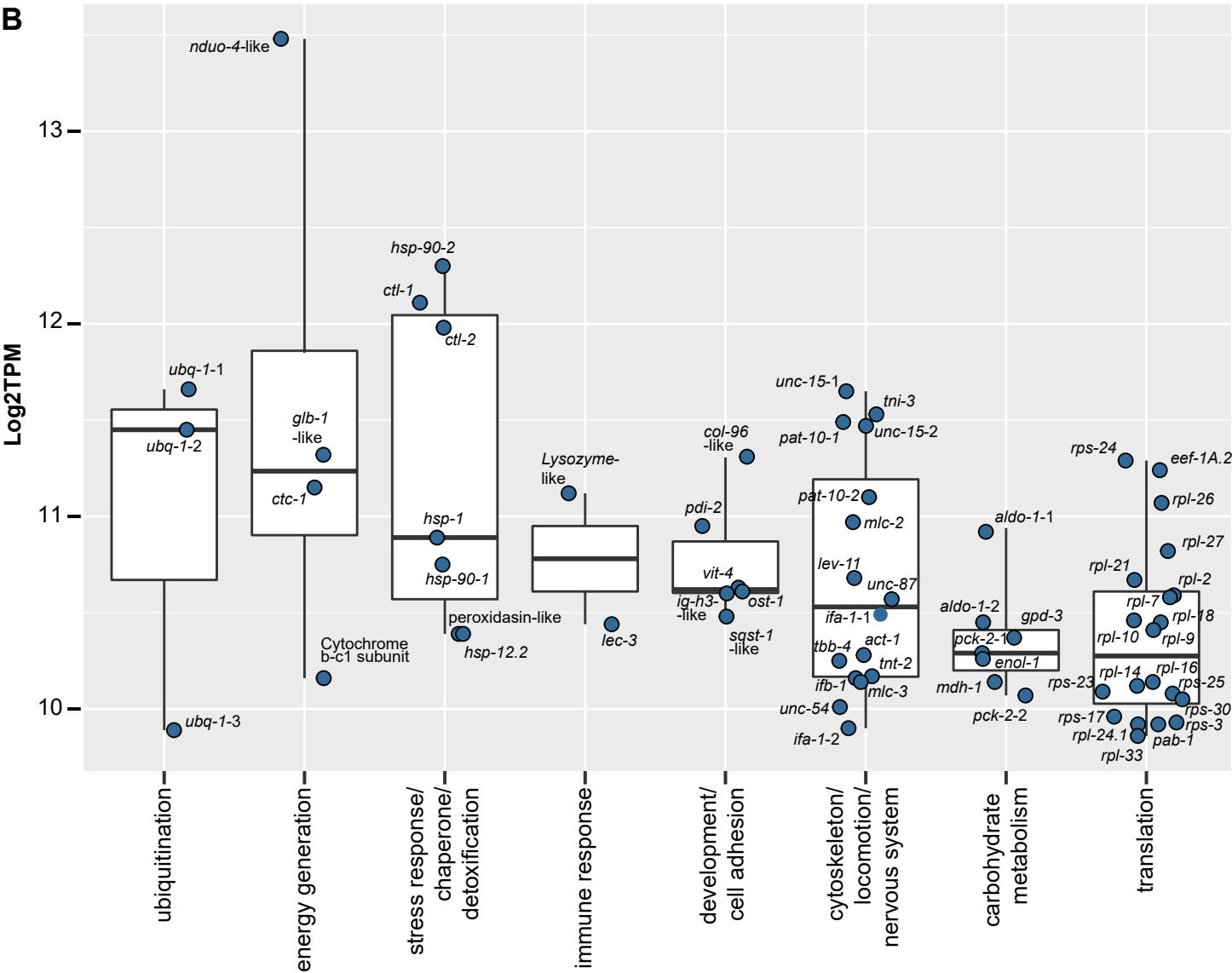


Figure 2

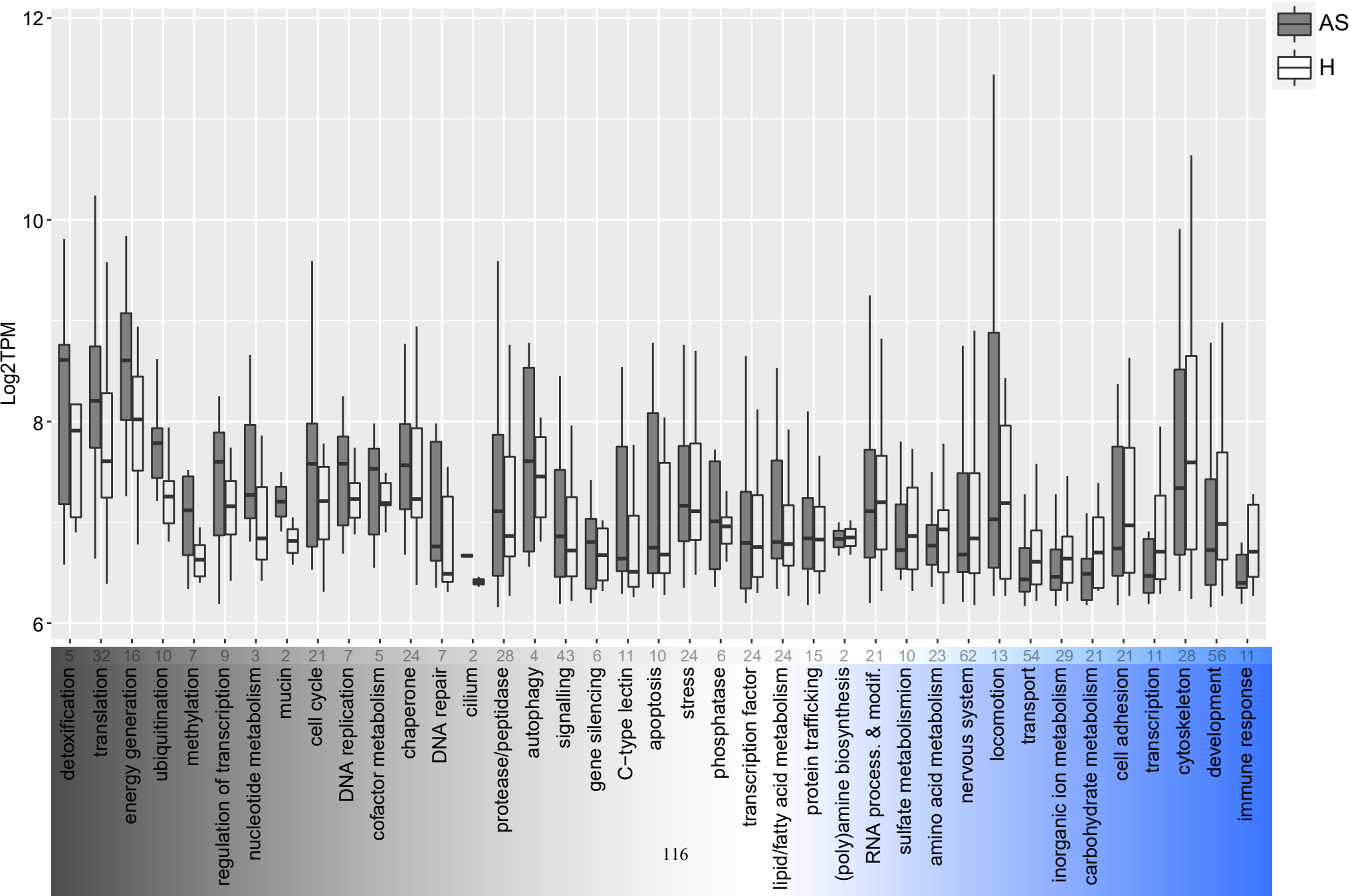


Figure 3

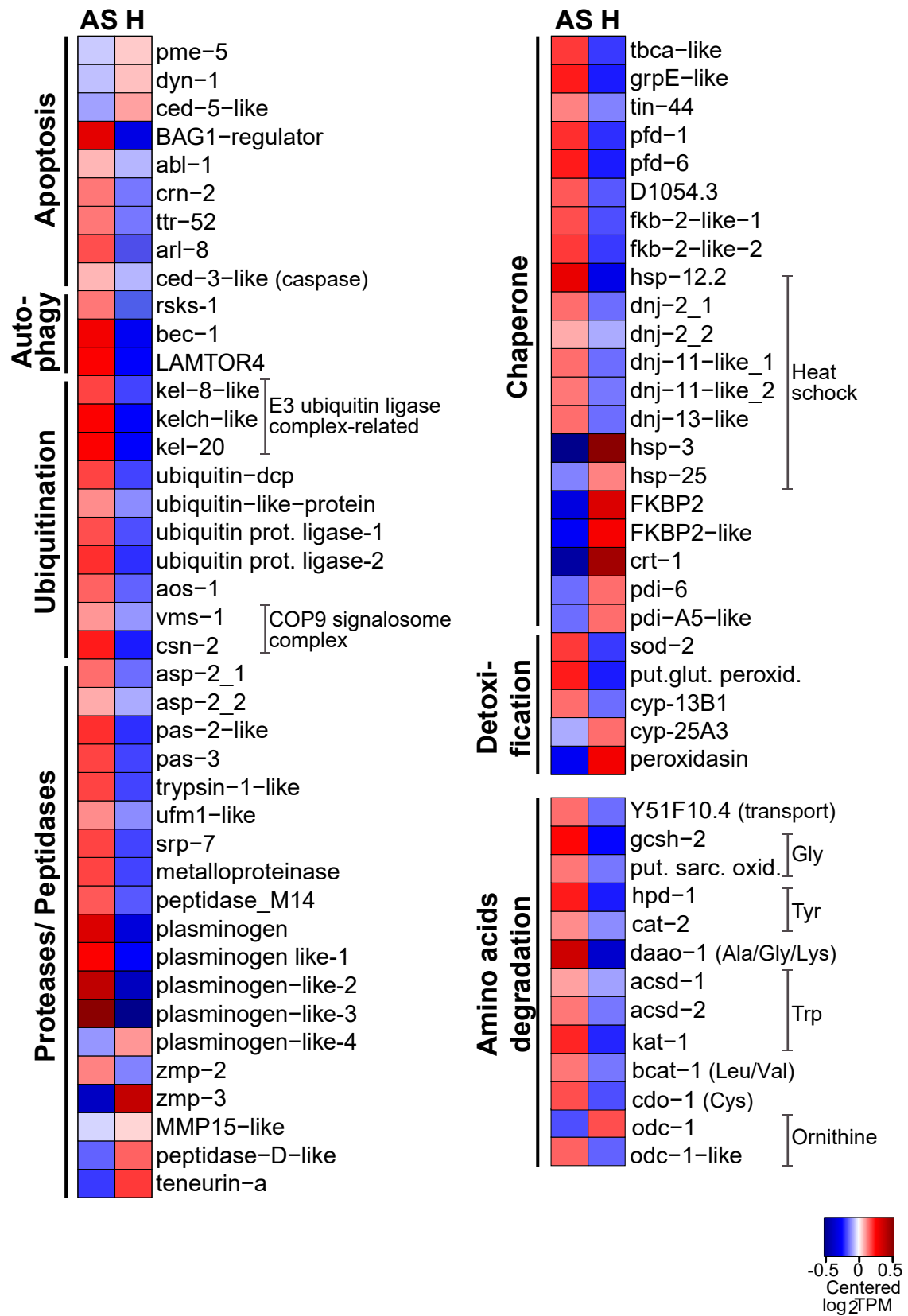
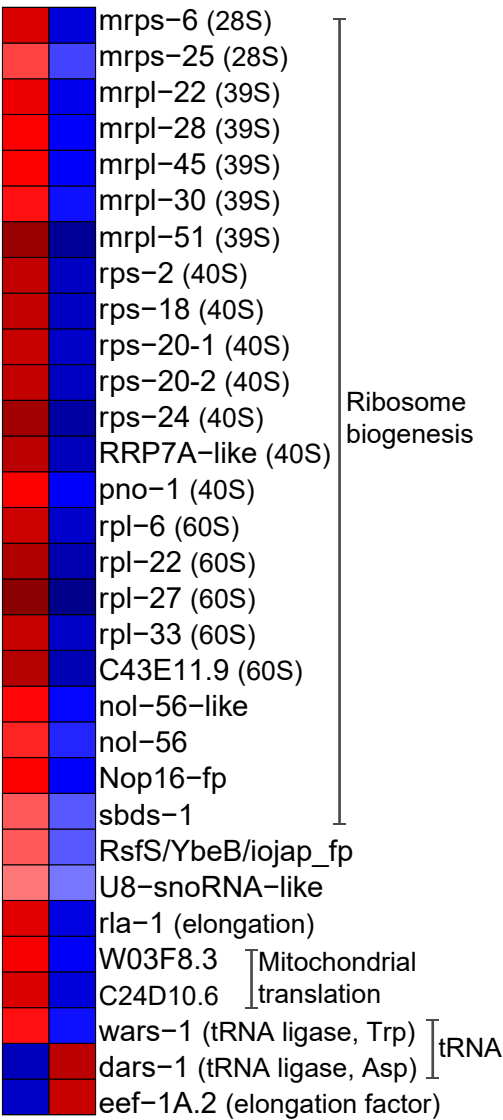


Figure 4

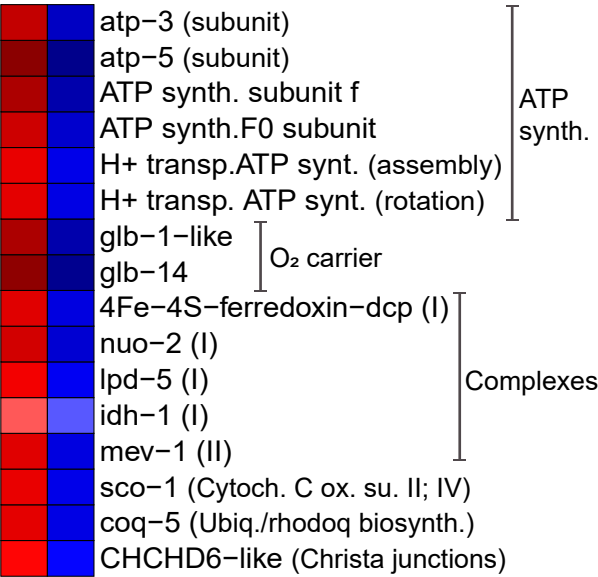
Translation

AS H



Energy generation

AS H



C-type lectins/mucins

AS H

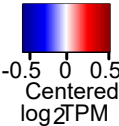
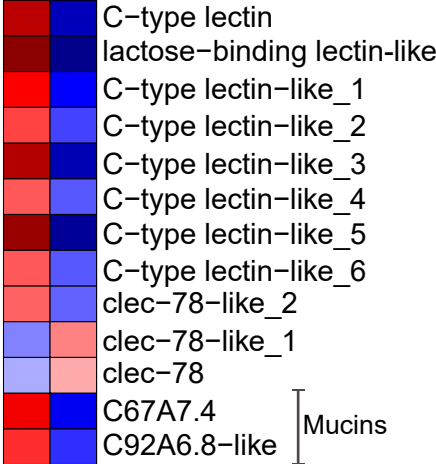
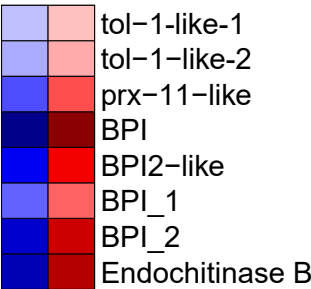


Figure 5

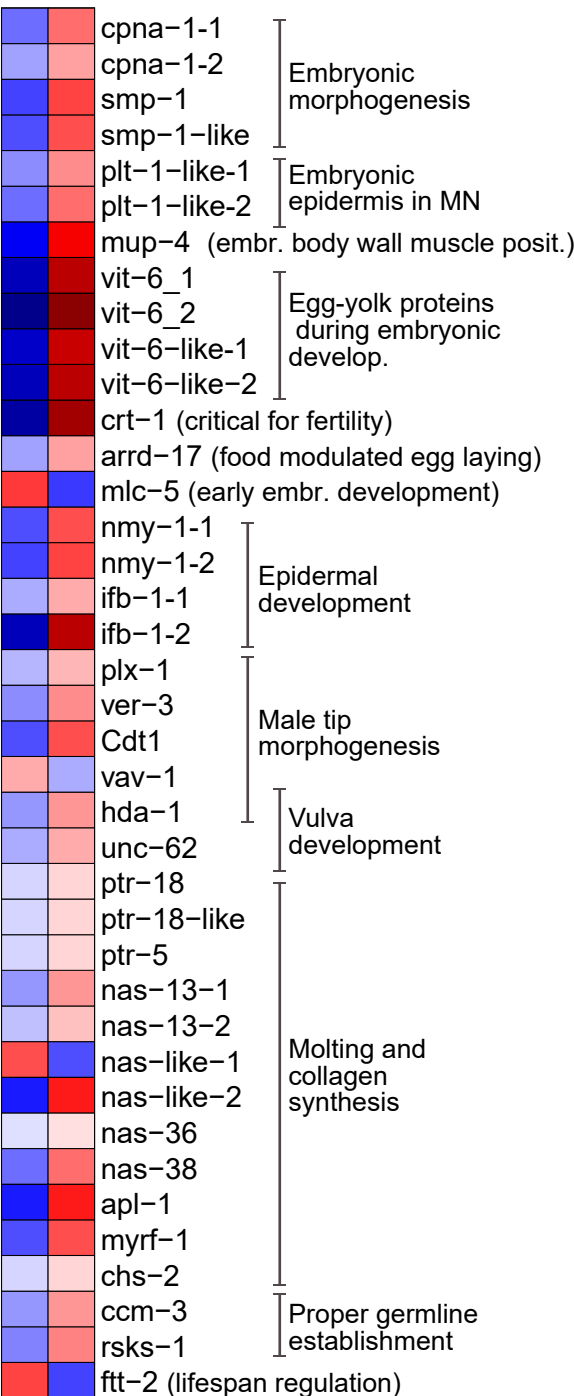
Immune system

AS H



Development

AS H



Nervous system

AS H

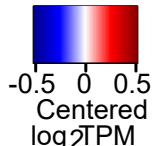
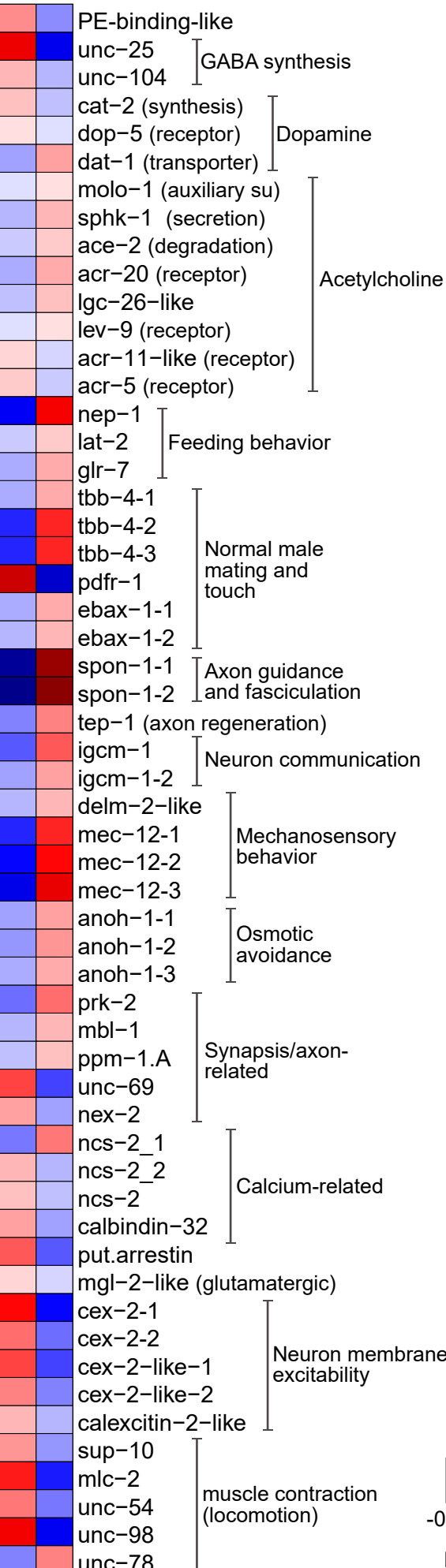


Figure 6

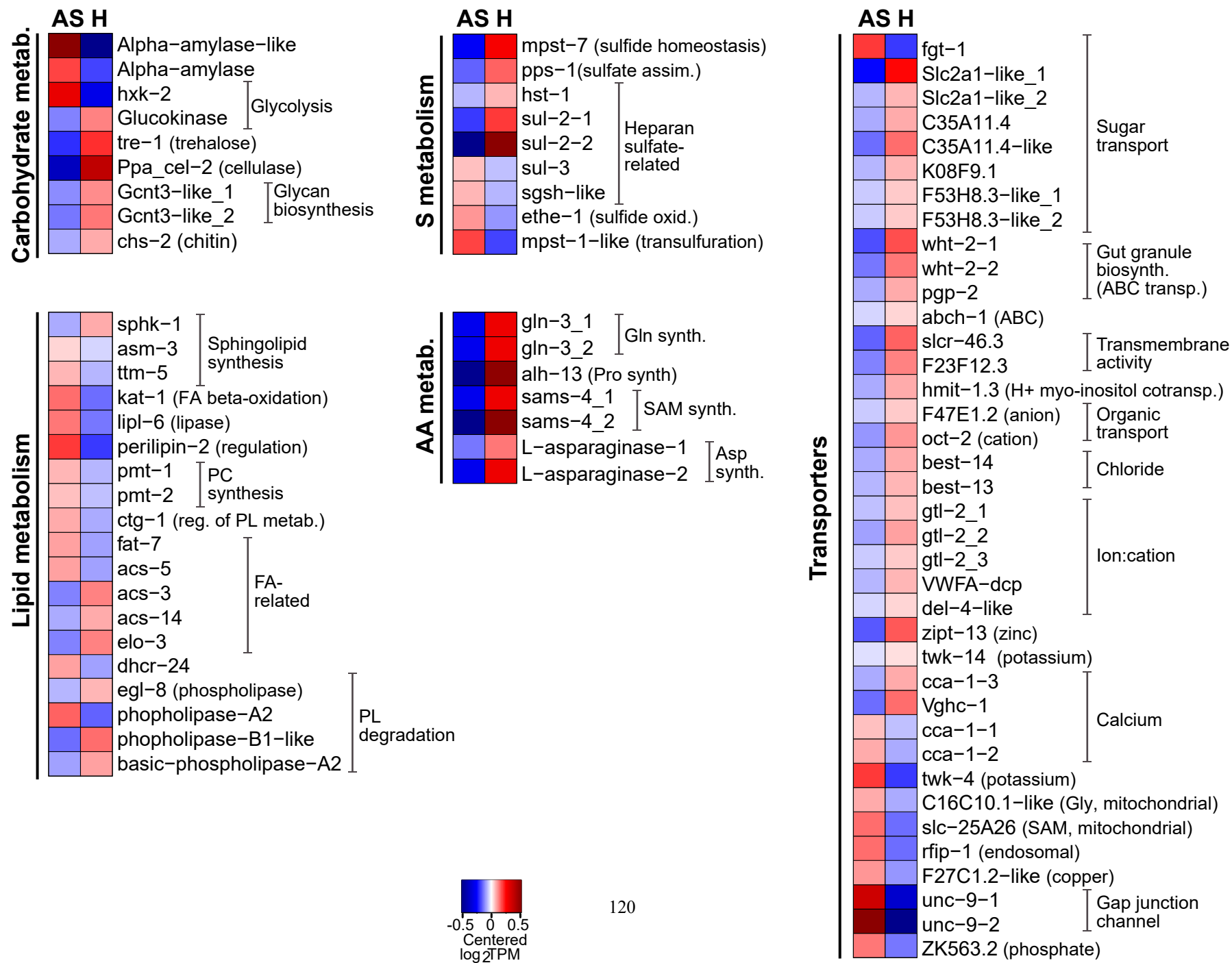


Figure 7

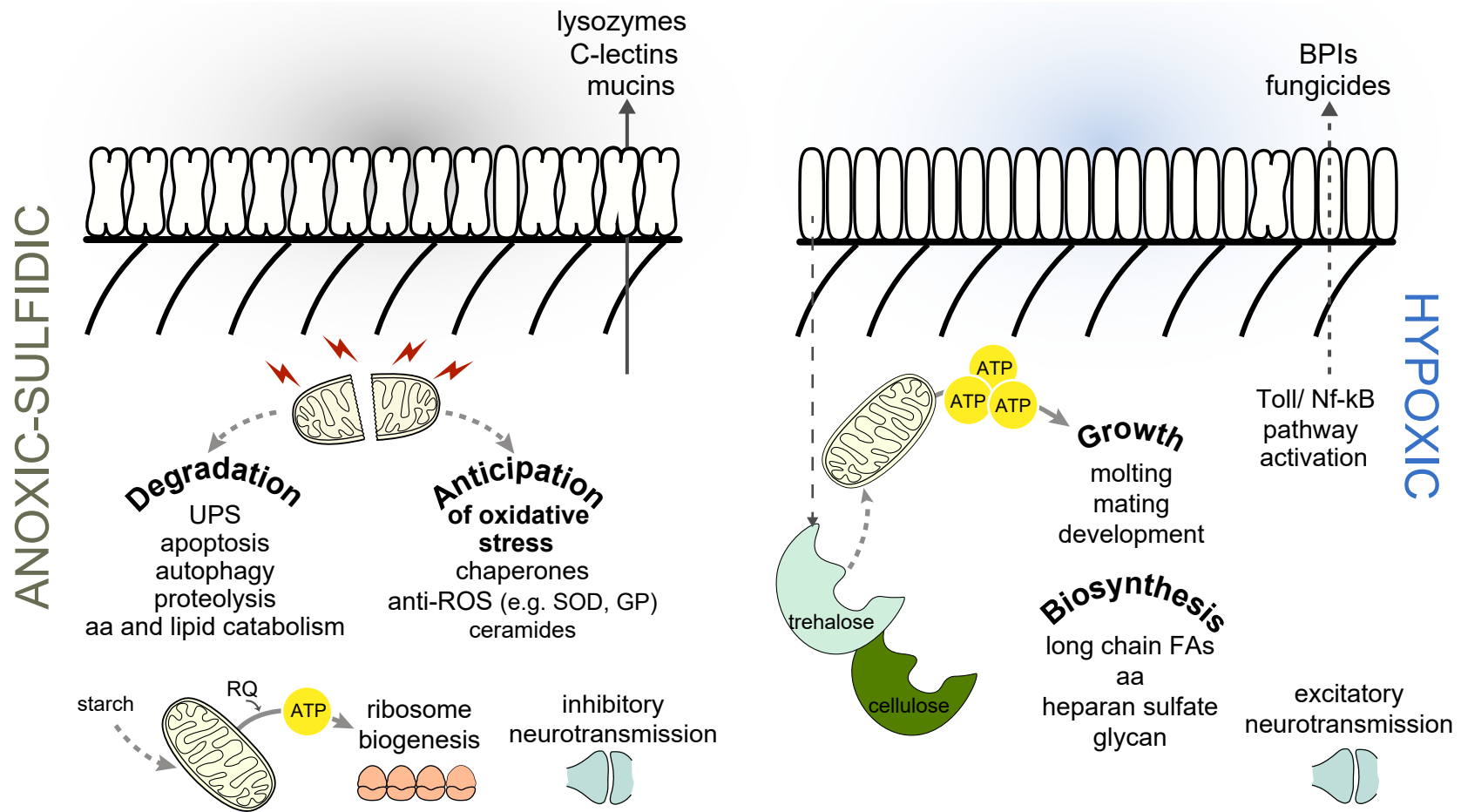
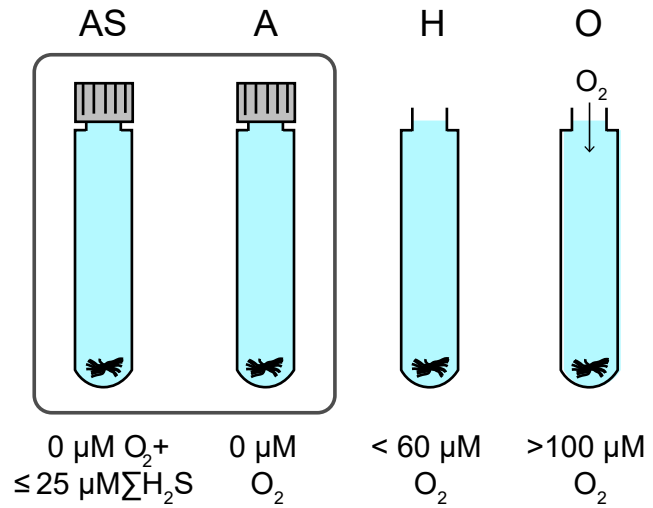
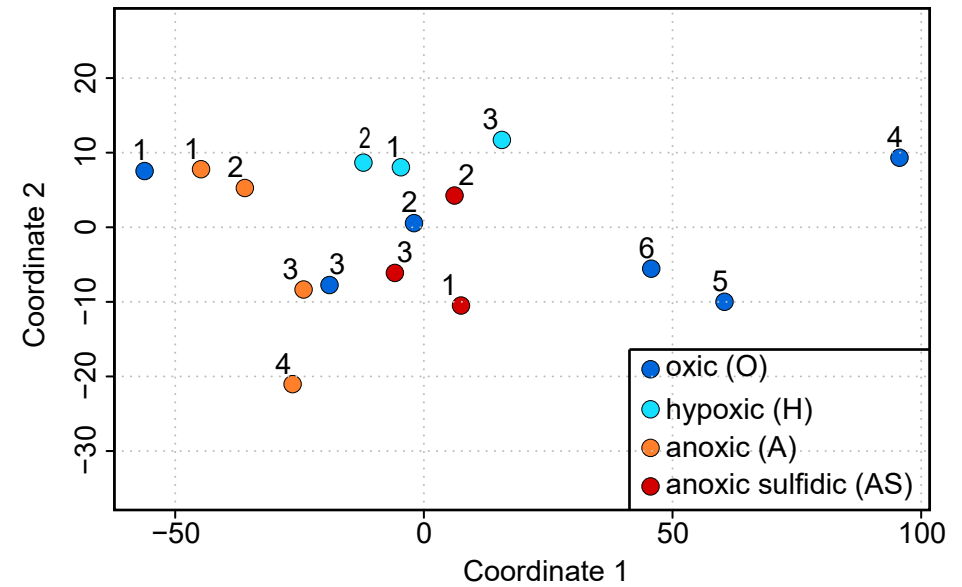


Figure S1

A



B



C

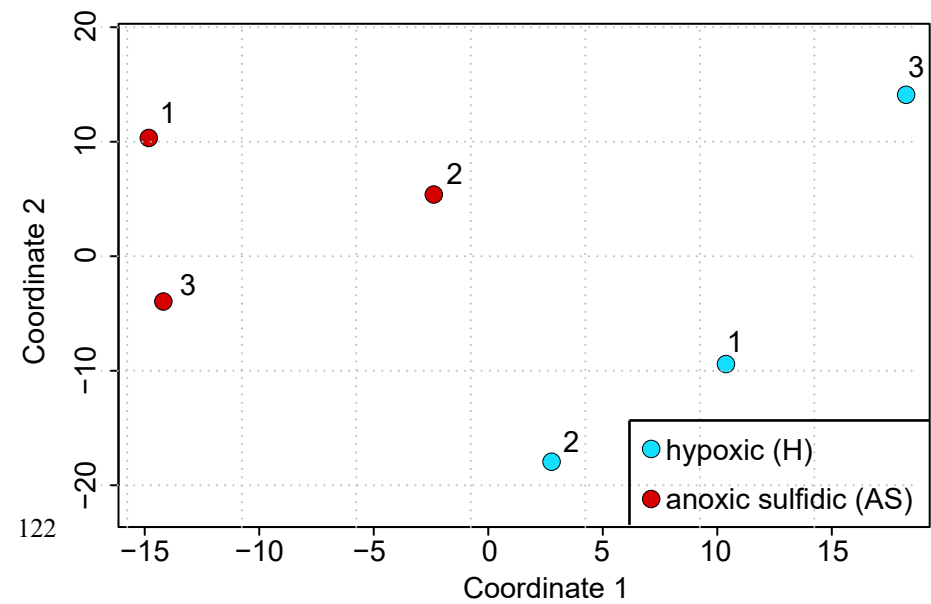
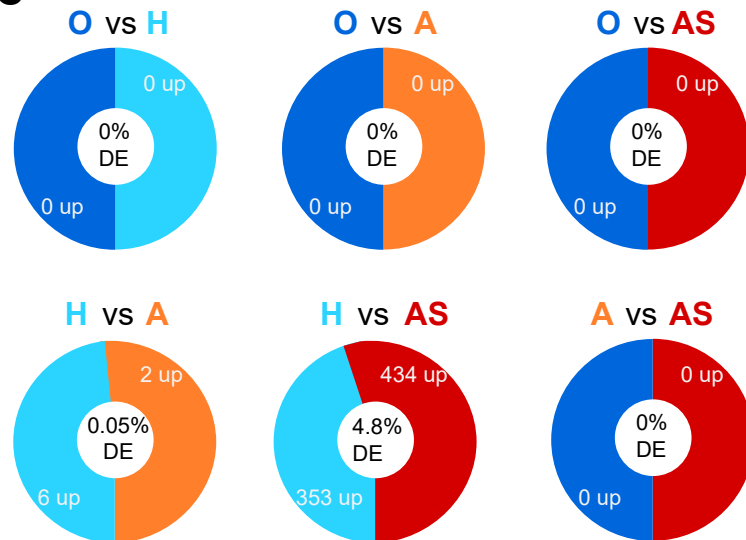
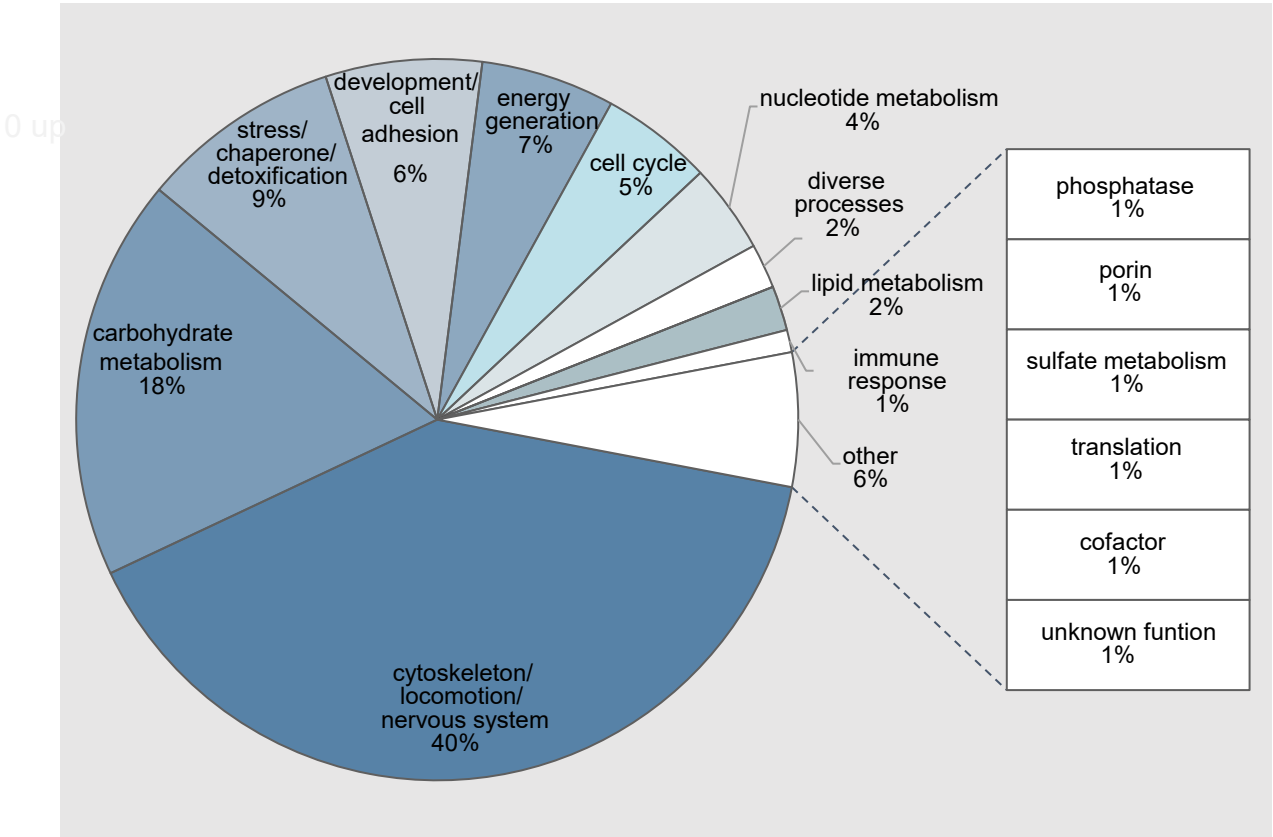


Figure S2

A



B

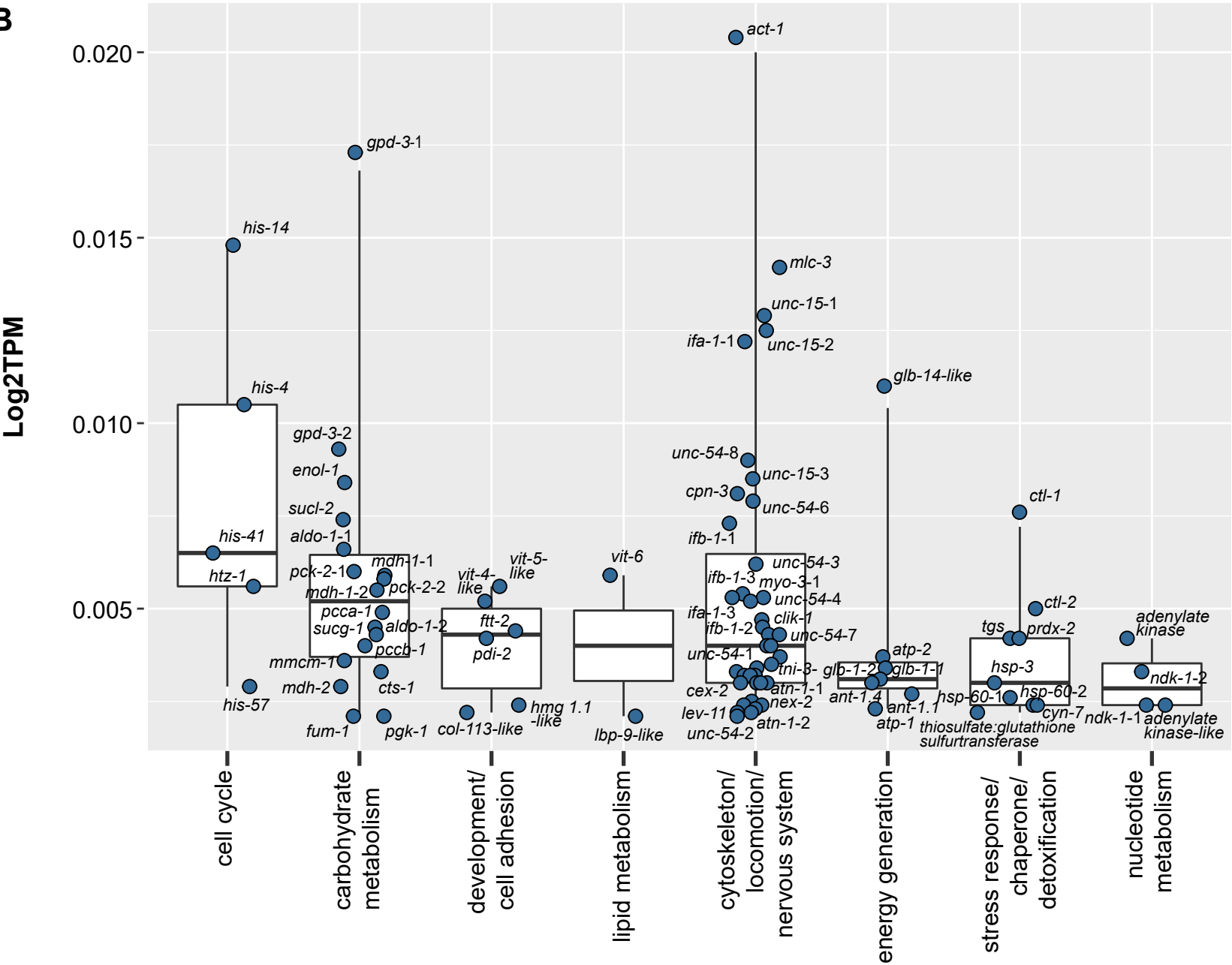


Figure S3

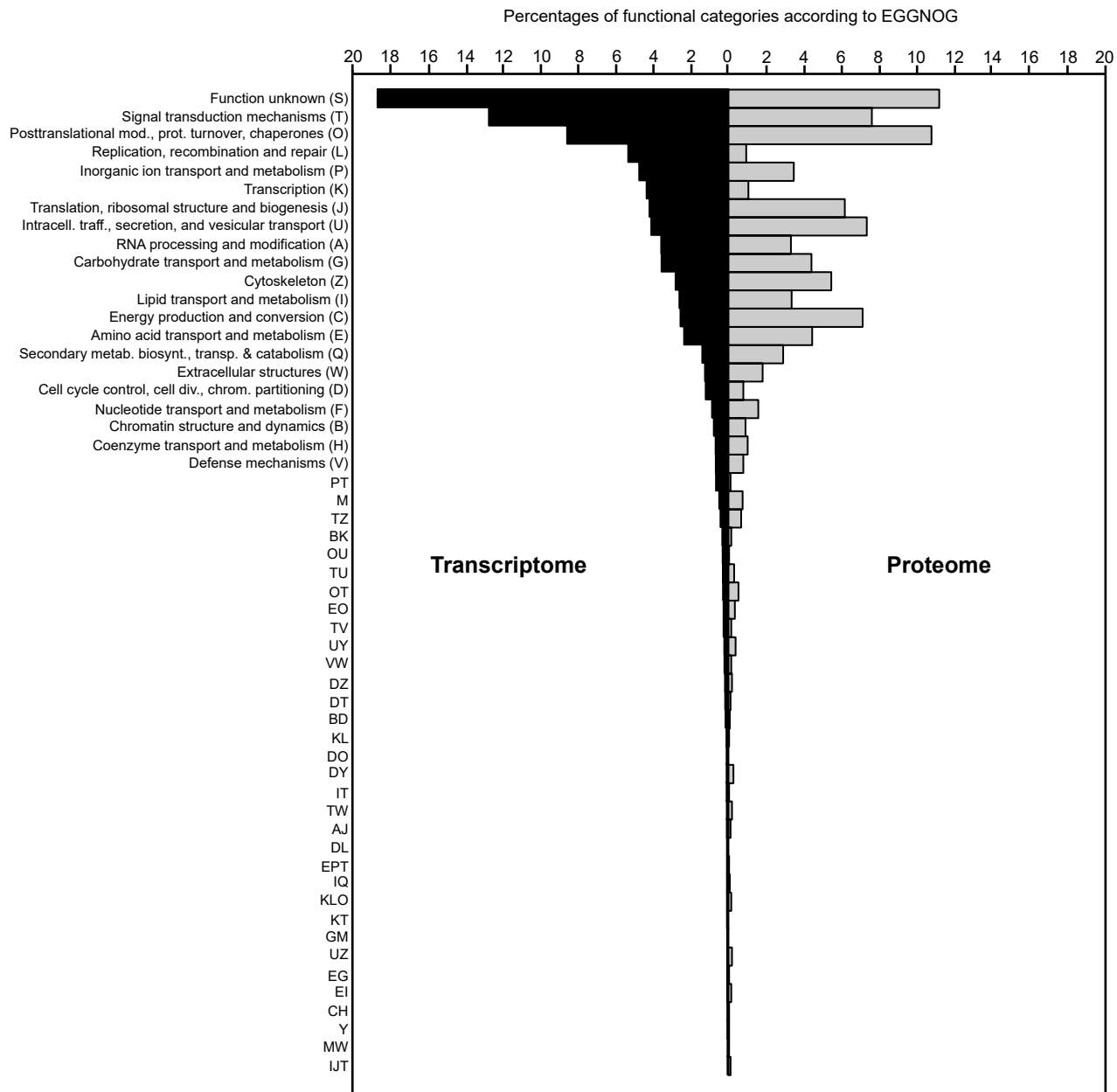
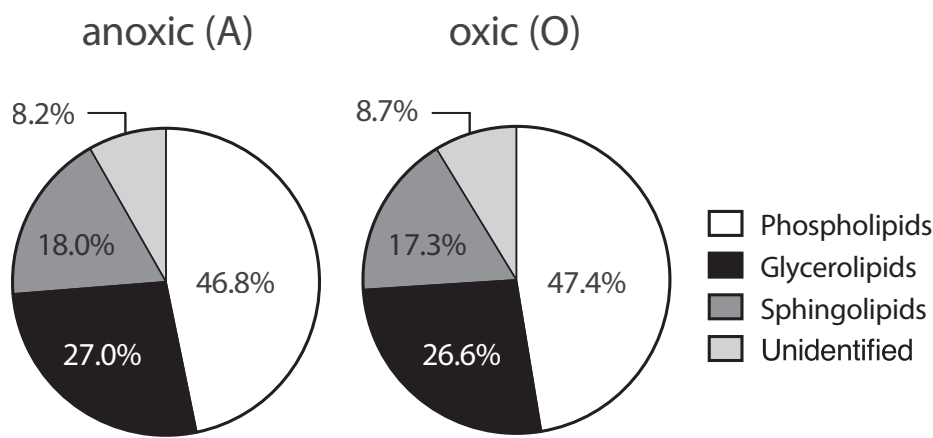


Figure S5.



CHAPTER IV

A Bidimensional Segregation Mode Maintains Symbiont Chromosome Orientation toward Its Host

Weber, P. M., Moessel, F. *, Paredes, G. F. *, Viehboeck, T., Vischer, N. O., & Bulgheresi, S.

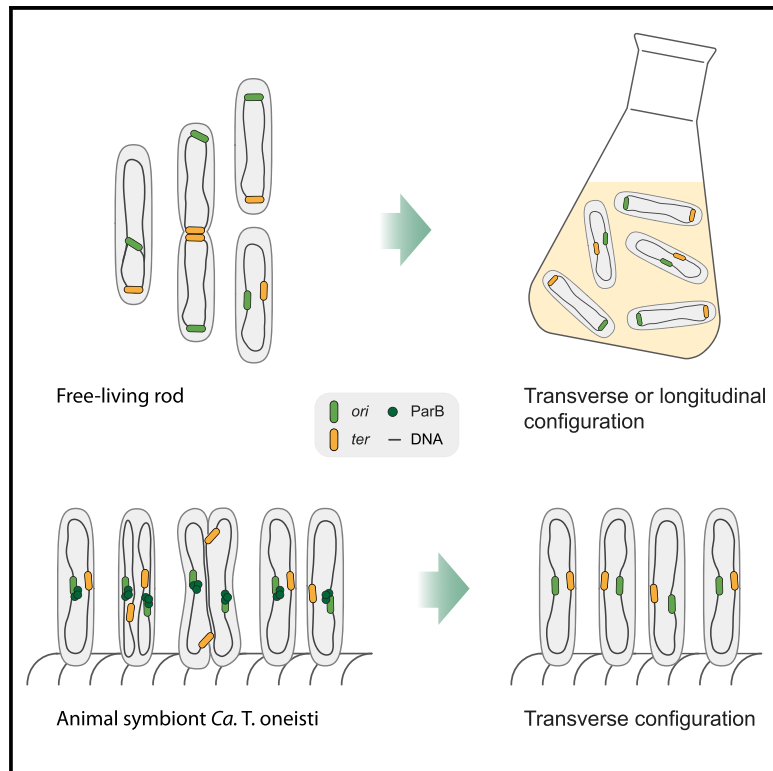
Published in Current Biology, 2019

*these authors contributed equally

Current Biology

A Bidimensional Segregation Mode Maintains Symbiont Chromosome Orientation toward Its Host

Graphical Abstract



Authors

Philipp M. Weber, Friedrich Moessel, Gabriela F. Paredes, Tobias Viehboeck, Norbert O.E. Vischer, Silvia Bulgheresi

Correspondence

silvia.bulgheresi@univie.ac.at

In Brief

Weber et al. report on the chromosome segregation of a longitudinally dividing gammaproteobacterium that lives attached to marine nematodes. They show that sister *ori* segregate along both the short and the length axis. Their data are consistent with the centromeric protein ParB mediating transgenerational maintenance of chromosome configuration.

Highlights

- Symbiont sister *ori* segregate along the short and the long cell axis (diagonally)
- ParB recapitulates *ori* localization and binds an *ori*-proximal *parS* site *in vitro*
- Septal sister *ter* migrate to midcell concomitantly with septation progression
- Bidimensional segregation endows maintenance of chromosome configuration



A Bidimensional Segregation Mode Maintains Symbiont Chromosome Orientation toward Its Host

Philipp M. Weber,¹ Friedrich Moessel,^{1,3} Gabriela F. Paredes,^{1,3} Tobias Viehboeck,¹ Norbert O.E. Vischer,² and Silvia Bulgheresi^{1,4,*}

¹Environmental Cell Biology Group, Department of Ecogenomics and Systems Biology, University of Vienna, Althanstrasse 14, 1090 Vienna, Austria

²Bacterial Cell Biology & Physiology, Swammerdam Institute of Life Sciences, Faculty of Science, University of Amsterdam, Science Park 904, 1098 Amsterdam, the Netherlands

³These authors contributed equally

⁴Lead Contact

*Correspondence: silvia.bulgheresi@univie.ac.at
<https://doi.org/10.1016/j.cub.2019.07.064>

SUMMARY

All living organisms require accurate segregation of their genetic material. However, in microbes, chromosome segregation is less understood than replication and cell division, which makes its decipherment a compelling research frontier. Furthermore, it has only been studied in free-living microbes so far. Here, we investigated this fundamental process in a rod-shaped symbiont, *Candidatus Thiosymbion oneisti*. This gammaproteobacterium divides longitudinally as to form a columnar epithelium ensheathing its nematode host. We hypothesized that uninterrupted host attachment would affect bacterial chromosome dynamics and set out to localize specific chromosomal loci and putative DNA-segregating proteins by fluorescence *in situ* hybridization and immunostaining, respectively. First, DNA replication origins (*ori*) number per cell demonstrated symbiont monoploidy. Second, we showed that sister *ori* segregate diagonally prior to septation onset. Moreover, the localization pattern of the centromere-binding protein ParB recapitulates that of *ori*, and consistently, we showed recombinant ParB to specifically bind an *ori*-proximal site (*parS*) *in vitro*. Third, chromosome replication ends prior to cell fission, and as the poles start to invaginate, termination of replication (*ter*) sites localize medially, at the leading edges of the growing septum. They then migrate to midcell, concomitantly with septation progression and until this is completed. In conclusion, we propose that symbiont ParB might drive chromosome segregation along the short axis and that tethering of sister *ter* regions to the growing septum mediates their migration along the long axis. Crucially, active bidimensional segregation of the chromosome allows transgenerational maintenance of its configuration, and therefore, it may represent an adaptation to symbiosis.

INTRODUCTION

The investigation of microorganisms with non-canonical growth modes is necessary to identify the conserved mechanisms underlying bacterial proliferation. *Candidatus Thiosymbion oneisti* forms a single-species community on the surface of its nematode host *Laxus oneistus* (*Stilbonematinae*) [1]. More precisely, each rod is attached by one pole (the proximal pole) to the host so that its long axis is perpendicular to the animal surface. Although *Stilbonematinae* regularly occur in tropical and temperate shallow water sediment, no *Ca. Thiosymbion* has been isolated in pure culture so far. Despite the impossibility of genetic manipulation, the reproductive mode of these *Gammaproteobacteria* is unique as *Ca. Thiosymbion* rods are the only prokaryotes reported to widen and undergo FtsZ-based longitudinal fission [2–4]. Because longitudinal fission allows for continuous attachment of the bacterial cell to the animal host, we hypothesized that (1) the orientation of the chromosome is invariable and transmitted from mother to daughter cells and that (2) this would require a DNA segregation mode different from that observed in bacteria that may adopt a free-living lifestyle, such as all model bacteria. Studies carried out on the latter revealed that, even though chromosome segregation occurs concomitantly with DNA replication, it follows a defined choreography [5–8]. Namely, it can be divided into three major steps: (1) separation and translocation of the region where replication starts (*ori*), (2) segregation of the bulk of the chromosome, and (3) separation of the region where replication terminates (*ter*) [9–11].

Segregation of the *ori* regions imposes the directionality of chromosome segregation and establishes the final configuration of the chromosome. A chromosomal *parABS* system drives or assists *ori* translocation in some bacterial species. This is closely related to the *parABS* plasmid system and consists of three components: a centromere site on the DNA (*parS*), a centromere-binding protein (ParB), and a Walker type ATPase (ParA) [10]. For instance, in the case of the *Vibrio cholerae*'s large chromosome (*chr1*) and of *Caulobacter crescentus*, one of the replicated ParB-bound *ori* regions stays at one pole, and the other moves to the opposite one following a retracting wave of nucleoid-bound ParA over the nucleoid [12–15]. Subsequently, a direct interaction between ParB and a pole-organizing



element, PopZ in *C. crescentus* [16, 17] and HupB in *V. cholerae* [18], anchors the translocated ParB-bound *ori* to the pole. In Actinobacteria, such as *Corynebacterium glutamicum* and in *Bacillus subtilis*, DivIVA appears to be the polar tether for the ParB-bound *ori*, albeit in the latter RacA is the functional homolog of ParB [19–24]. In order to propel itself along the ParA gradient, the ParB-bound *ori* region likely exploits the chromosomal elastic and/or the proteophoretic force through iterative interactions with ParA [25–27]. Notably, not only the ParB anchors but also the ParA and ParB localization patterns differ among bacteria. For example, instead of being tethered at the cell poles, ParB-bound *ori* is found near midcell in *Mycobacterium smegmatis* and displays a subpolar position in non-replicating *Myxococcus xanthus* [28–31]. Moreover, in *M. xanthus*, ParA is not nucleoid bound but instead is mainly confined to the DNA-free regions between the cell poles and the nucleoid [29, 30]. In bacteria lacking *parA* and *parB* genes, such as *Escherichia coli* [32], physical mechanisms underlie the translocation of the *ori* regions. Polymer dynamics in confined space anticipate that entropic forces will mediate the separation of freshly duplicated *ori* regions [33, 34]. Based on the finding that freshly replicated *ori* regions remain in close proximity for a protracted amount of time before they suddenly separate [35, 36], a “snap-release” mechanism has been put forward for *E. coli* *ori* segregation, by which entropic repulsion of DNA segments would drive the sister *ori* regions apart [37]. In *B. subtilis*, structural maintenance of chromosome (SMC) complexes that load in the vicinity of *ori* via Spo0J (the ParB homolog) may drive self-condensation and disentanglement of *ori*-proximal DNA loops [38–42]. Physical rather than biochemical phenomena were also invoked to explain bulk chromosome segregation [33, 34, 37, 43–48].

To guarantee complete segregation of sister chromosomes, DNA pumps, such as the FtsK protein (SpoIIIE, during *B. subtilis* sporulation), actively translocate DNA from one perspective daughter cell to the other [49–51]. FtsK binds the divisome at the growing septum, as well as specific FtsK-orienting polarized sequences (KOPS) on the chromosome [52, 53]. Numerous KOPS are distributed along both arms, and their *ori*-to-*ter* orientation confers directionality to the DNA translocation process [54–58]. KOPS guide the translocation of FtsK toward the *dif* site, another genetic element contained in the *ter* region that controls chromosome dynamics. The *dif* site serves indeed as the recognition sequence for the site-specific recombinase XerCD, which ensures resolution of chromosome dimers prior to cell division. The assembly of the recombination complex is facilitated by the aforementioned septum-tethered DNA translocase FtsK, which ensures the capture of the two recombining *dif* sites in the vicinity of the septum and activates the complex for recombination [59, 60]. About half of all presently sequenced bacterial genomes contain a canonical *dif* site, and several alternative ones were found in other bacteria [61]. Notably, special sites (*matS*) in *E. coli* bind MatP, which causes compaction of the region and tethers the domain to the closing division septum [62]. *matS*-containing *chr1* and *chr2* *ter* regions (*ter1* and *ter2*, respectively) are also compacted by MatP in *V. cholerae*, another gammaproteobacterium [63].

As for the overall arrangement of the genetic material, bacterial chromosomes can assume two major configurations, *ori-ter*

(longitudinal) and *left-ori-right* (transverse). In *ori-ter*, the origin is located at one cell pole, the terminus at the other pole, and both left and right chromosomal arms are parallel to the long axis of the cell [7]. This pattern has been observed in *C. crescentus* and *V. cholerae* *chr I*, for example. The *left-ori-right* pattern is rotated 90° with respect to *ori-ter*; namely, both *ori* and *ter* are centrally positioned so that the left and right arms reside in opposite cell halves. *E. coli* and other bacteria can switch between longitudinal and transverse arrangements, depending on the cell cycle stage and the growth conditions [35, 64–66].

Here, we present data indicating that, in longitudinally dividing Gammaproteobacteria, ParB/*parS* binding may mediate *ori* segregation along the cell short axis. Furthermore, we propose that tethering of sister *ter* regions to the newly assembled divisome makes them migrate toward one another along the cell long axis as septation proceeds and until, immediately prior to daughter cells' separation, they reach the center of the cell. Crucially, this bidimensional DNA segregation mode allows transgenerational maintenance of the transverse configuration in an animal symbiont.

RESULTS

Longitudinally Dividing *Ca. T. oneisti* Is Monoploid, and Its *ori* Is Segregated along the Cell Short Axis

Both the phylogenetic placement of *Ca. T. oneisti* and the characterization of its genome suggested that the symbiont genetic material is contained in a single, circular chromosome and that no extrachromosomal genetic elements (plasmids) are present [67] (Table S1). Moreover, the DNA appeared to be homogeneously distributed throughout the cell, except for an 8% drop in fluorescence signal in the polar cell fourths (Figure S1A). To determine the ploidy of *Ca. T. oneisti* and the localization pattern of its *ori*, we fixed it and subjected it to DNA fluorescence *in situ* hybridization (FISH) with a set of nine fluorescent probes targeting a 2,874-nt-long chromosomal region containing the *dnaA* and *dnaN* genes both predicted to be *ori*-proximal [68, 69] (*ori* probe; Figure S1B; Tables S3 and S5). This region also contained a duplex-unwinding region (also referred to as DNA unwinding element [DUE]) [70, 71] and binding sites for the initiator protein DnaA (DnaA boxes) [72] (Figure S1B). 69% (226) of the 327 cells analyzed by epifluorescence microscopy displayed one fluorescence focus, 25% (81) two foci, and 6% (20) three foci (Figure 1A), with this latter fraction accounting mostly for cells that started a second round of chromosome replication. Therefore, if we assume that one fluorescent focus equals one *ori* copy, we may conclude that the nematode symbiont is monoploid. This conclusion was also supported by counting the number of fluorescence foci obtained with an anti-ParB antibody and with probes targeting *ftsQAZ*- and *ter*-containing chromosomal regions (see below and Figures 1C, S1C, and 3A, respectively).

After determining *Ca. T. oneisti* ploidy, we analyzed the *ori* localization pattern throughout the symbiont life cycle. DNA-FISH-based visualization of *ori* revealed that, in non-dividing cells displaying only one focus, it occupies a near-midcell position (Figure 1B, left panel, and plot in Figure 1E). Moreover, the segregation of sister *ori* regions starts before the onset of septation, a process concomitant with symbiont cell growth [2]

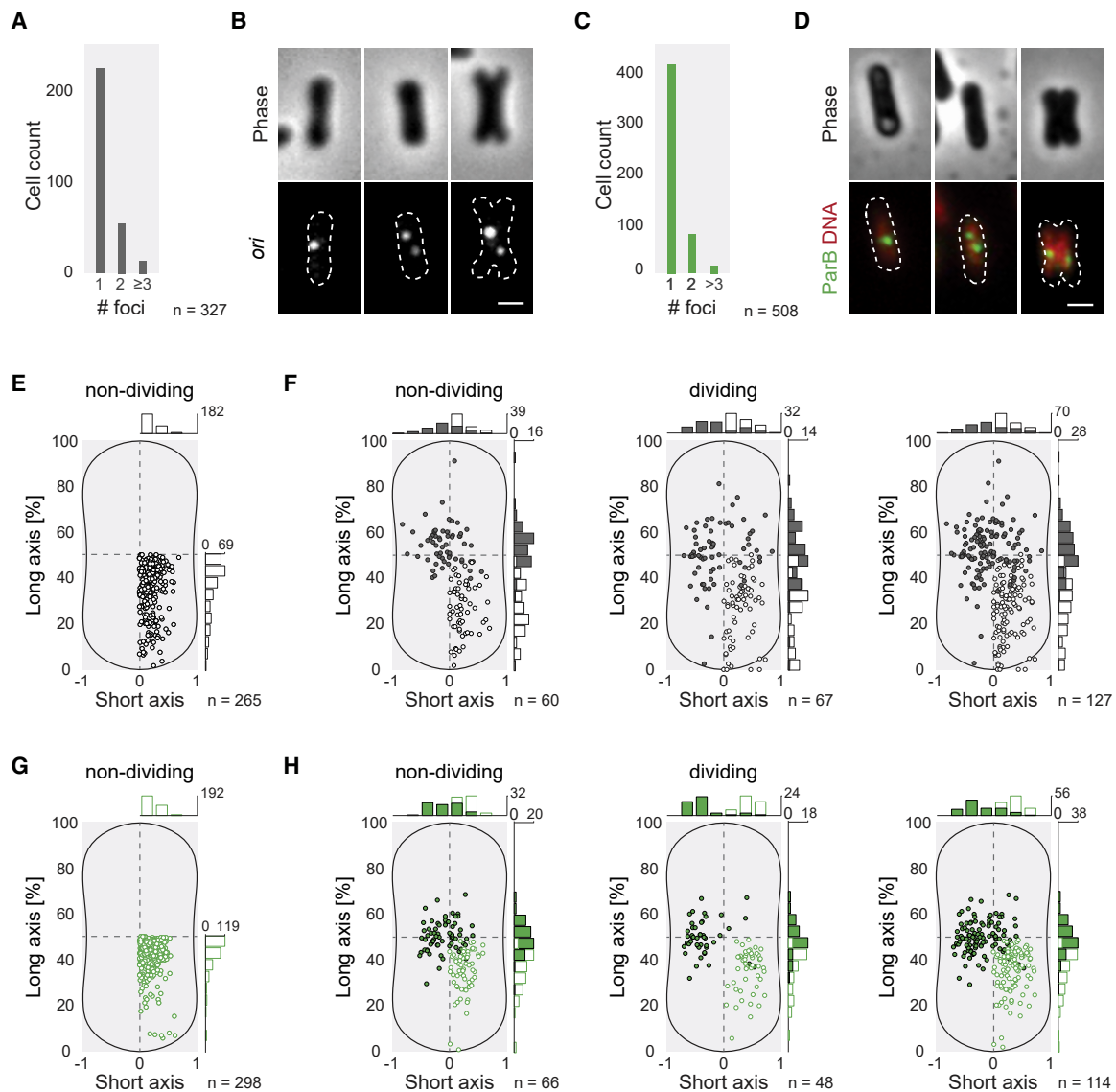


Figure 1. DNA FISH-Based Localization Pattern of *Ca. T. oneisti* *ori* and Immunostaining-Based ParB Localization Pattern

(A and C) Histograms showing number of *ori* (A) or ParB (C) foci per cell. Total number of analyzed cells (n) is 327 in (A) and 508 in (C).

(B and D) Images of three representative cells arranged from the thinnest (youngest) to the thickest (oldest) cell, from left to right. Upper panels show the phase-contrast images, and lower panels show *ori* signal in (B; white) or ParB (green) and DNA (red) signals in (D). Cell outlines were deduced from the corresponding phase-contrast images (white dotted lines). Scale bars, 1 μ m.

(E and F) Subcellular localization of *ori* fluorescence foci in non-dividing cells displaying one fluorescence focus only (E) and of *ori* fluorescence foci in cells displaying two fluorescence foci (F). In (F), *ori* foci found in non-dividing cells are displayed in the left plot, foci found in dividing cells are displayed in the middle plot, and foci found in both non-dividing and dividing cells are displayed in the right plot.

(G and H) Subcellular localization of ParB fluorescence foci in non-dividing cells displaying one fluorescence focus only (G) and of ParB foci in cells displaying two foci (F). In (H), *ori* foci found in non-dividing cells are displayed in the left plot, foci found in dividing cells are displayed in the middle plot, and foci found in both non-dividing and dividing cells are displayed in the right plot.

In (E)–(H), the position of each focus is plotted as fraction of the normalized cell width and length (%) of the cell that contained them. Dashed lines represent the long and the short cell axis, and midcell is defined as the point in which they intersect. See also Figures S1 and S2 and Tables S1–S3 and S5.

(representative image in Figure 1B, middle panel, and left plot in Figure 1F). Upon replication, sister *ori* regions are segregated along the short but also along the long axis (from here on, we will refer to this segregation mode as diagonal; Figure 1F; Table S2). Localization pattern of a 3,273-nt-long chromosomal region (Tables S3 and S5) containing the single-copy genes *ftsQ*, *ftsA*,

and *ftsZ*, which are *ori*-proximal in *E. coli* [73, 74], revealed a number of fluorescence foci (Figure S1C) and a diagonal migration pattern similar to that observed with the *ori* probe (Figures S1D and S1E). However, at least one of the two foci observed with the *ftsQAZ* probe appeared more polar, irrespectively of the cell cycle stage (Figure S1E).

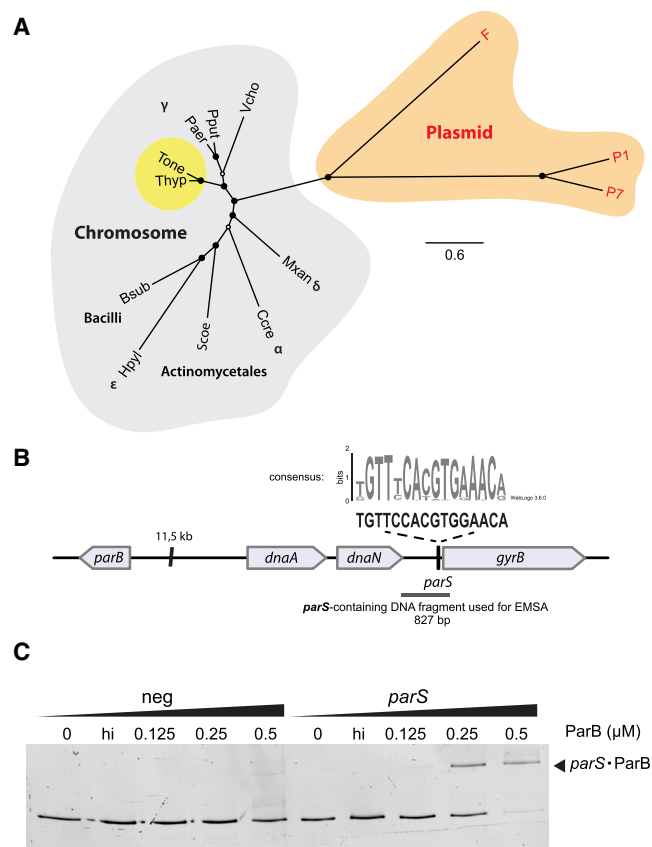


Figure 2. Phylogenetic Placement of *Ca. T. oneisti* ParB, Schematic Representation of the Chromosomal Region Containing the Symbiont *parS* Site, and *In Vitro* ParB-*parS* Binding Assay

(A) Unrooted phylogenetic tree including the ParB proteins of *Ca. T. oneisti* (*Tone*), *Ca. T. hypermnestrae* (*Thyp*), and of bacteria in which ParB was shown to facilitate either chromosome or plasmid segregation (*Bsub*, *Bacillus subtilis*; *Ccre*, *Caulobacter crescentus*; *Hpyl*, *Helicobacter pylori*; *Mxan*, *Myxococcus xanthus*; *Paer*, *Pseudomonas aeruginosa*; *Pput*, *Pseudomonas putida*; *Scoe*, *Streptomyces coelicolor*; *Vcho*, *Vibrio cholerae*). *Ca. T. oneisti* and *Ca. T. hypermnestrae* ParBs are on a yellow background, the ParB homologs that belong to the chromosomal group [5] are displayed on a gray background, and those belonging to the extrachromosomal group [5] on a red background. The analysis is based on a MAFFT alignment of full-length proteins (Table S4) and estimated under the LG+F+G4 model using ML analysis (IQ-TREE) with node support calculated by SH-aLRT. Scale bar represents 0.6% estimated sequence divergence. Open circles represent SH-aLRT values <80%, whereas closed circles represent SH-aLRT values ≥80% based on 10,000 replicates.

(B) Schematic representation of the chromosomal position of the *parS*-containing DNA fragment used in the electrophoretic mobility shift assay (EMSA) and bound by recombinant ParB *in vitro*. Sequence logo shows the consensus *parS* sequence [32] located between the *dnaN* and *gyrB* genes. The most conserved 11 nt are enlarged.

(C) Ethidium-bromide-stained acrylamide EMSA. Black arrowhead points to retarded DNA fragments containing the wild-type *parS* site; hi, heat inactivated; neg, DNA fragments containing a mutated *parS* site.

See also Figure S2 and Tables S1, S4, and S5.

In conclusion, in the monoploid *Ca. T. oneisti*, sister *ori* segregate before septation onset, and they do so diagonally. Sister *ftsQAZ*-containing chromosomal regions also migrate diagonally but are more polar throughout the cell cycle.

Symbiont ParB Recapitulates *ori* Localization Pattern

One of the generalities of bacterial chromosome segregation is that, when present, the *parABS* system contributes to it [32, 75–77]. The alignment of the predicted *Ca. T. oneisti* ParB protein sequence with other bacterial ParB proteins showed conservation of the box I and II and of the HTH motif required for the binding to *parS* [5, 78] (Figure S2A). Furthermore, probing western blots of symbiont protein extracts with a specific anti-ParB antibody showed that ParB is expressed (Figure S2B). Therefore, we tested whether ParB localization pattern would be consistent with a role in DNA segregation by immunostaining (Figure 1). Epifluorescence-microscopy-based analysis of fixed cells with a specific anti-ParB antibody showed that 82% (414), 15% (78), and 3% (16) of the 508 analyzed cells displayed one, two, or three fluorescence foci, respectively (Figure 1C). The fact that the percentages of cells bearing one, two, or three *ori* or ParB foci were similar (Figures 1A and 1C, respectively) and that ParB foci localization pattern resembled that of the *ori* region (see their apparent diagonal segregation in Figure 1D and plots in Figures 1G and 1H) indicated that symbiont ParB might bind the predicted centromeric *parS* and drive chromosome segregation. Consistently, phylogenetic analysis revealed that, among all ParB proteins reported to mediate DNA segregation, symbiont ParB is mostly related to those of *Pseudomonas* and *Vibrio*, that is to chromosome- and not to plasmid-encoded ParB proteins [79, 80–83] (Figure 2A).

In conclusion, our data indicate that native symbiont ParB may bind the chromosome in the vicinity of the *ori*.

Symbiont ParB Binds an *ori*-Proximal *parS* Site *In Vitro*

To further support a possible role of *Ca. T. oneisti* ParB in chromosome segregation, we tested its capacity to specifically bind symbiont *parS* *in vitro*. Therefore, we expressed and purified a His-tagged version of ParB (Figure S2B) and identified one *ori*-proximal *parS* site located between the *dnaN* and *gyrB* genes by searching the genome draft for the consensus sequence [32] (Figure 2B). Figure 2C shows that ≥0.125 μM symbiont recombinant ParB decreased the electrophoretic mobility of an 827-nt-long *parS* site-containing DNA fragment. However, recombinant ParB could not appreciably retard a DNA fragment bearing a *parS* site in which the 11 most conserved nucleotides [32] were mutated (Figure 2B). Thus, recombinant ParB appeared to specifically bind *parS* *in vitro*.

In conclusion, both ParB localization pattern and the electrophoretic mobility shift assay (EMSA) are consistent with native ParB binding an *ori*-proximal *parS* site in live symbiont cells.

Chromosome Transverse Configuration and Segregation of Sister *ter*

To determine the position of the *ter* region and, thereby, the overall arrangement of the symbiont chromosome, we took advantage of a 28-nt-long consensus sequence obtained by comparing 161 *dif*-related sequences from 137 proteobacterial species [84] (see STAR Methods for the symbiont *dif* site nucleotide sequence). We then subjected fixed *Ca. T. oneisti* to a set of 12 fluorescent probes targeting a 3,916-nt-long chromosomal region containing the predicted *dif* site (*ter* probe; Tables S3 and S5). First of all, the majority of the cells (56.7%) displayed one fluorescence focus only, confirming the monoploidy of the

symbiont (Figure 3A). Secondly, in these non-dividing cells, the *ter* position on the long axis resembled that of *ori*, whereas, on the short axis, *ter* appeared closer to the cell envelope than *ori* (leftmost panel in Figure 3B and Figures 3C and 3F). Given that both *ori* and *ter* occupied a near-midcell position at the beginning and at the end of the cell cycle, we concluded that the symbiont chromosome is not longitudinally but likely transversally organized (see schematic representation in Figure 4).

To analyze the localization pattern of the *ter* throughout the cell cycle, we grouped the cells into three width classes and plotted the total fluorescence emitted by each class against the normalized short axis or long axis (Figures 3D and 3E, respectively; in Figure 3E, we further subdivided the 263 widest cells of 3D into three width classes). Based on our analysis, sister *ter* regions appeared to localize medially in dividing cells (two rightmost representative cells in Figure 3B; plot in Figure 3D; demograph in Figure S3A) and to move to the center of the cell concomitantly with the invagination of the cell envelope and the growing septum (two leftmost representative cells in Figure 3B; plot in Figure 3E; demograph in Figure S3B). To better resolve the *ter* localization pattern in dividing cells, we also grouped them into three classes, depending on the position of the *ter* foci along the long axis, and plotted their total fluorescence against the short or the long axis, which confirmed rapprochement of the sister *ter* at midcell (left and right plot in Figure S3C, respectively). Notably, the presence of non-dividing cells bearing two fluorescence foci indicated that sister *ter* may segregate diagonally prior to septation onset (second leftmost panel in Figure 3B and leftmost panel in Figure 3G).

We conclude that sister *ter* may migrate away from each other diagonally before *Ca. T. oneisti* starts dividing and that, as septation begins, they localize medially at the divisome leading edges. Finally, as septation progresses, each *ter* migrates toward midcell.

DISCUSSION

We investigated chromosome dynamics in a longitudinally dividing bacterium and made a number of observations challenging simple predictions about DNA replication and segregation: (1) rod-shaped *Gammaproteobacteria* segregate their DNA along their short axis prior to cell division and likely via a *parABS* system; of note, this system has so far been known to mediate DNA segregation along the long axis only; (2) sister *ter* regions segregate away from one another in non-dividing cells, whereas in dividing cells sister *ter* are medial and migrate toward one another; and (3) diagonal (bidimensional) segregation of *ori*-, *ftsQAZ*-, and *ter*-containing regions in non-dividing cells and rapprochement of medial sister *ter* in dividing cells allow transgenerational maintenance of the chromosome configuration; this implies that the intracellular localization of specific genetic loci may be transmitted from mother to daughter cells (Figure 4).

According to the DNA-relay model [85], the ParB-translocating force is derived from the elastic dynamics of the DNA, which are harnessed each time ParA interacts with ParB. Therefore, as long as there is a molecule that interacts with and anchors the duplicated ParB at its final destination—the opposite lateral membrane—ParB motion could occur across the cell width. As we could not identify any of the genes encoding for the known

ParB anchors [16–18, 23, 24], a yet to be discovered molecule might mediate the attachment of ParB to the lateral sides of the cell. Moreover, the fact that (1) the segregation of both the symbiont *ori* and the *ori*-proximal *ftsQAZ* operon are diagonal and (2) the fact that *ori* and ParB foci are spread along the long axis suggest that, if existing, the putative *ori* anchor is not confined to the center of the lateral membrane. Namely, in non-dividing cells showing a single *ori* focus, we observed that 47% of the foci ($n = 124$) localized at 40%–50% of the long axis, 26% at 30%–40%, and 27% at 0%–30%.

An additional reason for the spreading of *ori* foci along the long axis could be the technique itself, as immunostaining-detected symbiont ParB foci were less spread than DNA-FISH-detected *ori* foci throughout the cell cycle (Figure 1). Along the same line, [86] observed a noisier localization pattern of chromosomal loci when applying DNA FISH versus fluorescent repressor-operator system (FROS) on *C. crescentus*, despite *ori*/ParB being tethered to the poles by PopZ. As a final remark on the spreading of *ori* signal along the long axis, it should be highlighted that we analyzed the localization patterns of chromosomal loci in cells that were not grown in culture. Instead, we fixed the symbiont cells upon collection from the environment while they were still attached to the worms. Therefore, it is possible that, at the moment of fixation, different symbiont cells were experiencing different environmental conditions and/or nutrients' availability. As reported for culturable bacteria, such as *E. coli*, growth conditions may significantly affect the position of their chromosomal loci [5].

From an evolutionary perspective, the existence of anchors on the symbiont lateral sides would imply that these physiologically correspond to the poles of *parABS*-utilizing *Gammaproteobacteria*, such as *Pseudomonas* and *Vibrio* species [81, 83]. It is tempting to speculate that the *Ca. T. oneisti* ancestor, likely a basal free-living flagellated gammaproteobacterium [87] possessing a long axis-oriented *parABS* system, attached to the nematode surface by one of its two lateral sides. Subsequently, as the bacterium-animal association became more and more stable, the *Ca. T. oneisti* predecessor would lose its flagellum [88], and the evolutionary pressure to maximize the number of cells per unit of nematode surface (or other yet unknown physiological constraints) would “squeeze” it laterally [89, 90]. In such an evolutionary scenario, the ancestrally polar *ori* and *ter* would have ended up occupying the cell center of the symbiont, or in other words, the typical longitudinal chromosome arrangement characteristic of flagellated, polar rods [12, 83, 91] would become transverse. Furthermore, the ancestral polar ParB anchor would become a lateral one and mediate chromosome segregation along the short cell axis. However, it should also be noted that membrane anchors, either polar or lateral, could be dispensable, as it is known, for instance, that plasmids are positioned to specific subcellular locations in a self-organizing manner [92, 93].

As for ParA, according to the reaction-diffusion model [94], it could form a lateral instead of a polar gradient. However, the establishment of a stable ParA gradient before DNA replication and segregation is not needed for directional segregation of ParB-*parS*. Indeed, the motion of ParB could be sufficient to establish asymmetry in ParA localization (i.e., between the back and the front of ParB-*parS*) and to drive directional motion. Although transcriptomics and proteomics revealed that the *parA*

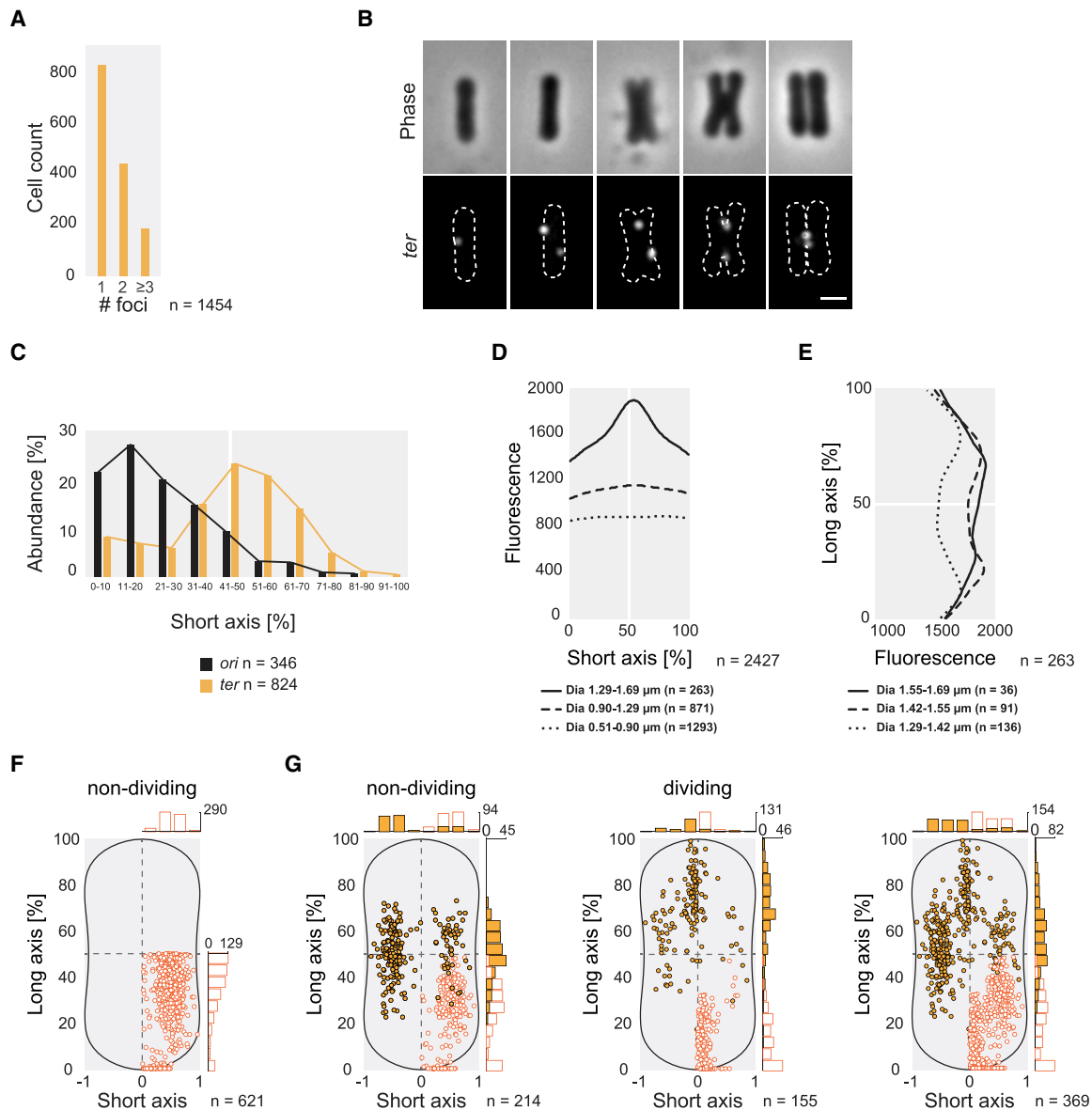


Figure 3. DNA FISH-Based Localization Pattern of *Ca. T. oneisti ter*

(A) Histogram showing number of *ter* fluorescence foci per cell. Total number of analyzed cells (n) is 1,454.

(B) Five representative cells probed with a *ter* probe arranged from the youngest to the oldest cell, from left to right. Upper panels show phase-contrast images of five cells arranged from the thinnest (youngest) to the thickest (oldest) cell, from left to right. Lower panels show the corresponding epifluorescence images of the *ter* signal (white). Cell outlines were deduced from the corresponding phase-contrast images (white dotted lines). Scale bar, 1 μ m.

(C) Histogram shows the distribution and abundances (%) of *ori* (n = 346) and *ter* (n = 824) fluorescence foci along the normalized cell width (%). 0% corresponds to the cell center, and 100% corresponds to the lateral membrane.

(D) We plotted the total fluorescence emitted by cells belonging to three width classes (0.51–0.90 μ m, n = 1,293, dotted line; 0.90–1.29 μ m, n = 871, dashed line; 1.29–1.69 μ m, n = 263, full line) along the short axis.

(E) The 263 widest cells analyzed in (D) (1.29–1.69 μ m) were subdivided into three additional width classes (1.29–1.42 μ m, n = 136, dotted line; 1.42–1.55 μ m, n = 91, dashed line; 1.55–1.69 μ m, n = 36, full line) and their fluorescence plotted along the long axis.

(F and G) Subcellular localization of *ter* fluorescence foci in cells displaying only one (F) or two fluorescence foci (G). In (G), *ter* foci found in non-dividing cells are shown in the left plot, foci found in dividing cells in the middle plot, and foci found in both non-dividing and dividing cells in the right plot. The position of each focus is plotted against the normalized cell width and length (%) of the cell that contained them. Dashed lines represent the long and the short cell axis, and midcell is defined as the point in which they intersect.

See also Figure S3 and Tables S1–S3 and S5.

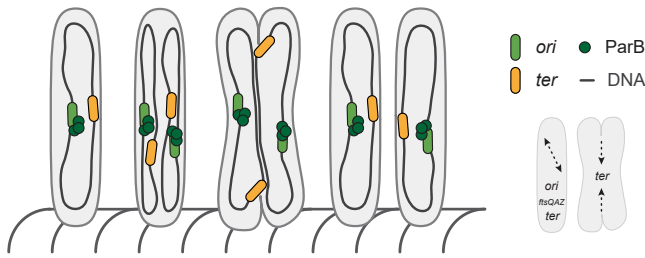


Figure 4. Schematic Representation of Chromosome Dynamics in the Animal Symbiont *Ca. T. oneisti*

Schematic representation of *ori* (light green), *ter* (orange), and ParB (dark green) localization patterns in *Ca. T. oneisti*. Cells are arranged from the youngest to the oldest from left to right. Diagonal segregation of *ori*, *ftsQAZ*, and *ter* in non-dividing cells is represented by a dashed double-headed arrow; rapprochement of sister *ter* in dividing cells is represented by two medial dashed arrows pointed against one another in scheme on the right (see Discussion).

gene is expressed (L. König, S. Markert, and S.B., unpublished data), the symbiont ParA localization pattern is currently unknown.

Given that several species (with the exception of *C. crescentus*, *M. xanthus*, and *V. cholerae* chromosome II) still segregate their chromosome normally in most cells, even when *parABS* is non-functional [12, 95–99], additional mechanisms might be in place to guarantee symbiont chromosome segregation in the absence of this system. For example, it has been proposed that the bacterial actin homolog contributes to DNA segregation in some bacteria [100–103] and that the Min system mediates active segregation of *ori* in *E. coli* [104]. As both *mreB* [2] and the *min* system are present and expressed in *Ca. T. oneisti* (L. König, S. Markert, and S.B., unpublished data), it will be compelling to assess their role in symbiont chromosome organization and segregation.

In *E. coli*, sister *ter* segregation immediately precedes daughter cells' separation so that DNA replication and segregation are concomitant [91, 105]. In contrast, in *Ca. T. oneisti*, sister *ter* appear already segregated in non-dividing cells, suggesting that a longer fraction of the chromosome segregation process occurs in the absence of DNA replication. Concerning what captures and tethers the *dif* site-containing *ter* region to the symbiont septum, *Ca. T. oneisti* FtsK is the best candidate, although no antibody is currently available to analyze the intracellular localization of this DNA translocase. In most bacteria, the assembly of the recombination complex is indeed facilitated by FtsK, which ensures the capture of the two *dif* sites in the vicinity of the septum and activates the complex for recombination [106]. This is likely mediated by DNA topoisomerases and the XerCD tyrosine recombinases, of which we have genomic-based evidence (GenBank: SMSC00000000.1), and would result in decatenation of duplicated intertwined circular chromosome. Despite both *E. coli* and *V. cholerae* possessing a *MatP/matS* system that causes compaction and tethering of the *ter* region to the closing division septum [62, 63], *Ca. T. oneisti* sister *ter* do not appear to be compacted. They indeed segregate from one another in non-dividing and toward one another in dividing cells. Consistently, we could identify neither a *matP* gene nor a *matS* site in the available genome draft (GenBank: SMSC00000000.1).

It was previously reported that different fluorochromes yielded different gene detection efficiencies, with Alexa 488 and Alexa Fluor 594 giving the strongest and most stable signal and the highest gene detection efficiency [107]. In our experimental system, only FISH probes labeled with Alexa Fluor 594 allowed us to detect an *ori*-, *ter*-, or *ftsQAZ*-containing chromosomal region. Therefore, given the impossibility of utilizing fluorochromes other than Alexa Fluor 594, the *ori*-, *ter*-, and *ftsQAZ*-specific probes could not be applied together but were each applied singularly.

In line with the hypothesis that *Ca. T. oneisti* evolved from a “squeezed” flagellated rod bearing a longitudinally (*ori-ter*) arranged chromosome, we expect each chromosome arm to be contained in either the proximal or the distal cell half of the symbiont. The fact that the *ftsQAZ* operon is in the polar cell third throughout the cell cycle indicates that not only *ori* and *ter* but also other chromosomal loci are non-randomly positioned and segregated. In *B. subtilis* and *E. coli*, midcell positioning of *ori*-proximal regions is maintained by the condensins SMC and MukB (a structural homolog of SMC), respectively [108–110]. As we do have genomics-based evidence (GenBank: SMSC00000000.1) that SMC is present in *Ca. T. oneisti*, this could compact large regions of the symbiont chromosome and, by interacting with ParB, organize the *ori*-proximal regions as observed in *B. subtilis* [38].

If we compare the symbiont nucleoid structure to that of other model bacteria, reports of both *E. coli* and of *B. subtilis* have suggested a variety of organizational patterns, including *ori-ter* or left-*ori*-right arrangement, as well as alternation between the two (see Introduction). Reports in *C. crescentus* and *V. cholerae* have been more consistent, with both bacteria invariably possessing *ori-ter* chromosome arrangement [12, 83, 91]. Despite assuming a transverse arrangement, the configuration of the symbiont genetic material is maintained throughout the cell cycle and therefore, in this regard, more similar to what observed in polarized bacteria.

As for why the symbiont chromosome configuration is maintained, we hypothesize that it might be advantageous to permanently position genetic loci mediating host interaction in the vicinity of the host (proximal cell half) and to confine loci involved in environmental response to the distal cell half. Determination of the 3D structure of the chromosome by chromosome conformation capture and development of live imaging techniques are necessary to unambiguously correlate the existence of a specific chromosome configuration with symbiont physiology. If we will indeed prove the existence of such a correlation, the range of cell biological adaptations to the symbiotic lifestyle will have to include positioning of the genetic material, a fundamental feature of cellular life. Moreover, from a chromosome-centric evolutionary perspective, even the peculiar reproductive mode of the symbiont (longitudinal division) might have evolved from the need to maintain a specific chromosome configuration.

STAR★METHODS

Detailed methods are provided in the online version of this paper and include the following:

- KEY RESOURCES TABLE
- LEAD CONTACT AND MATERIALS AVAILABILITY

- EXPERIMENTAL MODEL AND SUBJECT DETAILS
- METHOD DETAILS
 - Oxford Nanopore Technologies sequencing
 - DNA Fluorescence *In Situ* Hybridization
 - ParB alignment and phylogenetic tree
 - Expression of recombinant *Ca. T. oneisti* ParB
 - Antibodies and western blots
 - Identification of *Ca. T. oneisti* *parS* and electrophoretic mobility shift assay (EMSA)
 - Immunostaining and DNA staining
 - Fluorescence microscopy
- QUANTIFICATION AND STATISTICAL ANALYSIS
- DATA AND CODE AVAILABILITY

SUPPLEMENTAL INFORMATION

Supplemental Information can be found online at <https://doi.org/10.1016/j.cub.2019.07.064>.

A video abstract is available at <https://doi.org/10.1016/j.cub.2019.07.064#mmc3>.

ACKNOWLEDGMENTS

This work was supported by the Austrian Science Fund (FWF) grants P28593 (P.M.W. and S.B.) and P28743 (F.M. and T.V.), and the DK plus: Microbial Nitrogen Cycling (G.F.P. and P.M.W.). We thank the MPI for Marine Microbiology (Symbiosis group) and Marc Bramkamp and Kati Böhm (LMU Munich) for helping us apply the DNA FISH and EMSA protocols, respectively. We are indebted to the staff of the VBCF NGS Unit (Laura-Maria Bayer and Miriam Schalamun) for assistance with Oxford Nanopore MinION sequencing and to the Division of Computational Systems Biology, University of Vienna, for providing and maintaining the Life Science Compute Cluster (LiSC) (Florian Goldenberg and Thomas Rattei) and assisting with the MinION sequencing library preparation (Patrick Hyden). We are grateful to Nika Pende for reading and commenting on the manuscript and to Wolfgang Miller and the Genome Dynamics Lab for inspiring and constructive discussions. We thank Christoph Weigel for helping us identify the origin of replication and four anonymous reviewers for their very constructive comments that helped us to improve the first version of this manuscript. This work is contribution 1022 from the Carrie Bow Cay Laboratory, Caribbean Coral Reef Ecosystem Program, National Museum of Natural History, Washington, DC.

AUTHOR CONTRIBUTIONS

P.M.W. did most of the experiments, methodology, formal analysis, and visualization; provided resources; and reviewed and edited the manuscript. F.M. expressed and purified ParB recombinantly, performed the EMSA, and reviewed and edited the manuscript. G.F.P. contributed to the establishment of the DNA FISH protocol and reviewed and edited the manuscript. T.V. did the hybrid assembly of the symbiont genome and its annotation, ParB phylogenetic analysis, and data curation, and reviewed and edited the manuscript. N.O.E.V. wrote the XY shape inspector plugin for ImageJ. S.B. conceptualized and supervised the work, acquired funding, provided resources, wrote the original draft, and reviewed and edited the manuscript.

DECLARATION OF INTERESTS

The authors declare no competing interests.

Received: March 30, 2019

Revised: June 24, 2019

Accepted: July 22, 2019

Published: August 29, 2019

REFERENCES

1. Polz, M.F., Distel, D.L., Zarda, B., Amann, R., Felbeck, H., Ott, J.A., and Cavanaugh, C.M. (1994). Phylogenetic analysis of a highly specific association between ectosymbiotic, sulfur-oxidizing bacteria and a marine nematode. *Appl. Environ. Microbiol.* 60, 4461–4467.
2. Pende, N., Wang, J., Weber, P.M., Verheul, J., Kuru, E., Rittmann, S.K.R., Leisch, N., VanNieuwenhze, M.S., Brun, Y.V., den Blaauwen, T., and Bulgheresi, S. (2018). Host-polarized cell growth in animal symbionts. *Curr. Biol.* 28, 1039–1051.e5.
3. Leisch, N., Pende, N., Weber, P.M., Gruber-Vodicka, H.R., Verheul, J., Vischer, N.O.E., Abby, S.S., Geier, B., den Blaauwen, T., and Bulgheresi, S. (2016). Asynchronous division by non-ring FtsZ in the gammaproteobacterial symbiont of *Robbea hypermnestra*. *Nat. Microbiol.* 2, 16182.
4. Leisch, N., Verheul, J., Heindl, N.R., Gruber-Vodicka, H.R., Pende, N., den Blaauwen, T., and Bulgheresi, S. (2012). Growth in width and FtsZ ring longitudinal positioning in a gammaproteobacterial symbiont. *Curr. Biol.* 22, R831–R832.
5. Yamaichi, Y., and Niki, H. (2000). Active segregation by the *Bacillus subtilis* partitioning system in *Escherichia coli*. *Proc. Natl. Acad. Sci. USA* 97, 14656–14661.
6. Possoz, C., Junier, I., and Espéli, O. (2012). Bacterial chromosome segregation. *Front. Biosci.* 17, 1020–1034.
7. Wang, X., Montero Llopis, P., and Rudner, D.Z. (2013). Organization and segregation of bacterial chromosomes. *Nat. Rev. Genet.* 14, 191–203.
8. Wiggins, P.A., Cheveralls, K.C., Martin, J.S., Lintner, R., and Kondev, J. (2010). Strong intranucleoid interactions organize the *Escherichia coli* chromosome into a nucleoid filament. *Proc. Natl. Acad. Sci. USA* 107, 4991–4995.
9. Badrinarayanan, A., Le, T.B.K., and Laub, M.T. (2015). Bacterial chromosome organization and segregation. *Annu. Rev. Cell Dev. Biol.* 31, 171–199.
10. Bouet, J.Y., Stouf, M., Lebailly, E., and Cornet, F. (2014). Mechanisms for chromosome segregation. *Curr. Opin. Microbiol.* 22, 60–65.
11. Wang, X., and Rudner, D.Z. (2014). Spatial organization of bacterial chromosomes. *Curr. Opin. Microbiol.* 22, 66–72.
12. Fogel, M.A., and Waldor, M.K. (2006). A dynamic, mitotic-like mechanism for bacterial chromosome segregation. *Genes Dev.* 20, 3269–3282.
13. Ptacin, J.L., Lee, S.F., Garner, E.C., Toro, E., Eckart, M., Comolli, L.R., Moerner, W.E., and Shapiro, L. (2010). A spindle-like apparatus guides bacterial chromosome segregation. *Nat. Cell Biol.* 12, 791–798.
14. Schofield, W.B., Lim, H.C., and Jacobs-Wagner, C. (2010). Cell cycle co-ordination and regulation of bacterial chromosome segregation dynamics by polarly localized proteins. *EMBO J.* 29, 3068–3081.
15. Shebelut, C.W., Guberman, J.M., van Teeffelen, S., Yakhnina, A.A., and Gitai, Z. (2010). *Caulobacter* chromosome segregation is an ordered multistep process. *Proc. Natl. Acad. Sci. USA* 107, 14194–14198.
16. Bowman, G.R., Comolli, L.R., Zhu, J., Eckart, M., Koenig, M., Downing, K.H., Moerner, W.E., Earnest, T., and Shapiro, L. (2008). A polymeric protein anchors the chromosomal origin/ParB complex at a bacterial cell pole. *Cell* 134, 945–955.
17. Ebersbach, G., Galli, E., Möller-Jensen, J., Löwe, J., and Gerdes, K. (2008). Novel coiled-coil cell division factor ZapB stimulates Z ring assembly and cell division. *Mol. Microbiol.* 68, 720–735.
18. Yamaichi, Y., Bruckner, R., Ringgaard, S., Möll, A., Cameron, D.E., Briegel, A., Jensen, G.J., Davis, B.M., and Waldor, M.K. (2012). A multi-domain hub anchors the chromosome segregation and chemotactic machinery to the bacterial pole. *Genes Dev.* 26, 2348–2360.
19. Donovan, C., Sieger, B., Krämer, R., and Bramkamp, M. (2012). A synthetic *Escherichia coli* system identifies a conserved origin tethering factor in Actinobacteria. *Mol. Microbiol.* 84, 105–116.

20. Ben-Yehuda, S., Rudner, D.Z., and Losick, R. (2003). RacA, a bacterial protein that anchors chromosomes to the cell poles. *Science* 299, 532–536.
21. Ben-Yehuda, S., Fujita, M., Liu, X.S., Gorbatyuk, B., Skoko, D., Yan, J., Marko, J.F., Liu, J.S., Eichenberger, P., Rudner, D.Z., and Losick, R. (2005). Defining a centromere-like element in *Bacillus subtilis* by identifying the binding sites for the chromosome-anchoring protein RacA. *Mol. Cell* 17, 773–782.
22. Wu, L.J., and Errington, J. (1994). *Bacillus subtilis* SpoIIIE protein required for DNA segregation during asymmetric cell division. *Science* 264, 572–575.
23. Lenarcic, R., Halbedel, S., Visser, L., Shaw, M., Wu, L.J., Errington, J., Marenduzzo, D., and Hamoen, L.W. (2009). Localisation of DivIVA by targeting to negatively curved membranes. *EMBO J.* 28, 2272–2282.
24. Ramamurthi, K.S., and Losick, R. (2009). Negative membrane curvature as a cue for subcellular localization of a bacterial protein. *Proc. Natl. Acad. Sci. USA* 106, 13541–13545.
25. Surovtsev, I.V., and Jacobs-Wagner, C. (2018). Subcellular organization: a critical feature of bacterial cell replication. *Cell* 172, 1271–1293.
26. Lim, H.C., Surovtsev, I.V., Beltran, B.G., Huang, F., Bewersdorf, J., and Jacobs-Wagner, C. (2014). Evidence for a DNA-relay mechanism in ParABS-mediated chromosome segregation. *eLife* 3, e02758.
27. Sugawara, T., and Kaneko, K. (2011). Chemophoresis as a driving force for intracellular organization: Theory and application to plasmid partitioning. *Biophysics (Nagoya-Shi)* 7, 77–88.
28. Ginda, K., Santi, I., Bousbaine, D., Zakrzewska-Czerwińska, J., Jakimowicz, D., and McKinney, J. (2017). The studies of ParA and ParB dynamics reveal asymmetry of chromosome segregation in mycobacteria. *Mol. Microbiol.* 105, 453–468.
29. Harms, A., Treuner-Lange, A., Schumacher, D., and Søgaard-Andersen, L. (2013). Tracking of chromosome and replisome dynamics in *Myxococcus xanthus* reveals a novel chromosome arrangement. *PLoS Genet.* 9, e1003802.
30. Iniesta, A.A. (2014). ParABS system in chromosome partitioning in the bacterium *Myxococcus xanthus*. *PLoS ONE* 9, e86897.
31. Trojanowski, D., Ginda, K., Pióro, M., Hołówa, J., Skut, P., Jakimowicz, D., and Zakrzewska-Czerwińska, J. (2015). Choreography of the *Mycobacterium* replication machinery during the cell cycle. *MBio* 6, e02125–e14.
32. Livny, J., Yamaichi, Y., and Waldor, M.K. (2007). Distribution of centromere-like *parS* sites in bacteria: insights from comparative genomics. *J. Bacteriol.* 189, 8693–8703.
33. Youngren, B., Nielsen, H.J., Jun, S., and Austin, S. (2014). The multifork *Escherichia coli* chromosome is a self-duplicating and self-segregating thermodynamic ring polymer. *Genes Dev.* 28, 71–84.
34. Marko, J.F. (2009). Linking topology of tethered polymer rings with applications to chromosome segregation and estimation of the knotting length. *Phys. Rev. E Stat. Nonlin. Soft Matter Phys.* 79, 051905.
35. Bates, D., and Kleckner, N. (2005). Chromosome and replisome dynamics in *E. coli*: loss of sister cohesion triggers global chromosome movement and mediates chromosome segregation. *Cell* 121, 899–911.
36. Joshi, M.C., Bourniquel, A., Fisher, J., Ho, B.T., Magnan, D., Kleckner, N., and Bates, D. (2011). *Escherichia coli* sister chromosome separation includes an abrupt global transition with concomitant release of late-splitting intersister snaps. *Proc. Natl. Acad. Sci. USA* 108, 2765–2770.
37. Fisher, J.K., Bourniquel, A., Witz, G., Weiner, B., Prentiss, M., and Kleckner, N. (2013). Four-dimensional imaging of *E. coli* nucleoid organization and dynamics in living cells. *Cell* 153, 882–895.
38. Gruber, S., and Errington, J. (2009). Recruitment of condensin to replication origin regions by ParB/SpoOJ promotes chromosome segregation in *B. subtilis*. *Cell* 137, 685–696.
39. Marbouty, M., Courmac, A., Flot, J.F., Marie-Nelly, H., Mozziconacci, J., and Koszul, R. (2014). Metagenomic chromosome conformation capture (meta3C) unveils the diversity of chromosome organization in microorganisms. *eLife* 3, e03318.
40. Thanbichler, M. (2009). Closing the ring: a new twist to bacterial chromosome condensation. *Cell* 137, 598–600.
41. Marbouty, M., Le Gall, A., Cattoni, D.I., Courmac, A., Koh, A., Fiche, J.B., Mozziconacci, J., Murray, H., Koszul, R., and Nollmann, M. (2015). Condensin- and replication-mediated bacterial chromosome folding and origin condensation revealed by Hi-C and super-resolution imaging. *Mol. Cell* 59, 588–602.
42. Wang, X., Brandão, H.B., Le, T.B.K., Laub, M.T., and Rudner, D.Z. (2017). *Bacillus subtilis* SMC complexes juxtapose chromosome arms as they travel from origin to terminus. *Science* 355, 524–527.
43. Hadzadeh Yazdi, N., Guet, C.C., Johnson, R.C., and Marko, J.F. (2012). Variation of the folding and dynamics of the *Escherichia coli* chromosome with growth conditions. *Mol. Microbiol.* 86, 1318–1333.
44. Hong, S.H., and McAdams, H.H. (2011). Compaction and transport properties of newly replicated *Caulobacter crescentus* DNA. *Mol. Microbiol.* 82, 1349–1358.
45. Umbarger, M.A., Toro, E., Wright, M.A., Porreca, G.J., Baù, D., Hong, S.H., Fero, M.J., Zhu, L.J., Marti-Renom, M.A., McAdams, H.H., et al. (2011). The three-dimensional architecture of a bacterial genome and its alteration by genetic perturbation. *Mol. Cell* 44, 252–264.
46. Jun, S., and Mulder, B. (2006). Entropy-driven spatial organization of highly confined polymers: lessons for the bacterial chromosome. *Proc. Natl. Acad. Sci. USA* 103, 12388–12393.
47. Junier, I., Boccard, F., and Espéli, O. (2014). Polymer modeling of the *E. coli* genome reveals the involvement of locus positioning and macro-domain structuring for the control of chromosome conformation and segregation. *Nucleic Acids Res.* 42, 1461–1473.
48. Lampo, T.J., Kuwada, N.J., Wiggins, P.A., and Spakowitz, A.J. (2015). Physical modeling of chromosome segregation in *Escherichia coli* reveals impact of force and DNA relaxation. *Biophys. J.* 108, 146–153.
49. Aussel, L., Barre, F.X., Aroyo, M., Stasiak, A., Stasiak, A.Z., and Sherratt, D. (2002). FtsK is a DNA motor protein that activates chromosome dimer resolution by switching the catalytic state of the XerC and XerD recombinases. *Cell* 108, 195–205.
50. Lesterlin, C., Pages, C., Dubarry, N., Dasgupta, S., and Cornet, F. (2008). Asymmetry of chromosome Replichores renders the DNA translocase activity of FtsK essential for cell division and cell shape maintenance in *Escherichia coli*. *PLoS Genet.* 4, e1000288.
51. Sharp, M.D., and Pogliano, K. (2002). MinCD-dependent regulation of the polarity of SpoIIIE assembly and DNA transfer. *EMBO J.* 21, 6267–6274.
52. Wang, L., and Lutkenhaus, J. (1998). FtsK is an essential cell division protein that is localized to the septum and induced as part of the SOS response. *Mol. Microbiol.* 29, 731–740.
53. Yu, X.C., Tran, A.H., Sun, Q., and Margolin, W. (1998). Localization of cell division protein FtsK to the *Escherichia coli* septum and identification of a potential N-terminal targeting domain. *J. Bacteriol.* 180, 1296–1304.
54. Bigot, S., Saleh, O.A., Lesterlin, C., Pages, C., El Karoui, M., Dennis, C., Grigoriev, M., Allemand, J.F., Barre, F.X., and Cornet, F. (2005). KOPS: DNA motifs that control *E. coli* chromosome segregation by orienting the FtsK translocase. *EMBO J.* 24, 3770–3780.
55. Bigot, S., Saleh, O.A., Cornet, F., Allemand, J.F., and Barre, F.X. (2006). Oriented loading of FtsK on KOPS. *Nat. Struct. Mol. Biol.* 13, 1026–1028.
56. Levy, O., Ptacin, J.L., Pease, P.J., Gore, J., Eisen, M.B., Bustamante, C., and Cozzarelli, N.R. (2005). Identification of oligonucleotide sequences that direct the movement of the *Escherichia coli* FtsK translocase. *Proc. Natl. Acad. Sci. USA* 102, 17618–17623.
57. Löwe, J., Ellonen, A., Allen, M.D., Atkinson, C., Sherratt, D.J., and Grainge, I. (2008). Molecular mechanism of sequence-directed DNA loading and translocation by FtsK. *Mol. Cell* 31, 498–509.
58. Pease, P.J., Levy, O., Cost, G.J., Gore, J., Ptacin, J.L., Sherratt, D., Bustamante, C., and Cozzarelli, N.R. (2005). Sequence-directed DNA translocation by purified FtsK. *Science* 307, 586–590.

59. May, P.F.J., Zawadzki, P., Sherratt, D.J., Kapanidis, A.N., and Arciszewska, L.K. (2015). Assembly, translocation, and activation of XerCD-dif recombination by FtsK translocase analyzed in real-time by FRET and two-color tethered fluorophore motion. *Proc. Natl. Acad. Sci. USA* **112**, E5133–E5141.
60. Keller, A.N., Xin, Y., Boer, S., Reinhardt, J., Baker, R., Arciszewska, L.K., Lewis, P.J., Sherratt, D.J., Löwe, J., and Grainge, I. (2016). Activation of Xer-recombination at dif: structural basis of the FtsK γ -XerD interaction. *Sci. Rep.* **6**, 33357.
61. Castillo, F., Benmohamed, A., and Szatmari, G. (2017). Xer site specific recombination: double and single recombinase systems. *Front. Microbiol.* **8**, 453.
62. Bailey, M.W., Bisicchia, P., Warren, B.T., Sherratt, D.J., and Männik, J. (2014). Evidence for divisome localization mechanisms independent of the Min system and SlmA in *Escherichia coli*. *PLoS Genet.* **10**, e1004504.
63. Demarre, G., Galli, E., Muresan, L., Paly, E., David, A., Possoz, C., and Barre, F.X. (2014). Differential management of the replication terminus regions of the two *Vibrio cholerae* chromosomes during cell division. *PLoS Genet.* **10**, e1004557.
64. Cass, J.A., Kuwada, N.J., Traxler, B., and Wiggins, P.A. (2016). *Escherichia coli* chromosomal loci segregate from midcell with universal dynamics. *Biophys. J.* **110**, 2597–2609.
65. Niki, H., Yamaichi, Y., and Hiraga, S. (2000). Dynamic organization of chromosomal DNA in *Escherichia coli*. *Genes Dev.* **14**, 212–223.
66. Wang, X., Montero Llopis, P., and Rudner, D.Z. (2014). *Bacillus subtilis* chromosome organization oscillates between two distinct patterns. *Proc. Natl. Acad. Sci. USA* **111**, 12877–12882.
67. Antipov, D., Hartwick, N., Shen, M., Raiko, M., Lapidus, A., and Pevzner, P.A. (2016). plasmidSPAdes: assembling plasmids from whole genome sequencing data. *Bioinformatics* **32**, 3380–3387.
68. Sernova, N.V., and Gelfand, M.S. (2008). Identification of replication origins in prokaryotic genomes. *Brief. Bioinform.* **9**, 376–391.
69. Yoshikawa, H., and Ogasawara, N. (1991). Structure and function of DnaA and the DnaA-box in eubacteria: evolutionary relationships of bacterial replication origins. *Mol. Microbiol.* **5**, 2589–2597.
70. Bramhill, D., and Kornberg, A. (1988). A model for initiation at origins of DNA replication. *Cell* **54**, 915–918.
71. Katayama, T., Kasho, K., and Kawakami, H. (2017). The DnaA cycle in *Escherichia coli*: activation, function and inactivation of the initiator protein. *Front. Microbiol.* **8**, 2496.
72. Schaper, S., and Messer, W. (1995). Interaction of the initiator protein DnaA of *Escherichia coli* with its DNA target. *J. Biol. Chem.* **270**, 17622–17626.
73. Roos, M., van Geel, A.B.M., Aarsman, M.E.G., Veuskens, J.T., Woldringh, C.L., and Nanninga, N. (2001). The replicated ftsQAZ and minB chromosomal regions of *Escherichia coli* segregate on average in line with nucleoid movement. *Mol. Microbiol.* **39**, 633–640.
74. Flärdh, K., Palacios, P., and Vicente, M. (1998). Cell division genes ftsQAZ in *Escherichia coli* require distant cis-acting signals upstream of *ddlB* for full expression. *Mol. Microbiol.* **30**, 305–315.
75. Ramachandran, R., Jha, J., and Chatteraj, D.K. (2014). Chromosome segregation in *Vibrio cholerae*. *J. Mol. Microbiol. Biotechnol.* **24**, 360–370.
76. Lin, D.C., and Grossman, A.D. (1998). Identification and characterization of a bacterial chromosome partitioning site. *Cell* **92**, 675–685.
77. Passot, F.M., Calderon, V., Fichant, G., Lane, D., and Pasta, F. (2012). Centromere binding and evolution of chromosomal partition systems in the Burkholderiales. *J. Bacteriol.* **194**, 3426–3436.
78. Dubarry, N., Pasta, F., and Lane, D. (2006). ParABS systems of the four replicons of *Burkholderia cenocepacia*: new chromosome centromeres confer partition specificity. *J. Bacteriol.* **188**, 1489–1496.
79. Gerdes, K., Møller-Jensen, J., and Bugge Jensen, R. (2000). Plasmid and chromosome partitioning: surprises from phylogeny. *Mol. Microbiol.* **37**, 455–466.
80. Godfrin-Estevenson, A.M., Pasta, F., and Lane, D. (2002). The parAB gene products of *Pseudomonas putida* exhibit partition activity in both *P. putida* and *Escherichia coli*. *Mol. Microbiol.* **43**, 39–49.
81. Vallet-Gely, I., and Boccard, F. (2013). Chromosomal organization and segregation in *Pseudomonas aeruginosa*. *PLoS Genet.* **9**, e1003492.
82. Lagage, V., Boccard, F., and Vallet-Gely, I. (2016). Regional control of chromosome segregation in *Pseudomonas aeruginosa*. *PLoS Genet.* **12**, e1006428.
83. Fogel, M.A., and Waldor, M.K. (2005). Distinct segregation dynamics of the two *Vibrio cholerae* chromosomes. *Mol. Microbiol.* **55**, 125–136.
84. Carnoy, C., and Roten, C.A. (2009). The dif/Xer recombination systems in proteobacteria. *PLoS ONE* **4**, e6531.
85. Surovtsev, I.V., Campos, M., and Jacobs-Wagner, C. (2016). DNA-relay mechanism is sufficient to explain ParA-dependent intracellular transport and patterning of single and multiple cargos. *Proc. Natl. Acad. Sci. USA* **113**, E7268–E7276.
86. Viollier, P.H., Thanbichler, M., McGrath, P.T., West, L., Meewan, M., McAdams, H.H., and Shapiro, L. (2004). Rapid and sequential movement of individual chromosomal loci to specific subcellular locations during bacterial DNA replication. *Proc. Natl. Acad. Sci. USA* **101**, 9257–9262.
87. Pende, N., Leisch, N., Gruber-Vodicka, H.R., Heindl, N.R., Ott, J., den Blaauwen, T., and Bulgheresi, S. (2014). Size-independent symmetric division in extraordinarily long cells. *Nat. Commun.* **5**, 4803.
88. Petersen, J.M., Kemper, A., Gruber-Vodicka, H., Cardini, U., van der Geest, M., Kleiner, M., Bulgheresi, S., Mußmann, M., Herbold, C., Seah, B.K.B., et al. (2016). Chemosynthetic symbionts of marine invertebrate animals are capable of nitrogen fixation. *Nat. Microbiol.* **2**, 16195.
89. Thanbichler, M. (2018). Cell division: symbiotic bacteria turn it upside down. *Curr. Biol.* **28**, R306–R308.
90. den Blaauwen, T. (2018). Is longitudinal division in rod-shaped bacteria a matter of swapping axis? *Front. Microbiol.* **9**, 822.
91. Viollier, P.H., Thanbichler, M., McGrath, P.T., West, L., Meewan, M., McAdams, H.H., and Shapiro, L. (2004). Rapid and sequential movement of individual chromosomal loci to specific subcellular locations during bacterial DNA replication. *Proc. Natl. Acad. Sci. USA* **101**, 9257–9262.
92. Ho, T.Q., Zhong, Z., Aung, S., and Pogliano, J. (2002). Compatible bacterial plasmids are targeted to independent cellular locations in *Escherichia coli*. *EMBO J.* **21**, 1864–1872.
93. Garner, E.C., Campbell, C.S., Weibel, D.B., and Mullins, R.D. (2007). Reconstitution of DNA segregation driven by assembly of a prokaryotic actin homolog. *Science* **315**, 1270–1274.
94. Surovtsev, I.V., Lim, H.C., and Jacobs-Wagner, C. (2016). The slow mobility of the ParA partitioning protein underlies its steady-state patterning in *Caulobacter*. *Biophys. J.* **110**, 2790–2799.
95. Ireton, K., Gunther, N.W., 4th, and Grossman, A.D. (1994). *spo0J* is required for normal chromosome segregation as well as the initiation of sporulation in *Bacillus subtilis*. *J. Bacteriol.* **176**, 5320–5329.
96. Yamaichi, Y., Fogel, M.A., McLeod, S.M., Hui, M.P., and Waldor, M.K. (2007). Distinct centromere-like *parS* sites on the two chromosomes of *Vibrio* spp. *J. Bacteriol.* **189**, 5314–5324.
97. Lewis, R.A., Bignell, C.R., Zeng, W., Jones, A.C., and Thomas, C.M. (2002). Chromosome loss from *par* mutants of *Pseudomonas putida* depends on growth medium and phase of growth. *Microbiology* **148**, 537–548.
98. Hołowska, J., Trojanowski, D., Janczak, M., Jakimowicz, D., and Zakrzewska-Czerwińska, J. (2018). The origin of chromosomal replication is asymmetrically positioned on the mycobacterial nucleoid, and the timing of its firing depends on HupB. *J. Bacteriol.* **200**, e00044–18.
99. Jakimowicz, D., Brzostek, A., Rumijowska-Galewicz, A., Zydek, P., Dołzbiasz, A., Smulczyk-Krawczyński, A., Zimniak, T., Wojtasz, L., Zawilak-Pawlik, A., Kois, A., et al. (2007). Characterization of the mycobacterial chromosome segregation protein ParB and identification of its target in *Mycobacterium smegmatis*. *Microbiology* **153**, 4050–4060.

100. Gitai, Z., Dye, N.A., Reisenauer, A., Wachi, M., and Shapiro, L. (2005). MreB actin-mediated segregation of a specific region of a bacterial chromosome. *Cell* 120, 329–341.
101. Kruse, T., Blagoev, B., Lobner-Olesen, A., Wachi, M., Sasaki, K., Iwai, N., Mann, M., and Gerdes, K. (2006). Actin homolog MreB and RNA polymerase interact and are both required for chromosome segregation in *Escherichia coli*. *Genes Dev.* 20, 113–124.
102. Karczmarek, A., Martínez-Arteaga, R., Alexeeva, S., Hansen, F.G., Vicente, M., Nanninga, N., and den Blaauwen, T. (2007). DNA and origin region segregation are not affected by the transition from rod to sphere after inhibition of *Escherichia coli* MreB by A22. *Mol. Microbiol.* 65, 51–63.
103. Shebelut, C.W., Jensen, R.B., and Gitai, Z. (2009). Growth conditions regulate the requirements for *Caulobacter* chromosome segregation. *J. Bacteriol.* 191, 1097–1100.
104. Di Ventura, B., Knecht, B., Andreas, H., Godinez, W.J., Fritsche, M., Rohr, K., Nickel, W., Heermann, D.W., and Sourjik, V. (2013). Chromosome segregation by the *Escherichia coli* Min system. *Mol. Syst. Biol.* 9, 686.
105. Nielsen, H.J., Li, Y., Youngren, B., Hansen, F.G., and Austin, S. (2006). Progressive segregation of the *Escherichia coli* chromosome. *Mol. Microbiol.* 61, 383–393.
106. May, P.F.J., Pinkney, J.N.M., Zawadzki, P., Evans, G.W., Sherratt, D.J., and Kapanidis, A.N. (2014). Tethered fluorophore motion: studying large DNA conformational changes by single-fluorophore imaging. *Biophys. J.* 107, 1205–1216.
107. Barrero-Canosa, J., Moraru, C., Zeugner, L., Fuchs, B.M., and Amann, R. (2017). Direct-geneFISH: a simplified protocol for the simultaneous detection and quantification of genes and rRNA in microorganisms. *Environ. Microbiol.* 19, 70–82.
108. Niki, H., Imamura, R., Kitaoka, M., Yamanaka, K., Ogura, T., and Hiraga, S. (1992). *E. coli* MukB protein involved in chromosome partition forms a homodimer with a rod-and-hinge structure having DNA binding and ATP/GTP binding activities. *EMBO J.* 11, 5101–5109.
109. Danilova, O., Reyes-Lamothé, R., Pinskaya, M., Sherratt, D., and Possoz, C. (2007). MukB colocalizes with the oriC region and is required for organization of the two *Escherichia coli* chromosome arms into separate cell halves. *Mol. Microbiol.* 65, 1485–1492.
110. Sullivan, N.L., Marquis, K.A., and Rudner, D.Z. (2009). Recruitment of SMC by ParB-parS organizes the origin region and promotes efficient chromosome segregation. *Cell* 137, 697–707.
111. Li, H., and Durbin, R. (2010). Fast and accurate long-read alignment with Burrows-Wheeler transform. *Bioinformatics* 26, 589–595.
112. Wick, R.R., Judd, L.M., Gorrie, C.L., and Holt, K.E. (2017). Unicycler: resolving bacterial genome assemblies from short and long sequencing reads. *PLoS Comput. Biol.* 13, e1005595.
113. Gremme, G., Steinbiss, S., and Kurtz, S. (2013). GenomeTools: a comprehensive software library for efficient processing of structured genome annotations. *IEEE/ACM Trans. Comput. Biol. Bioinformatics* 10, 645–656.
114. Vallenet, D., Engelen, S., Mornico, D., Cruveiller, S., Fleury, L., Lajus, A., Rouy, Z., Roche, D., Salvignol, G., Scarpelli, C., and Médigue, C. (2009). MicroScope: a platform for microbial genome annotation and comparative genomics. *Database (Oxford)* 2009, bap021.
115. Katoh, K., and Standley, D.M. (2013). MAFFT multiple sequence alignment software version 7: improvements in performance and usability. *Mol. Biol. Evol.* 30, 772–780.
116. Nguyen, L.T., Schmidt, H.A., von Haeseler, A., and Minh, B.Q. (2015). IQ-TREE: a fast and effective stochastic algorithm for estimating maximum-likelihood phylogenies. *Mol. Biol. Evol.* 32, 268–274.

STAR★METHODS

KEY RESOURCES TABLE

REAGENT or RESOURCE	SOURCE	IDENTIFIER
Antibodies		
Rabbit polyclonal anti-Ca. T. oneisti ParB	This paper; Eurogentec	N/A
Monoclonal anti-His antibody	Sigma	Product number: SAB1305538; RRID: AB_2687993
Bacterial and Virus Strains		
<i>Escherichia coli</i> Strain number: BI21 (DE3)	Invitrogen	Catalog number: C601003
<i>Escherichia coli</i> Strain number: Top10	Invitrogen	Catalog number: C404010
Chemicals, Peptides, and Recombinant Proteins		
Ampicillin	Duchefa	Catalog number: A0104
IPTG	This study	N/A
H-Thr-ParB	This study	N/A
Critical Commercial Assays		
HisTrap HP	GE Healthcare	Catalog number: 17524701
Ulysis Nucleic Acid Labeling Kit	ThermoFisher	Catalog number: U21654
Deposited Data		
Ca. T. oneisti genome draft	This paper	GenBank: SMSC000000000; https://www.ncbi.nlm.nih.gov/nuccore/SMSC000000000
Ca. T. oneisti <i>parS</i> containing fragment	This paper	GenBank: MK650415; https://www.ncbi.nlm.nih.gov/nuccore/MK650415
Ca. T. hypermnestrae ParB amino acid sequence	This paper	GenBank: MK650416; https://www.ncbi.nlm.nih.gov/nuccore/MK650416
Experimental Models: Organisms/Strains		
<i>Candidatus</i> Thiosymbion oneisti	Environmental sample	N/A
Oligonucleotides		
T.oneisti_parB_F = (5'-ATGTCTACGAAGAAAAAGGGC-3')	This paper	N/A
T.oneisti_parB_R = (5'-CTACTTTATATGAGCAAG-3')	This paper	N/A
FWD_primer_parB = (5'-GAGGCCCAAGGGGTTA TGCTAGCTACTTTATATGAGCAAGGA-3'),	This paper	N/A
REV_primer_parB = (5'-GTGCCGCGCGGCAGC ATGTCTACGAAGAAAAAGGG-3')	This paper	N/A
FWD_To_pET-15b = (5'-GCTGCCGCGCGGCACCAAG-3')	This paper	N/A
REV_To_pET-15b = (5'-CTAGCATAACCCCTTGGGG-3')	This paper	N/A
To_parS_EMSA_dnaN_F1 = (5'-GTGGTAATGCCGATGAG ACTTTG-3')	This paper	N/A
To_parS_EMSA_R1.1 = (5'-AACCATATGATGAAGGCCA GTTCC-3')	This paper	N/A
To_parSmut11_F1 = (5'- GCAGGGTAAATGTTCCGGCA CCTCC-3')	This paper	N/A
To_parSmut11_R = (5'-[Phosphorylation]ACA GGG TAC ATA GAA CAG CAC TGT CCA GCG TT-3')	This paper	N/A
Oligonucleotides for FISH probe synthesis (see Table S3)	This manuscript	N/A
Recombinant DNA		
Plasmid pET-15b-His-ParB, see Method Details	This paper	N/A
Plasmid pJET1.2- <i>parS</i> fragment	This paper	N/A
Plasmid pJET1.2- <i>parS</i> -mut11 fragment	This paper	N/A
Software and Algorithms		
ImageJ	NIH	https://imagej.nih.gov/ij/
ObjectJ	University of Amsterdam	https://sils.fnwi.uva.nl/bcb/objectj/

(Continued on next page)

Continued

REAGENT or RESOURCE	SOURCE	IDENTIFIER
XY-Shape Inspector	This manuscript	https://sils.fnwi.uva.nl/bcb/objectj/examples/XY-Shape-Inspector/MD/xy-shape-inspector.html
ProRes Capture Pro 2.8.8	Jenoptik	https://www.jenoptik.us
Photoshop CS6	Adobe Systems	https://www.adobe.com
Illustrator CS6	Adobe Systems	https://www.adobe.com
Snapgene	GSL Biotech L Biotech	https://www.snapgene.com/

LEAD CONTACT AND MATERIALS AVAILABILITY

Further information and requests for resources and reagents should be directed to and will be fulfilled by the Lead Contact, Silvia Bulgheresi (silvia.bulgheresi@univie.ac.at).

This study did not generate new unique reagents.

EXPERIMENTAL MODEL AND SUBJECT DETAILS

Sediment samples were collected on multiple field trips (2015–2019) in ~1 m depth from a sand bar off Carrie Bow Cay, Belize (16° 48' 11.01"N, 88° 4' 54.42"W). Specimens of *L. oneistus* were extracted from the sediment by stirring the sand in seawater and pouring the supernatant through a mesh sieve (125 µm opening size). The retained material was transferred into a Petri dish and single nematodes were handpicked using pipettes under a dissecting microscope. For DNA FISH, nematodes were fixed in 3 or 4% PFA for 12–14 hr at 4°C, washed with 70% ethanol and stored at –20°C. For Western Blotting and immunostaining, nematodes were transferred to methanol and stored at –20°C. For gDNA extraction, bacteria were dissociated by 2 min incubation in 3.5% MgSO₄, pelleted and stored in methanol at –20°C. Symbiotic nematodes were transported from Carrie Bow Cay to the University of Vienna deep-frozen.

METHOD DETAILS**Oxford Nanopore Technologies sequencing**

Total genomic DNA was extracted using Genomic-tip 20/G (QIAGEN) following the manufacturer's instruction, with elution into 20 µL of PCR molecular grade water. After clean-up using 1X AMPure XP beads (Beckman Coulter), the library was prepared using the ONT 1D ligation sequencing kit (SQK-LSK109) and subsequently 70 ng were loaded onto a R9.4 flow cell (FLO-MIN106) and sequenced on a MinION for 26 hr. Base calling was performed locally with ONT's Albacore v2.3.3, and resulting fastq-files were trimmed using Porechop v0.2.1 (<https://github.com/rwwick/Porechop>). For the hybrid assembly, metagenomic Illumina HiSeq 2 × 100 bp paired-end reads were mapped to the symbiont *Ca. T. oneisti* genome [88] using the bwa v0.7.16a aln algorithm [111] and the mapped reads together with the reads acquired by ONT sequencing were assembled using Unicycler v0.4.6 [112]. Completeness, contamination and strain heterogeneity was calculated in CheckM v1.0.7 with the lineage_wf workflow. Fasta statistics were calculated using genometools v1.5.9 seqstat module [113]. The assembly was annotated automatically on the MicroScope platform [114]. This Whole Genome Shotgun project has been deposited at DDBJ/ENA/GenBank under the accession GenBank: SMSC00000000.1.

DNA Fluorescence In Situ Hybridization

We used the genome draft of *Ca. T. oneisti* (SMSC00000000.1) to design specific primers against the *Ca. T. oneisti ori* and *ter* regions, as well as against a region containing the *ftsQAZ* operon (Table S3; symbiont *dif* site sequence: ATGCGCATAATGTATATTATG TAAAGT). Worms were rehydrated in phosphate-buffered saline (PBS) and bacteria were detached from the worms by sonication. Subsequently, 1 µL of bacterial suspension was used as template in each 25 µL PCR reaction (primers' sequences and PCR conditions are listed in Tables S3 and S5). A 2,874 nt-long fragment containing the *dnaA* and *dnaN* genes (Figure S1B), a 3,273 nt-long fragment containing the *ftsQAZ* operon and a 3,916 nt-long fragment containing the predicted *dif* site were amplified from *Ca. T. oneisti* genomic DNA. Each purified fragment was then used as template to PCR-amplify dsDNA polynucleotide probes (referred to as *ori*, *ftsQAZ* and *ter*, respectively) that were subsequently chemically labeled with the Alexa Fluor 594 using the Ulysis Nucleic Acid Labeling Kit (ThermoFisher) following the same modifications to the manufacturers' protocol as in [107]. Single *L. oneistus* nematodes were rehydrated in PBS and bacteria were detached by sonication. For the hybridization procedure, we followed a slightly modified version of the direct-gene FISH protocol [107]. After letting the cell suspension dry onto a well of a Poly-L-lysine coated Epoxy-slide, cells were dehydrated in a series of increasing ethanol concentrations and permeabilized with freshly prepared lysozyme solution for 1 hr on ice. *Ca. T. oneisti ori*, *ftsQAZ* and *ter* probes were diluted in hybridization buffer containing 35% (*ori* and *ftsQAZ* probes) or 45% (*ter* probe) formamide to a final concentration of 62 pg/µL and each probe was applied to the cells individually. Slides were transferred into a hybridization chamber and incubated for 40 min at 85°C and subsequently at 46°C for 2 hr. Washing buffer was applied

to the cells once briefly and once for 15 min at 48°C and, finally, cells were incubated in PBS for 20 min at room temperature. Upon a quick wash in ddH₂O and, subsequently, in absolute ethanol, cells were air-dried and mounted in 4.5 µl Vectashield mounting medium (Vector Labs) per microscopic slide well.

ParB alignment and phylogenetic tree

Selected ParB sequences (Table S4) were retrieved from GenBank and aligned using mafft v7.397 [115]. The alignment was visually inspected and poorly aligned or misaligned regions were removed. The maximum-likelihood tree with SH-like aLRT support values (10,000 replicates) was inferred using IQ-TREE v1.6.2 [116].

Expression of recombinant *Ca. T. oneisti* ParB

The 912 nt-long *parB* gene was amplified from *Ca. T. oneisti* and used as a template to obtain the fragments for the Gibson assembly (see Table S5 for primers' sequences and PCR conditions). The *Ca. T. oneisti parB* gene was cloned into the pET-15b vector (Novagen) by Gibson assembly and a His-tagged ParB recombinant protein (His-ToParB) was expressed in *E. coli* strain BL21 (DE3) (Invitrogen). The *parB* recombinant strain was grown at 37°C in Lysogeny Broth (LB) medium with 100 µg/ml ampicillin. The recombinant protein expression was induced at OD₆₀₀ = 0.6 in 1 mM IPTG and 0.2% L-arabinose. After 3 hr induction, the cell culture (125 ml) was pelleted by centrifuging 10 min at 4,500 rpm and resuspended in 4 mL lysis buffer (20 mM Na₂HPO₄-NaH₂PO₄, 15 mM imidazole, 0.5 M NaCl, pH 7.4) supplemented with 4 µl of proteinase inhibitor cocktail (Sigma). Cell lysates were obtained by sonication and after a 45 min-long centrifugation at 30,000 rpm at 4°C soluble fractions were applied to a HisTrap (GE Healthcare) column packed with nickel chelate resin and connected to an EP-1 Econo pump (BioRAD) at 4°C at a flow rate of 0.2 ml/min. Washing was performed with 4 mL lysis buffer at a flow rate of 0.5 ml/min. Bound recombinant ParB was eluted by applying 5 mL elution buffer (20 mM Na₂HPO₄-NaH₂PO₄, 0.5 M imidazole, 0.5 M NaCl, pH 7.4) at a flow rate of 0.2 ml/min. Eluted 1 mL fractions were subjected to SDS-PAGE to select those that appeared to contain recombinant ParB only. Finally, 1 mL of eluate was dialyzed against 250 mL PBS overnight at 4°C and subsequently used for functional assays.

Antibodies and western blots

Methanol fixed deep-frozen worms were rehydrated in PBS and, subsequently, proteins from *Ca. T. oneisti* dissociated from its host or from *E. coli* cells expressing recombinant ParB were separated by reduced sodium dodecyl sulfate (SDS)-polyacrylamide gel electrophoresis (PAGE) on NuPAGE 4%–12% Bis-Tris pre-cast MOPS gel (Invitrogen), respectively, and each blotted onto Hybond ECL nitrocellulose membranes (Amersham Biosciences). Membranes were blocked for 45 min in PBS containing 5% (wt/vol) nonfat milk (PBMS) at room temperature and incubated overnight at 4°C with either a 1:50 dilution of custom, peptide rabbit polyclonal anti-*Ca. T. oneisti* ParB antibody (Eurogentec) or with a 1:1,000 dilution of a monoclonal anti-His antibody (Sigma) in PBMS. For the negative control, the primary antibody was omitted. After five 6 min-long washes in PBMS and one final wash in PBS containing 0.1% Tween20, the blots were incubated for 1 hr at room temperature with a horseradish peroxidase-conjugated anti-rabbit or anti-mouse secondary antibody (1:10,000; Amersham Biosciences) in PBMS. Protein-antibody complexes were visualized using ECL Plus detection reagents (Amersham Biosciences).

Identification of *Ca. T. oneisti parS* and electrophoretic mobility shift assay (EMSA)

To identify *Ca. T. oneisti parS* we used the consensus sequence from 1,030 *parS* sequences identified from 276 prokaryotic genomes [32] against the genome draft (Figure 2B). Sequence logos of *parS* sequences were generated via the WebLogo3 webpage (<http://weblogo.threeplusone.com/>).

An 827 nt-long *parS*-containing DNA fragment was amplified from *Ca. T. oneisti* (GenBank: MK650415; see Table S5 for PCR cycling conditions), cloned into pJET1.2/blunt vector (ThermoFisher, K1231) and used as a template to synthesize the DNA fragment used in the EMSA. The 827 nt-long *parS*-containing DNA fragment was subsequently PCR amplified out of the vector and residual vector was digested with DpnI (New England Biolabs, R0176S) for 5 min at RT and 1 hr at 37°C. For the negative control, the eleven most conserved nucleotides of the *parS* consensus sequence GTTCAGTGAAC (enlarged nucleotides in Figure 2B) were mutated into, respectively, ACCTGACAGGT via PCR mutagenesis using the ToparSmut11_F1 and To parSmut11_R primers. After a digest with DpnI for 5 min at RT and 1 hr at 37°C and a clean-up, the pJET1.2-*parS*-mut11 fragment was circularized for 20 min at RT with T4 DNA ligase (ThermoFisher, EL0011) and transformed into competent *E. coli* Top10 cells. The cleaned-up plasmid was then used to PCR amplify the 827 nt-long *parS*-mut11-containing DNA fragment, which was subsequently digested with DpnI to remove the residual vector.

500 nM, 250 nM or 125 nM affinity purified recombinant ParB was incubated with 200 ng DNA containing either the wild-type or the mutated *parS* site in 20 µl at 30°C for 30 min. As an additional negative control, 500 nM ParB was heat-inactivated by incubating 30 min at 94°C in the presence of 1 mM DTT prior incubation with the DNA fragment containing the wild-type or the mutated *parS* site. Samples were mixed with 2x Native Dye (100 mM NaCl, 100 mM imidazole, 4 mM 6-aminocaproic acid, 2 mM EDTA, 20% glycerol) and 20 µl of each were loaded onto a 4%–16% Native PAGE Bis-Tris Gels (Invitrogen). The gel was run in 1x Anode (50 mM Bis-Tris, pH 7.0) and 1x Cathode (50 mM Tricine, 15 mM Bis-Tris) buffer at 4°C. Sample separation was done with a stepwise increase of voltage (i.e., 50 V for 20 min, 100 V for 30 min, 150 V for 30 min, 200 V for 30 min). The SDS-PAGE was stained in an ethidium bromide gel bath for 15 min and visualized under UV light.

Immunostaining and DNA staining

Deep-frozen methanol fixed nematodes were rehydrated and washed in PBS containing 0.1% Tween 20 (PBT), followed by permeabilization of the bacterial peptidoglycan by incubation for 15 min with 0.1% (wt/vol) lysozyme at room temperature. Blocking was carried out for 1 hr in PBT containing 2% (wt/vol) bovine serum albumin (blocking solution) at room temperature. *Ca. T. oneisti* was incubated with a 1:500 dilution of peptide rabbit polyclonal anti-*Ca. T. oneisti* ParB antibody (Eurogentec). All primary antibodies were incubated in blocking solution overnight at 4°C. Upon incubation with primary antibody (or without, in the case of the negative control) samples were washed three times in PBT and incubated with a 1:500 dilution of secondary Alexa 488-conjugated anti-rabbit antibody (Jackson ImmunoResearch, USA) in blocking solution for 1 hr at room temperature. Unbound secondary antibody was removed by three washing steps in PBT and thereupon incubated in 5 µg/ml Hoechst 33342 PBT for 15 min. After two washing steps to remove unbound DNA stain, worms were sonicated for 45 s in order to dissociate *Ca. T. oneisti* from its host prior mounting. 1.5 µl of the bacterial suspension was mixed with 0.75 µl of Vectashield mounting medium (Vector Labs) and applied to a 1% agarose covered microscopy slide.

Fluorescence microscopy

Slides containing symbiont cells subjected to DNA FISH or immunostaining were imaged using a Nikon Eclipse NI-U microscope equipped with a MFCool camera (Jenoptik). Images were acquired using the ProgRes Capture Pro 2.8.8 software (Jenoptik).

QUANTIFICATION AND STATISTICAL ANALYSIS

Microscopic images were processed using the public domain program ImageJ in combination with plugin ObjectJ and XY-shape inspector. Cell outlines were traced and morphometric measurements recorded. Fluorescent intensities were measured within the cell boundaries and the positions of the fluorescence foci (i.e., points of maximal fluorescent emissions) were plotted as fraction of the normalized cell width and length of the cell that contained them. Automatic cell recognition was double-checked manually. For the average fluorescence plots, cells were automatically grouped into morphological classes based on phase-contrast images, each cell was resampled to the same length and the fluorescence intensities added up and averaged. For representative images, the background subtraction function of ImageJ was used and brightness and contrast were adjusted for better visibility. Data analysis was performed using Excel 2017 (Microsoft Corporation, USA), plots were created with Excel 2017 and figures were compiled using Photoshop CC and Illustrator CC (Adobe Systems, USA). Gene features were plotted using the DNAFeaturesViewer Python library (<https://github.com/Edinburgh-Genome-Foundry/DnaFeaturesViewer>).

DATA AND CODE AVAILABILITY

The symbiont genome has been deposited at DDBJ/ENA/GenBank under the accession number GenBank: SMSG000000000.1. *Ca. T. oneisti* *parS*-containing DNA fragment and the ParB amino acid sequence have been deposited in DDBJ/ENA/GenBank under the accession numbers GenBank: MK650415 and MK650416, respectively. The documentation for the ImageJ plugin XY-shape inspector can be accessed here: <https://sils.fnwi.uva.nl/bcb/objectj/examples/XY-Shape-Inspector/MD/xy-shape-inspector.html>.

Current Biology, Volume 29

Supplemental Information

A Bidimensional Segregation Mode Maintains

Symbiont Chromosome Orientation toward Its Host

Philipp M. Weber, Friedrich Moessel, Gabriela F. Paredes, Tobias Viehboeck, Norbert O.E. Vischer, and Silvia Bulgheresi

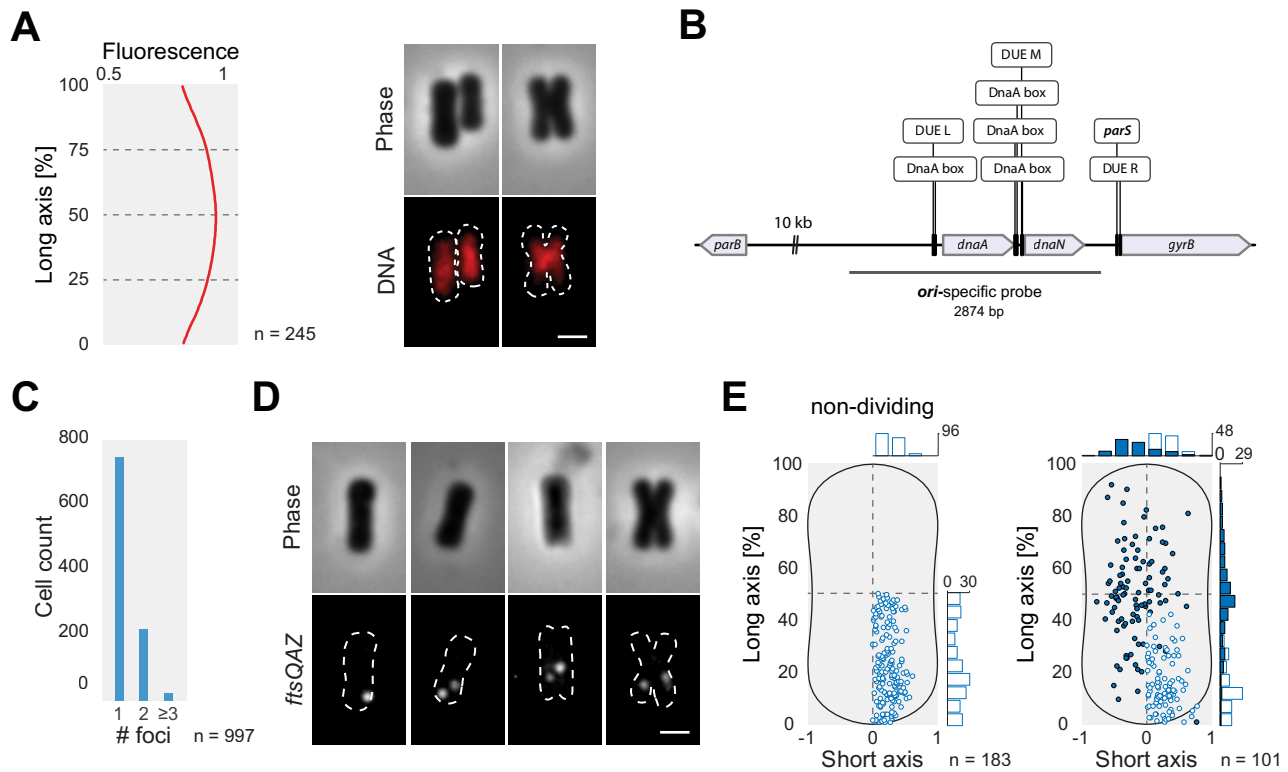


Figure S1. DNA distribution, schematic representation of the predicted *ori* and FISH-based *ftsQAZ* localization pattern in *Ca. T. oneisti*. Related to Figure 1, Table S1, S2, S3 and S5.

(A) Left panel shows average DNA fluorescence expressed in arbitrary units (a.u.) plotted against the normalized cell length (%). Right panel shows images of three representative cells stained with Hoechst 33342. Upper panels show the phase contrast images and lower panels show DNA signal (red) and cell outlines deduced from the corresponding phase contrast images (white dotted lines). Scale bar is 1 μ m. (B) Predicted *Ca. T. oneisti* origin of replication with DNA unwinding element (DUE; L, M and R), DnaA boxes and *parS* site. (C) Histogram showing number of *ftsQAZ* foci per cell. Total number of analyzed cells (n) is 997. (D) Images of four representative cells arranged from the thinnest (youngest) to the thickest (oldest) cell, from left to right. Upper panels show the phase contrast images and lower panels show *ftsQAZ* signal (white). Cell outlines were deduced from the corresponding phase contrast images (white dotted lines). Scale bar is 1 μ m. (E) Left plot shows *ftsQAZ* subcellular localization in cells that show one fluorescent focus and the right plot shows cells with two *ftsQAZ* foci. The position of each focus is plotted against the normalized cell width and length (%) of the cell that contained them. Dashed lines represent the long and the short cell axis and midcell is defined as the point in which they intersect.

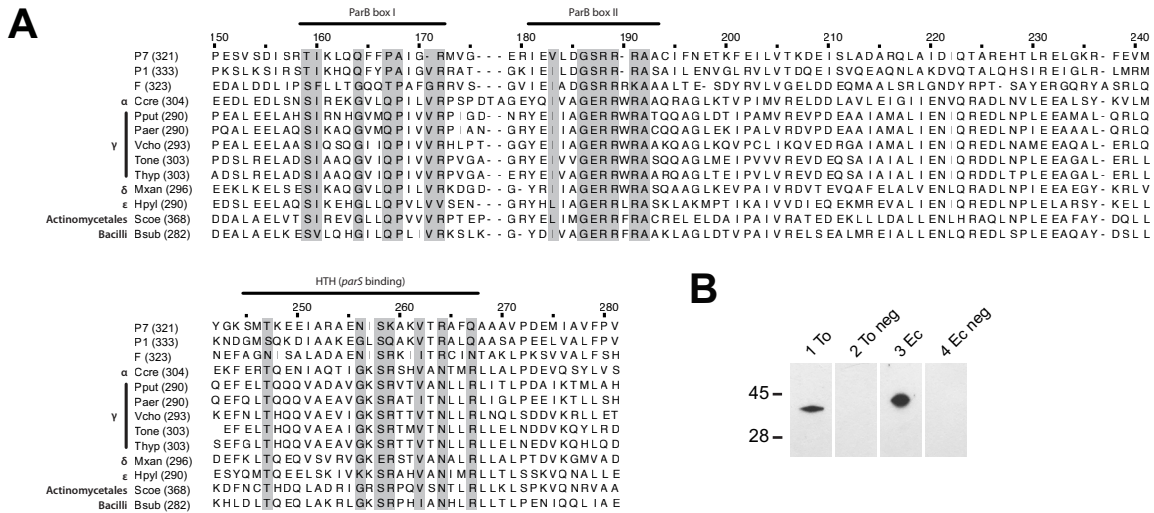


Figure S2. *Ca. T. oneisti* ParB protein alignment and expression. Related to Figures 1, 2, Table S4 and S5.

(A) Alignment of ParB (140 aa-278 aa) of *Ca. T. oneisti*, *Ca. T. hypermnestreae* and of bacteria where it was shown to mediate chromosome segregation (see main text and Table S5). Residues that are conserved in the ParB Boxes I and II and in the HTH motif in at least ten ParB proteins are in grey [5,78]. P7: *E. coli* plasmid; P1: *E. coli* plasmid; F: *E. coli* plasmid; Ccre: *Caulobacter crescentus*; Pput: *Pseudomonas putida*; Paer, *Pseudomonas aeruginosa*; Vcho: *Vibrio cholerae*; Tone: *Ca. T. oneisti*; Thyp: *Ca. T. hypermnestreae*; Mxan: *Myxococcus xanthus*; Hpyl: *Helicobacter pylori*; Scoe: *Streptomyces coelicolor*; Bsub: *Bacillus subtilis*. (B) Western blots of protein extracts of *Ca. T. oneisti* (lanes 1 and 2, To and To neg, respectively) and of *E. coli* cells expressing recombinant ParB (lanes 3 and 4, Ec and Ec neg) probed with a specific anti-ParB antibody (lanes 1 and 3) or with the secondary antibody only (lanes 2 and 4). Native ParB predicted MW is 33 kDa and recombinant ParB 35 kDa. Numbers indicate apparent MWs expressed in kDa.

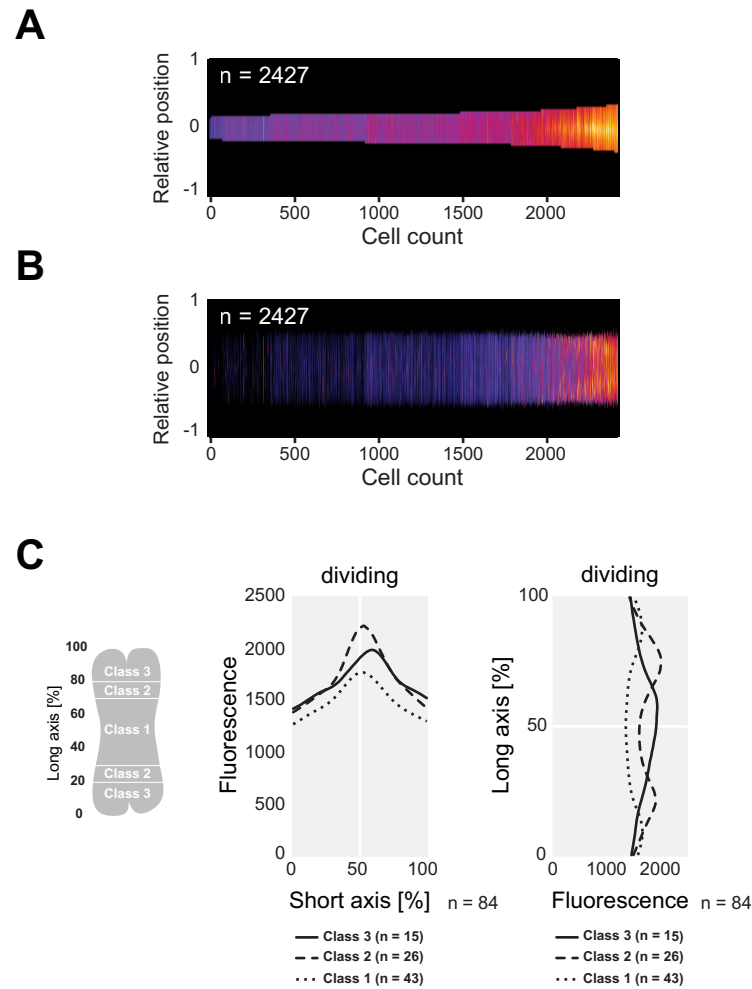


Figure S3. FISH-based *ter* localization pattern in *Ca. T. oneisti*. Related to Figure 3, Table S1, S2, S3 and S5.

(A and B) Demographs showing FISH-based *ter* localization of 2,427 *Ca. T. oneisti* cells. The *ter* probe fluorescence emitted by each cell is represented as a pixel-wide bar whose length corresponds to the short axis (A) or the long axis (B) of the cell. Symbiont cells were arranged according to increasing width from left to right. (C) Dividing cells ($n = 84$) were grouped into three classes depending on the position of the *ter* foci along the long axis (cells with central foci belonged to class 1, cells with pericentral foci to class 2 and cells with polar foci to class 3, see scheme) and the total fluorescence emitted by each class was plotted against the short (left plot) or the long cell axis (right plot).

Genome size [Mb]	4.36
Number of contigs	216
Average G+C content [%]	58.69
Protein coding density [%]	83.05
Number of coding sequences (CDS)	5155
Number of tRNA	46
Number of rRNA	3
CheckM Completeness [%]	94.28
CheckM Contamination [%]	0.75
CheckM Strain heterogeneity [%]	0.00
Number of plasmids	0 ¹
Number of predicted <i>ori</i>	1 ²
Number of predicted <i>dif</i> sites	1 ³

¹ No circular sequences were assembled when using SPAdes v3.12.0 with the flag '--plasmid'.

² Predicted *ori* features are visualized in Figure 2 and Figure S1.

³ One *dif* site was identified using a *dif* consensus sequence.

Table S1. *Ca. T. oneisti* genome features. Related to Figures 1, 2, 3, S1 and S3.

			distance between two <i>ori</i> foci	
			Short axis	Long axis
<i>ori</i>	All (n = 127)	average	0.46	0.26
		stdev	0.29	0.17
	Non-dividing (n = 60)	average	0.39	0.28
		stdev	0.29	0.16
	Dividing (n = 67)	average	0.52	0.24
		stdev	0.28	0.18
<i>ftsQAZ</i>	All (n = 102)	average	0.42	0.34
		stdev	0.29	0.19
	Non-dividing (n = 59)	average	0.37	0.37
		stdev	0.28	0.19
	Dividing (n = 43)	average	0.47	0.30
		stdev	0.28	0.19
<i>ter</i>	All (n = 369)	average	0.50	0.38
		stdev	0.42	0.24
	Non-dividing (n = 214)	average	0.62	0.26
		stdev	0.45	0.16
	Dividing (n = 155)	average	0.32	0.55
		stdev	0.30	0.22

Table S2. Distance between sister *ori*, *ftsQAZ* and *ter* foci along the short and the long cell axis. Related to Figures 1, 3, S1 and S3.

Target	Probe no.	Primer	Sequence (5'-3')	Product (nt)
ori region (2,874 nt)	1	1F_oriC	GTGGGAATCTGGAATCAATGTGCC	301
		1R_oriC	GGGACTTCACCTGAGGTACGAATG	
	2	2F_oriC	CTGACCCCCGAGTTTACGTTTG	309
		2R_oriC	GATAAGCAGCGTATTGACGGTTCG	
	3	3F_oriC	GATGATGTCCAGTTCTTCGCGG	299
		3R_oriC	CGGATATTCGAGCGGACATGTCT	
	4	4F_oriC	AGATCTCGAGGGGGCATTACG	304
		4R_oriC	GGTGTGATCCCTTCCTCCAAAG	
	5	5F_oriC	CACGGTGATCCACGCAACA	350
		5R_oriC	CGACCCCTCCTACCTTTGTGA	
	6	6F_oriC	CTCCCAATACTCGGCAATCTGC	347
		6R_oriC	GCCGTTTTTCTCGAAGAGATGCTTC	
	7	7F_oriC	GTTTGCAATGGCACATCAAGATGTC	303
		7R_oriC	TAGCGGCCATCAACAAGCTTC	
	8	8F_oriC	CCGGATTACGAGCGGGTAGTA	316
		8R_oriC	CGCTACCGTCTGAATCTTTAAACCC	
	9	9F_oriC	CTGCGGAATAAAGGTAAGGAGAAGG	300
		9R_oriC	GACAGCCTCTAAGGTCCACAC	
ftsQAZ containing region (3,273 nt)	1	ftsQAZ_F	TCTACTGATGCGTTGGGAGC	317
		Los_ftsQAZ_R1	GAGTAGCACCGGTTTCGG	
	2	Los_ftsQAZ_2F	GGAATGGACCAGGATGCCTT	338
		Los_ftsQAZ_2R	GGGACTTTAGTTTTGCTGACCG	
	3	LosftsA_start_F	ATGTTGAGACGAGGCGAAAAGAAT	276
		Los_ftsQAZ_3R	GTTGAGGCTGCGGATATGG	
	4	Los_ftsQAZ_4F	ATTACCGCCATCAAGGAGCG	282
		Los_ftsQAZ_4R	CTGCTCCAAGACCAAGTCG	
	5	Los_ftsQAZ_5F	GGATGAGAAGGAGCTGGGC	312
		Los_ftsQAZ_5R	TCCTCGTAGCGTGGCTCTA	
	6	Los_ftsQAZ_6F	GCTCTTGGGTCTGCTCCAA	328
		LosftsA_stop_R	TCAGAAATTGCCTTGAAACCAGCT	
	7	Los_ftsQAZ_7F	CCTCCATGAGATCCTGCAAG	311
		Los_ftsQAZ_7R	CCTCCTTGCCACCTTG	
	8	Los_ftsQAZ_8F	TTGGAGGACAAGGAACGCAT	291
		Los_ftsQAZ_8R	GAGACTCATTTCTTACCGAGCA	
	9	Los_ftsQAZ_9F	ACGATGTGCTCCTGAACG	311
		Los_ftsQAZ_9R	GTCGTCTGTCGCAAGTC	
	10	Los_ftsQAZ_10F	ATCGATCCCGACCTGAGC	304
		ftsQAZ_R	TGATTCAGTCCGCCTGATGG	
ter region (3,916 nt)	1	To_dif_1_f	CCATCGGGTGAAGATTCTCC	307
		To_dif_1_r	CAGGAGGTCATTTGAACCGA	
	2	To_dif_2_f	ATGCCCTGAGTCTGGATGTCA	333
		To_dif_2_r	ACCCAGTGATCGAGCTCGTC	
	3	To_dif_3_f	ATACGGTGTTCTGGGCGCA	316
		To_dif_3_r	TCCCCGACGATCGTTGCC	
	4	To_dif_4_f	CAATCAGCTCCCAATGGACGA	323
		To_dif_4_r	CCGAGATGAATGGCCGCA	

Target	Probe no.	Primer	Sequence (5'-3')	Product (nt)
ter region (3,916 nt)	5	To_dif_5_f	AAGAAGCCGCCGCGGTGGA	328
		To_dif_5_r	CCGTTCTGTTCTTGAGGAGTGG	
	6	To_dif_6_f	AGTAGGACCAGAGTTCCAGGC	302
		To_dif_6_r	TGGGACCGGTGGCTGGATT	
	7	To_dif_7_f	GGCATCCGGTCATGGATCG	302
		To_dif_7.1_r	AAGGGACCGGACAGCCGCTA	
	8	To_dif_8_f	GCACCAAGCCCCAACGCAA	320
		To_dif_8_r	TCGAGATCGGTCGCTTTGCC	
	9	To_dif_9.1_f	CCAGCATCGAGTCGGTACGC	332
		To_dif_9.1_r	TCAACCCACCCTCTACGAGTCC	
	10	To_dif_10_f	GGACCTCGACCGATTTGCAG	310
		To_dif_10_r	TTACTGCACCGCCGTTTCG	
	11	To_dif_11_f	GGCAAAGTGGCTGACCTCAAG	307
		To_dif_11_r	CGGTTGGTGGATCTTCATCG	
	12	To_dif_12_f	TCGGCCCCTCTGAAAAGGTC	339
		To_dif_12_r	GCGCTTTTCTAGGCGGTTTTG	

Table S3. DNA FISH PCR primers. Related to Figures 1, 3, S1, S3 and Table S5.

Abbrev.	Annotation/Organism	chr/ plasmid	GeneBank	aa-sequence length
P7	Enterobacteria phage P7	plasmid	AAQ07528.1	321 aa
P1	<i>Escherichia coli</i> virus P1	plasmid	YP006527.1	333 aa
F	sopB (plasmid) [<i>Escherichia coli</i> K-12]	plasmid	BAA97917.1	323 aa
Vcho	putative chromosome-partitioning protein ParB [<i>Vibrio cholerae</i>]	chr	SNC57145.1	293 aa
Pput	putative chromosome-partitioning protein ParB [<i>Pseudomonas putida</i>]	chr	PNG85025.1	290 aa
Bsub	site-specific DNA-binding protein [<i>Bacillus subtilis</i> subsp. <i>subtilis</i> str. 168]	chr	NP391976.1	282 aa
Ccre	chromosome partitioning protein ParB [<i>Caulobacter vibrioides</i> NA1000]	chr	YP002519241.4	304 aa
Hpyl	putative chromosome-partitioning protein ParB [<i>Helicobacter pylori</i>]	chr	GCF06275.1	290 aa
Paer	putative chromosome-partitioning protein ParB [<i>Pseudomonas aeruginosa</i>]	chr	AXS75203.1	290 aa
Scoe	ParB [<i>Streptomyces coelicolor</i> A3(2)]	chr	AAF16004.1	368 aa
Mxan	ParB/RepB/Spo0J family partition protein [<i>Myxococcus xanthus</i>]	chr	WP011557382.1	296 aa
Tone	ParB/RepB/Spo0J family partition protein [<i>Candidatus Thiosymbion oneisti</i>]	chr	WP089729459	303 aa
Thyp	THYP1385H_v1_1700001 ID:48089279 parB putative chromosome-partitioning protein ParB [<i>Candidatus Thiosymbion hypermnestreae</i> 1385H]	chr	MK650416	303 aa

Table S4. ParB sequences. Related to Figure 2 and S2. Species names' abbreviations and GeneBank accession numbers of ParB sequences used to construct the phylogenetic tree shown in Figure 2A and the amino acid sequence alignment shown in Figure S2A.

Target	Primer	Product (nt)	Cycling conditions
<i>ori</i>	see Table S3	Initial 2,874 nt-long fragment	98°C for 5 min, followed by 30 cycles at 98°C for 20 s, 58°C for 20 s, 72°C for 120 s, followed by a final elongation step at 72°C for 5 min.
	see Table S3	~300 nt-long probes (P1-P9)	95°C for 5 min, followed by 31 cycles at 94°C for 60 s, 57°C for 45 s, 72°C for 45 s, followed by a final elongation step at 72°C for 10 min.
<i>ftsQAZ</i>	see Table S3	Initial 3,273 nt-long fragment	98°C for 5 min, followed by 31 cycles at 98°C for 20 s, 57°C for 20 s, 72°C for 120 s, followed by a final elongation step at 72°C for 5 min.
	see Table S3	~300 nt-long probes (P1-P10)	95°C for 5 min, followed by 31 cycles at 95°C for 45 s, 57°C for 45 s, 72°C for 30 s, followed by a final elongation step at 72°C for 5 min.
<i>ter</i>	see Table S3	Initial 3,916 nt-long fragment	98°C for 5 min, followed by 31 cycles at 98°C for 20 s, 63°C (-0.3°C every cycle) for 20 s, 72°C for 125 s, followed by a final elongation step at 72°C for 5 min.
	see Table S3	~300 nt-long probes (P1-P12)	98°C for 5 min, followed by 32 cycles at 98°C for 20 s, 55°C for 20 s, 72°C for 15 s, followed by a final elongation step at 72°C for 5 min.
<i>parB</i>	T.oneisti_parB_F (5'-ATGTC-TACGAAGAAAAAGGGC-3'), T.oneisti_parB_R (5'-CTACT-TTATATGAGCAAG-3')	912	98°C for 5 min, followed by 31 cycles at 98°C for 20 s, 45°C (-0.3) for 20 s, 72°C for 35 s, followed by a final elongation step at 72°C for 5 min.
<i>parB-overhang</i>	FWD_primer_parB (5'-GAGGCCCAAGG-GGTTATGCTAGCTACT-TTATATGAGCAAGGA-3'), REV_primer_parB (5'-GTGC-CGCGCGGCAGCATGTC-TACGAAGAAAAAGGG-3')	951	98°C for 5 min, followed by 31 cycles at 98°C for 20 s, 50°C for 20 s, 72°C for 30 s, followed by a final elongation step at 72°C for 5 min.
<i>pET-15b</i>	FWD_To_pET-15b (5'-GCTGCCGCGCGGCAC-CAG-3'), REV_To_pET-15b (5'-CTAGCATAACCCCTTGG-GG-3')	5,708	98°C for 5 min, followed by 31 cycles at 98°C for 20 s, 50°C for 20 s, 72°C for 180 s, followed by a final elongation step at 72°C for 5 min.
<i>parS</i> -containing fragment and <i>parS</i> mut11 containing fragment (used in EMSA)	To_parS_EMSA_dnaN_F1 (5'-GTGGTAATGCCGAT-GAGACTTTG-3'), To_parS_EMSA_R1.1 (5'-AACCATAT-GATGAAGGCCAGTTCC-3')	827	98°C for 5 min, followed by 31 cycles at 98°C for 20 s, 63°C (-0.3) for 20 s, 72°C for 60 s, followed by a final elongation step at 72°C for 5 min.

Table S5. PCR cycling conditions. Related to Figures 1, 2, 3, S1, S2, S3, Table S2 and S3. DNA FISH PCR cycling conditions and conditions applied to amplify *Ca. T. oneisti parB*, clone it into an expression vector by Gibson assembly and to amplify DNA fragments used in EMSA.

CHAPTER IV

Ftsz-Mediated Fission of a Cuboid Bacterial Symbiont

Weber, P., Paredes, G. F. *, Viehboeck, T. *, Pende, N., Volland, JM., Gros, O., Ott, J., & Bulgheresi, S.

Accepted at iScience, and available online at:
https://papers.ssrn.com/sol3/papers.cfm?abstract_id=3885987

*these authors contributed equally

FtsZ-mediated fission of a cuboid bacterial symbiont

Philipp M. Weber¹, Gabriela F. Paredes^{1*}, Tobias Viehboeck^{1,6*}, Nika Pende^{1,2}, Jean-Marie Volland^{1,3}, Olivier Gros⁴, Jörg Ott⁵ and Silvia Bulgheresi^{1,7, 8}

¹ Department of Ecogenomics and Systems Biology, Environmental Cell Biology Group, University of Vienna, Vienna, Althanstrasse 14, A-1090 Vienna, Austria

² Evolutionary Biology of the Microbial Cell Unit, Department of Microbiology, Institut Pasteur, 25-28 Rue du Dr Roux, 75015 Paris, France.

³ Department of Energy Joint Genome Institute, Lawrence Berkeley National Laboratory, Berkeley, CA 94720, USA / LRC Systems, Menlo Park, CA, 94025 USA

⁴ C3MAG, UFR Des Sciences Exactes Et Naturelles, Université Des Antilles, BP 592, 97159 Pointe-à-Pitre, Guadeloupe, France.

⁵ Department of Limnology and Bio-Oceanography, University of Vienna, Althanstrasse 14, A-1090 Vienna, Austria

⁶ Division of Microbial Ecology, Center for Microbiology and Environmental Systems Science University of Vienna, A-1090 Vienna, Austria

⁷ Lead Contact

⁸ Correspondence: silvia.bulgheresi@univie.ac.at

* These authors contributed equally

SUMMARY

Less than a handful of cuboid and squared cells have been described in nature which makes them a rarity. Here, we show how *Candidatus* Thiosymbion cuboideus, a cube-like gammaproteobacterium, reproduces on the surface of marine free-living nematodes. Morphometric analysis showed that most non-dividing *Ca. T. cuboideus* cells are squared and 1.3 μm -thick on average. Immunostaining of symbiont cells with an anti-fimbriae antibody revealed that they are host-polarized, as these appendages exclusively localized at the host-proximal (animal-attached) pole. Moreover, by applying a fluorescently labelled metabolic probe to track new cell wall insertion *in vivo*, we observed that the host-attached pole started to septate before the distal one. Proximal-to-distal

insertion of new cell wall material at the septum displayed a similar localization pattern as the tubulin homolog FtsZ. Although this has been shown to arrange into squares in synthetically remodelled cuboid cells, here we show that FtsZ may also mediate the division of naturally occurring ones. This implies that, even in natural settings, membrane roundness is not required for FtsZ function.

Prokaryotic cells have evolved an enormous diversity of cell shapes and sizes. While most model bacteria are spheres or rod-like, recently more uncommon shapes, including corkscrews, crescents, or stars, are receiving increasing attention (Caccamo and Brun, 2017; Kysela et al., 2016). However, no squared bacteria and only two archaea have been described so far, *Haloquadratum walsbyi* (Walsby, 1980) and *Haloarcula quadrata* (Oren, 1999).

In bacteria, the rigid peptidoglycan (PG) layer of the cell envelope provides mechanical strength and determines the cell shape. By investigating the molecular mechanisms of PG synthesis, substantial progress has been made in understanding the morphogenesis of model rods such as *Escherichia coli*. Here, the task of directing the PG synthesis machinery is split between the actin homolog MreB and the tubulin homolog FtsZ. While short MreB filaments are spiralling along the envelope to elongate the cell corpus, FtsZ polymerizes exclusively at the septal plane determining the end of the cell cycle (McQuillen and Xiao, 2020; Shi et al., 2018). In the case of model rods and cocci, FtsZ polymerizes into a ring-like structure at septation onset or, at least, during its last step (Eswara and Ramamurthi, 2017). However, in synthetically remodelled cells, fluorescently tagged FtsZ could polymerize into other shapes (including squares), while displaying the usual dynamics (Söderström et al., 2018).

Here, we investigated the reproduction mode of *Candidatus Thiosymbion cuboideus*, a cube-like sulfur-oxidizing gammaproteobacterium, exclusively found attached to the cuticle of marine free-living nematodes (*Stilbonematinae*). We discovered that in this ectosymbiont both FtsZ and newly synthesised peptidoglycan (PG) localize at the septum in a proximal-to-distal fashion, implying that symbiont growth starts at the host-attached pole and that the tubulin homologue mediates septal PG insertion. We conclude that membrane roundness is not required for FtsZ-based division under natural settings.

RESULTS

The ectosymbiont of the marine nematode *Catanema* sp. “Guadeloupe” belongs to the candidate genus *Candidatus* Thiosymbion and bears the *fts* gene. To molecular identify the symbiont of the nematode *Catanema* sp. “Guadeloupe”, we dissociated it from its host, extracted its genomic DNA (gDNA) and sequenced it. We found the *Ca. T. cuboideus* genome to be 5.0 Mb in size and to be 96.91% complete (Table S1). A 16S rRNA gene-based phylogenetic tree (Figure S1, Table S2) shows that *Ca. T. cuboideus* clusters together with other *Candidatus* Thiosymbion bacteria that cover *Stilbonematinae*. Furthermore, *Ca. T. cuboideus* possesses the complete *fts* operon, including an *ftsZ* gene whose product is 94% identical to that of the longitudinally dividing *Ca. T. oneisti* and 75% identical to that of the model rod-shaped bacterium *Escherichia coli* (Figure S2A, B).

We conclude that *Ca. T. cuboideus* belongs to the *Candidatus* genus Thiosymbion and that FtsZ may mediate its division.

***Ca. T. cuboideus* cells are cuboid.** *Ca. T. cuboideus* cells form a tightly packed monolayer on the cuticle of its marine nematode host *Catanema* sp. “Guadeloupe” (Figure 1A). Henceforth, we will refer to the sides of the symbiont, which are parallel to the nematode surface and whose length corresponds to that of the cell long axis, as poles, namely the proximal (host-attached) pole and the distal (free) pole (Figure 2C). The average length and width of non-dividing cells were 1.87 μm and 1.72 μm , respectively. Further, we found 54% of the population to be squared (i.e., axes length difference is less than 15%, $n = 212$; Figure S3A; Table S3). As for the average symbiont thickness, it was 1.31 μm , as revealed by morphometric analysis of cells imaged by 3D SIM microscopy ($n = 15$; Figures 1C, S3B).

All in all, based on 2D and 3D morphometric analyses, *Ca. T. cuboideus* cells are cuboid.

Polarity and asynchronous septation of *Ca. T. cuboideus*. To confirm the nature of the filamentous structures observed by scanning electron microscopy (SEM) that are situated between the symbiont proximal cell pole and nematode cuticle (Figure 1B, right panel and S3D), we immunostained dissociated *Ca. T. cuboideus* cells with an anti-fimbriae antibody. The localization of the epifluorescence signal to one cell

side, as previously described for *Ca. Thiosymbion hypermnestrae* (Leisch et al., 2016), indicated that the proximal filamentous structures displayed by *Ca. T. cuboideus* were indeed fimbriae (Figure 2A top panel, 2B left plot, S3E). To determine the growth mode of the cube-like symbiont, we incubated it *in vivo* (i.e., as it was still attached to the nematode host), with a clickable bio-orthogonal PG precursor D-amino acid dipeptide ethynyl-D-alanyl-D-alanine (EDA-DA). We found that the cell walls of symbionts that were incubated in EDA-DA for 3 hr were completely stained and that, additionally, dividing cells fluoresced at the nascent septum (Figure 2A, middle panel; S3C). In cells that showed an indentation of the proximal membrane (early septation stage or stage 1), we detected new PG incorporation only at the proximal pole. In cells displaying indentations at both poles (later septation stage or stage 2), proximal and distal EDA-DA signals appeared (Figure 2A, middle panel; 2B middle plot; S3E).

We conclude that *Ca. T. cuboideus* cells are host-polarized and that septal growth is asynchronous, starting at the proximal pole, followed by the distal pole.

FtsZ localization pattern recapitulates that of new PG insertion. To determine whether FtsZ localization would be consistent with septal PG insertion in cuboid bacteria, we immunostained dissociated symbionts with an anti-FtsZ antibody. We found that the FtsZ localization pattern resembled the pattern of insertion of newly inserted PG. Indeed, at early septation stages, cells displayed a proximal focus of fluorescence, whereas, at later septation stages, they displayed two, one at the proximal and one at the distal pole. Moreover, a weaker FtsZ signal was also visible in correspondence of the nascent septum, i.e. between the two foci (Figure 2A, bottom panel; 2B right plot; S3C).

In conclusion, the FtsZ localization pattern is consistent with this tubulin homolog mediating septal PG insertion in cuboid cells.

***Ca. T. cuboideus* FtsZ polymerizes into either straight or sharp-cornered filaments.** To gain a better resolution and a 3D image of the FtsZ localisation pattern of immunostained *Ca. T. cuboideus* cells, we performed 3D SIM microscopy. We detected different types of FtsZ arrangements at the septation plane, ranging from foci to straight or sharp-cornered filaments (Figure 3, Supplementary Movies 1-4). Importantly, the latter arrangements were the largest, as we could detect neither a continuous FtsZ ring nor a square. We conclude that FtsZ can mediate cell division by

polymerizing into a discontinuous square, implying that membrane curvature is not required for FtsZ function in a naturally occurring cuboid bacterium.

DISCUSSION

Although Polz et al. (1992) reported on corn-kernel shaped symbionts attached to the cuticle of *Catanema* sp. 1 from Croatia, no cell population thereof was subjected to rigorous morphometric analysis. This makes *Ca. T. cuboideus* the first bacterium shown to be cube-like. Aside from the squared archaeal species, which were described as either flat (Oren, 1999) or only 0.25 μm thick (Stoeckenius, 1981), only two more examples of cuboid cells are known, both belonging to the eukaryotic kingdom of life: the first example are the cells that build the compound eyes (ommatidia) of decapod crustaceans (Palmer et al., 2018). The second example, are cells that build tightly sealed, surface epithelia lining human organs (e.g., kidneys, ovaries). These, however, appeared as prisms when viewed from the top (Krstić, 1985). We hypothesise that, in a *Ca. T. cuboideus* “epithelium”, a cuboid shape would be better suited than a rod-like for maximizing contact areas between neighbouring cells. If we recently showed that *Ca. T. oneisti* might import phospholipids, ammonia and organic compounds from its host and sulfide, oxygen, urea, and CO_2 from the environment, we still do not know which molecules Thiosymbion cells exchange among themselves (Paredes et al., 2020). Therefore, the kind of cell physiology that would drive the evolution of a cube-like cell awaits discovery.

We investigated the reproduction mode of a sulfur-oxidizing cube-like gammaproteobacterium, that naturally thrives on the surface of marine free-living nematodes. The proximal localization of fimbriae suggests that this symbiont uses these appendages to attach to its nematode host, and that septal growth is asynchronous likely due to its monopolar attachment to the host. Both these features are reminiscent of a phylogenetically related nematode symbiont, *Ca. T. hypermnestrae* (Leisch et al., 2016; Pende et al., 2018). It is possible that both symbionts start septal growth at the host-attached pole, to guarantee host attachment to both daughter cells, even prior to septation completion.

The cytoskeleton is the major shape determinant for eukaryotic and prokaryotic cells. According to current models, in order to mediate bacterial septation, FtsZ polymerizes into a highly dynamic, discontinuous and heterogeneous ring. Notably, it has been suggested that cell pole morphogenesis in rod-shaped cells relies on those

FtsZ dynamics and structure, just like the controlled elongation of the lateral walls relies on the actin homolog MreB (McQuillen and Xiao, 2020). Although the *mreB* gene was identified in *Ca. T. cuboideus*, successful cultivation and genetic manipulation of *Ca. T. cuboideus* are necessary to track the localization pattern of fluorescently labelled FtsZ and MreB *in vivo* to understand their role in its morphogenesis.

In bacteria that were artificially forced to become cuboid, while their growth and division was pharmacologically halted, FtsZ polymerized into sharp-cornered Z-squares (Söderström et al., 2018). Although fabricated microchambers that hold the cells upright should be used for improved resolution along the Z axis, we could not detect continuous Z-squares in *Ca. T. cuboideus*. However, differently to what observed in another asynchronously dividing symbiont (Pende et al., 2018), we could detect sharp-cornered, staple-like FtsZ filaments (Figure 3 bottom panel, Supplementary Movie 4). This implies that FtsZ does not have to polymerize into half rings or arcs to mediate division and that membrane roundness is not required for FtsZ function under natural settings.

Even though only a handful of squared or cuboid shapes have been reported in prokaryotic and eukaryotic cells so far, squareness might be more widespread than currently assumed. To know whether the natural occurrence of cube-like cells is truly that rare or whether they are simply undersampled, we need to screen the Earth microbiome for morphological diversity by using high throughput techniques. Only then we will have a more complete picture of the morphological diversity likely concealed behind rods and cocci.

AUTHOR CONTRIBUTIONS

P.M.W. did most of the experiments, formal analysis, visualization, provided resources and reviewed and drafted the manuscript; G.F.P. did the sampling, the PG precursor incubations in the field, the SEM images and revised the manuscript. T.V. did PG precursor incubations in the field, Nanopore sequencing, the assembly of the genome, bioinformatic analyses and revised the manuscript. N.P. did preliminary bioinformatic analyses and experiments, acquired the WGA 3D SIM images with P.M.W., the FtsZ 3D SIM images and revised the manuscript. J.-M.V. did the TEM images and revised the manuscript. SEM and TEM were performed at the Core Facility Cell Imaging and Ultrastructure Research, University of Vienna. J.O. helped with the sorting of the nematodes and revised the manuscript. O.G. provided substantial technical support

and workspace. S.B. conceptualized and supervised the work, acquired funding, provided resources and revised the manuscript.

ACKNOWLEDGEMENTS

This work was supported by the Austrian Science Fund (FWF) projects P28593 (P.M.W, G.F.P., T.V.) and FWF DK+ Microbial nitrogen cycling (G.F.P.), a DOC-fellowship from the Austrian Academy of Science (P.M.W.), a uni:docs fellowship (N.P.) and three PhD completion grants from the University of Vienna (N.P., G.F.P. and P.M.W.). The authors acknowledge the Cell Imaging and Ultrastructure Research Core Facility of the University of Vienna. We are extremely grateful to Lijuan Zhang and Kareem Elsayad (Vienne Biocenter Core Facility for Advanced Microscopy) for technical support with the 3D SIM. Further, the authors would like to acknowledge Aurélien Dauphin and the Cell and Tissue Imaging Platform - PICT-IBiSA (member of France–Bioimaging ANR-10-INBS-04) of the Genetics and Developmental Biology Department (UMR3215/U934) of Institut Curie for help with 3D SIM. This work was supported by the European Research Council (ERC EPIGENETIX N°250367). We are also indebted to the staff of the VBCF NGS Unit (Laura-Maria Bayer and Miriam Schalamun) for assistance with Oxford Nanopore MinION sequencing and to Florian Goldenberg and Thomas Rattei (Division of Computational Systems Biology, University of Vienna) for providing and maintaining the Life Science Compute Cluster (LiSC), to Harald Gruber-Vodicka and Nicole Dubilier (Max Planck Institute for Marine Microbiology, Symbiosis Group, Bremen) for providing Illumina raw reads of the *Ca. T. cuboideus* genome and full length sequences of the *ftsZ* genes to Friedrich Moessel for helping with nematode collection.

DECLARATION OF INTEREST

The authors declare no competing interests.

FIGURES

Figure 1. *Ca. T. cuboideus* cells are cuboid. (A) A scanning electron micrograph (SEM) and a transmission electron micrograph (TEM) showing the bacterial coat from the top (left) and a section of it coating the nematode cuticle (right). (B) SEM images display three representative *Ca. T. cuboideus* cells arranged from the youngest to the oldest (three leftmost panels) and a cell that is attached to the worm's cuticle

(rightmost panel). (C) 3D-Structured illumination microscopy (SIM) images of cells stained with fluorescent Wheat Germ Agglutinin. Upper row shows a non-dividing and a dividing cell in front view (left) and 90° shifted side view (right) and lower panel show multiple *Ca. T. cuboideus* cells in different stages of the cell cycle (cyan). Scale bars correspond to 1 µm.

Figure 2. *Candidatus T. cuboideus* cells localize FtsZ at their septum. (A) Three representative images showing cells immunostained with an anti-fimbriae antibody (top), an anti-FtsZ antibody (middle), or PG metabolic probe EDA-DA (bottom). White dotted cell outline is the cell shape deduced from phase contrast images. (B) Quantitative analyses of fluorescence patterns corresponding to the different cell cycle stages. (C) Model of *Ca. T. cuboideus* growth and division. Scale bars corresponds to 1 µm.

Figure 3. *Ca. T. cuboideus* FtsZ forms either foci or straight or sharp-cornered filaments. 3D Structured illumination microscopy (SIM) images of cells immunostained with an anti FtsZ antibody. No membrane indentations appear in the two top cells, whereas the two bottom cells are invaginated. The left column shows the front view and the right column a 90° shifted side view. Scale bar corresponds to 1 µm.

Supplementary Figure 1. 16S rRNA gene-based phylogenetic placement of *Ca. T. cuboideus*. Maximum-likelihood reconstruction of 16S rRNA-genes of ectosymbionts of marine nematodes (*Stilbonematinae*). The tree was rooted using *Allochromatium vinosum* DSM 180, *Marichromatium purpuratum* 984 and *Thiocapsa marina* 5811 as an outgroup. Black circles indicate ultrafast bootstrap support values of ≥ 95%, all other node support values (< 95%) are depicted by open circles. For better readability, some branches have been collapsed and number of sequences is noted in brackets. See Supplementary table 2 for a list of GenBank accession numbers

Supplementary Figure 2. FtsZ identity heatmap and FtsZ amino acid sequence alignment (A) Heatmap showing the identity of pairwise-aligned FtsZ sequences in percentage. Sequences are clustered via hierarchical clustering (complete linkage method) using Euclidean distances. (B) Alignment of FtsZ sequences of *Escherichia*

coli DH5 α , *Ca. T. oneisti*, *Ca. T. cuboideus*, and of ectosymbionts of *Eubostrichus dianeae* and *E. fertilis*. Five distinct functional regions of FtsZ are indicated, NTP (dashed line), Globular Core (thick black line), C-terminal linker (thick white line), C-terminal tail (CTT, thin black line) and C-terminal variable region (CTV, dashed line end) (Casiraghi et al., 2020; Silber et al., 2020).

Supplementary Figure 3. Morphometry, localization patterns of EDA-DA, FtsZ, fimbriae and DNA, as well as transmission electron micrographs (TEM) of *Candidatus T. cuboideus*. (A) Scatter plot shows the length and width of 259 *Ca. T. cuboideus* cells, grouped into the categories dividing (red, n = 44), non-dividing (blue and green, n = 212) and squared (n = 122). (B) Boxplot shows the length, width, and depth of 15 cells imaged with 3D SIM microscopy. Box is the interquartile range (IQR), where the lower edge is 25th percentile (1st quartile [Q1]) and the upper edge the 75th percentile (3rd quartile [Q3]). Whiskers show the range between the lowest value (Min) and the highest value (Max). Line inside each box indicates the median. (C) Demographs of *Ca. T. cuboideus* cells labeled with a PG metabolic probe (EDA-DA) for 180 minutes (left, n = 108) and immunostained with anti-FtsZ antibody (right). Each cell is represented as a pixel-wide bar whose and cells were sorted according to increasing length from left to right. (D) TEM images display fimbrial structures between the symbiont cell and the host cuticle (white arrowheads). (E) Epifluorescence images of four representative *Ca. T. cuboideus* cells, sorted by increasing length from left to right, incubated with EDA-DA and immunostained with an anti-fimbriae antibody. Plot shows normalized fluorescence emitted by 62 *Ca. T. cuboideus* cells (a.u.) plotted against their cell width (%). (F) Representative symbiont cells stained with Hoechst and sorted from the youngest to the oldest. Plot shows the total fluorescence (a.u.) emitted by short cells (long axis < 2 μ m; n=45) and long cells (long axis > 2 μ m; n=186) plotted against their length (%).

Supplementary Table 1 Ca. T. cuboideus genome features.

Genome size [Mb]	5.006632
Number of contigs	16
Average G+C content [%]	57.51
Protein coding density [%]	82.67
Number of coding sequences (CDS)	6316
Number of tRNAs	45
Number of rRNAs	3 (1 operon)
CheckM Completeness [%]	96.61
CheckM Contamination [%]	2.28
CheckM Strain heterogeneity [%]	16.67

Supplementary Table 2. 16S rRNA-gene sequences used for the phylogenetic reconstruction displayed in Fig. S1 (from Scharhauser et al. 2020).

Ca. T. hypermnestrae	KP943980.1
Ca. T. hypermnestrae	EU711428.1
Ca. T. hypermnestrae	LR746256.1
Ca. T. oneisti	LR746261.1
Ca. T. oneisti	KT826595.1
Ca. T. oneisti	KF278591.1
Ectosymbiont of <i>Catanema 'crete1'</i>	LR746257.1
Ectosymbiont of <i>Catanema 'crete1'</i>	LR746258.1
Ectosymbiont of <i>Catanema sp.</i>	EU711426.1
Ectosymbiont of <i>Catanema sp. 'belize1'</i>	KP943972.1
Ectosymbiont of <i>Catanema sp. 'st andrea'</i>	KP943973.1
Ectosymbiont of <i>Eubostrichus cf. dianeae</i>	KP943975.1
Ectosymbiont of <i>Eubostrichus cf. topiarius</i>	LR746246.1
Ectosymbiont of <i>Eubostrichus cf. topiarius</i>	LR746244.1
Ectosymbiont of <i>Eubostrichus cf. topiarius</i>	LR746245.1
Ectosymbiont of <i>Eubostrichus cf. topiarius</i>	LR746242.1
Ectosymbiont of <i>Eubostrichus cf. topiarius</i>	LR746243.1
Ectosymbiont of <i>Eubostrichus cf. topiarius</i>	KP943974.1
Ectosymbiont of <i>Eubostrichus dianeae</i>	LR746262.1
Ectosymbiont of <i>Eubostrichus dianeae</i>	LR746247.1
Ectosymbiont of <i>Eubostrichus dianeae</i>	KF278587.1
Ectosymbiont of <i>Eubostrichus fertilis</i>	KF278590.1
Ectosymbiont of <i>Laxus cf. cosmopolitus</i>	EU711427.1
Ectosymbiont of <i>Laxus cf. cosmopolitus</i>	KP943986.1
Ectosymbiont of <i>Laxus cf. cosmopolitus</i>	LR746259.1
Ectosymbiont of <i>Laxus sp. 'heron1'</i>	KP943987.1
Ectosymbiont of <i>Laxus sp. 'heron2'</i>	KP943988.1
Ectosymbiont of <i>Leptonemella aphanothecae</i>	KP943979.1

Ectosymbiont of <i>Leptonemella aphanothecae</i>	LR746248.1
Ectosymbiont of <i>Leptonemella juliae</i>	KP943977.1
Ectosymbiont of <i>Leptonemella vestari</i>	KP943976.1
Ectosymbiont of <i>Leptonemella vicina</i>	KP943978.1
Ectosymbiont of <i>Leptonemella vicina</i>	KU921521.1
Ectosymbiont of <i>Paralaxus 'heron1'</i>	KP943985.1
Ectosymbiont of <i>Paralaxus 'oahu1'</i>	LR746253.1
Ectosymbiont of <i>Paralaxus 'oahu1'</i>	LR746252.1
Ectosymbiont of <i>Paralaxus bermudensis</i>	LR746255.1
Ectosymbiont of <i>Paralaxus bermudensis</i>	LR746250.1
Ectosymbiont of <i>Paralaxus bermudensis</i>	LR746249.1
Ectosymbiont of <i>Paralaxus cocos</i>	LR746254.1
Ectosymbiont of <i>Paralaxus cocos</i>	KP943984.1
Ectosymbiont of <i>Stilbonema 'heron1'</i>	KP943983.1
Ectosymbiont of <i>Stilbonema 'heron2'</i>	KP943982.1
Ectosymbiont of <i>Stilbonema 'st andrea1'</i>	KP943981.1
Ectosymbiont of <i>Stilbonema majum</i>	LR746260.1
Ectosymbiont of <i>Stilbonema majum</i>	HM776017.1
Ectosymbiont of <i>Stilbonematinae gen. B</i>	KP943971.1
Ectosymbiont of <i>Paralaxus 'heron1'</i>	LR746251.1
<i>Allochromatium vinosum</i> DSM 180	CP001896.112452.113967
<i>Marichromatium purpuratum</i> 984	CP007031.294591.296118
<i>Thiocapsa marina</i> 5811	AF112998.1
Ca. T. cuboideus	WYCW01000004.1.400935.402467

Supplementary Table 3. Phase contrast images-based morphometry of dissociated Ca. T. cuboideus cells

Number of cells (n)		Length (μm)	Width (μm)
All (256)	average	2.01	1.70
	stdev	0.45	0.11
Non-dividing (212)	average	1.87	1.71
	stdev	0.32	0.14
Dividing (44)	average	2.70	1.64
	stdev	0.31	0.14

REFERENCES

- Altschul, S.F., Gish, W., Miller, W., Myers, E.W., Lipman, D.J., 1990. Basic local alignment search tool. *J. Mol. Biol.* 215.
- Boetzer, M., Pirovano, W., 2014. SSPACE-LongRead: Scaffolding bacterial draft genomes using long read sequence information. *BMC Bioinformatics* 15, 1–9.
- Caccamo, P.D., Brun, Y. V., 2017. The Molecular Basis of Noncanonical Bacterial Morphology. *Trends Microbiol.*
- Capella-Gutiérrez, S., Silla-Martínez, J.M., Gabaldón, T., 2009. trimAl: A tool for automated alignment trimming in large-scale phylogenetic analyses. *Bioinformatics* 25.
- Casiraghi, A., Suigo, L., Valoti, E., Straniero, V., 2020. Targeting bacterial cell division: A binding site-centered approach to the most promising inhibitors of the essential protein FtsZ. *Antibiotics*. <https://doi.org/10.3390/antibiotics9020069>
- Eswara, P.J., Ramamurthi, K.S., 2017. Bacterial Cell Division: Nonmodels Poised to Take the Spotlight. *Annu. Rev. Microbiol.*
- Goldammer, H., Hollerschwandtner, E., Elisabeth, N.H., Frade, P.R., Reipert, S., 2016. Automatized Freeze Substitution of Algae Accelerated by a Novel Agitation Module. *Protist* 167.
- Hoang, D.T., Chernomor, O., Von Haeseler, A., Minh, B.Q., Vinh, L.S., 2018. UFBoot2: Improving the ultrafast bootstrap approximation. *Mol. Biol. Evol.* 35.
- Kalyaanamoorthy, S., Minh, B.Q., Wong, T.K.F., Von Haeseler, A., Jermini, L.S., 2017. ModelFinder: Fast model selection for accurate phylogenetic estimates. *Nat. Methods* 14.
- Katoh, K., Standley, D.M., 2013. MAFFT multiple sequence alignment software version 7: Improvements in performance and usability. *Mol. Biol. Evol.* 30.
- Krstić, R. V, 1985. General Histology of the Mammal: An Atlas for Students of Medicine and Biology. Springer-Verlag Berlin Heidelberg.
- Kysela, D.T., Randich, A.M., Caccamo, P.D., Brun, Y. V., 2016. Diversity takes shape: understanding the mechanistic and adaptive basis of bacterial morphology. *PLoS Biol.* 14, 1–15.
- Leisch, N., Pende, N., Weber, P.M., Gruber-Vodicka, H.R., Verheul, J., Vischer, N.O.E., Abby, S.S., Geier, B., den Blaauwen, T., Bulgheresi, S., 2016. Asynchronous division by non-ring FtsZ in the gammaproteobacterial symbiont of *Robbea hypermnestra*. *Nat. Microbiol.* 2, 16182.

353 McQuillen, R., Xiao, J., 2020. Insights into the Structure, Function, and Dynamics of
 354 the Bacterial Cytokinetic FtsZ-Ring. *Annu. Rev. Biophys.* 49, 309–341.
 355 Minh, B.Q., Schmidt, H.A., Chernomor, O., Schrempf, D., Woodhams, M.D., Von
 356 Haeseler, A., Lanfear, R., Teeling, E., 2020. IQ-TREE 2: New Models and
 357 Efficient Methods for Phylogenetic Inference in the Genomic Era. *Mol. Biol. Evol.*
 358 37.
 359 Nadalin, F., Vezzi, F., Policriti, A., 2012. GapFiller: A de novo assembly approach to
 360 fill the gap within paired reads. *BMC Bioinformatics* 13.
 361 Oren, A., 1999. *Haloarcula quadrata* sp. nov., a square, motile archaeon isolated
 362 from a brine pool in Sinai (Egypt). *Int. J. Syst. Bacteriol.* 49.
 363 Palmer, B.A., Hirsch, A., Brumfeld, V., Aflalo, E.D., Pinkas, I., Sagi, A., Rosenne, S.,
 364 Oron, D., Leiserowitz, L., Kronik, L., Weiner, S., Addadi, L., 2018. Optically
 365 functional isoxanthopterin crystals in the mirrored eyes of decapod crustaceans.
 366 *Proc. Natl. Acad. Sci. U. S. A.* 115.
 367 Paredes, G.F., Viehboeck, T., Lee, R., Palatinszky, M., Mausz, M.A., Reipert, S.,
 368 Schintlmeister, A., Volland, J.M., Hirschfeld, C., Wagner, M., Berry, D., Markert,
 369 S., Bulgheresi, S., König, L., 2020. Anaerobic sulfur oxidation underlies
 370 adaptation of a chemosynthetic symbiont to oxic-anoxic interfaces. *bioRxiv*.
 371 <https://doi.org/10.1101/2020.03.17.994798>
 372 Parks, D.H., Imelfort, M., Skennerton, C.T., Hugenholtz, P., Tyson, G.W., 2015.
 373 CheckM: Assessing the quality of microbial genomes recovered from isolates,
 374 single cells, and metagenomes. *Genome Res.* 25, 1043–1055.
 375 Pende, N., Wang, J., Weber, P.M., Verheul, J., Kuru, E., Rittmann, S.K.M.R., Leisch,
 376 N., VanNieuwenhze, M.S., Brun, Y. V., den Blaauwen, T., Bulgheresi, S., 2018.
 377 Host-Polarized Cell Growth in Animal Symbionts. *Curr. Biol.* 28, 1039-1051.e5.
 378 Polz, M.F., Felbeck, H., Novak, R., Nebelsick, M., Ott, J.A., 1992. Chemoautotrophic,
 379 sulfur-Oxidizing symbiotic bacteria on marine nematodes: Morphological and
 380 biochemical characterizarion. *Microb. Ecol.* 24, 313–329.
 381 Scharhauser, F., Zimmermann, J., Ott, J.A., Leisch, N., Gruber-Vodicka, H.R., 2020.
 382 Morphology of obligate ectosymbionts reveals *Paralaxus* gen. nov.: A new
 383 circumtropical genus of marine stilbonematine nematodes. *Zool. Scr.* 49, 379–
 384 394.
 385 Schneider, C.A., Rasband, W.S., Eliceiri, K.W., 2012. NIH Image to ImageJ: 25
 386 years of image analysis. *Nat Meth* 9, 671–675.

- Seemann, T., 2014. Prokka: Rapid prokaryotic genome annotation. *Bioinformatics* 30.
- Shi, H., Bratton, B.P., Gitai, Z., Huang, K.C., 2018. How to Build a Bacterial Cell: MreB as the Foreman of *E. coli* Construction. *Cell* 172, 1294–1305.
- Silber, N., Matos De Opitz, C.L., Mayer, C., Sass, P., 2020. Cell division protein FtsZ: From structure and mechanism to antibiotic target. *Future Microbiol.* <https://doi.org/10.2217/fmb-2019-0348>
- Söderström, B., Badrutdinov, A., Chan, H., Skoglund, U., 2018. Cell shape-independent FtsZ dynamics in synthetically remodeled bacterial cells. *Nat. Commun.* 9, 4323.
- Stoeckenius, W., 1981. Walsby's square bacterium: Fine structure of an orthogonal procaryote. *J. Bacteriol.* 148.
- Trump, B.F., Ericsson, J.L., 1965. The Effect of The Fixative Solution on The Ultrastructure of Cells and Tissues. *Lab. Invest.* 14.
- van der Ploeg, R., Verheul, J., Vischer, N.O.E., Alexeeva, S., Hoogendoorn, E., Postma, M., Banzhaf, M., Vollmer, W., den Blaauwen, T., 2013. Colocalization and interaction between elongasome and divisome during a preparative cell division phase in *Escherichia coli*. *Mol. Microbiol.* 87, 1074–1087.
- Vischer, N.O.E., Verheul, J., Postma, M., van den Berg van Saparoea, B., Galli, E., Natale, P., Gerdes, K., Luirink, J., Vollmer, W., Vicente, M., den Blaauwen, T., 2015. Cell age dependent concentration of *Escherichia coli* divisome proteins analyzed with ImageJ and ObjectJ. *Front. Microbiol.* 6.
- Walker, B.J., Abeel, T., Shea, T., Priest, M., Abouelliel, A., Sakthikumar, S., Cuomo, C.A., Zeng, Q., Wortman, J., Young, S.K., Earl, A.M., 2014. Pilon: An integrated tool for comprehensive microbial variant detection and genome assembly improvement. *PLoS One* 9, e112963.
- Walsby, A.E., 1980. A square bacterium. *Nature* 283.
- Wick, R.R., Judd, L.M., Gorrie, C.L., Holt, K.E., 2017. Unicycler: Resolving bacterial genome assemblies from short and long sequencing reads. *PLoS Comput. Biol.* 13, 1–22.

STAR METHODS

Ectosymbiont collection. *Catanema* sp. "Guadeloupe" individuals were collected between March and August 2019 from sand bars in Guadeloupe, French West Indies ("Ilet à Cochons", 16°12'53.76"N 61°32'05.74"W) at approximately 1 m depth. The sand was collected with the aid of cores and nematodes were extracted by gently stirring the sand in seawater and subsequently pouring it onto a 212 µm mesh sieve. Single worms (1-2 mm length, representing adults) were handpicked by forceps (Dumont 3, Fine Science Tools, Canada) under a dissecting microscope. *Catanema* sp. nematodes were identified based on morphological characteristics (Scharhauser et al., 2020).

Transmission electron microscopy. Live worms were plunge frozen in liquid propane at -179°C, cryo-substituted rapidly in acetone using the agitation module described in Goldammer et al. (2016) and transferred in absolute ethanol. Dehydrated samples were then embedded in medium-grade LR White resin. Polymerization was performed under nitrogen atmosphere at 40°C for three days. Alternatively (Figure S1), live worms were chemically fixed in a modified Trump's fixative solution (2.5% glutaraldehyde, 2% paraformaldehyde in sodium cacodylate 0.1 mol L⁻¹; 1100 mOsm.L⁻¹; pH 7.2; Trump and Ericsson, 1965) and further dehydrated in ascending ethanol series before embedding in Agar Low Viscosity Resin (Agar Scientific®). Thin sections (70nm) were placed on Formvar®-coated slot grids and stained with 0.5% uranyl acetate and 3% lead citrate prior to imaging with a Zeiss® Libra 120 transmission electron microscope.

Scanning electron microscopy. Whole worms were fixed in modified Trump's fixative solution (2.5% glutaraldehyde and 2% paraformaldehyde in 0.1 M sodium cacodylate buffer, 1000 mOsm L⁻¹, pH 7.2) (Trump and Ericsson, 1965). To dissociate the bacteria, 10 nematodes were washed three times by pipetting them up and down in 100 µL of 0.1 M sodium cacodylate buffer. 50 µl of the bacterial suspension was spotted on a poly-L-lysine-coated glass slide and let sink for 15 min for proper attachment. The samples were then dehydrated in an ascending ethanol series, followed by 100 % acetone, and critical-point drying (Leica EM CPD300, Leica Microsystems, Wetzlar, Germany). Finally, they were mounted on stubs and sputter-coated with gold (JEOL JFC-2300HR, Tokyo, Japan), and observed on an IT 300 scanning electron microscope (JEOL).

EDA-DA incubation of live symbionts. To track symbiont cell wall growth, batches of approx. 50 live symbiotic nematodes were each incubated in a 1.5 mL tube containing 500 µl of 10 mM ethynyl-D-alanyl-D-alanine (EDA-DA, a D-amino acid carrying a clickable ethynyl group; kind gift of Michael S. VanNieuwenhze, Indiana University) in filter sterilized natural seawater (FSW) for 180 min and subsequently washed once in FSW, transferred to methanol, and stored at -20°C. Nematodes were transported from Guadeloupe to Vienna deep-frozen.

Click-chemistry. Deep frozen methanol fixed nematodes were rehydrated and washed in PBS containing 0.1% Tween 20 (PBT). Blocking was carried out for 30 min in PBS containing 0.1% Tween 20 (OBT) and 2% (wt/vol) bovine serum albumin (blocking solution) at room temperature. An Alexa488 fluorophore was covalently bound to EDA-DA via copper catalyzed click-chemistry by following the user manual protocol for the Click-iT reaction cocktail (Click-iT EdU Imaging Kit, Invitrogen). The nematodes were incubated with the Click-iT reaction cocktail for 30 min at RT in the dark. Unbound dye was removed by a 10-min wash in PBT and one wash in PBS. Worms were sonicated for 40 s to dissociate *Ca. T. cuboideus* prior mounting.

Immunostaining. Deep-frozen methanol fixed nematodes were rehydrated and washed in PBT, followed by blocking for 1 h in PBT containing 2% (wt/vol) bovine serum albumin (blocking solution) at room temperature. *Ca. T. cuboideus* were incubated with a 1:200 dilution of commercially available rabbit polyclonal anti-*E. coli* FtsZ antibody (Agrisera) in blocking solution, as well as with a 1:500 dilution of sheep polyclonal anti-*E. coli* K88 fimbrial protein AB/FaeG antibody (ab35292, Abcam). Both the anti-*E. coli* FtsZ antibody (Agrisera) and the anti-*E. coli* K88 fimbrial protein AB/FaeG antibody (ab35292, Abcam) were previously shown to specifically recognize the FtsZ and the fimbriae of other Thiosymbion ectosymbionts (Leisch et al., 2012, 2016; Pende et al., 2014). All primary antibodies were incubated overnight at 4°C in blocking solution. Upon incubation with primary antibody (or without in the case of the negative control) samples were washed three times in PBT and incubated with secondary Alexa488 conjugated anti-rabbit (Jackson ImmunoResearch, USA) for anti-*E. coli* FtsZ antibody and Alexa555 conjugated anti-sheep antibody (Thermo Fisher Scientific) for anti-*E. coli* K88 fimbrial AB/FaeG antibody at 1:500 dilution in blocking solution for 1 h at room temperature. Unbound secondary antibody was removed by three washing steps in PBT and worms were sonicated for 40 s to dissociate *Ca. T.*

cuboideus cells from their hosts prior mounting. 1 μ L of the bacterial solution was mixed with 0.5 μ L of Vectashield mounting medium (Vector Labs).

Wheat germ agglutinin staining. Deep-frozen methanol-fixed nematodes were rehydrated and washed in PBS, followed by incubation in 20 μ g/mL FITC labelled Wheat germ agglutinin (W834, Invitrogen) in PBS for 1h at room temperature. Unbound WGA was removed by three washing steps in PBS and worms were sonicated for 40 s to dissociate *Ca. T. cuboideus* cells from their hosts prior mounting. 1 μ L of the bacterial solution was mixed with 0.5 μ L of Vectashield mounting medium (Vector Labs).

Three-Dimensional Structured Illumination Microscopy (3D SIM) imaging and analysis. Cell suspensions were applied on high precision coverslips (No. 1.5H, Sigma-Aldrich) coated with 0.01% (wt/vol) of Poly-L-Lysin. After letting the cell dry onto the surface of the coverslip, antifade mounting medium (Vectashield) was applied and the coverslip was sealed to a slide. 3D SIM was performed on a Delta Vision OMX v4 microscope equipped with an Olympus 60X/1.42 Oil Plan Apo N objective or an Olympus 100X/1.42 Oil Plan Apo N objective and 2 sCMOS or EMCCD cameras. The samples were excited with lasers at 488 nm, the emission was detected through emission filters 477/32 nm (Center/Bandpass). The image reconstruction and registration were performed using the SoftWoRx image software running under Linux operating system. For further image analysis of SIM image z stacks we used Fiji (ImageJ) Version 2.0.0-rc-54/1.51i. Namely, brightness and contrast were adjusted, stacks were fused to a single image (z projection, maximum intensity), stacks were rotated 90° (resliced) prior z projection for the 90° side view, and videos were created via 3D projection. Regions of interest were cut out and, for uniformity, placed on a black squared background. Figures were compiled using Illustrator CC (Adobe Systems Inc. USA).

Cell size and fluorescence measurements. Symbiont cells were dissociated from fixed *Catanema* sp. "Guadeloupe" nematodes by sonication. Cell suspensions were applied to an 1% agarose covered microscopy slide and imaged using a Nikon Eclipse Ni microscope equipped with a MFCool camera (Jenoptik, Germany). Epifluorescence images were acquired using ProgRes Capture Pro 2.8.8 software (Jenoptik) and processed using the public domain program ImageJ (Schneider et al., 2012) in combination with plugin ObjectJ and a modified version of Coli-Inspector (van

der Ploeg et al., 2013; Vischer et al., 2015). Cell length, width and fluorescence patterns were measured automatically. Automatic cell recognition was double-checked manually. For the average fluorescence plots and for the demographs, cells were automatically grouped into morphological classes based on phase-contrast images, each cell was resampled to the same length and the fluorescence intensities added up and averaged. For assessing early and late septation stages cells were grouped based on constriction based on visual inspection. Data analysis was performed using Excel 365 (Microsoft Corporation, USA), plots were created with R Studio (1.4.1103) and figures were compiled using Illustrator CC (Adobe Systems Inc. USA).

DNA extraction, sequencing and genome assembly of *Ca. T. cuboideus*.

500 *Catanema* sp. individuals collected between July and August 2018 were used for DNA extraction and genome assembly of the *Catanema* sp. ectosymbiont. The bacteria were detached from the worms by dipping the nematodes into ddH₂O for 1 min, then transferring them to 0.2 µM-filtered seawater for 5 min, after which the symbiont-free nematodes were discarded, and the bacterial suspensions pooled and collected by centrifugation. The bacterial fraction was carefully resuspended in TLB (100 mM NaCl, 10 mM Tris-HCl pH 8, 25 mM EDTA pH 8, 0.5% v/v SDS), 10 µL RNase A (20 mg/ml, Thermo Fisher) and 10 µL lysozyme in lysozyme buffer (100 mg/ml in 20 mM Tris-HCl pH 8, 2 mM EDTA pH 8.0, 1% v/v Triton X-100) added, mixed by inverting the tube and incubated at 37°C. After 1 h, 30 µL Proteinase K (20 mg/ml) was added, the tube inverted and incubated for 50°C for 1 h. For the phenol-chloroform extraction, the lysate was mixed with 500 µL Phenol:Chloroform:Isoamyl alcohol (25:24:1, v/v Thermo Fisher Scientific), vortexed for 1 min and centrifuged for 5 min at 4°C and 16 000 x g. The aqueous phase was transferred to a new tube, 500 µL Chloroform:Isoamyl alcohol (24:1) added, vortexed for 1 min and again centrifuged. The aqueous phase was then mixed with 0.3 volumes 7.5 M NH₄OAc (pH 5.2), 20 µg glycogen and 2 volumes of ice-cold ethanol 100%. The solution was incubated for 15 min at room temperature and the DNA subsequently pelleted by centrifugation for 30 min at 4°C and 16 000 x g. The supernatant was carefully taken off, and the DNA pellet washed with 80% ethanol. The supernatant was completely taken off, and the DNA pellet allowed to air dry for 5 min. DNA was resuspended in 20 µL of PCR molecular grade water for 1 h at 37°C.

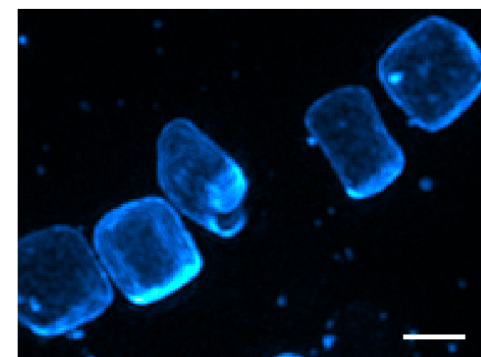
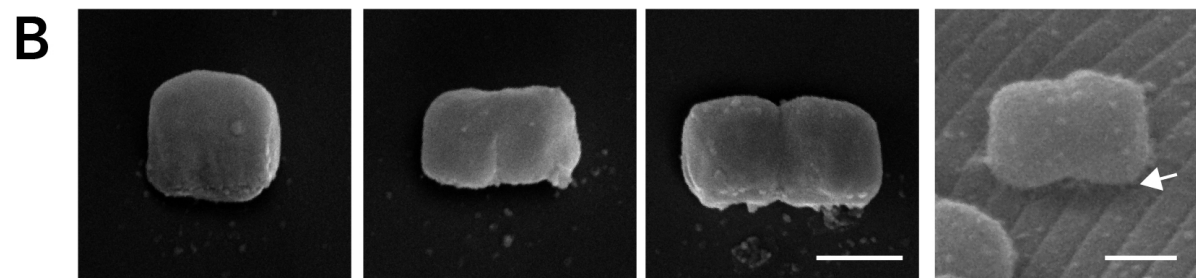
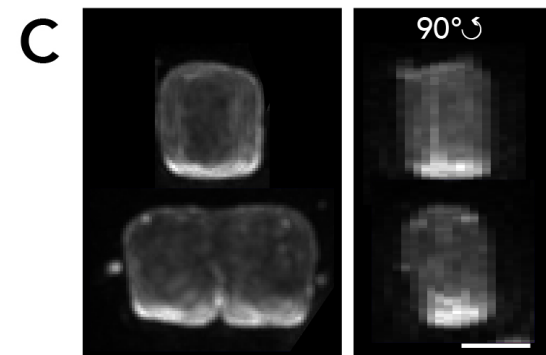
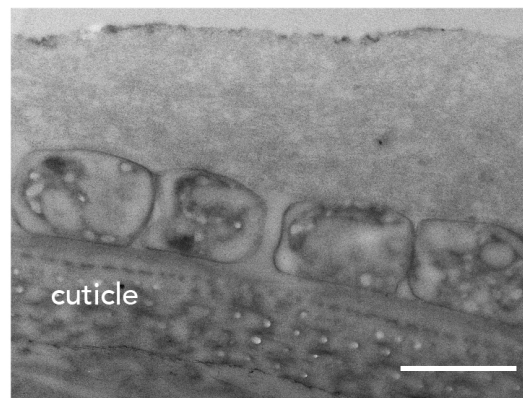
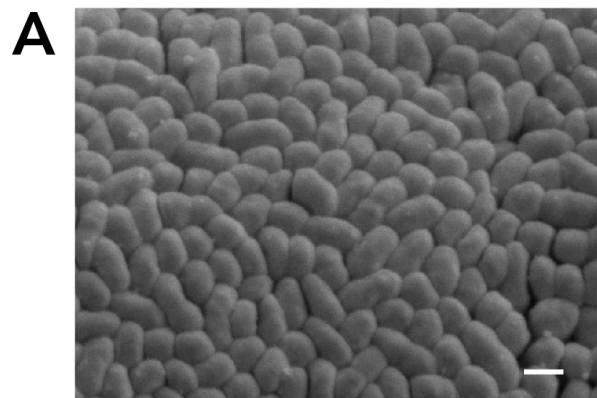
The library for Oxford Nanopore Technologies (ONT) sequencing was prepared using the ONT 1D ligation sequencing kit (SQK-LSK109) and sequenced on a R9.4 flow cell (FLO- MIN106) on a MinION for 48 h. Base calling was performed locally with ONT's Guppy Basecalling Software v3.2.4+d9ed22f, and resulting fastq-files were trimmed using Porechop version 0.2.1 (<https://github.com/rrwick/Porechop>).

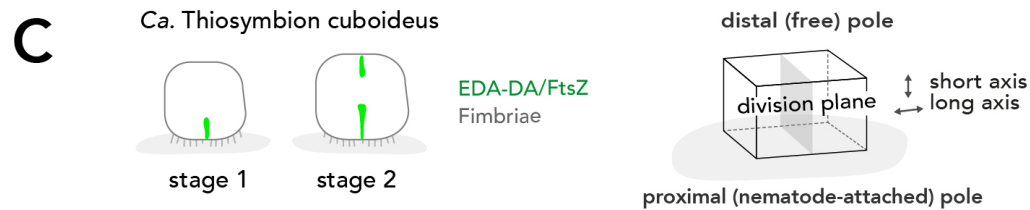
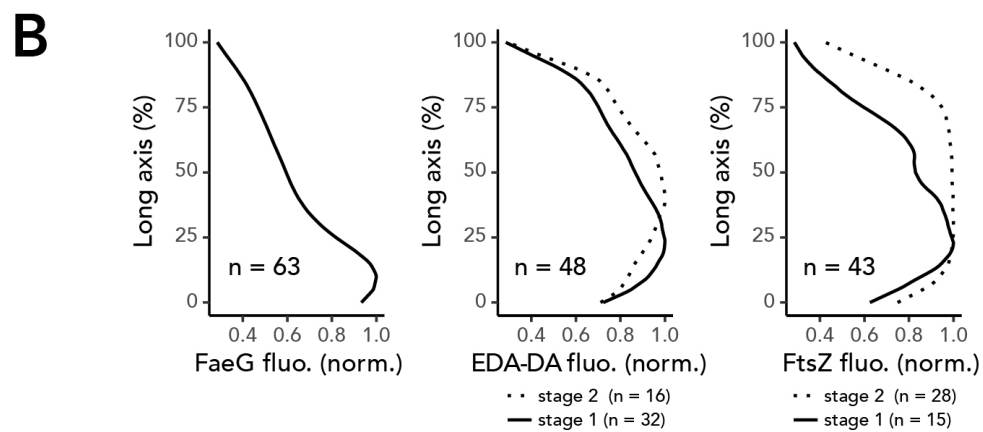
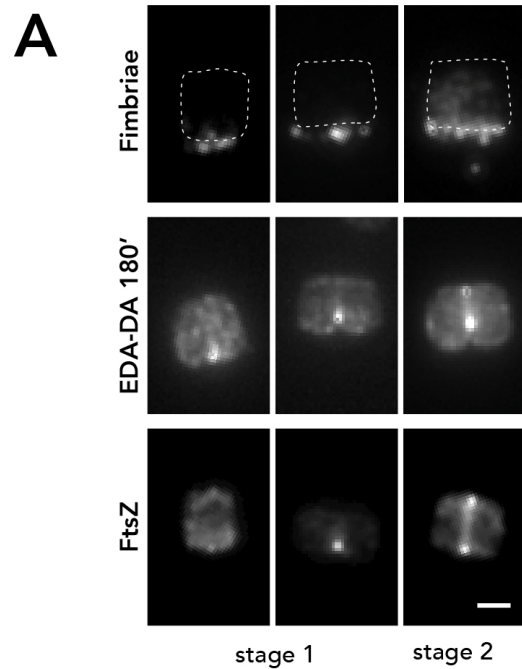
For the assembly, raw Illumina reads were quality filtered and trimmed using bbduk version 37.61 (<https://sourceforge.net/projects/bbmap/>) by a minimum quality value of 2 and minimum length of 50. Unicycler version 0.4.6 (Wick et al., 2017) was used in 'bold' mode to assemble the trimmed Illumina and ONT reads, with SPAdes version 3.13.1 in 'careful mode. The assembly was manually binned using the mmgenome2 tool (<https://github.com/KasperSkytte/mmgenome2>). The bin was further scaffolded using SSPACE LongRead version 1.1 (Boetzer and Pirovano, 2014) with the trimmed ONT reads, and ambiguous bases replaced using Gapfiller.pl version 1.10 (Nadalin et al., 2012), followed by 10 rounds of Pilon version 1.22 (Walker et al., 2014) using BWA-aln mapped reads, and contigs shorter than 200 bp were discarded.

The genome completeness was assessed using checkM version 1.0.18 (Parks et al., 2015) with the gammaproteobacterial marker gene set using the taxonomy workflow. Assembled contigs were annotated using Prokka 1.14.6 (Seemann, 2014). The genome sequence has been deposited at GenBank under the accession WYCW000000000.1. Raw reads, basecalled with Guppy Basecalling Software 4.2.2+effbaf8, have been deposited in SRA under the accession SRR13336336.

Symbiont phylogeny and FtsZ sequence alignment. For the 16S phylogenetic analysis, *Ca. Thiosymbion* 16S sequences from Scharhauser et al. 2021 were retrieved together with 16S sequences from 3 outgroup species (see Table S1 for accession numbers). The alignment was performed with mafft v7.427 (L-INS-I mode, Katoh and Standley, 2013), trimmed in TrimAl v1.4.rev15 (-gt 0.7, Capella-Gutiérrez et al., 2009) and the maximum likelihood phylogeny reconstructed using IQ-TREE v2.1.2 (Minh et al., 2020) with the best-fit model automatically selected by ModelFinder Plus (Kalyaanamoorthy et al., 2017) and 1,000 ultrafast bootstraps (Hoang et al., 2018). The phylogeny was outgroup-rooted and visualized in FigTree v1.4.4 (<http://tree.bio.ed.ac.uk/software/figtree/>).

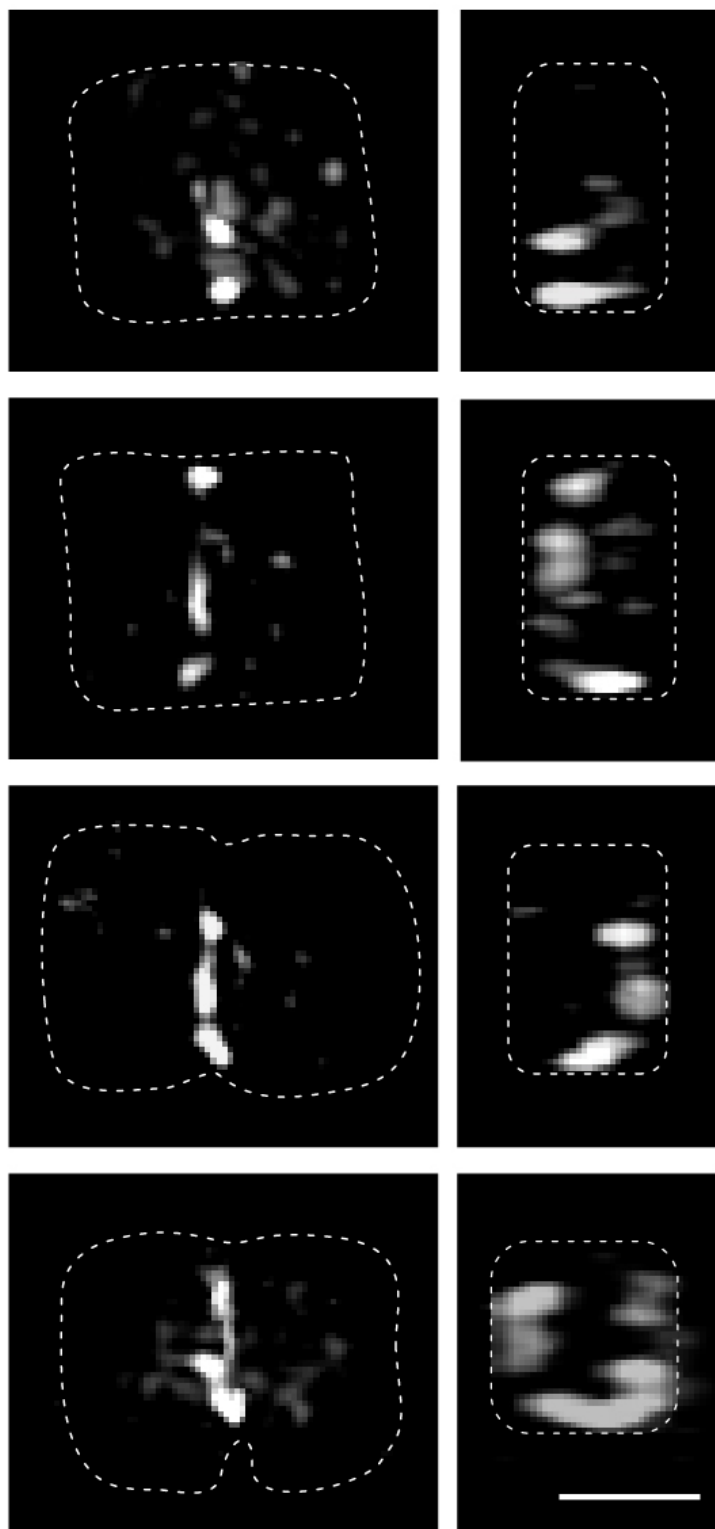
FtsZ sequences were aligned using mafft and visualized with ggmsa in R (<http://www.R-project.org/>). Identities were retrieved by a pairwise blastp (Altschul et al., 1990) and plotted with heatmap.2 in R (<http://www.R-project.org/>).

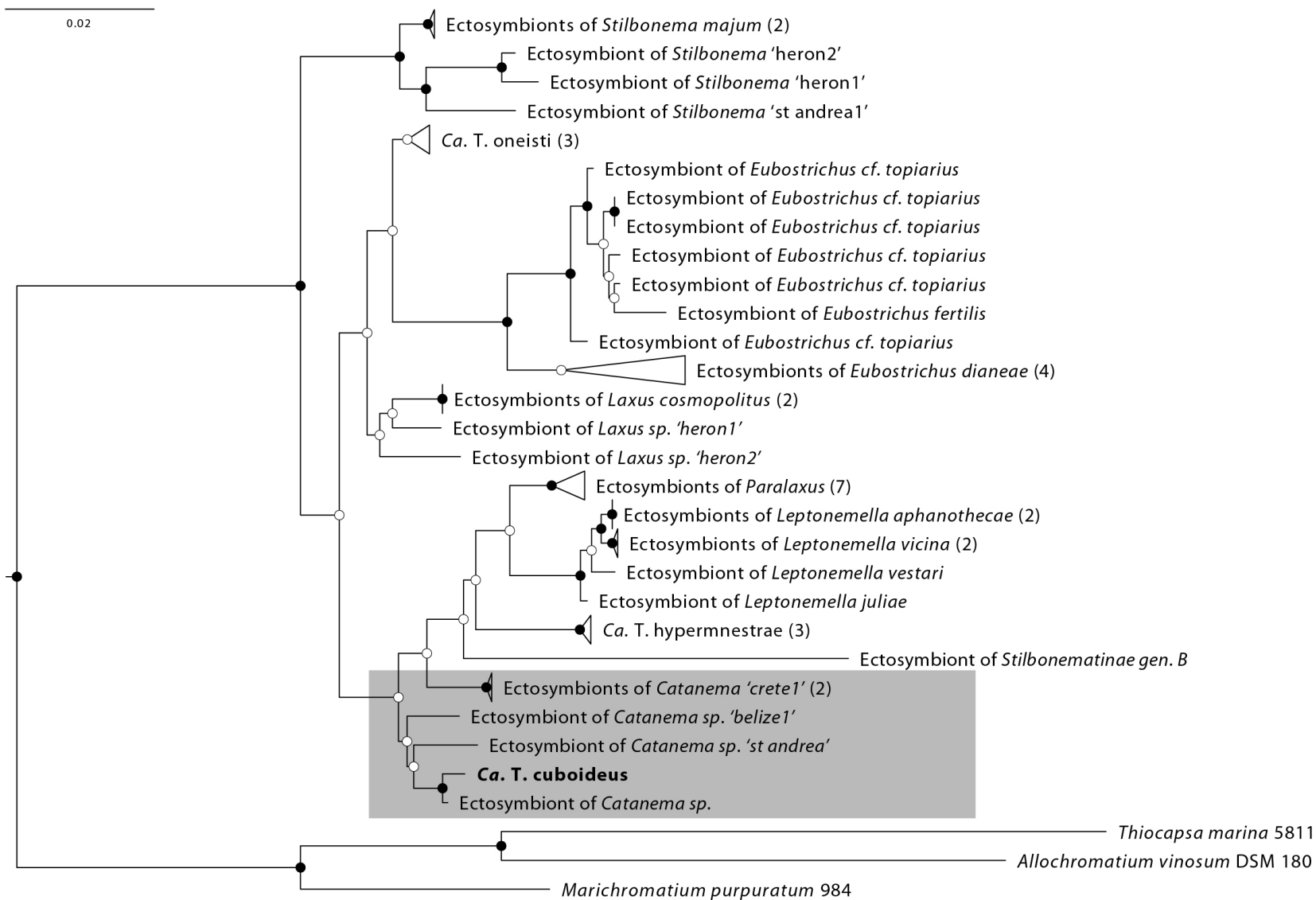




FtsZ

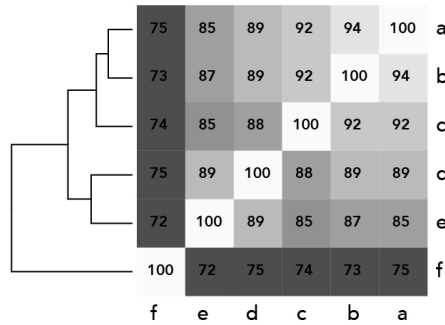
90°



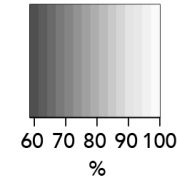


A

FtsZ



- a) *Ca. T. cuboideus*
 b) *Ca. T. oneisti*
 c) *Ca. T. hypermnestreae*
 d) Ectosymbiont of *Eubostrichus dianeae*
 e) Ectosymbiont of *Eubostrichus fertilis*
 f) *E. coli* DH5a



B

NTP

E. coli DH5a (AOO68522.1) M-F E P M E L - - T N D A V I K V I G V G G G G N A V E H M V R R I E G V E F F A V N T D A Q A L R K T A V G Q T I Q I G S G I T K G L G A G A N P E V G R N A A D E D R D A L R A A L E G A D M
Ca. T. oneisti (AFK79040.1) M-F E L V D T - N G Q A V I K V I G V G G G G N A V N Q M V E S S I E G V D F I C A N T D S Q A L K S S N V K T I L Q L G A D I T K G L G A G A D P K V G K E A A L E D K E R I H D A L E G A D M
Ca. T. hypermnestreae (ANC67818.1) M-F E L M D T - N G Q D A V I K V I G V G G G G N A V N Q M V D S A I E G V D F I C A N T D S Q A L K H S N A K T I L Q L G A D I T K G L G A G A D P K V G Q E A A L E D R E R I H D A L E G A D M
Ectosymbiont of *Eubostrichus dianeae* M-F E L V D N - N N P H A V I K V I G V G G G G N A V N Q M M E S S I E G V E F I C A N T D S Q A L K E S K V K T I L Q L G A D V T R G L G A G A N P Q V G K D A A L E D K Q R I H E V L D G A D M
Ectosymbiont of *Eubostrichus fertilis* M-K F E L V D N P N S Q N A V I K V I G V G G G G N A V N Q M M D S S I E G V E F I C A N T D S Q A L K E S K A K T I I Q L G A E T T R G L G A G A K P Q V G K D A A M E D K Q Q I Q Q A L D G A D M
Ca. T. cuboideus M-F E L M D T - N G Q D A V I K V I G V G G G G N A V N Q M V D S S I E G V D F I C A N T D S Q A L Q H S N V K T I L Q L G A D I T R G L G A G A D P K V G K Q A A L E D K E R I H D A L D G A D M

Globular Core

E. coli DH5a (AOO68522.1) V F I A A G M G G G T G T G A A P V V A E V A K D L G I L T V A V V T K P F N F E G K K R M A F A E Q G I T E L S K H V D S L I T I P N D K L L K V L G R G I S L L D A F G A A N D V L K G A V Q G I A
Ca. T. oneisti (AFK79040.1) V F I T A G M G G G T G T G A A P V V A Q V A R E L G I L T V A V V T K P F A F E G A K R M K V A V E G I S E L A S H V D S L I T I P N E K L L A V L G K E M S L L N S F K A A N D V L L N A T Q G I A
Ca. T. hypermnestreae (ANC67818.1) V F I T A G M G G G T G T G A A P I V A Q I A R E L G I L T V A V V T K P F A F E G A K R M Q V A L E G I S E L A N H V D S L I T I P N E K L L A V L G K E M S L L N A F K A A N D V L L N A T Q G I A
Ectosymbiont of *Eubostrichus dianeae* I F I T A G M G G G T G T G A A P I V A Q V A R E L G I L T V A V V T K P F V F E G S K R M K V A M D G I A E L T D H V D S L I T I P N E K L L A V L G K E M T L L N A F K A A N N V L L N A T Q G I A
Ectosymbiont of *Eubostrichus fertilis* I F I T A G M G G G T G T G A A P I V A Q V A K E L D I L T V A V V T K P F V F E G S K R M N I A R D G I D E L A K H V D S L I T I P N E K L L A V L G K E M T L L S A F K E A N N V L L N A T Q G I A
Ca. T. cuboideus V F I T A G M G G G T G T G A A P V V A Q V A R E L G I L T V A V V T K P F A F E G T K R M K V A M E G I S E L A D N V D S L I T I P N E K L L A V L G K E M S L L N A F K A A N D V L L N A T Q G I A

E. coli DH5a (AOO68522.1) E L I T R P G L M N V D F A D V R T V M S E M G Y A M M G S G V A S G E D R A E E A A E M A I S S P L L E D I D L S G A R G V L V N I T A G F D L R L D E F E T V G N T I R A F A S D N A T V V I G T S
Ca. T. oneisti (AFK79040.1) E L I T R P G L I N V D F A D V K T V M A E M G Q A M M G T G I A S G E Q R A R E A A E A A I N S P L L E D I D L A G A K G I L V N I T A G M S L S I G E F F D E V G N T V R D F A D D D A I V V V G T V
Ca. T. hypermnestreae (ANC67818.1) E L I T C P G L I N V D F A D I K T V M A E M G Q A M M G T G A A S G E Q R A R D A A E A A I N S P L L E D I D L A G A K G I L V N I T A G M S L S I G E F F D E V G N T V R D F A D D D A T V V V G T V
Ectosymbiont of *Eubostrichus dianeae* E L I T R P G L I N V D F A D V K T V M A E M G Q A M M G T G S A K G E Q R A R E A A E A A I H S P L L E D I D L A G A K G I L V N I T A G M D L S I G E F F D E V G N T V R D F A D D E A M V V V G T V
Ectosymbiont of *Eubostrichus fertilis* E L I T R P G L I N V D F A D V K T V M A E M G Q A M M G T G N A K G E Q R A E K A A K D A I N S P L L E D I D L S G A R G I L V N I T A G M D L S I G E F F D E V G N T V R E F A D E E A M V V V G T V
Ca. T. cuboideus E L I T C P G L I N V D F A D V K T V M A E M G Q A M M G T G V A S G E Q R A R E A A E A A I R S P L L E D I D L A G A R G I L V N I T A G P S L S I G E F F D E V G N T V R D F A D D D A I V V V G T V

C-terminal linker

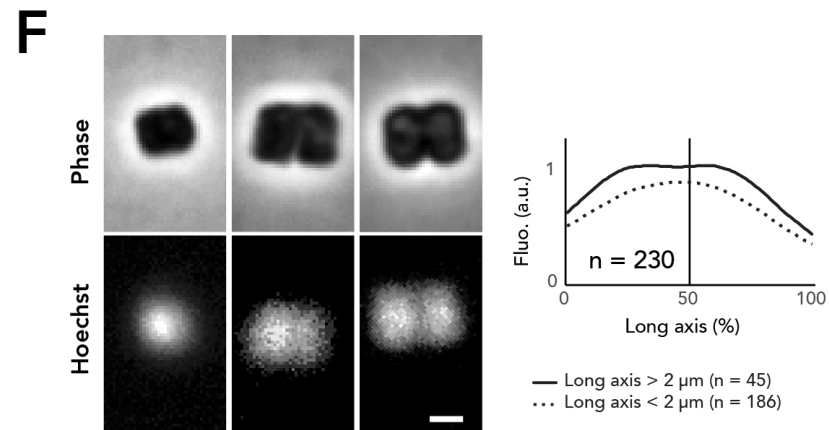
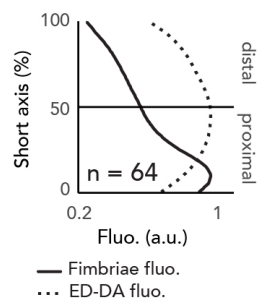
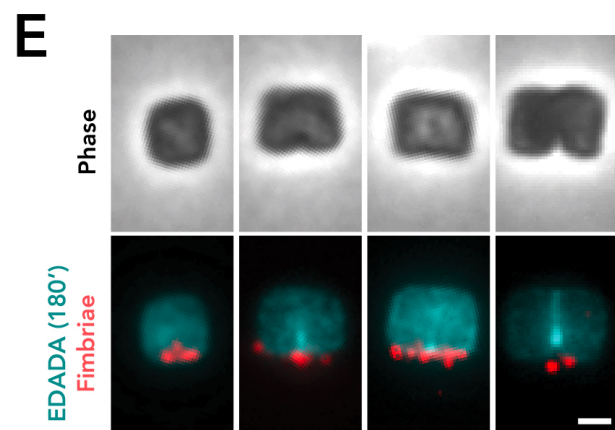
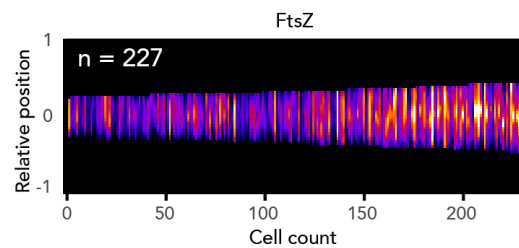
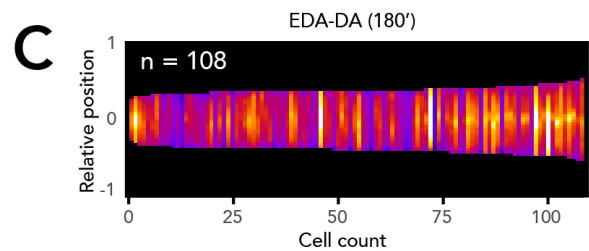
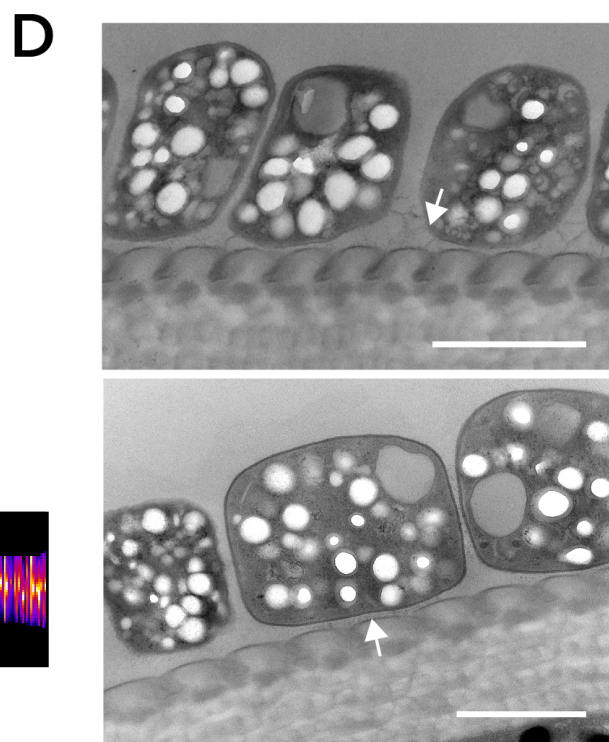
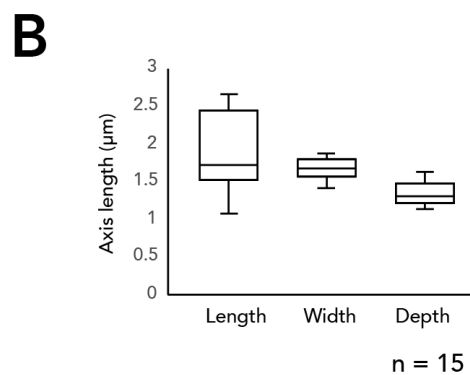
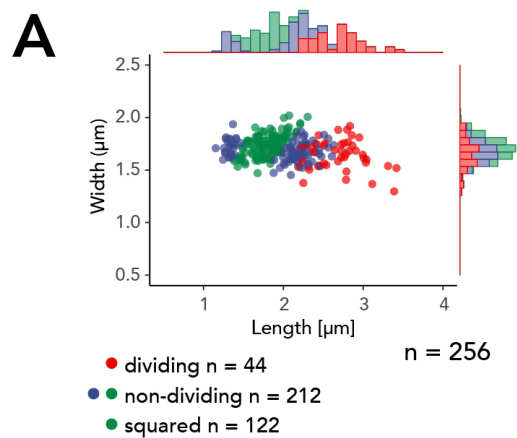
E. coli DH5a (AOO68522.1) L D P D M N D E L R V T V V A T G I G M D K R P E - - - - - I T L V T N - - - - - K Q V Q Q P V M D R Y Q - - - Q H G M A P L - - T Q E Q K P V A K V V N D N A P Q T A K E P D Y
Ca. T. oneisti (AFK79040.1) I D P D L S E E L R V T V V A T G L G E G R K A Q L S K P A M G - E S P I H L V P R G G T G S V T P D Y R D M E R P A V Y R K G - - Y Q G V A A A A V A Q A H P D A V E - - - - - E T D L D Y
Ca. T. hypermnestreae (ANC67818.1) I D S N L S E E L R V T V V A T G L G K R N K A Q - P R L A V G - E P A L H L V S N G I T E T A T P D Y R L D R P A V Y R N K G - - H Q G G T A A A A T Q A Q A D T A G - - - - - E K N L D Y
Ectosymbiont of *Eubostrichus dianeae* I D P E L E D E L R V T V V A T G L G E G G G V E A P K P A T G - Q A P I H L V A N R A A E S V A P D Y R E M E R P A V H R K G G - - - - - A R A Q T E P - - - - - D D D L D Y
Ectosymbiont of *Eubostrichus fertilis* I D P E L E D E L R V T V V A T G L G E G L A M E A P K P V R G H Q A P I H L V A N G S E E S P P T D Y R A M D R P T V S R K R G G S Q V G M A A A A R A Q A E P V S G A - - - - - E D D L D Y
Ca. T. cuboideus I D P D L N E D L R V T V V A T G L G E G R K A R V S K S A L G - G S P I H L V P N E V A E S V T P D Y R E M D R P A V Y R K G - - - H Q G V A A A - - V Q T Q P D A V G - - - - - E T D L D Y

CTT

CTV

E. coli DH5a (AOO68522.1) L D I P A F L R K Q A D
Ca. T. oneisti (AFK79040.1) L D I P A F L R H Q A D
Ca. T. hypermnestreae (ANC67818.1) L D I P A F L R R Q A N
Ectosymbiont of *Eubostrichus dianeae* L D I P A F L R R Q A D
Ectosymbiont of *Eubostrichus fertilis* L D I P A F L R R Q A D
Ca. T. cuboideus L D I P A F L R R Q A D

NTP: N-terminal peptide
 CTT: C-terminal tail
 CTV: C-terminal variable region



CHAPTER V

CONCLUSIVE DISCUSSION

CONCLUSIVE REMARKS

OUTLOOK

CONCLUSIVE DISCUSSION

My thesis aimed at better understanding the unique symbiosis between an animal, the nematode *Laxus oneistus*, and the one bacterial species coating its surface, the gammaproteobacterium *Candidatus Thiosymbion oneisti*. Namely, we applied omics and stable isotope-based techniques to elucidate how the bacterium (Chapter II) and the nematode (Chapter III) react to environmental changes (in particular to oxygen, as the worm occurs at oxic-anoxic interfaces). Moreover, we tried to link symbiont physiology with cell biology by investigating how longitudinally dividing symbionts configure and segregate their chromosomes and how a cube-like symbiont divides (Chapter IV). Given that the obtained results are extensively discussed in their respective chapters (Chapters II, III, and IV), this Conclusive Discussion will only tackle selected key discoveries from Chapters II, III, and IV.

5.1 Novel insights on *Candidatus Thiosymbion oneisti* physiology

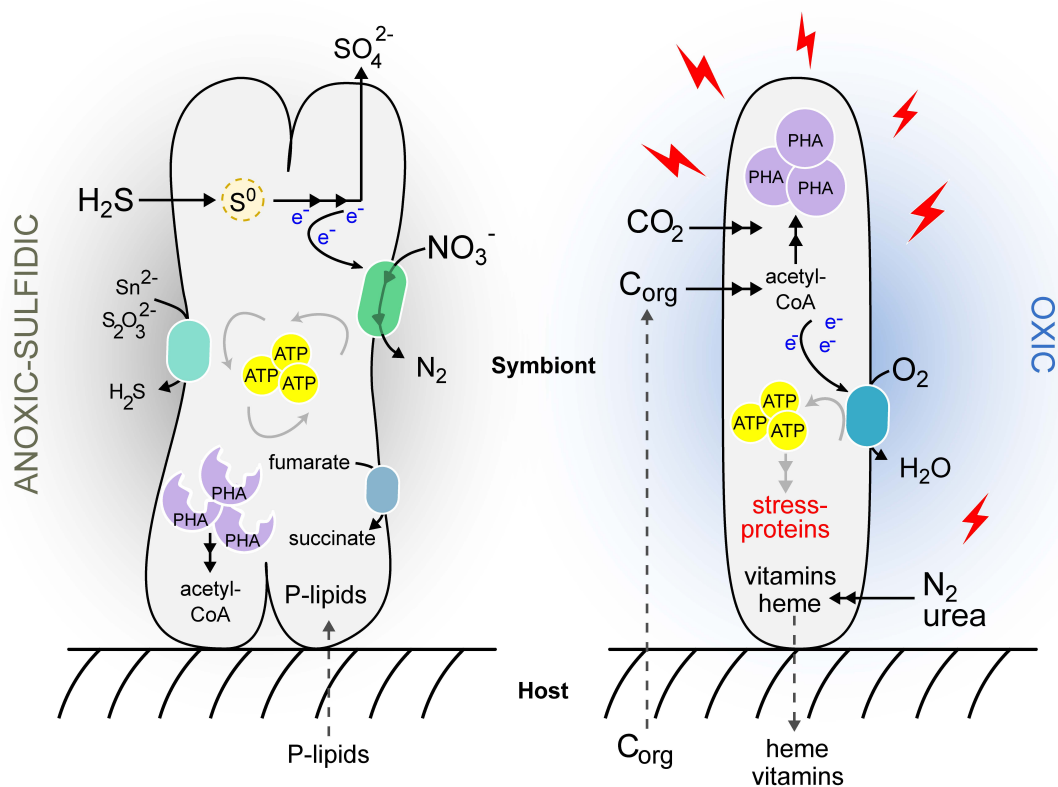


Figure 1. Schematic representation of *Ca. T. oneisti*'s suggested metabolism in deep anoxic and in superficial sand (Paredes et al., 2021). Note that the illustrated processes likely occur under both anoxic, sulfidic (AS) and oxic (O) conditions, but the model highlights those proposed to be dominant in one condition over the other. C_{org}: small organic compounds, PHA: polyhydroxyalkanoates, P-lipids: phospholipids.

Oxygen is to a certain extent essential to life (Semenza, 2007; Lane and Martin, 2010). Even anoxia-tolerant animals that are capable of sustaining long anoxic periods (e.g., days or months) need at some point to respire it if they want to continue living (Hochachka and Lutz, 2001). In the chemosynthetic symbioses arena, its relevance has not gone unnoticed. Indeed, as illustrated in Dubilier et al., 2008, despite being remarkably metabolically versatile, chemosynthetic symbionts share the ability to respire the electron acceptor with the highest energy yield: oxygen. However, in the marine environment, frequently, this substrate is found spatially separated from the electron donors needed for energy generation and biomass buildup (Canfield and Thamdrup, 2009; Luther et al., 2011). For example, oxygen is present in upper sand layers, while sulfide is predominantly present in deeper anoxic sand.

On the one hand, the need to bridge the gap between oxygen and sulfide likely pushed some sulfur-oxidizing free-living bacteria, referred to as cable bacteria, to elongate (Nielsen et al., 2010; Pfeffer et al., 2012). On the other hand, some other thiotrophs evolved stable associations with animals which, thanks to their behavior, may expose their symbionts to both substrates (reviewed in Ott et al., 2004a, b; Stewart et al., 2005; Cavanaugh et al., 2006; Dubilier et al., 2008). An example of such behavior is the vertical migration of Stilbonematinae across the upper oxygenated and deeper anoxic sulfidic sediment layers (Ott and Novak., 1989; Schiemer et al., 1990; Ott et al., 1991). If up to this work, the worm migrations through the chemocline were regarded as the primal reason for the bacteria to associate with its host, its response to oxygen revealed unexpected evolutionary scenarios (Figure 1).

Loose coupling between sulfur oxidation and inorganic carbon fixation

Paredes et al., 2021 (Chapter II) is the first study describing the global physiological response of an animal ectosymbiont (*Ca. Thiosymbion oneisti*) to oxygen. Collectively, our data indicated that this oxidant (and to a much lesser degree sulfide) was the main factor affecting sym-

biont gene expression. Moreover, our analysis supports previous observations of Stilbonematinae ectosymbionts showing aerobic and anaerobic sulfur oxidation (Schiemer et al., 1990; Hentschel et al., 1999). However, it invites to revise the vertical migration premise that posits: once in the presence of oxygen, the sulfur oxidation of the symbiont powers carbon fixation (Ott et al., 1991; Polz et al., 2000; Ott et al., 2004a, b). Indeed, although sulfur oxidation genes were upregulated under anoxia, this was not accompanied by the upregulation of autotrophic carbon fixation genes. On the contrary, the latter (e.g., *cbbS*, the small subunit of RuBisCO) had a higher expression in the presence of oxygen. Importantly, however, bulk isotope ratio mass spectrometry (EA-IRMS) values indicated no significant difference in the incorporation of ^{13}C -labeled CO_2 between anoxic and oxic conditions. Therefore, we hypothesized that this discrepancy between the transcriptomic and the EA-IRMS data might be related to the dual nature of RuBisCO, which uses both O_2 and CO_2 as substrates (Jordan and Ogren, 1981; Badger and Bek, 2008). Thus, this might reflect a tradeoff between the carboxylase and oxygenase activity when oxygen is present.

The apparent loose coupling between sulfur oxidation and inorganic carbon fixation in *Ca. T. oneisti* was surprising, as the concept of thiotrophy is deeply connected to the fuel of primary productivity (carbon fixation) (Van Dover et al., 2000; Dubilier et al., 2008). Indeed, there is vast evidence that reduced sulfur compounds enhance carbon fixation in thiotrophic symbionts (e.g., Cavanaugh et al., 1983; Schiemer et al., 1990; Childress et al., 1991; Markert et al., 2007; Scott et al., 2007; Ponsard et al., 2013; Seston et al., 2016).

In addition, we hypothesized that in anoxic sulfidic layers, sulfur oxidation might be greatly supported by denitrification. Upholding evidence was the upregulation in the anoxic sulfidic condition (AS), of the four denitrification enzyme complexes (Nap, Nir, Nor, Nos), and of Complex II of the electron transport chain (ETC), known to also be involved in denitrification (Chen et al., 2013). Therefore, my results urge to reconsider the importance of nitrate, not only in nitrogen assimilation, but also in respiration (Dubilier et al., 2008). Besides nitrate (Hentschel et al., 1999; Petersen et al., 2016), genomics, transcriptomics and proteomics indicated that *Ca. Thiosymbion* might use additional anaerobic electron acceptors such as fumarate, polysulfide or thiosulfate.

Enhanced mixotrophy in the presence of oxygen

Thiotrophic symbionts are canonically viewed as autotrophs (Cavanaugh et al., 2006; Dubilier et al., 2008). However, there is increasing evidence of their complex metabolism, which can even comprise obligate heterotrophy (Seah et al., 2019). Based on genomics, *Ca. T. oneisti* is capable of using several organic carbon compounds as electron donors and thus it might engage in mixotrophy (Petersen et al., 2016; Paredes et al., 2021). Indeed, transcriptomics indicated that, in addition to carbon fixation, their heterotrophic metabolism seems to be stimulated in the presence of oxygen, likely resulting in a higher carbon availability under this condition. Consistently, we observed the upregulation of storage compounds-related genes (e.g., PHA, trehalose, and glycogen) in the presence of oxygen. Based on these lines of evidence, heterotrophy might be an important strategy for nutrient acquisition in *Ca. T. oneisti*; hence, pigeonholing it as thiotroph would oversimplify its metabolism.

Nitrogen fixation appears to be stimulated in oxic conditions

The first study that identified nitrogen fixation genes in *Ca. T. oneisti* (Petersen et al., 2016) hypothesized that diazotrophy would only occur in deep anoxic sediment layers due to the oxygen-sensitive nature of the nitrogenase (Hill et al., 1988). Although stable isotope-based techniques could show symbiotic nitrogen fixation under neither anoxic nor oxic conditions (G.F. Paredes and W. Mohr, unpublished data), genes related to nitrogen fixation (e.g., *nifB*, *nifD*, *nifK*) were, unexpectedly, upregulated in the presence of oxygen. In Paredes et al. (2021), and as shown for other nitrogen-fixing bacteria (Bentzon et al., 2015), we put forward that fixed nitrogen, aside from being assimilated, might function as an electron sink to maintain redox homeostasis under heterotrophic conditions. Indeed, under oxic conditions, a higher carbon availability could create nitrogen limitation, and hence, the need to spark nitrogen uptake (Sorgo et al., 2002; Rogers et al., 2006; Elgharably et al., 2011; Petersen et al., 2016). The latter could explain that, aside from nitrogen fixation-related genes, urea assimilation genes were also upregulated. Furthermore, enhanced nitrogen assimilation might be linked to the global stress response observed in the presence of oxygen, requiring nitrogen-containing compounds, such as vitamins (Paredes et al., 2021).

Interestingly, the ability to perform nitrogen fixation was shown in *Candidatus* Thiodiazotropha endoloripes, the endosymbiont of the lucinid clam *Loripes lucinalis*. Although this inhabits the oxygen-exposed gills of the animal, the strategy adopted to avoid nitrogenase inhibition is unknown (Petersen et al., 2016). The external location of *Ca. T. oneisti* makes the upregulation of nitrogen fixation genes under oxic conditions even more puzzling.

5.2 Novel insights on *Laxus oneistus* physiology

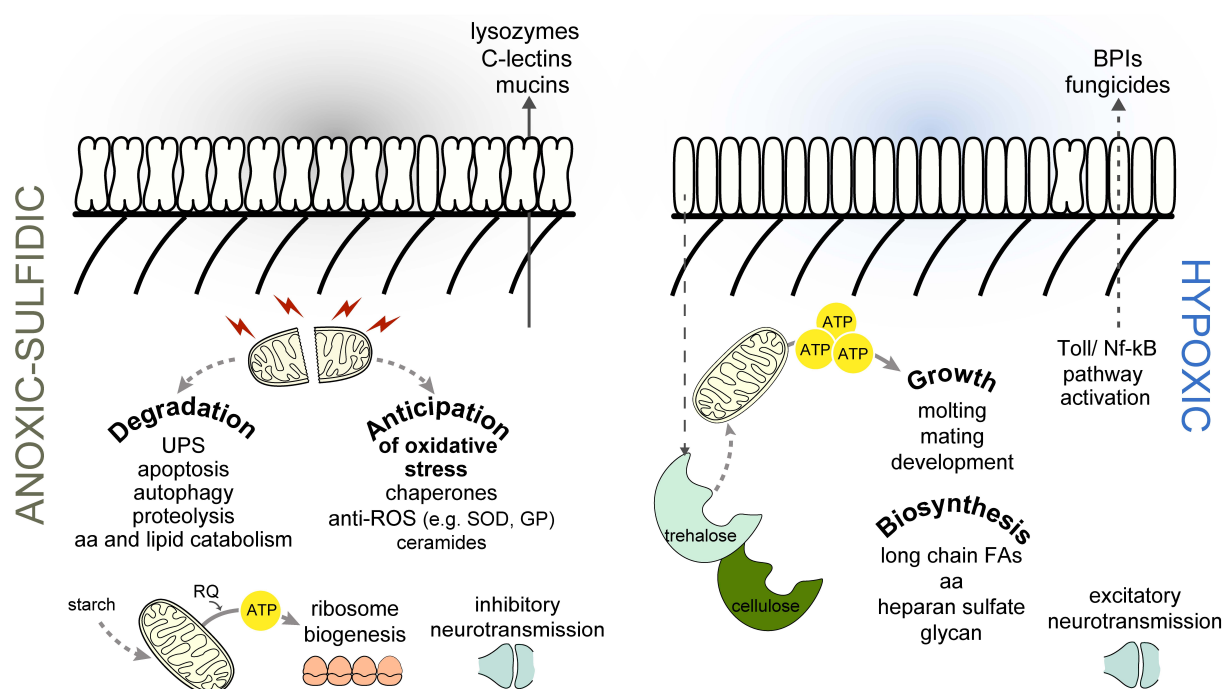


Figure 2. Schematic representation of *Laxus oneistus*' suggested metabolism in deep anoxic and in superficial sand (Paredes et al., *under review*). Note that the illustrated processes likely occur under both conditions, but the model highlights those proposed to be dominant in one condition over the other. AA: amino acids, BPIs: Bactericidal/permeability-increasing proteins, FA: fatty acids, GP: glutathione peroxidase, RQ: rhodoquinone, UPS: Ubiquitin-proteasome system, SOD: superoxide dismutase.

A wealth of physiological studies on chemosynthetic symbionts are available (e.g., Markert et al., 2007; Zbinden et al., 2008; Kleiner et al., 2012; Seston et al., 2016; Jäckle et al., 2019; Seah et al., 2020; Paredes et al., 2021) and significant progress has been made in understanding the physiology of host bearing chemosynthetic endosymbionts (e.g., Bettencourt et al., 2010; Osca et al., 2014; Wippler et al., 2016; Hinzke et al., 2019; Wang et al., 2019; Yuen et al., 2019;

Yang et al., 2020; Ip et al., 2021). However, much less is known about animals harboring external chemosynthetic bacteria (Lin et al., 2021). In Chapter III, we described the physiological response to oxygen of such an animal, *Laxus oneistus*, by means of the first *de novo* transcriptome of a Stilbonematinae (Paredes et al., *under review*). The latter comprised 22,072 taxonomy-filtered transcripts with at least one functional annotation, a value similar to what was obtained for the transcriptome of the Lucinid clam *Loripes orbiculatus* (20,163) (Yuen et al., 2019). Moreover, 74.9% of the predicted protein-encoding genes (i.e. 16,526 out of 22,072) were expressed.

Vertical migrations: natural ischemic/reperfusion events

Several organisms such as free-living nematodes (e.g., *Caenorhabditis elegans*), pathogenic nematodes, and marine animals are likely to experience oxygen depletion in their natural habitats (Fenchel and Finlay, 1995; Danovaro et al., 2016; Kitazume et al., 2018). Despite this, they all eventually require the reintroduction of sufficient amounts of oxygen for their development and reproduction (Hochachka and Lutz, 2001). Oddly enough, also the re-exposure to oxygen can be deadly as it abruptly introduces reactive oxygen species (ROS) back to the organism (Hermes-Lima and Zenteno-Savín, 2002; Kalogeris et al., 2016; Galli and Richards, 2014). This scenario resembles what in medicine is called ischemia/reperfusion injury events. The first as proxy of oxygen shortage (hypoxia or anoxia), and the second as synonym of re-oxygenation (Borutaite et al., 1995; Moncada and Erusalimsky, 2002; Kowaltowski et al., 2009; Fago et al., 2015). Therefore, several anoxia-tolerant organisms anticipate reoxygenation by upregulating their antioxidant defense (reviewed in Hermes-Lima and Zenteno-Savín, 2002). In the case of *L. oneistus* ischemic/reperfusion events can be expected due to the behavioral tactic of migrating across anoxic sulfidic and oxygenated sediment layers (Ott et al., 1991). While the first environment might offer the advantage of not having to cope with predators that shun toxic compounds such as sulfide (Fenchel and Riedl, 1970), up until my thesis, nothing was known about how *L. oneistus* might react to oxygen.

***Laxus oneistus* does not enter suspended animation in anoxic sulfidic conditions**

Transcriptomics analysis of *L. oneistus* incubated in anoxia showed that it kept engaging in energy-demanding processes (e.g., ribosome biogenesis) even after 24 h. Moreover, *L. oneistus* did not stop moving even after a 6-day-long incubation in anoxia (Paredes et al., *under review*). This was remarkable as suspended animation (i.e., movement arrest, metabolic depression, and developmental arrest) is commonly adopted to survive ATP scarcity due to oxygen deprivation by animals, including the model organisms *Artemia franciscana*, *Drosophila melanogaster*, and *C. elegans* (Hochachka and Lutz, 2001; Clegg, 1997; Wingrove and O’Farrell, 1999; Van Voorhies and Ward, 2000; Padilla et al., 2002; Kitazume et al., 2018). For example, *D. melanogaster* undergoes suspended animation only after approximately 5 h in anoxia (Haddad, 2006) and some nematodes (e.g., *C. elegans*, *Bursaphelenchus xylophilus*) after 7 h (Kitazume et al., 2018).

Based on what is presented in Chapter III and further discussed below, we hypothesize that *L. oneistus* avoids entering suspended animation by regulating gene expression. Indeed, 4.8 % of the expressed genes (i.e. 787 out of 16,526) were found to be differentially expressed between the anoxic sulfidic (AS) and hypoxic (H) conditions (Figure 2), the ones preferred by the worm (Ott and Novak, 1989; Paredes et al., 2021). Differentially expressed genes will be further discussed below.

Chaperones and detoxification genes are upregulated in anoxic sulfidic conditions

In turtles, ROS production has been reported up to 4 h upon anoxia onset, where the intracellular conditions might still be hypoxic; however, it then ceased (Milton et al., 2007). Therefore, as ROS are not generated in anoxia (Hermes-Lima and Zenteno-Savín, 2002), we postulate that the apparent upregulation of antioxidant genes (e.g., superoxide dismutase and glutathione peroxidase) and chaperones found in AS worms might be an anticipatory response to re-oxygenation. Indeed, as previously anticipated, to withstand a massive reintroduction of ROS, anoxia-tolerant animals upregulate their oxidative defense before switching from an anoxic environment to an oxygenated one (reviewed in Hermes-Lima and Zenteno-Savín, 2002).

Alternatively, the presence of residual oxygen in the tissue of *L. oneistus* nematodes incubated in anoxic seawater could also cause ROS production (Nystul and Roth, 2004; Selivanov et al., 2009).

AS worms may turn damaged cellular components into food and may respire them by rewiring the ETC

The transcriptional profile of *L. oneistus* suggests that catabolic processes are relevant in anoxic sulfidic conditions. Namely, we found upregulation of genes related to degradation processes such as the ubiquitin-proteasome system (UPS), autophagy, apoptosis, and genes mediating amino acids and fatty acids degradation. Degradation processes might turn damaged cellular components (e.g., mitochondria) and misfolded proteins into nutrients and thus contribute to their recycling (Thompson et al., 2005). Of note, mitochondria of AS worms may be damaged by ROS generated by residual intracellular oxygen (Nystul and Roth, 2004; Kim and Jin, 2015), or independently from ROS, as expected in anoxia (Galli et al., 2014).

Surprisingly, *L. oneistus* upregulated both genes involved in mitochondrial and cytoplasmic ribosome biogenesis. These energy-demanding processes (Powers, 2004) might be supported by the energy generation-related genes, which were all upregulated in AS worms. These included genes related to complexes I, II, IV, and V of the ETC and a mitochondrial gene (*coq-5*). The latter is putatively involved in the synthesis of the anaerobic electron carrier rhodoquinone (RQ) (Buceta et al., 2019). We propose that ETC is rewired in such a way as to use RQ and fumarate as the electron carrier and acceptor, respectively (Buceta et al., 2019; Del Borrello et al., 2019). This would sustain cellular ATP production and enable *L. oneistus* to avoid suspended animation.

Managing a poison: sulfide detoxification in anoxic sulfidic conditions

A main issue for marine meiofauna inhabiting sulfidic sediments is how to detoxify this toxic compound (reviewed in Cavanaugh et al., 2006). Common strategies are the accumulation of sulfur-rich amino acids such as taurine (Conway and Capuzzo, 1992; Pruski et al., 2000, 2003; Joyner et al., 2003) and the mitochondrial oxidation of sulfide into thiosulfate assisted by cytochrome *c* (Powell and Somero, 1986; O'Brien and Vetter, 1990; Yong and Searcy, 2001).

Given that a cysteine dioxygenase (which catalyzes taurine synthesis; Rose et al., 2017) and a cytochrome c subunit (Williams et al., 2005) were upregulated under anoxic sulfidic conditions, the worm might also mediate sulfide detoxification through the formation of taurine and mitochondrial sulfide oxidation. Additionally, *L. oneistus* might detoxify sulfide through the use of persulfide dioxygenases (*ethe-1*) (Budde et al., 2011).

Biosynthetic processes are predominant in hypoxia

For most animals, including humans, low oxygen concentrations can be harmful (Lutz et al., 1996; Fago et al., 2015). Nematodes, instead, are known to thrive and even extend their lifestyle in hypoxia (Leiser et al., 2013; Kitazume et al., 2018). They may achieve this due to the lack of a circulatory system and mainly rely on oxygen diffusion (Hochachka et al., 1993). Our data indicate that *L. oneistus* is well-adapted to hypoxia. Indeed, we observed an overall upregulation of genes related to energy-costly biological processes, such as development, feeding, mating behavior, as well as carbohydrate metabolism, and amino acid and lipid synthesis in H worms (relative to AS worms). These might be supported by the enhanced excitatory neuronal response, and by glycolysis coupled with oxidative phosphorylation, as suggested by the upregulation of acetylcholine-related genes and sugar transporters, respectively.

Additionally, trehalose might be a well-liked carbon source in hypoxia, as a trehalase gene (*tre-1*) was found upregulated under this condition. Interestingly, this sugar can act as an osmotic protectant and membrane stabilizer under different stressors (Crowe et al., 1987; Carpenter et al., 1988). Therefore, to maintain membrane integrity, animals experiencing anoxia (and thus at the risk of membrane depolymerization) (Galli et al., 2014) might prefer to mainly mobilize trehalose when again in the presence of oxygen (Clegg et al., 1997).

Impact of oxygen on host immunity

When *L. oneistus* was incubated in anoxic sulfidic conditions, genes related to immune effectors such as lectins, mucins, and one lysozyme, all likely involved in the specific attachment of its symbiont (Nussbaumer et al., 2004, Bulgheresi et al., 2006, 2011; Koropatkin et al., 2012; Ott et al., 2021) were upregulated (Paredes et al., *under review*). Interestingly, the latter fosters symbiont proliferation (Paredes et al., 2021).

On the other hand, Toll receptor-related genes and several antimicrobial-encoding genes (e.g., Bactericidal/permeability-increasing proteins (BPIs) and fungicides) were all upregulated in hypoxia. In oxygenated environments, this response might have evolved to protect the worm from predation and from pathogenic members of the bacterioplankton (Dang and Lovell, 2016; M. Mussman, personal communication). BPIs might also serve to control symbiont proliferation (e.g., Login et al., 2011) and/or might be needed for the host to develop (Krasity et al., 2011; Nyholm and McFall-Ngai, 2021). Most notably, transcripts of the nuclear transcription factor kappa B (NF- κ B) were identified in all host transcriptomes. This factor belongs to the highly conserved Toll/NF- κ B signal transduction pathway involved in the regulation of the immune response of animals to microbe-associated molecular patterns (MAMPs) (Hoffmann et al., 1999; Goodson et al., 2020). This observation was striking as, up to this study, no nematode was known to possess an NF- κ B orthologue (Pujol et al., 2001; Ott et al., 2021). Further studies lie ahead to prove whether this factor is required for the *Laxus*-Thiosymbion symbiosis establishment.

Putative inter-partner metabolic exchange

To find out the physiological processes an ectosymbiotic worm must engage with, irrespectively of the environmental concentrations, we pooled all the available 16 transcriptomes (O, H, A, AS), and detected the 100 most abundant transcripts out of the 16,526 predicted protein-encoding genes. Genes involved in ubiquitination, energy generation, oxidative stress and immune response, development, cell adhesion, cytoskeleton, locomotion, nervous system, carbohydrate metabolism, and translation were among the most expressed in *L. oneistus*. In contrast to what was shown for other chemosynthetic animals, the main processes undertaken by *L. oneistus* could not be directly related to its symbiotic lifestyle. Namely, transcriptomics of deep-sea mussels, the tubeworm *R. pachyptila*, and shallow-water clams showed that they greatly engage in symbiont recognition, establishment, control, and recycling (Sun et al., 2017, Hinzke et al., 2019; Yuen et al., 2019). However, when comparing transcriptomes of the gutless oligochaete *O. algarvensis* and *L. oneistus*, we could observe a partial overlap of the highest expressed gene categories (e.g., energy generation, oxidative stress). We ascribe this overlap to the fact that the two worms share the same habitat (Woyke et al., 2006).

Although omics and stable isotope-based techniques (Chapters II and III) might allude to a low degree of metabolic interdependence between *Laxus* and its Thiosymbiont, we determined putative nutritional links between the partners. Namely, lipidomics showed that phosphatidylcholine was more abundant in the anoxic symbiont, even though the latter cannot synthesize it (Paredes et al., 2021). Thus, the upregulation of genes (*pmt-1* and *pmt-2*, Brendza et al., 2007) related to its biosynthesis in AS worms (Paredes et al., *under review*) could be an indication of worm-to-symbiont lipid transfer.

Additionally, metabolomics detected hydrocarbons in the symbiont fraction (e.g., hexadecane, eicosane, docosane), which based on the symbiont genome draft and the host transcriptome, could also be host-derived. Further comparison of the symbiont genome and the nematode transcriptome allows us to hypothesize symbiont-to-host transfer of sucrose, heme, all B-vitamins, essential amino acids (except B6 and threonine, respectively), and a wide array of small organic carbon compounds (e.g., acetate, lactate, propionate). Metabolomics also supported the symbiont-to-host transfer of sucrose and trehalose (Paredes et al., *under review*).

Finally, it is hypothesized that Stilbonematinae might gain carbon and energy from grazing on their bacteria (Ott et al., 2004a, b). Hints of bacterial digestion were the high expression of a gene encoding acid phosphatase (*acp-7*-like) (among the top 100 expressed transcripts across all conditions), and the upregulation of two acid phosphatases and two arylsulfatases in H worms, all considered markers of lysosomal activity (Yuen et al., 2019).

5.3 Linking the physiology of *Candidatus Thiosymbion* with its cell biology

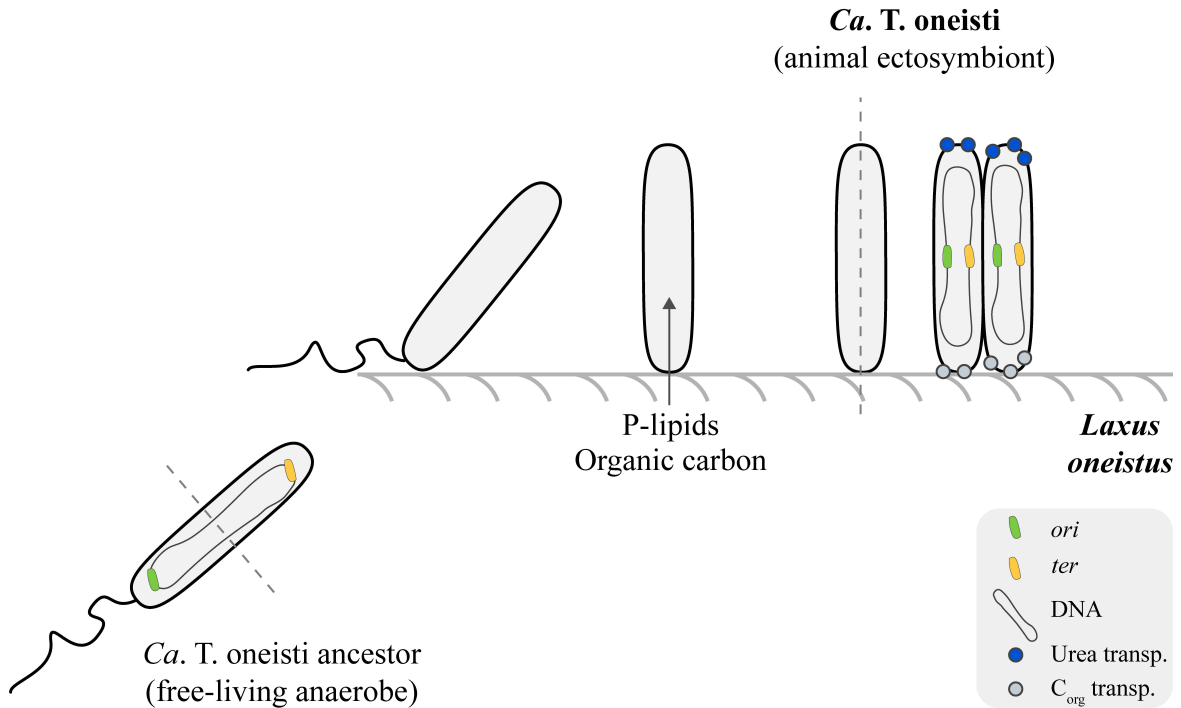


Figure 3. Schematic representation of *Ca. T. oneisti* transitioning from a free-living (likely a flagellated anaerobe with an *ori-ter* (longitudinal) chromosome configuration) to a symbiotic form (with fixed left-*ori*-right (transverse) chromosome configuration), and switching from transverse to longitudinal fission (dashed lines) (Weber et al., 2019). We propose that aside from oxygen exposure, the nutritional compounds gained from the nematode, such as phospholipids (P-lipids) and/or organic carbon compounds (Paredes et al., 2021) might have served such transition and the evolution of its reproduction mode and that a fixed chromosome configuration would enable the localization of genetic loci into an environmental side (blue dots) and a host side (grey dots). Modified from Weber et al., 2019. C_{org}: Organic carbon compounds transporter genes, DNA: Deoxyribonucleic acid, *ori*: origin of replication, *ter*: terminus of replication, Urea transp.: urea transporter genes.

Although longitudinal division is a rarity (Bulgheresi et al., 2016), up to this work, its understanding in a physiological and ecological context was not attempted: Chapter II (Paredes et al., 2021) puts *Ca. T. oneisti* longitudinal fission in a physiological and ecological context, while Chapter IV addresses how its chromosome is segregated (Weber et al., 2019).

In Paredes et al. (2021), we observed a significantly higher number of dividing symbionts under the AS condition. Namely, we counted 21.4 % versus 30.1 % dividing cells under the H and AS conditions, respectively. Consistently, several symbiont cell division genes (e.g.,

ftsE, *ftsX*, *damX*, *ftsN*; Typas et al., 2011) were upregulated under AS. This was remarkable as a higher proliferation of a thiotroph in anaerobic relative to aerobic conditions has, to the best of our knowledge, not been reported (e.g., see Justin et al., 1978; Timmer-ten Hoor et al., 1981; Sorokin et al., 2004; Nunoura et al., 2014). We propose that sulfur oxidation coupled to denitrification and, perhaps, host-to-symbiont phospholipid transfer support bacterial growth under AS conditions. Conversely, lower *Ca. Thiosymbion* proliferation in the presence of oxygen, might be related to the global stress response, and we speculate that oxidative stress might be hampering symbiont proliferation in oxygenated sand (Nyström et al., 1992, 2001, 2002; Aldsworth 1999; Page and Peti, 2016).

Concerning Chapter IV, by using a combination of DNA fluorescence *in situ* hybridization (FISH), and immunofluorescence labeling, we discovered that in the monoploid *Ca. T. oneisti*, a bidimensional segregation mode endows maintenance of chromosome configuration throughout generations. Namely, the two sister *ori* segregate along the short and the long cell axis (diagonally), likely helped by the ParABS chromosome segregation system. But the bidirectional segregation mode of *Ca. T. oneisti* chromosome is not the only extraordinary feature of this symbiont. Another peculiarity is that, even though its chromosome configuration is transversal (left-*ori*-right), it is fixed. Up to this work, only unipolar flagellated bacteria (e.g., *Pseudomonas aeruginosa* and *Vibrio cholerae*), which display longitudinal (*ori-ter*) configurations, were known to have fixed chromosome configurations (Fogel and Waldor, 2005; Vallet-Gely and Boccard, 2013). In Weber et al. (2019) we propose that *Ca. T. oneisti* evolved a fixed chromosome configuration (i.e. the chromosome orientation toward the host is maintained throughout the generations) to permanently position loci ascribed to the symbiotic lifestyle in the vicinity of the worm (e.g., C_{org} uptake genes), and confine those related to the environment to the distal cell pole (e.g., urea uptake genes) (Figure 3). Further studies, beyond the scope of this work, (e.g., combining imaging techniques and high-resolution mapping of the 3D chromosome structure by chromosome conformation capture (3C); Hagège et al., 2007) would be needed to confirm our hypothesis.

Chapter IV also reports the reproduction mode of the cuboid bacterium *Candidatus Thiosymbion cuboideus* (Weber et al., *accepted*). This symbiont lives attached to the Stilbonematinae *Catanema sp.* and forms a continuous monolayer on the surface of the worm (Polz et al., 1992). Besides being the first bacteria shown to be cube-like, its division is FtsZ-mediated. Notably, 3D-Structured illumination microscopy (SIM) microscopy revealed that FtsZ mostly

polymerized into either sharp-cornered or straight filaments. Therefore, this implies that membrane roundness is not required for the tubulin homolog FtsZ to function. Moreover, we showed that *Ca. T. cuboideus* peptidoglycan insertion and FtsZ localization patterns not only were similar but also host-polarized. Namely, in early division stages, both septation and FtsZ localization started first at the cell proximal pole (the one adjacent to the nematode cuticle), followed by the distal pole; that is, asynchronous division). Based on the latter, we proposed that FtsZ could be mediating septal peptidoglycan insertion in these cube-like symbionts.

Although the kind of bacterial physiology that drove the evolution of a cuboid shape is still eluding us, we hypothesize that, as *Ca. T. oneisti*, *Ca. T. cuboideus* FtsZ-mediated fission could have evolved to serve the physiological needs of the bacteria (and the host). In other words, the suit of putative nutritional benefits (e.g., lipids, organic compounds) that the symbiont could be gaining from its host, might have driven the evolution of their division modes, which guarantees uninterrupted host attachment to both daughter cells (Figure 3). However, in comparison to a rod-shaped symbiont, its cuboid shape would maximize the contact surface area with the neighboring cells (and with the nematode).

A comprehensive comparative omics study between the different *Ca. Thiosymbion* symbionts and the different Stilbonematinae worms (and in an ecological context, for example, different oxygen concentrations) awaits to elucidate specific host-microbe interactions in the *Catanema sp.* ectosymbiosis.

CONCLUSIVE REMARKS

As coined in Petersen and Yuen (2020), *Ca. T. oneisti* is metabolically an “all-rounder”. With a 4.35 Mb-sized genome – as large as those of some thiotrophic free-living bacteria (e.g., see Weissgerber et al., 2011; Kyndt et al., 2020) – *Ca. Thiosymbion* does not show hints of metabolic reduction. Indeed, it can synthesize a wide array of compounds, ranging from all amino acids (except threonine) to all B vitamins, and use a suite of nitrogen compounds, carbon sources, and electron acceptors. Of note, our data highlighted the importance of anaerobic electron acceptors and heterotrophy for energy generation, both largely overlooked.

Based on the top expressed transcripts under all conditions, *L. oneistus* highly engages in processes that might not be directly related to the symbiotic lifestyle (e.g., ubiquitination, energy-generation, cytoskeleton, locomotion). Taken together, although we found putative nutritional links, our data support a weak metabolic interdependence between this nematode and its bacterium.

We speculate that *Ca. T. oneisti* evolved from an obligate anaerobe as its most closely related free-living relatives are anoxygenic phototrophic purple sulfur bacteria of the family *Chromatiaceae* (e.g., *Allochromatium vinosum*) (Petersen et al. 2016; Zimmerman et al., 2016). Additional genetic hints of *Ca. T. oneisti* anaerobic ancestry described in Paredes et al. (2021) are the capability of using several anaerobic electron acceptors, of synthesizing (as *L. oneistus*; Paredes et al., *under review*) the anaerobic electron carrier rhodoquinone, and the global down-regulation of stress-related genes in the absence of oxygen. If anoxia seems to be the preferred condition for *Ca. T. oneisti*, the host seems to be suffering instead, as it mostly engages in degradation pathways that might be crucial for recycling under nutrient scarcity. On the contrary, in superficial sand, it appears that it is the symbiont to be globally stressed, while the host engages in several biosynthetic and developmental processes. Therefore, it is fascinating that, despite the apparent dramatically different needs the two partners have, the *Laxus*-Thiosymbion symbiosis evolved. Importantly, the fact that *L. oneistus* has not been found without its symbiont (and vice versa) attests to the success of this symbiosis.

All in all, host vertical migrations might ultimately have allowed each partner to expand its ancestral habitat: on the one hand, symbiont exposure to oxygen likely pushed the evolution

of systems to resist oxidative stress and to harvest the most from superficial sand (e.g., oxidative phosphorylation, mixotrophy, and urea uptake). On the other hand, being in anoxic, sulfidic sand frees the nematode from predation and gives it access to decomposed organic matter (Fenchel and Riedl 1970; Reise and Ax, 1979; Hentschel et al., 1999). Looking at the *Laxus*-Thiosymbion holobiont, the maximization of symbiont sulfur oxidation in anoxia would shield the worm from sulfide poisoning, where it most needs it (Hentschel et al., 1999; Paredes et al., 2021).

OUTLOOK

The *Laxus*-Thiosymbion association thrives in oxic-anoxic interfaces. My thesis is a valuable addition to what is known regarding the physiological potential of both partners, and how they respond to oxygen. Namely, it provides novel insights on a pivotal topic: the effect of the environment on the physiology and reproduction of the *Laxus*-Thiosymbion consortium. Although we now know what the partners might exchange (e.g., lipids, organic compounds, heme), future studies are needed to unequivocally confirm the transfer of these nutrients. Once confirmed, the gained information might become the basis of future attempts to cultivate this partnership. In this final section, I propose some approaches that can further aid in understanding what pushed two seemingly incompatible partners to hold onto each other so that nematode-bacterium ectosymbioses could evolve.

- 1) Couple our Omics, EA-IRMS, and Raman spectroscopy analysis with enzymatic and biochemical measurements. For example, determine if the observed symbiont gene expression positively correlates with its enzymatic characterization. This may comprise: measurements of sulfide oxidation, thiosulfate oxidation, nitrate respiration, and rates of ammonia assimilation. As for the host, measurements of ATP turnover rates, intracellular pH (e.g., changes in K^+ , Ca^{2+} , and Na^+ fluxes) and oxygen, neuronal electric activity, fermentation products (e.g., lactate), and storage compounds (e.g., glycogen and trehalose) might help to unravel other strategies used for anoxic survival.
- 2) Nematode distribution in sediment cores from Belize, and Guadeloupe (JM. Volland, personal communication), indicated that Stilbonematinae nematodes have different habitat distribution, and thus a varying tolerance toward oxygen and sulfide. For example, *Stilbonema* and *Robbea* occur more superficially (S. Bulgheresi and G. Paredes, unpublished data), whereas *L. oneistus* is found mainly in deeper sulfidic layers (Paredes et al., 2021). Therefore, *in situ* transcriptomics of *L. oneistus* and co-occurring Stilbonematinae could aid in explaining the distribution of Stilbonematinae in the sand.
- 3) Thanks to the optimization of whole worm transcriptomics (Paredes et al., 2021; Paredes et al., *under review*), we will be able to apply laser microdissection to compare

transcripts from symbiotic versus non-symbiotic tissues of the *Laxus oneistus* nematode. This approach could confirm and identify additional symbiosis-related genes.

- 4) The lack of host genomes hinders the comprehensive study of chemosynthetic adaptations. The genome of *L. oneistus* is estimated to be around 1 Gb and has approximately 95 % repeats (T. Viehboeck, personal communication). Currently, its genome, and that of another Stilbonematinae nematode, *Stilbonema majum*, are being assembled using PacBio long-read sequencing (Sanger Institute, Blaxter Group, United Kingdom).
- 5) The tracing and visualization of incorporated radiolabeled reduced organic substrates (e.g., amino acids or lipids) using NanoSIMS might help confirm and identify additional nutritional interactions.
- 6) Transmission electron microscopy (TEM) coupled with fluorescence *in situ* hybridization (FISH) targeting the gut of Stilbonematinae could prove whether *L. oneistus* feeds upon and digests its symbiont; as proposed in Jensen, 1987; Ott and Novak, 1989; Ott et al., 1991.
- 7) Cultivation of the *Laxus*-Thiosymbion consortium based on what we have learned on the partner's habitat (*in situ* measurements) and physiology (omics and stable isotope-based techniques), could turn the *Laxus*-Thiosymbion association into a model symbiosis.

REFERENCES

1. Aldsworth, T. G., Sharman, R. L., & Dodd, C. E. R. (1999). Bacterial suicide through stress. *Cellular and Molecular Life Sciences CMLS*, 56(5), 378-383.
2. Armenteros, M., Ruiz-Abierno, A., & Decraemer, W. (2014). Taxonomy of Stilbonematinae (Nematoda: Desmodoridae): description of two new and three known species and phylogenetic relationships within the family. *Zoological Journal of the Linnean Society*, 171(1), 1-21.
3. Badger, M. R., & Bek, E. J. (2008). Multiple Rubisco forms in proteobacteria: their functional significance in relation to CO₂ acquisition by the CBB cycle. *Journal of experimental botany*, 59(7), 1525-1541.
4. Bendezú, F. O., & de Boer, P. A. (2008). Conditional lethality, division defects, membrane involution, and endocytosis in mre and mrd shape mutants of *Escherichia coli*. *Journal of bacteriology*, 190(5), 1792-1811.
5. Brendza, K. M., Haakenson, W., Cahoon, R. E., Hicks, L. M., Palavalli, L. H., Chiappelli, B. J., ... & Jez, J. M. (2007). Phosphoethanolamine N-methyltransferase (PMT-1) catalyses the first reaction of a new pathway for phosphocholine biosynthesis in *Caenorhabditis elegans*. *Biochemical Journal*, 404(3), 439-448.
6. Bauer-Nebelsick, M., Blumer, M., Urbancik, W., & Ott, J. A. (1995). The glandular sensory organ of Desmodoridae (Nematoda)-ultrastructure and phylogenetic implications. *Invertebrate Biology*, 211-219.
7. Bayer, C., Heindl, N. R., Rinke, C., Lückner, S., Ott, J. A., & Bulgheresi, S. (2009). Molecular characterization of the symbionts associated with marine nematodes of the genus *Robbea*. *Environmental Microbiology Reports*, 1(2), 136-144.
8. Bentzon-Tilia, M., Severin, I., Hansen, L. H., & Riemann, L. (2015). Genomics and ecophysiology of heterotrophic nitrogen-fixing bacteria isolated from estuarine surface water. *MBio*, 6(4), e00929-15.
9. Bettencourt, R., Pinheiro, M., Egas, C., Gomes, P., Afonso, M., Shank, T., & Santos, R. S. (2010). High-throughput sequencing and analysis of the gill tissue transcriptome from the deep-sea hydrothermal vent mussel *Bathymodiolus azoricus*. *BMC genomics*, 11(1), 1-17.

10. Bongrand, C., Koch, E. J., Moriano-Gutierrez, S., Cordero, O. X., McFall-Ngai, M., Polz, M. F., & Ruby, E. G. (2016). A genomic comparison of 13 symbiotic *Vibrio fischeri* isolates from the perspective of their host source and colonization behavior. *The ISME journal*, 10(12), 2907-2917.
11. Borutaite, V., Mildaziene, V., Brown, G. C., & Brand, M. D. (1995). Control and kinetic analysis of ischemia-damaged heart mitochondria: which parts of the oxidative phosphorylation system are affected by ischemia?. *Biochimica et Biophysica Acta (BBA)-Molecular Basis of Disease*, 1272(3), 154-158.
12. Bright, M., & Sorgo, A. (2003). Ultrastructural reinvestigation of the trophosome in adults of *Riftia pachyptila* (Annelida, Siboglinidae). *Invertebrate Biology*, 122(4), 347-368.
13. Bright M, Bulgheresi S (2010) A complex journey: transmission of microbial symbionts. *Nature Reviews Microbiology*, 8, 218–230.
14. Buceta, P. M. R., Romanelli-Cedrez, L., Babcock, S. J., Xun, H., VonPaige, M. L., Higley, T. W., ... & Salinas, G. (2019). The kynurenine pathway is essential for rhodoquinone biosynthesis in *Caenorhabditis elegans*. *Journal of Biological Chemistry*, 294(28), 11047-11053.
15. Budde, M. W., & Roth, M. B. (2011). The response of *Caenorhabditis elegans* to hydrogen sulfide and hydrogen cyanide. *Genetics*, 189(2), 521-532.
16. Bulgheresi, S., Schabussova, I., Chen, T., Mullin, N. P., Maizels, R. M., & Ott, J. A. (2006). A new C-type lectin similar to the human immunoreceptor DC-SIGN mediates symbiont acquisition by a marine nematode. *Applied and Environmental Microbiology*, 72(4), 2950-2956.
17. Bulgheresi, S., Gruber-Vodicka, H. R., Heindl, N. R., Dirks, U., Kostadinova, M., Breiteneder, H., & Ott, J. A. (2011). Sequence variability of the pattern recognition receptor Mermaid mediates specificity of marine nematode symbioses. *The ISME journal*, 5(6), 986-998.
18. Bulgheresi, S. (2016). Bacterial cell biology outside the streetlight. *Environmental microbiology*, 18(8), 2305-2318.
19. Canfield, D. E., & Thamdrup, B. O. (2009). Towards a consistent classification scheme for geochemical environments, or, why we wish the term ‘suboxic’ would go away. *Geobiology* 7:385–392.

20. Carpenter, J. F., & Crowe, J. H. (1988). Modes of stabilization of a protein by organic solutes during desiccation. *Cryobiology*, 25(5), 459-470.
21. Cavanaugh, C. M. (1983). Symbiotic chemoautotrophic bacteria in marine invertebrates from sulphide-rich habitats. *Nature*, 302(5903), 58-61.
22. Cavanaugh, C. M., McKiness, Z. P., Newton, I. L., & Stewart, F. J. (2006). Marine chemosynthetic symbioses. *The prokaryotes*, 1, 475-507.
23. Clegg, J. (1997). Embryos of *Artemia franciscana* survive four years of continuous anoxia: the case for complete metabolic rate depression. *The Journal of Experimental Biology*, 200(3), 467-475.
24. Chen, J., & Strous, M. (2013). Denitrification and aerobic respiration, hybrid electron transport chains and co-evolution. *Biochimica et Biophysica Acta (BBA)-Bioenergetics*, 1827(2), 136-144.
25. Childress, J. J., Fisher, C. R., Favuzzi, J. A., & Sanders, N. K. (1991). Sulfide and carbon dioxide uptake by the hydrothermal vent clam, *Calymene magnifica*, and its chemoautotrophic symbionts. *Physiological zoology*, 64(6), 1444-1470.
26. Childress, J. J., & Girguis, P. R. (2011). The metabolic demands of endosymbiotic chemoautotrophic metabolism on host physiological capacities. *Journal of Experimental Biology*, 214(2), 312-325.
27. Conway, N., Capuzzo, J. M., & Fry, B. (1989). The role of endosymbiotic bacteria in the nutrition of *Solemya velum*: evidence from a stable isotope analysis of endosymbionts and host. *Limnology and Oceanography*, 34(1), 249-255.
28. Conway, N. M., & Capuzzo, J. E. M. (1992). High taurine levels in the *Solemya velum* symbiosis. *Comparative Biochemistry and Physiology Part B: Comparative Biochemistry*, 102(1), 175-185.
29. Corliss, J. B., Dymond, J., Gordon, L. I., Edmond, J. M., von Herzen, R. P., Ballard, R. D., ... & van Andel, T. H. (1979). Submarine thermal springs on the Galapagos Rift. *Science*, 203(4385), 1073-1083.
30. Crowe, J. H., Crowe, L. M., Carpenter, J. F., & Wistrom, C. A. (1987). Stabilization of dry phospholipid bilayers and proteins by sugars. *Biochemical Journal*, 242(1), 1.
31. Dando, P. R., & Spiro, B. (1993). Varying nutritional dependence of the thyasirid bivalves *Thyasira sarsi* and *T. equalis* on chemoautotrophic symbiotic bacteria, demonstrated by isotope ratios of tissue carbon and shell carbonate. *Marine Ecology-Progress Series*, 92, 151-151.

32. Dang, H., & Lovell, C. R. (2016). Microbial surface colonization and biofilm development in marine environments. *Microbiology and molecular biology reviews*, 80(1), 91-138.
33. Danovaro, R., Gambi, C., Dell'Anno, A., Corinaldesi, C., Pusceddu, A., Neves, R. C., & Kristensen, R. M. (2016). The challenge of proving the existence of metazoan life in permanently anoxic deep-sea sediments. *BMC biology*, 14(1), 1-7.
34. de Bary A (1879) *Die Erscheinung der Symbiose*. Verlag von Karl J, Trübner, Strassburg.
35. Del Borrello, S., Lautens, M., Dolan, K., Tan, J. H., Davie, T., Schertzberg, M. R., ... & Fraser, A. G. (2019). Rhodoquinone biosynthesis in *C. elegans* requires precursors generated by the kynurenine pathway. *Elife*, 8, e48165.
36. den Blaauwen, T. (2013). Prokaryotic cell division: flexible and diverse. *Current opinion in microbiology*, 16(6), 738-744.
37. Douglas, A. E., & Smith, D. C. (1989). Are endosymbioses mutualistic?. *Trends in ecology & evolution*, 4(11), 350-352.
38. Douglas, A. E. (1994). *Symbiotic interactions* (No. 577.85 D733s). Oxon, GB: Oxford University Press, 1994.
39. Dubilier, N., Bergin, C., & Lott, C. (2008). Symbiotic diversity in marine animals: the art of harnessing chemosynthesis. *Nature Reviews Microbiology*, 6(10), 725-740.
40. Elgharably, A., & Marschner, P. (2011). Microbial activity and biomass and N and P availability in a saline sandy loam amended with inorganic N and lupin residues. *European Journal of Soil Biology*, 47(5), 310-315.
41. Fago, A., & Jensen, F. B. (2015). Hypoxia tolerance, nitric oxide, and nitrite: lessons from extreme animals. *Physiology*, 30(2), 116-126.
42. Felbeck H (1981) Chemoautotrophic potential of the hydrothermal vent tube worm, *Riftia pachyptila* Jones (Vestimentifera). *Science*, 213, 336–338.
43. Fenchel, T. M., & Riedl, R. J. (1970). The sulfide system: a new biotic community underneath the oxidized layer of marine sand bottoms. *Marine Biology*, 7(3), 255-268.
44. Fenchel, T., & Finlay, B. J. (1995). *Ecology and evolution in anoxic worlds*. Oxford; New York: Oxford University Press, 1995.
45. Foe, V. E., & Alberts, B. M. (1985). Reversible chromosome condensation induced in *Drosophila* embryos by anoxia: visualization of interphase nuclear organization. *The Journal of cell biology*, 100(5), 1623-1636.

46. Fogel, M. A., & Waldor, M. K. (2005). Distinct segregation dynamics of the two *Vibrio cholerae* chromosomes. *Molecular microbiology*, 55(1), 125-136.
47. Galli, G. L., & Richards, J. G. (2014). Mitochondria from anoxia-tolerant animals reveal common strategies to survive without oxygen. *Journal of Comparative Physiology B*, 184(3), 285-302.
48. Gally, C., & Bessereau, J. L. (2003). GABA is dispensable for the formation of junctional GABA receptor clusters in *Caenorhabditis elegans*. *Journal of Neuroscience*, 23(7), 2591-2599.
49. Ghanbari, M., Kneifel, W., & Domig, K. J. (2015). A new view of the fish gut microbiome: advances from next-generation sequencing. *Aquaculture*, 448, 464-475.
50. Gilbert, S. F., Sapp, J., & Tauber, A. I. (2012). A symbiotic view of life: we have never been individuals. *The Quarterly review of biology*, 87(4), 325-341.
51. Goff, L. J. (1982). Symbiosis and parasitism: another viewpoint. *BioScience*, 32(4), 255-256.
52. Goffredi, S. K. (2010). Indigenous ectosymbiotic bacteria associated with diverse hydrothermal vent invertebrates. *Environmental Microbiology Reports*, 2(4), 479-488.
53. Goodrich-Blair, H. (2007). They've got a ticket to ride: *Xenorhabdus nematophila*–*Steinernema carpocapsae* symbiosis. *Current opinion in microbiology*, 10(3), 225-230.
54. Haddad, G. G. (2006). Tolerance to low O₂: lessons from invertebrate genetic models. *Experimental physiology*, 91(2), 277-282.
55. Hagège, H., Klous, P., Braem, C., Splinter, E., Dekker, J., Cathala, G., ... & Forné, T. (2007). Quantitative analysis of chromosome conformation capture assays (3C-qPCR). *Nature protocols*, 2(7), 1722-1733.
56. Hentschel, U., Berger, E. C., Bright, M., Felbeck, H., & Ott, J. A. (1999). Metabolism of nitrogen and sulfur in ectosymbiotic bacteria of marine nematodes (Nematoda, Stilbonematinae). *Marine Ecology Progress Series*, 183, 149-158.
57. Hermes-Lima, M., & Zenteno-Savín, T. (2002). Animal response to drastic changes in oxygen availability and physiological oxidative stress. *Comparative Biochemistry and Physiology Part C: Toxicology & Pharmacology*, 133(4), 537-556.
58. Hill, S. (1988). How is nitrogenase regulated by oxygen?. *FEMS microbiology reviews*, 4(2), 111-129.

59. Hinzke, T., Kleiner, M., Breusing, C., Felbeck, H., Häsler, R., Sievert, S. M., ... & Markert, S. (2019). Host-microbe interactions in the chemosynthetic *Riftia pachyptila* symbiosis. *Mbio*, 10(6), e02243-19.
60. Hochachka, P. W., Lutz, P. L., Sick, T. J., & Rosenthal, M. (1993). Surviving hypoxia: mechanisms of control and adaptation. CRC Press.
61. Hochachka, P. W., & Lutz, P. L. (2001). Mechanism, origin, and evolution of anoxia tolerance in animals☆. *Comparative Biochemistry and Physiology Part B: Biochemistry and Molecular Biology*, 130(4), 435-459.
62. Ip, J. C. H., Xu, T., Sun, J., Li, R., Chen, C., Lan, Y., ... & Qiu, J. W. (2021). Host–endosymbiont genome integration in a deep-sea chemosymbiotic clam. *Molecular Biology and Evolution*, 38(2), 502-518.
63. Jäckle, O., Seah, B. K., Tietjen, M., Leisch, N., Liebeke, M., Kleiner, M., ... & Gruber-Vodicka, H. R. (2019). Chemosynthetic symbiont with a drastically reduced genome serves as primary energy storage in the marine flatworm *Paracatenula*. *Proceedings of the National Academy of Sciences*, 116(17), 8505-8514.
64. Jannasch, H. W. (1985). Review Lecture-The chemosynthetic support of life and the microbial diversity at deep-sea hydrothermal vents. *Proceedings of the Royal society of London. Series B. Biological sciences*, 225(1240), 277-297.
65. Jensen, P. (1987). Feeding ecology of free-living aquatic nematodes. *Marine Ecology Progress Series*, 35(1/2), 187-196.
66. Jordan, D. B., & Ogren, W. L. (1981). Species variation in the specificity of ribulose biphosphate carboxylase/oxygenase. *Nature*, 291(5815), 513-515.
67. Joyner, J. L., Peyer, S. M., & Lee, R. W. (2003). Possible roles of sulfur-containing amino acids in a chemoautotrophic bacterium-mollusc symbiosis. *The Biological Bulletin*, 205(3), 331-338.
68. Justin, P., & Kelly, D. P. (1978). Growth kinetics of *Thiobacillus denitrificans* in anaerobic and aerobic chemostat culture. *Microbiology*, 107(1), 123-130.
69. Kalogeris, T., Baines, C. P., Krenz, M., & Korthuis, R. J. (2016). Ischemia/reperfusion. *Comprehensive Physiology*, 7(1), 113.
70. Kampfer, S., Sturmbauer, C., & Ott, J. (1998). Phylogenetic analysis of rDNA sequences from adenophorean nematodes and implications for the *Adenophorea-Seicernentea* controversy. *Invertebrate Biology*, 29-36.

71. Karl, D. M., Wirsén, C. O., & Jannasch, H. W. (1980). Deep-sea primary production at the Galapagos hydrothermal vents. *Science*, 207(4437), 1345-1347.
72. Kawazura, T., Matsumoto, K., Kojima, K., Kato, F., Kanai, T., Niki, H., & Shiomi, D. (2017). Exclusion of assembled MreB by anionic phospholipids at cell poles confers cell polarity for bidirectional growth. *Molecular microbiology*, 104(3), 472-486.
73. Kim, K. W., & Jin, Y. (2015). Neuronal responses to stress and injury in *C. elegans*. *FEBS letters*, 589(14), 1644-1652.
74. Kitazume, H., Dayi, M., Tanaka, R., & Kikuchi, T. (2018). Assessment of the behaviour and survival of nematodes under low oxygen concentrations. *PloS one*, 13(5), e0197122.
75. Kleiner, M., Wentrup, C., Lott, C., Teeling, H., Wetzel, S., Young, J., ... & Dubilier, N. (2012). Metaproteomics of a gutless marine worm and its symbiotic microbial community reveal unusual pathways for carbon and energy use. *Proceedings of the National Academy of Sciences*, 109(19), E1173-E1182.
76. Kowaltowski, A. J., de Souza-Pinto, N. C., Castilho, R. F., & Vercesi, A. E. (2009). Mitochondria and reactive oxygen species. *Free Radical Biology and Medicine*, 47(4), 333-343.
77. Krasity, B. C., Troll, J. V., Weiss, J. P., & McFall-Ngai, M. J. (2011). LBP/BPI proteins and their relatives: conservation over evolution and roles in mutualism. *Biochemical Society Transactions*, 39(4), 1039-1044.
78. Kyndt, J. A., & Meyer, T. E. (2020). Genome Sequences of *Allochromatium palmeri* and *Allochromatium humboldtianum* Expand the *Allochromatium* Family Tree of Purple Sulfur Photosynthetic Bacteria within the Gammaproteobacteria and Further Refine the Genus. *Microbiology Resource Announcements*, 9(33), e00774-20.
79. Lane, N., & Martin, W. (2010). The energetics of genome complexity. *Nature*, 467(7318), 929-934.
80. Lin, W., Shi, H., Zou, C., Ren, J., Jian, Y., Liu, L., ... & Ruan, L. (2021). De novo transcriptome assembly of the deep-sea hydrothermal vent, shrimp *Rimicaris exoculate* (Crustacea: Decapoda), from the south Mid-Atlantic Ridge. *Marine Genomics*, 100876.
81. Lee, J. J., Cervasco, M. H., Morales, J., Billik, M., Fine, M., & Levy, O. (2010). Symbiosis drove cellular evolution. *Symbiosis*, 51(1), 13-25.

82. Leisch, N., Verheul, J., Heindl, N. R., Gruber-Vodicka, H. R., Pende, N., den Blaauwen, T., & Bulgheresi, S. (2012). Growth in width and FtsZ ring longitudinal positioning in a gammaproteobacterial symbiont. *Current Biology*, 22(19), R831-R832.
83. Leisch, N., Pende, N., Weber, P. M., Gruber-Vodicka, H. R., Verheul, J., Vischer, N. O., ... & Bulgheresi, S. (2016). Asynchronous division by non-ring FtsZ in the gammaproteobacterial symbiont of *Robbea hypermnestra*. *Nature microbiology*, 2(1), 1-5.
84. Leiser, S. F., Fletcher, M., Begun, A., & Kaeberlein, M. (2013). Life-span extension from hypoxia in *Caenorhabditis elegans* requires both HIF-1 and DAF-16 and is antagonized by SKN-1. *Journals of Gerontology Series A: Biomedical Sciences and Medical Sciences*, 68(10), 1135-1144.
85. Login, F. H., Balmand, S., Vallier, A., Vincent-Monégat, C., Vigneron, A., Weiss-Gayet, M., ... & Heddi, A. (2011). Antimicrobial peptides keep insect endosymbionts under control. *Science*, 334(6054), 362-365.
86. Lonsdale P (1977) Clustering of suspension-feeding macrobenthos near abyssal hydrothermal vents at oceanic spreading centers. *Deep Sea Research*, 24, 857–863.
87. Luther, G. W., Findlay, A. J., MacDonald, D. J., Owings, S. M., Hanson, T. E., Beinart, R. A., & Girguis, P. R. (2011). Thermodynamics and kinetics of sulfide oxidation by oxygen: a look at inorganically controlled reactions and biologically mediated processes in the environment. *Frontiers in microbiology*, 2, 62.
88. Lutz, P. L., Nilsson, G. E., & Pérez-Pinzón, M. A. (1996). Anoxia tolerant animals from a neurobiological perspective. *Comparative Biochemistry and Physiology Part B: Biochemistry and Molecular Biology*, 113(1), 3-13.
89. Margulis, L., & Fester, R. (Eds.). (1991). *Symbiosis as a source of evolutionary innovation: speciation and morphogenesis*. Mit Press.
90. Markert, S., Arndt, C., Felbeck, H., Becher, D., Sievert, S. M., Hügler, M., ... & Schweder, T. (2007). Physiological proteomics of the uncultured endosymbiont of *Riftia pachyptila*. *Science*, 315(5809), 247-250.
91. Martin, B. D., & Schwab, E. (2013). Current usage of symbiosis and associated terminology. *International Journal of Biology*, 5(1), 32.
92. McFall-Ngai, M. J., & Gordon, J. I. (2006). Experimental Models of Symbiotic Host-Microbial Relationships: Understanding the Underpinnings of Beneficence and the Origins of Pathogenesis. *Evolution of microbial pathogens*, 147-166.

93. McFall-Ngai, M. (2008). Are biologists in 'future shock'? Symbiosis integrates biology across domains. *Nature Reviews Microbiology*, 6(10), 789-792.
94. McFall-Ngai, M., Hadfield, M. G., Bosch, T. C., Carey, H. V., Domazet-Lošo, T., Douglas, A. E., ... & Wernegreen, J. J. (2013). Animals in a bacterial world, a new imperative for the life sciences. *Proceedings of the National Academy of Sciences*, 110(9), 3229-3236.
95. McFall-Ngai, M. (2015). Out of sight, out of mind. *Environmental microbiology reports*, 7(1), 29-30.
96. Milton, S. L., Nayak, G., Kesaraju, S., Kara, L., & Prentice, H. M. (2007). Suppression of reactive oxygen species production enhances neuronal survival in vitro and in vivo in the anoxia-tolerant turtle *Trachemys scripta*. *Journal of neurochemistry*, 101(4), 993-1001.
97. Minic, Z., Simon, V., Penverne, B., Gaill, F., & Hervé, G. (2001). Contribution of the bacterial endosymbiont to the biosynthesis of pyrimidine nucleotides in the deep-sea tube worm *Riftia pachyptila*. *Journal of Biological Chemistry*, 276(26), 23777-23784.
98. Minic, Z., & Hervé, G. (2003). Arginine metabolism in the deep sea tube worm *Riftia pachyptila* and its bacterial endosymbiont. *Journal of Biological Chemistry*, 278(42), 40527-40533.
99. Moncada, S., & Erusalimsky, J. D. (2002). Does nitric oxide modulate mitochondrial energy generation and apoptosis?. *Nature reviews Molecular cell biology*, 3(3), 214-220.
100. Moran, N. A., McCutcheon, J. P., & Nakabachi, A. (2008). Genomics and evolution of heritable bacterial symbionts. *Annual review of genetics*, 42, 165-190.
101. Moya A, Peretó J, Gil R, Latorre A (2008) Learning how to live together: genomic insights into prokaryote–animal symbioses. *Nature Reviews Genetics*, 9, 218–229.
102. Murfin, K. E., Lee, M. M., Klassen, J. L., McDonald, B. R., Larget, B., Forst, S., ... & Goodrich-Blair, H. (2015). *Xenorhabdus bovienii* strain diversity impacts coevolution and symbiotic maintenance with *Steinernema* spp. nematode hosts. *MBio*, 6(3), e00076-15.
103. Nebelsick, M., Blumer, M., Novak, R., & Ott, J. (1992). A new glandular sensory organ in *Catanema* sp. (Nematoda, Stilbonematinae). *Zoomorphology*, 112(1), 17-26.

104. Newton, I. L. G., Woyke, T., Auchtung, T. A., Dilly, G. F., Dutton, R. J., Fisher, M. C., ... & Cavanaugh, C. M. (2007). The *Calymmatobacterium magnificum* chemoautotrophic symbiont genome. *Science*, 315(5814), 998-1000.
105. Nielsen, L. P., Risgaard-Petersen, N., Fossing, H., Christensen, P. B., & Sayama, M. (2010). Electric currents couple spatially separated biogeochemical processes in marine sediment. *Nature*, 463(7284), 1071-1074.
106. Nunoura, T., Takaki, Y., Kazama, H., Kakuta, J., Shimamura, S., Makita, H., ... & Takai, K. (2014). Physiological and genomic features of a novel sulfur-oxidizing gammaproteobacterium belonging to a previously uncultivated symbiotic lineage isolated from a hydrothermal vent. *PLoS One*, 9(8), e104959.
107. Nussbaumer, A.D., Bright, M., Baranyi, C., Beisser, C.J., and Ott, J.A. (2004) Attachment mechanism in a highly specific association between ectosymbiotic bacteria and marine nematodes. *Aquat Microb Ecol* 34:239–246
108. Nussbaumer, A. D., Fisher, C. R., & Bright, M. (2006). Horizontal endosymbiont transmission in hydrothermal vent tubeworms. *Nature*, 441(7091), 345-348.
109. Nyholm, S. V., & McFall-Ngai, M. (2004). The winnowing: establishing the squid–*Vibrio* symbiosis. *Nature Reviews Microbiology*, 2(8), 632-642.
110. Nyholm, S. V., & McFall-Ngai, M. J. (2021). A lasting symbiosis: how the Hawaiian bobtail squid finds and keeps its bioluminescent bacterial partner. *Nature Reviews Microbiology*, 1-14.
111. Nyström, T., & Neidhardt, F. C. (1992). Cloning, mapping and nucleotide sequencing of a gene encoding a universal stress protein in *Escherichia coli*. *Molecular microbiology*, 6(21), 3187-3198.
112. Nyström, T. (2001). Not quite dead enough: on bacterial life, culturability, senescence, and death. *Archives of Microbiology*, 176(3), 159-164.
113. Nyström, T. (2002). Translational fidelity, protein oxidation, and senescence: lessons from bacteria. *Ageing research reviews*, 1(4), 693-703.
114. Nystul, T. G., & Roth, M. B. (2004). Carbon monoxide-induced suspended animation protects against hypoxic damage in *Caenorhabditis elegans*. *Proceedings of the National Academy of Sciences*, 101(24), 9133-9136.
115. O'Brien, J. O. H. N., & Vetter, R. D. (1990). Production of thiosulphate during sulphide oxidation by mitochondria of the symbiont-containing bivalve *Solemya reidi*. *Journal of Experimental Biology*, 149(1), 133-148.

116. Oren, A., Ventosa, A., Gutiérrez, M. C., & Kamekura, M. (1999). *Haloarcula quadrata* sp. nov., a square, motile archaeon isolated from a brine pool in Sinai (Egypt). *International Journal of Systematic and Evolutionary Microbiology*, 49(3), 1149-1155.
117. Osca, D., Templado, J., & Zardoya, R. (2014). The mitochondrial genome of *Ifremeria nautilei* and the phylogenetic position of the enigmatic deep-sea *Abyssochrysoidea* (Mollusca: Gastropoda). *Gene*, 547(2), 257-266.
118. Ott, J., Rieger, G., Rieger, R., & Enderes, F. (1982). New mouth less interstitial worms from the sulfide system: Symbiosis with prokaryotes. *Marine Ecology*, 3(4), 313-333.
119. Ott, J. A., & Novak, R. (1989). Living at an interface: Meiofauna at the oxygen/sulfide boundary of marine sediments.
120. Ott, J. A., Novak, R., Schiemer, F., Hentschel, U., Nebelsick, M., & Polz, M. (1991). Tackling the sulfide gradient: a novel strategy involving marine nematodes and chemoautotrophic ectosymbionts. *Marine Ecology*, 12(3), 261-279.
121. Ott, J. A., Bauer-Nebelsick, M., & Novotny, V. (1995). THE GENUS *LAXUS* COBB, 1984 (STILBONEMATINAE: NEMATODA): DESCRIPTION OF TWO NEW SPECIES WITH ECTOSYMBIOTIC CHEMOAUTOTROPHIC BACTERIA. *Proceedings of the Biological Society of Washington*, 108(3), 508-527.
122. Ott, J., Bright, M. & Bulgheresi, S. (2004a). Symbioses between marine nematodes and sulfur-oxidizing chemoautotrophic bacteria. *Symbiosis* 36, 103–126
123. Ott, J., Bright, M., & Bulgheresi, S. (2004b). Marine microbial thiotrophic ectosymbioses. *Oceanogr Mar Biol Annu Rev*, 42, 95-118.
124. Ott, J. A., Gruber-Vodicka, H. R., Leisch, N., & Zimmermann, J. (2014a). Phylogenetic confirmation of the genus *Robbea* (Nematoda: Desmodoridae, Stilbonematinae) with the description of three new species. *Systematics and Biodiversity*, 12(4), 434-455.
125. Ott, J. A., Leisch, N., & Gruber-Vodicka, H. R. (2014b). *Eubostrichus fertilis* sp. n., a new marine nematode (Desmodoridae: Stilbonematinae) with an extraordinary reproductive potential from Belize, Central America. *Nematology*, 16(7), 777-787.
126. Ott, J., Bulgheresi, S., Gruber-Vodicka, H., Gruhl, A., König, L. & Leisch, N. 2022. "Meiofauna Meets Microbes: Chemosynthetic Symbioses", in 'Frontiers in Meibenthos Research – Profiles, Links and Perspectives in the Benthic Biome, eds. Giere, O. & Schratzberger, M. (in prep.); Springer, 2022

127. Pace, N. R., Sapp, J., & Goldenfeld, N. (2012). Phylogeny and beyond: Scientific, historical, and conceptual significance of the first tree of life. *Proceedings of the National Academy of Sciences*, 109(4), 1011-1018.
128. Padilla, P. A., Nystul, T. G., Zager, R. A., Johnson, A. C., & Roth, M. B. (2002). Dephosphorylation of cell cycle-regulated proteins correlates with anoxia-induced suspended animation in *Caenorhabditis elegans*. *Molecular biology of the cell*, 13(5), 1473-1483.
129. Page, R., & Peti, W. (2016). Toxin-antitoxin systems in bacterial growth arrest and persistence. *Nature chemical biology*, 12(4), 208-214.
130. Paracer, S., & Ahmadjian, V. (2000). *Symbiosis: an introduction to biological associations*. Oxford University Press.
131. Paredes, G. F., Viehboeck, T., Lee, R., Palatinszky, M., Mausz, M. A., Reipert, S., ... Bulgheresi, S. & König, L. (2021). Anaerobic sulfur oxidation underlies adaptation of a chemosynthetic symbiont to oxic-anoxic interfaces. *Msystems*, 6(3), e01186-20.
132. Pende, N., Leisch, N., Gruber-Vodicka, H. R., Heindl, N. R., Ott, J., Den Blaauwen, T., & Bulgheresi, S. (2014). Size-independent symmetric division in extraordinarily long cells. *Nature communications*, 5(1), 1-10.
133. Pende, N., Wang, J., Weber, P. M., Verheul, J., Kuru, E., Simon, K. M. R., ... & Bulgheresi, S. (2018). Host-polarized cell growth in animal symbionts. *Current Biology*, 28(7), 1039-1051.
134. Perreau, J., & Moran, N. A. (2021). Genetic innovations in animal-microbe symbioses. *Nature Reviews Genetics*, 1-17.
135. Petersen, J. M., Kemper, A., Gruber-Vodicka, H., Cardini, U., Van Der Geest, M., Kleiner, M., ... & Weber, M. (2016). Chemosynthetic symbionts of marine invertebrate animals are capable of nitrogen fixation. *Nature microbiology*, 2(1), 1-11.
136. Petersen, J. M., & Yuen, B. (2020). The symbiotic “all-rounders”: partnerships between marine animals and chemosynthetic nitrogen-fixing bacteria. *Applied and Environmental Microbiology*, 87(5), e02129-20.
137. Pfeffer, C., Larsen, S., Song, J., Dong, M., Besenbacher, F., Meyer, R. L., ... Schramm, A., Risgaard-Petersen, N., & Nielsen, L. P. (2012). Filamentous bacteria transport electrons over centimetre distances. *Nature*, 491(7423), 218-221.

138. Polz, M. F., Felbeck, H., Novak, R., Nebelsick, M., & Ott, J. A. (1992). Chemoautotrophic, sulfur-oxidizing symbiotic bacteria on marine nematodes: morphological and biochemical characterization. *Microbial Ecology*, 24(3), 313-329.
139. Polz, M. F., Distel, D. L., Zarda, B., Amann, R., Felbeck, H., Ott, J. A., & Cavanaugh, C. M. (1994). Phylogenetic analysis of a highly specific association between ectosymbiotic, sulfur-oxidizing bacteria and a marine nematode. *Applied and Environmental Microbiology*, 60(12), 4461-4467.
140. Polz, M. F., Ott, J. A., Bright, M., & Cavanaugh, C. M. (2000). When bacteria hitch a ride. *ASM news*, 66(9), 531-539.
141. Ponsard, J., Cambon-Bonavita, M. A., Zbinden, M., Lepoint, G., Joassin, A., Corbari, L., ... & Compere, P. (2013). Inorganic carbon fixation by chemosynthetic ectosymbionts and nutritional transfers to the hydrothermal vent host-shrimp *Rimicaris exoculata*. *The ISME journal*, 7(1), 96-109.
142. Powell, E. N., Crenshaw, M. A., & Rieger, R. M. (1979). Adaptations to sulfide in the meiofauna of the sulfide system. I. 35S-sulfide accumulation and the presence of a sulfide detoxification system. *Journal of experimental marine biology and ecology*, 37(1), 57-76.
143. Powell, M. A., & Somero, G. N. (1986). Adaptations to sulfide by hydrothermal vent animals: sites and mechanisms of detoxification and metabolism. *The Biological Bulletin*, 171(1), 274-290.
144. Powers, T. (2004). Ribosome biogenesis: giant steps for a giant problem. *Cell*, 119(7), 901-902.
145. Pruski, A. M., Fiala-Médioni, A., Fisher, C. R., & Colomines, J. C. (2000). Composition of free amino acids and related compounds in invertebrates with symbiotic bacteria at hydrocarbon seeps in the Gulf of Mexico. *Marine Biology*, 136(3), 411-420.
146. Pruski, A. M., & Fiala-Médioni, A. (2003). Stimulatory effect of sulphide on thiotaurine synthesis in three hydrothermal-vent species from the East Pacific Rise. *Journal of experimental biology*, 206(17), 2923-2930.
147. Reise, K., & Ax, P. (1979). A meiofaunal "thiobios" limited to the anaerobic sulfide system of marine sand does not exist. *Marine biology*, 54(3), 225-237.
148. Rogers, A., Gibon, Y., Stitt, M., Morgan, P. B., Bernacchi, C. J., Ort, D. R., & Long, S. P. (2006). Increased C availability at elevated carbon dioxide concentration improves N assimilation in a legume. *Plant, Cell & Environment*, 29(8), 1651-1658.

149. Rosati, G. (2004) Ectosymbiosis in Ciliated Protozoa. In Symbiosis: Mechanisms and Model Systems. Seckbach, J.(ed.). Dordrecht, Netherlands: Springer, pp. 475–488.10.1007/0-306-48173-1_30.
150. Rose, P., Moore, P. K., & Zhu, Y. Z. (2017). H₂S biosynthesis and catabolism: new insights from molecular studies. Cellular and Molecular Life Sciences, 74(8), 1391-1412.
151. Rowlett, V. W., & Margolin, W. (2015). The Min system and other nucleoid-independent regulators of Z ring positioning. Frontiers in microbiology, 6, 478.
152. Russell SL. 2019. Transmission mode is associated with environment type and taxa across bacteria-eukaryote symbioses: a systematic review and meta-analysis. FEMS Microbiol Lett 366.
153. Saffo, M. B. (1992). Coming to Terms with a Field: Words and Concepts in Symbiosis. Symbiosis. 14: 17-31.
154. Scharhauser, F., Zimmermann, J., Ott, J. A., Leisch, N., & Gruber-Vodicka, H. R. (2020). Morphology of obligate ectosymbionts reveals *Paralaxus* gen. nov.: A new circumtropical genus of marine stilbonematine nematodes. Zoologica scripta, 49(3), 379-394.
155. Schiemer, F., Novak, R., & Ott, J. (1990). Metabolic studies on thiobiotic free-living nematodes and their symbiotic microorganisms. Marine Biology, 106(1), 129-137.
156. Scott, K. M., & Cavanaugh, C. M. (2007). CO₂ uptake and fixation by endosymbiotic chemoautotrophs from the bivalve *Solemya velum*. Applied and Environmental Microbiology, 73(4), 1174-1179.
157. Seah, B. K., Antony, C. P., Huettel, B., Zarzycki, J., Schada von Borzyskowski, L., Erb, T. J., ... & Gruber-Vodicka, H. R. (2019). Sulfur-oxidizing symbionts without canonical genes for autotrophic CO₂ fixation. MBio, 10(3), e01112-19.
158. Selivanov, V. A., Votyakova, T. V., Zeak, J. A., Trucco, M., Roca, J., & Cascante, M. (2009). Bistability of mitochondrial respiration underlies paradoxical reactive oxygen species generation induced by anoxia. PLoS computational biology, 5(12), e1000619.
159. Semenza, G. L. (2007). Life with oxygen. Science, 318(5847), 62-64.
160. Seston, S. L., Beinart, R. A., Sarode, N., Shockey, A. C., Ranjan, P., Ganesh, S., ... & Stewart, F. J. (2016). Metatranscriptional response of chemoautotrophic *Ifremeria nautili* endosymbionts to differing sulfur regimes. Frontiers in microbiology, 7, 1074.

161. Shigenobu, S., Watanabe, H., Hattori, M., Sakaki, Y., & Ishikawa, H. (2000). Genome sequence of the endocellular bacterial symbiont of aphids *Buchnera sp.* APS. Nature, 407(6800), 81-86.
162. Smith, D. C. (1979). From extracellular to intracellular: the establishment of a symbiosis. Proceedings of the Royal Society of London. Series B. Biological Sciences, 204(1155), 115-130.
163. Smith, D. C., & Douglas, A. E. (1987). The biology of symbiosis. Edward Arnold (Publishers) Ltd.
164. Smith, J. M. (1991). A Darwinian view of symbiosis. Symbiosis as a source of evolutionary innovation, 26-39.
165. Sogin, E. M., Kleiner, M., Borowski, C., Gruber-Vodicka, H. R., & Dubilier, N. (2021). Life in the Dark: Phylogenetic and Physiological Diversity of Chemosynthetic Symbioses. Annual Review of Microbiology, 75.
166. Sorgo, A., Gaill, F., Lechaire, J. P., Arndt, C., & Bright, M. (2002). Glycogen storage in the *Riftia pachyptila* trophosome: contribution of host and symbionts. Marine Ecology Progress Series, 231, 115-120.
167. Sorokin, D. Y., Tat'yana, P. T., Antipov, A. N., Muyzer, G., & Kuenen, J. G. (2004). Anaerobic growth of the haloalkaliphilic denitrifying sulfur-oxidizing bacterium *Thi-alkalivibrio thiocyanodenitrificans* sp. nov. with thiocyanate. Microbiology, 150(7), 2435-2442.
168. Stewart, F. J., Newton, I. L., & Cavanaugh, C. M. (2005). Chemosynthetic endosymbioses: adaptations to oxic–anoxic interfaces. Trends in Microbiology, 13(9), 439-448.
169. Sudakaran, S., Kost, C., & Kaltenpoth, M. (2017). Symbiont acquisition and replacement as a source of ecological innovation. Trends in Microbiology, 25(5), 375-390.
170. Sun, J., Zhang, Y., Xu, T., Zhang, Y., Mu, H., Zhang, Y., ... & Qian, P. Y. (2017). Adaptation to deep-sea chemosynthetic environments as revealed by mussel genomes. Nature Ecology & Evolution, 1(5), 1-7.
171. Taylor, J. D. & Glover, E. A. Lucinidae (Bivalvia) — the most diverse group of chemosymbiotic molluscs. Zool. J. Linn. Soc. 148, 421–438 (2006).
172. Tchesunov, A. V. (2013). Marine free-living nematodes of the subfamily Stilbonematinae (Nematoda, Desmodoridae): taxonomic review with descriptions of a few species from the Nha Trang Bay, Central Vietnam. Meiofauna Marina, 20, 71-94.

173. Thomas, J. H. (1990). Genetic analysis of defecation in *Caenorhabditis elegans*. *Genetics*, 124(4), 855-872.
174. Thompson, A. R., & Vierstra, R. D. (2005). Autophagic recycling: lessons from yeast help define the process in plants. *Current opinion in plant biology*, 8(2), 165-173.
175. Timmer-ten Hoor, A. (1981). Cell yield and bioenergetics of *Thiomicrospira denitrificans* compared with *Thiobacillus denitrificans*. *Antonie van Leeuwenhoek*, 47(3), 231-243.
176. Trojan, D., Schreiber, L., Bjerg, J. T., Bøggild, A., Yang, T., Kjeldsen, K. U., & Schramm, A. (2016). A taxonomic framework for cable bacteria and proposal of the candidate genera *Electrothrix* and *Electronema*. *Systematic and applied microbiology*, 39(5), 297-306.
177. Turney, P. D. (2020). Symbiosis promotes fitness improvements in the Game of Life. *Artificial Life*, 26(3), 338-365.
178. Tyler, P. A., & Young, C. M. (2003). Dispersal at hydrothermal vents: a summary of recent progress. *Hydrobiologia*, 503(1), 9-19.
179. Typas, A., Banzhaf, M., Gross, C. A., & Vollmer, W. (2012). From the regulation of peptidoglycan synthesis to bacterial growth and morphology. *Nature Reviews Microbiology*, 10(2), 123-136.
180. Vallet-Gely, I., & Boccard, F. (2013). Chromosomal organization and segregation in *Pseudomonas aeruginosa*. *PLoS genetics*, 9(5), e1003492.
181. Van Dover, C. (2000). The ecology of deep-sea hydrothermal vents. Princeton University Press.
182. Van Voorhies, W. A., & Ward, S. (2000). Broad oxygen tolerance in the nematode *Caenorhabditis elegans*. *Journal of Experimental Biology*, 203(16), 2467-2478.
183. Volland, J. M., Schintlmeister, A., Zambalos, H., Reipert, S., Mozetič, P., Espada-Hinojosa, S., ... & Bright, M. (2018). NanoSIMS and tissue autoradiography reveal symbiont carbon fixation and organic carbon transfer to giant ciliate host. *The ISME journal*, 12(3), 714-727.
184. Walsby, A. E. (1980). A square bacterium. *Nature*, 283(5742), 69-71.
185. Wang, X., Llopis, P. M., & Rudner, D. Z. (2013). Organization and segregation of bacterial chromosomes. *Nature Reviews Genetics*, 14(3), 191-203.

186. Wang, H., Zhang, H., Wang, M., Chen, H., Lian, C., & Li, C. (2019). Comparative transcriptomic analysis illuminates the host-symbiont interactions in the deep-sea mussel *Bathymodiolus platifrons*. *Deep Sea Research Part I: Oceanographic Research Papers*, 151, 103082.
187. Weber, P. M., Moessel, F., Paredes, G. F., Viehboeck, T., Vischer, N. O., & Bulgheresi, S. (2019). A bidimensional segregation mode maintains symbiont chromosome orientation toward its host. *Current Biology*, 29(18), 3018-3028.
188. Weber, P., Paredes, G. F., Viehboeck, T., Pende, N., Volland, J. M., Gros, O., ... & Bulgheresi, S. Ftsz-Mediated Fission of a Cuboid Bacterial Symbiont. *Available at SSRN* 3885987.
189. Wieser, W. (1959). Eine ungewöhnliche Assoziation zwischen Blaualgen und freilebenden marinen Nematoden. *Österreichische Botanische Zeitschrift*, 106(1/2), 81-87.
190. Wilbanks, E. G., Jaekel, U., Salman, V., Humphrey, P. T., Eisen, J. A., Facciotti, M. T., ... & Orphan, V. J. (2014). Microscale sulfur cycling in the phototrophic pink berry consortia of the Sippewissett Salt Marsh. *Environmental microbiology*, 16(11), 3398-3415.
191. Williams, J. C., Sue, C., Banting, G. S., Yang, H., Glerum, D. M., Hendrickson, W. A., & Schon, E. A. (2005). Crystal structure of human SCO1: implications for redox signaling by a mitochondrial cytochrome c oxidase “assembly” protein. *Journal of Biological Chemistry*, 280(15), 15202-15211.
192. Wingrove, J. A., & O'farrell, P. H. (1999). Nitric oxide contributes to behavioral, cellular, and developmental responses to low oxygen in *Drosophila*. *Cell*, 98(1), 105-114.
193. Winogradsky, S. (1887). Über schwefelbakterien. *Bot. Ztg*, 45(31-37), 488-610.
194. Wippler, J., Kleiner, M., Lott, C., Gruhl, A., Abraham, P. E., Giannone, R. J., ... & Dubilier, N. (2016). Transcriptomic and proteomic insights into innate immunity and adaptations to a symbiotic lifestyle in the gutless marine worm *Olavius algarvensis*. *BMC genomics*, 17(1), 1-19.
195. Weissgerber, T., Zigann, R., Bruce, D., Chang, Y. J., Detter, J. C., Han, C., ... & Dahl, C. (2011). Complete genome sequence of *Allochromatium vinosum* DSM 180 T. *Standards in genomic sciences*, 5(3), 311-330.

196. Woese, C. R., & Fox, G. E. (1977). Phylogenetic structure of the prokaryotic domain: the primary kingdoms. *Proceedings of the National Academy of Sciences*, 74(11), 5088-5090.
197. Woese, C. R., Kandler, O., & Wheelis, M. L. (1990). Towards a natural system of organisms: proposal for the domains Archaea, Bacteria, and Eucarya. *Proceedings of the National Academy of Sciences*, 87(12), 4576-4579.
198. Woyke, T., Teeling, H., Ivanova, N. N., Huntemann, M., Richter, M., Gloeckner, F. O., ... & Dubilier, N. (2006). Symbiosis insights through metagenomic analysis of a microbial consortium. *Nature*, 443(7114), 950-955.
199. Yang, Y., Sun, J., Sun, Y., Kwan, Y. H., Wong, W. C., Zhang, Y., ... & Qian, P. Y. (2020). Genomic, transcriptomic, and proteomic insights into the symbiosis of deep-sea tubeworm holobionts. *The ISME journal*, 14(1), 135-150.
200. Yong, R., & Searcy, D. G. (2001). Sulfide oxidation coupled to ATP synthesis in chicken liver mitochondria. *Comparative Biochemistry and Physiology Part B: Biochemistry and Molecular Biology*, 129(1), 129-137.
201. Yuen, B., Polzin, J., & Petersen, J. M. (2019). Organ transcriptomes of the lucinid clam *Loripes orbiculatus* (Poli, 1791) provide insights into their specialized roles in the biology of a chemosymbiotic bivalve. *BMC genomics*, 20(1), 1-14.
202. Zaremba-Niedzwiedzka, K., Caceres, E. F., Saw, J. H., Bäckström, D., Juzokaite, L., Vancaester, E., ... Schramm, A., Baker, B. J., Spang, A & Ettema, T. J. (2017). Asgard archaea illuminate the origin of eukaryotic cellular complexity. *Nature*, 541(7637), 353-358.
203. Zbinden, M., Shillito, B., Le Bris, N., de Montlaur, C. D. V., Roussel, E., Guyot, F., ... & Cambon-Bonavita, M. A. (2008). New insights on the metabolic diversity among the epibiotic microbial community of the hydrothermal shrimp *Rimicaris exoculata*. *Journal of Experimental Marine Biology and Ecology*, 359(2), 131-140.
204. Zimmermann, J., Wentrup, C., Sadowski, M., Blazejak, A., Gruber-Vodicka, H. R., Kleiner, M., ... & Dubilier, N. (2016). Closely coupled evolutionary history of ecto-and endosymbionts from two distantly related animal phyla. *Molecular ecology*, 25(13), 3203-3223

APPENDIX

ZUSAMMENFASSUNG

ACKNOWLEDGEMENTS

ZUSAMMENFASSUNG

In meiner Dissertation habe ich eine faszinierende Symbiose zwischen einem Tier und einem Bakterium erforscht, nämlich die der marinen, interstitiellen Nematoden, die zur Familie der Stilbonematinae gehören. Diese sind außergewöhnlich, da jeder Wurm auf seiner Oberfläche einen einzigen Phylotyp von schwefeloxidierenden Gammaproteobakterien trägt, die zur Gattung *Candidatus* Thiosymbion gehören. Obwohl sie weltweit in Meeressedimenten mit niedrigem Wasserstand verbreitet sind und aufgrund ihres hohen Vorkommens möglicherweise die geochemischen Zyklen der Sedimente beeinflussen, wissen wir immer noch nicht, warum diese beiden Organismen in Symbiose leben. Auf der Grundlage ökologischer Studien wurde lange Zeit angenommen, dass die Symbionten mit Nematoden assoziiert sind, um deren vertikale Wanderungen durch die Redoxzone zu nutzen, d. h. um abwechselnd Zugang zu O₂ in den oberen Sandschichten und zu Schwefelwasserstoff in den tieferen Schichten zu erhalten. Bis zu dieser Arbeit war jedoch die physiologische Reaktion des Holobionten auf die Bedingungen unerforscht, die er bei seiner Wanderung durch den Sand antrifft. Im Rahmen meiner Doktorarbeit habe ich daher die physiologische Reaktion von *Laxus oneistus* auf beide Bedingungen analysiert, indem ich eine breite Palette von Techniken angewandt habe, darunter vergleichende Analyse von mRNA, Lipiden, Proteinen und Metaboliten, qPCR, Stabil-Isotopen Analyse mittels Raman-Spektroskopie und nanoSIMS und Messungen der physikalisch-chemischen Umweltparameter. Um die Physiologie der Symbionten mit ihrer Zellbiologie zu verknüpfen, habe ich außerdem ultrastrukturelle Studien durchgeführt und DNA-Fluoreszenz-in-situ-Hybridisierung (FISH) angewandt.

Die im Rahmen meiner Doktorarbeit gesammelten Ergebnisse führten zu vier Publikationen, die sich konzeptionell in drei Teile gliedern lassen: 1) Reaktion der Symbionten auf Sauerstoff (Paredes et al., 2021); 2) Reaktion des Wirtes auf Sauerstoff (Paredes et al., unter Begutachtung); 3) Zellbiologie der Symbionten (Weber, Moessel, Paredes et al., 2019; Weber, Paredes et al., zur Publikation akzeptiert). In Bezug auf Teil (1) konnten wir zeigen, dass unter Fehlen von Sauerstoff Gene für die Schwefeloxidation hochreguliert wurden und die Symbionten weniger gestresst zu sein schienen und sich stärker vermehrten. Unter Sauerstoff hingegen wurden Gene, die an der Assimilation von Kohlenstoff und Stickstoff beteiligt sind,

Appendix

hochreguliert. Wir vermuten daher, dass der von den Tieren vermittelte Zugang zu Sauerstoff eher die Kohlenstoffspeicherung und die Synthese von Vitaminen und Cofaktoren fördert als die Schwefeloxidation. Außerdem könnte der Symbiont von den organischen Verbindungen und Lipiden des Wirtes profitieren. In Teil (2) haben wir gezeigt, dass der Wirt ohne Sauerstoff weder in einen bewegungslosen Ruhezustand überging noch seinen Stoffwechsel zu unterdrücken schien. Stattdessen wurden Abbauwege (z. B. das Ubiquitin-Proteasom-System, Autophagie und Apoptose) sowie Gene, die den Aufbau der Symbiose vermitteln könnten (z. B. Lektine, Muzine), hochreguliert. War hingegen Sauerstoff vorhanden, schien er kostspielige biologische Prozesse wie Entwicklung, Fütterung, Paarung und Fortbewegung zu aktivieren und auch Immunantwort und Effektoren (z. B. Fungizide, BPIs) hochzuregulieren. Schließlich zeigten wir in Teil (3) eine feste Chromosomenkonfiguration in *Ca. Thiosymbion* und stellten die Hypothese auf, dass dies die Lokalisierung von Membranproteinen erleichtern könnte und dies wiederum für die Symbiose zwischen Wurm und Bakterium vorteilhaft sein könnte. Schließlich haben wir die Morphologie und die Fortpflanzungsweise des ersten jemals beschriebenen würfelförmigen Bakteriums *Ca. T. cuboideus* charakterisiert.

ACKNOWLEDGEMENTS

I thought this section would be the quickest to write, but it turned out to be among the most difficult ones. I am at a loss for words to express my gratitude to the people who shared this experience with me, in good times and the difficult ones. With my best effort, here it goes!

- First and foremost to my supervisor, Silvia. I remember the first time we talked about the doctoral project, and you welcomed me with the ever-smiling personality that identifies you. Now, on the other end of this journey, I fall short of words to express my heartfelt gratitude for the constant input, guidance and dedication throughout these years. I admire the ease with which you are able to detect innovative ideas and write papers, your ability to learn and deepen different topics and overall your positive attitude toward life and through adversity. It has been wonderful working with you side by side and I am confident that future projects will bring us back together again☺.
- To Tobi and Phili, "my chickens". Thank you for all the moments of hard work and also for the laughter and friendship that we have spent together. It has been a joy working with you. To *my little brother*, Tobi, I admire your organization and accuracy in developing tasks and your constant learning of new things. Thank you for all the support in our multiple field trips and all the brainstormed ideas and discussions. Don't miss me too much☺. To Phili, I admire your innovative ideas, as well as your talent with all sorts of microscopy, graphics software, and your excellent communication skills. Thank you for all the scientific input throughout the years and all the tips on Adobe Illustrator, and comments on cell biology☺.
- To Lena, I am very grateful for everything you taught me regarding transcriptomics, as well as for our spirited discussions that always lead to improving the quality of our work. Among the many things that I admire from you is your environmental conscience. Indeed, congratulations for having co-founded together with Philipp, Logan, Melina, Ipek, Thomas, and Kevin, Green Labs Austria, with a lot of effort and from scratch!
- My sincere appreciation to the other (former) members of the Environmental Cell Biology Group: Friedl, Nicole, Mary, Belma, Amir, Nika, and Jean-Marie.
- My special thanks to the *godfather* of the Stilbonematinae, Jörg Ott. It would not have been possible to have had my doctoral studies without your seminal and groundbreaking work on the ectosymbiotic nematodes. I am also thankful for all the insightful discussions through the years.

Appendix

- I also want to thank the insightful discussions with Christa Schleper, Monika Bright, Salvador Espada Hinojosa, Florian Scharhauser, Filipa Sousa, Simon Rittmann, Ulisse Cardini, Jill Petersen, Carolina Reyes, and Wolfgang Miller.
- I am very grateful to all my collaborators: Jean-Marie Volland, Stephanie Markert, Michaela Mausz, Yin Chen, Arno Schintlmeister, Raymond Lee, Siegfried Reipert, Marton Palatinszky, David Berry, Michael Wagner, Andreas Maier, and Manuel Liebeke; and to the Max-Planck Institute for Marine Microbiology: Wiebke Mohr, Marcel Kuypers, Niko Leisch, Harald Gruber-Vodicka and Nicole Dubilier, for continuous scientific and technical support.
- My special thanks to Olivier Gros, for granting me the privilege to perform my secondment in his laboratory in Guadeloupe, and for all help in sampling collection and equipment organization. I also would like to extend my gratitude to Adrien Grimonprez for helping in sampling collection.
- My sincere gratitude to the Carrie Bow Cay Marine Field Station and the Caribbean Coral Reef Ecosystem Program. Especially to the station managers, Zach, Edd, Bonnie, Scott, and Lisa, for your continuous help during fieldwork. Thank you very much, Bonnie, for accompanying me to the hospital of Dangriga☺, and my dear Martha for all your wonderful stories and delicious cuisine!
- I am indebted to Nathalia for her continuous support in all administrative matters. Moreover, many thanks to Andrea and Ulf for all the technical support in the laboratory.
- To Eri cherry, Ip (kelebek), Babsi, Meli, Logan, Tommi, Michael, Max, Lisi, Ruth, Isa, Kevin, Angus, Sinje, Hyak, Rafa, Thiago; and to overall the Archaea Biology and Ecogenomics Unit, **gracias chicos!** It has been a joy working with you. My special thanks to Logan for sharing your scripts and for all the tips on the visa application☺.
- Mariciña, our coffee breaks where we talked about our achievements and frustrations always made me recharge with good energy! Muito obrigada! te quiero☺
- I would like to thank the University of Vienna for awarding me the Dissertation Completion Grant and the DK+ grant (Microbial Nitrogen Cycling) for financing my doctoral work.
- Thank you to the anonymous reviewers because your comments and suggestions greatly aid in improving the quality of our work.
- Last but not least, my sincere gratitude to my doctoral opponents Margaret McFall-Ngai, Andreas Schramm, and Monika Bright, as well as Gerhard Herndl for heading the committee of my defense.

Appendix

To the University “outsiders”

- Para mis padres Hildebrando y Marcela. No tengo palabras para expresar cuánto les quiero, les extraño, les admiro. No habría logrado lo que tengo sin su apoyo incondicional. Aunque estén lejos, siempre estamos juntos y les amo desde el infinito hasta el más allá☺.
- Para mis hermanos, Tana y Brando. Son mis mejores amigos y siempre han sido mi ejemplo a seguir. Les amo y gracias por todo su apoyo y por las risas que nos echamos. También quiero agradecer a Lupo y a mi sobrina Micaela, por existir y hacer la familia más grande y feliz☺.
- Para mi ubelito Abel y mi abuelita Mima, que los quiero con todo mi corazón.
- Para mis tios Patty, Harvey, Yola, Manuel, Aida, Flory, Esther, Amalia, Albert, Beto, Cunshe, Shanty, Ricardo, Andi y en general a todo mi familia. Por todo su cariño y apoyo.
- Un agradecimiento muy especial a mis primos Catty, Uchi y a Arturo, que fueron mi mayor inspiración para convertirme en científica.
- An die Faas-Gehlen: Karl, Kinni, Pou, Geddi, Karin, Elmer, Moni, Goddi, Tinnars, Alexi, primo Alex, Anne, Uwe, Daniel, Susane, Matt, Cristine, Ben, Sandra (die Familie ist so groß!) Vielen dank, dass ihr mich mit offenen Armen in eurer Familie aufgenommen habt☺.
- Abschließend möchte ich Johannes danken. Ich weiß, dass die letzten Monate des Ph.D. besonders schwierig waren, weil ich so gestresst war☺, aber ich danke dir, dass du es mit mir ausgehalten hast, und auch für deine ständige Unterstützung in so vielerlei Hinsicht. Du bist die netteste, freundlichste und disziplinierteste Person, die ich kenne, die einzige, die meine (häufigen) dummen Witze erträgt, und ich bin dankbar, dass sich unsere Wege gekreuzt haben. Gracias *mi amore*!